KU LEUVEN

ARENBERG DOCTORAL SCHOOL
Faculty of Engineering Science

Automated quantification of preterm brain maturation using electroencephalography

Ninah Koolen

Supervisor:
Prof. dr. ir. S. Van Huffel
Prof. dr. G. Naulaers, co-supervisor
Prof. dr. ir. M. De Vos, co-supervisor
(University of Oxford)
Prof. dr. S. Vanhatalo, co-supervisor
(University of Helsinki)

Dissertation presented in partial fulfillment of the requirements for the degree of Doctor in Engineering

December 2015

Automated quantification of preterm brain maturation using electroencephalography

Ninah KOOLEN

Examination committee:
Prof. dr. ir. Y. Willems, chair
Prof. dr. ir. S. Van Huffel, supervisor
Prof. dr. G. Naulaers, co-supervisor
Prof. dr. ir. M. De Vos, co-supervisor
(University of Oxford)
Prof. dr. S. Vanhatalo, co-supervisor
(University of Helsinki)
Prof. dr. ir. M. Moonen
Prof. dr. ir. R. Puers
dr. M. Toet
(University Medical Center Utrecht)
Prof. dr. ir. C. van Pul
(Technical University Eindhoven and Máxima Medical Center, Veldhoven)

Dissertation presented in partial fulfillment of the requirements for the degree of Doctor in Engineering

December 2015

© 2015 KU Leuven – Faculty of Engineering Science
Uitgegeven in eigen beheer, Ninah Koolen, Kasteelpark Arenberg 10 box 2446, B-3001 Leuven (Belgium)

Alle rechten voorbehouden. Niets uit deze uitgave mag worden vermenigvuldigd en/of openbaar gemaakt worden door middel van druk, fotokopie, microfilm, elektronisch of op welke andere wijze ook zonder voorafgaande schriftelijke toestemming van de uitgever.

All rights reserved. No part of the publication may be reproduced in any form by print, photoprint, microfilm, electronic or any other means without written permission from the publisher.

Voorwoord

Beste lezer,

Graag wil ik u bedanken om aanwezig te zijn op mijn publieke doctoraatsverdediging. De weg tot dit punt was een rollercoaster met vele hoogtes en laagtes, door goed of slecht weer, alleen of met gezelschap. De rit duurt vier jaar, gordels vast and there you go!

De start valt wel te vernoemen, vol motivatie startte ik goedlachs als altijd. Al tijdens mijn masterproef bij prof. Sabine Van Huffel werd duidelijk, met het aanstekelijke enthousiasme van mijn begeleider Ivan Gligorijevic, dat het domein van de neurowetenschappen gecombineerd met technologie mij fascineerde. Dit spreekt duidelijk tot de verbeelding, wat als we het neurale netwerk in de menselijke hersenen volledig kunnen begrijpen? Als vervolg, stelde Prof. Van Huffel mij voor om een doctoraat te starten op de diepe hersenstimulatie, ze verwoordde het als "Je kunt nu op de trein springen, nu dit onderwerp van neuromodulatie opkomt". Niettegenstaande interessant, maar ik wou iets praktischer, meer samenwerking met het ziekenhuis, direct nut was van belang. Dus sprong ik op een andere trein, die van de neonatale hersenanalyse, waar ik geen seconde spijt van heb gehad.

Telkens ik mijn onderwerp uitlegde, in slechts een paar regels, konden mijn familie, vrienden, vreemden, conferentiecollega's, jury's om beurzen te verkijgen, zich vinden in het onderwerp. Telkens werd het onmiskenbaar belang voor de maatschappij afgetekend. Helaas, wat ik daarbij niet altijd vermeldde, vanzelfsprekend misschien (?), was het vele uren programmeerwerk om tot deze analyses te komen. Natuurlijk start je vol optimisme, maar al gauw blijkt dat er vele paden te bewandelen zijn, om te komen tot interessante kenmerken die het patroon van de hersenontwikkeling bij te vroeg geborenen definiëren. Hoewel misschien een contradictie, in deze niche blijkt het onderzoeksgebied ruim te zijn, en raakte ik de weg soms even kwijt. Gelukkig kon ik op heel wat ondersteuning rekenen van de mensen om mij heen, om steeds weer een

herboren motivatie te vinden om nu, met een zekere voldaanheid, deze rit af te ronden. Klaar voor nieuwe avonturen.

Daarbij wil ik graag al de mensen bedanken die bijgedragen hebben tot het verwezenlijken van dit doctoraat.

In de eerste plaats wil ik graag mijn oprechte dank betuigen aan mijn supervisor, Prof. Sabine Van Huffel. Allereerst om mij in te leiden tot de biomedische signaalverwerking, en vervolgens te introduceren in het doctoraatsleven. Ook voor de waardevolle suggesties, continue begeleiding en aanmoediging tijdens alle fasen van dit proefschrift. Van mijn motivatie was u altijd overtuigd, waarbij u ook geloofde in mijn capaciteiten. Dankzij de vele sociale momenten, die u organiseerde binnen de afdeling BIOMED, voelde ik mij als een PhD student met een individueel onderwerp nauwer betrokken bij een groep met een gemeenschappelijk doel, een doel waar u uw levenswerk van heeft gemaakt. Het doel om als ingenieurs bij te dragen tot tools om de geneeskunde te ondersteunen!

Ten tweede wil ik ook graag mijn diepe dank betuigen aan mijn co-supervisors Prof. Maarten De Vos, Prof. Gunnar Naulaers en Prof. Sampsa Vanhatalo. Maarten, jij was altijd daar om mij te inspireren met nieuwe ideeën, met die kritische kijk op het onderzoek. Maar ook bij het schrijven van papers, ik mocht alles niet beginnen overdrijven :-) Jij was daar om mij telkens aan te moedigen, om te evolueren in de juiste richting en de touwtjes aan elkaar te knopen. Eveneens Gunnar, ook u hebt mij hierbij geholpen. Om te beginnen introduceerde u mij tot de wereld van de neonatologie en de grote 'toppers' in dit veld, waaronder uzelf, o.a. op de conferentie Brain Monitoring and Neuroprotection in the Newborn. U bleef steeds geloven in mij om begrijpbare algoritmes te ontwikkelen, al dan niet gepaard gaande van een mopje :-) U verbond de hele NeoGuard groep, bestaande uit actief betrokken ingenieurs en medici. Dit vooruitstrevende project motiveerde mij zeker, omdat het mij het belang van dit onderzoek liet inzien. And last but not least, just added during the last year of my PhD, Sampsa, I really want to thank you. You also showed me the importance of this research by concrete examples. I am very happy that I met you, of course not only for the stay in your BABA (Baby Brain activity) lab in Helsinki during half a year, but even more for all the knowledge that you shared with me, whether it was medical, technical or about life. You are a robust bridge between engineers and clinicians. Let's say, the bridge! Your innovative ideas lead to brilliant discussions and the not excludable work :-). This fruitful collaboration pushed me forward with big steps. Kiitos paljon!

Vervolgens wil ik ook de leden die mijn examencommissie vervolledigen bedanken, Prof. Marc Moonen, Prof. Bob Puers, Prof. Carola van Pul, Mona Toet en de voorzitter Prof. Yves Willems. Dankzij de verschillende achtergronden, hebben jullie inzichten de kwaliteit van dit werk nog verbeterd op zowel klinisch als

algoritmisch vlak. Alsook om deel te willen uitmaken van dit laatste stuk van de vierjarige rit.

Ik ben zeer blij met de financiële steun van het IWT (Agentschap voor Innovatie voor Wetenschap en Technologie), die mij een vier-jarige beurs aanbood tot het verwezenlijken van "strategisch basisonderzoek". Alsook met de twee beurzen voor internationale mobiliteit van het FWO (Fonds Wetenschappelijk Onderzoek), die mij toelieten om tweemaal gedurende drie maanden in Helsinki te verblijven.

Zeer belangrijk, want onmisbaar om tot de resultaten te komen die zijn opgenomen in dit werk, zijn mijn collega's van het Universitair Ziekenhuis Leuven, namelijk Anneleen Dereymaeker, Jan Vervisch en Prof. Katrien Jansen. Ik wil jullie bedanken voor alle fijne discussies, al het werk van de labeling en de selectie van de patiënten. Ook voor de vele publicaties die we samen hebben geschreven ;-). Jullie hebben mij veel medische kennis bijgebracht. Het enthousiasme tijdens de vele meetings in het ziekenhuis werkte aanstekelijk, stapje voor stapje werd de vraag naar meer groter!

I would also like to thank my fellow and former researchers at the Department of Electrical Engineering, in particular those of the BIOMED-group! I shared magnificent and unforgettable moments with many of you during conferences, the summer school (with swag'ahs and menus), during lunch breaks and Kubb/frisbee-breaks, during Christmas parties and many other social evenings ;-). We had some great talks, about the PhD rollercoaster, about life and fun. Especially my offices mates, Rob, Bori, Yipeng, Amir, Vladimir and Ivan, but also Griet, Laure, Adrian, Carolina, Alexander, Tim, Nicolas, Lieven, Nico, Otto, Thomas, Barath, Ofelie, Neetha, Steven, Vanya, Ben, Anca, Diana, Kris, Devy, Kirsten, Katrien, Maria Isabel, Rosy, Wang, Milica, Bogdan, Michal and Wout. So, have a lot of fun and laughter in your further (PhD) life!

Voor een constante inspiratie wil ik ook al mijn vrienden hartelijk bedanken. Eline, Sylvie, Susanna. Met jullie heb ik altijd vele gedachtes kunnen uitwisselen tijdens al de toffe babbels, gelach en natuurlijk gepaard met de nodige morele steun. Het maakt niet uit hoe ver we uit elkaar zitten, elkaar een maand(en) niet zien, ik weet dat ik altijd op jullie kan rekenen! Suski, thanks for the amazing talks as a colleague and friend. Pidän paljon naurua Suomessa ;-) Evenzeer belangrijk zijn al mijn studievrienden, vrienden uit Leuven, friends from Helsinki en vele anderen! Velen ken ik al jaren, en ik heb veel plezierige momenten beleefd tijdens deze geweldige jaren in Leuven, in België, around Europe, around the world. The sky is the limit! Te gek! :-)

Tenslotte wil ik natuurlijk mijn dankbaarheid uitdrukken aan mijn fantastische familie. Vooral aan mijn ouders, mijn broer Derck en mijn zus Inez. Jullie

zijn die sterke ruggesteun die een PhD student nodig heeft. Jullie hebben in al mijn keuzes geloofd, in alles wat ik tijdens mijn studies en mijn doctoraat heb gedaan. Ik ga niet zeggen dat alles gemakkelijk is geweest, maar de gesprekken tijdens moeilijke tijden, afgewisseld met gejuich en gelach tijdens vrolijke tijden, en bovendien de fijne vakanties, hebben me alles helpen te relativeren. Jullie staan altijd voor me klaar! Dat alles heeft bijgedragen tot dit promotiewerk. Wie had dit durven denken bijna 27 jaar geleden ;-)

Ninah

December 2015

Abstract

Around 10 percent of all human births is premature, which means that annually about 15 million babies are born before 37 completed weeks of gestation. About one third of the admissions to the Neonatal Intensive Care Unit (NICU) consists of this patient group. Due to complications, 1 million babies die from premature delivery, and it is therefore the most important cause of neonatal death. In general, premature and immature babies have a high risk for neurological abnormalities by maturation in extra-uterine life. Even though improved health care has increased the survival changes of these neonates, they are sensitive to brain damage and consequently, neurocognitive disabilities.

Nowadays, critical information about the brain development can be extracted from the electroencephalography (EEG). Clinical experts visually assess evolving EEG characteristics over both short and long periods to evaluate maturation of patients at risk and, if necessary, to start neuroprotective treatment. However, (semi-) automated monitoring of objective and quantitative EEG variables and its validated use is nearly non-existent in neonates, whereas high need exists in the NICUs. To bridge this gap, the aim of this PhD research was to develop supporting software for the automatic analysis of preterm EEG patterns.

The first part of this work investigates the ability to quantify the maturational change in EEG discontinuity. Early cortical brain activity alternates between two activity modes: periods of relative quiescence (interburst intervals or IBIs) are interrupted by spontaneous activity transients (bursts). This EEG pattern will evolve into a more continuous pattern as a biomarker of maturation. An accurate burst detection algorithm is developed using the multichannel line length (LL) information. Based on the LL characteristics, the suppression curve (SC) is derived representing the 'level of discontinuity'. Both SC properties and IBI lengths show statistically significant correlation with postmenstrual age. Moreover, this developmental shift from intermittent to continuous activity can be captured in a line length histogram. A subset of relevant histogram features is derived and combined into a data-driven EEG index, which holds promise to

facilitate automated EEG assessment.

The second part of this work explored the functional brain connectivity in both healthy patients and patients with developmental neurological disorders. Evaluation of interhemispheric symmetry and synchrony still rely on visual, qualitative EEG assessment without clearly quantifiable definitions. Symmetry characteristics were investigated by the channel symmetry index, and served as input for one-class Support Vector Machine classifiers to distinguish pathological from physiological asymmetry. Interhemispheric synchrony (IHS) was estimated using a quantitative measure, the activation synchrony index (ASI). At term age, it showed to be an objective feature of normal neonatal brain function by significant correlation to clinical, visual classification of normal vs. abnormal. Moreover, a robust and statistically significant increase in ASI is observed with early development of synchrony in cortical activations. Hence, ASI-based metrics provide diagnostic value, even at individual level, which strongly supports its use as a functional biomarker.

In conclusion, the EEG patterns can be assessed over longer time intervals and patients at risk can be identified by automated means. The knowledge and expertise of medical experts is aggregated in the implemented algorithms, which adapt automatically at an individual patient level. A feature set of EEG indexes is reported and promising for implementation of preterm developmental growth charts. This feature set provides a unique set of classifiers to detect deviations from normal brain maturation. In this way, automated analysis would add significantly to the normal manual assessment and could therefore become of high value for devising a markedly improved neonatal assessment capability at the NICU. Furthermore, our work opens up possibilities for a more objective and reliable quantification of therapeutic interventions, paving the way forward for more precise administration of medications.

Beknopte samenvatting

Circa 10 procent van alle baby's wordt te vroeg geboren. Dit betekent dat jaarlijks ongeveer 15 miljoen baby's wereldwijd geboren wordt vóór de 37e week van de zwangerschap. Ongeveer een derde van de opnames in de Neonatal Intensive Care Unit (NICU) bestaat uit deze groep patiënten. Als gevolg van complicaties van de vroeggeboorte sterven 1 miljoen baby's, waardoor dit de belangrijkste oorzaak is van neonatale kindersterfte. In het algemeen hebben premature baby's een hoog risico op neurologische afwijkingen bij de verdere ontwikkeling na de geboorte. Hoewel door de betere gezondheidszorg de overlevingskansen van pasgeborenen zijn toegenomen, zijn ze gevoelig voor hersenschade en bijgevolg neurocognitieve handicaps.

Tegenwoordig kan belangrijke informatie over de hersenontwikkeling worden afgeleid uit het elektro-encefalogram (EEG). Klinische experts beoordelen visueel de evoluerende EEG kenmerken op zowel korte als lange termijn om de maturatie van risicopatienten te evalueren en, indien nodig, neuroprotectieve behandeling op te starten. Echter, (semi-) automatische monitoring van objectieve en kwantitatieve EEG variabelen en het gevalideerd gebruik hiervan, is bijna onbestaande bij pasgeborenen, terwijl hiernaar grote behoefte bestaat in de NICU. Om hieraan tegemoet te komen, was het doel van dit promotieonderzoek ondersteunende software te ontwikkelen voor de automatische analyse van premature EEG patronen.

Het eerste deel van dit werk onderzoekt de mogelijkheid om de ontwikkeling in de discontinuiteit van het EEG patroon te kwantificeren. Corticale hersenactiviteit wisselt tussen twee verschillende niveaus van activiteit: periodes van relatieve rust (interburst intervallen of IBIs) worden onderbroken door periodes van spontane activiteit (burst). Als een teken van ontwikkeling zal dit discontinu EEG patroon evolueren naar een continu patroon. We hebben een nauwkeurig burst detectie algoritme ontwikkeld op basis van de lijn lengte (LL) informatie. De suppressie curve (SC) wordt op basis van deze LL kenmerken bepaald, en reflecteert de mate van discontinuïteit. Zowel SC karakteristieken, als de IBI

lengtes tonen statistisch significante correlatie met de postmenstruele leeftijd. Bovendien kan de verandering van een discontinu naar een continu patroon worden weergegeven met het LL histogram. Een subset van relevante histogram kenmerken is afgeleid en dan gecombineerd in een EEG maturatie-index, die veelbelovend lijkt voor geautomatiseerde EEG evaluatie.

Het tweede deel van dit werk onderzoekt de functionele connectiviteit in de hersenen bij zowel gezonde patiënten als patiënten met een neurologische ontwikkelingsstoornis. De klinische evaluatie van interhemisferische symmetrie en synchronie gebeurt nog steeds op basis van visuele en kwalitatieve EEG inspectie zonder gebruik van kwantificeerbare definities. De mate van symmetrie wordt bepaald met de kanaal symmetrie-index, die vervolgens met behulp van een Support Vector Machine pathologische asymmetrie onderscheidt van fysiologische asymmetrie. Interhemisferische synchronie (IHS) wordt berekend aan de hand van een kwantitatieve maat, de activatie synchronie index (ASI). Op terme leeftijd, blijkt dit een objectieve parameter te zijn om normale neonatale hersenfunctie te kwantificeren. Er wordt een significante correlatie gevonden met de klinische, visuele beoordeling (normaal versus abnormaal). Bovendien wordt een robuuste en statistisch significante stijging van de ASI parameter waargenomen bij de vroege ontwikkeling van synchronie van corticale activiteit. Op basis van deze resultaten, kunnen we stellen dat de ASI-gebaseerde kenmerken een diagnostische waarde verschaffen. Dit geldt zelfs voor individuele patienten, wat het gebruik als een functionele biomarker ondersteunt.

We kunnen concluderen dat het mogelijk is om EEG patronen kwantitatief te evalueren over langere tijdsintervallen en op deze manier ook risicopatiënten te identificeren. De kennis en expertise van de medische deskundigen wordt bijeengebracht in de geïmplementeerde algoritmes, die zich automatisch aanpassen aan de individuele patiënt. Een set van EEG indexen wordt gerapporteerd, die veelbelovend is voor de totstandkoming van premature ontwikkelings grafieken. Op basis van deze feature set kunnen afwijkingen op de normale hersenontwikkeling worden opgespoord. Op deze manier kan een geautomatiseerde en objectieve analyse de visuele EEG evaluatie aanzienlijk verlichten. Het kan daarom van grote waarde zijn voor de optimalisering van de neonatale analyse op de NICU. Bovendien opent ons werk mogelijkheden voor een objectieve en betrouwbare kwantificering van therapeutische interventies, en daarbij voor een meer nauwkeurige toediening van medicatie.

Nomenclature

Metrics

Hz	Hertz
ms	milliseconds
mV	millivolt
mg	milligram
μV	microvolt
s	seconds
h	hour
g	gram
kg	kilogram
kOhm	kiloOhm
w	weeks

Abbreviations

AC	Algebraic Connectivity
aEEG	amplitude integrated ElectroEncephaloGram
AMP	Amplitude
ANOVA	ANalysis Of VAriance
AS	Active Sleep
ASI	Activation Synchrony Index
BAC	Brain Activity Cycling
BBSI	Bilateral Brain Symmetry Index
BSI	Brain Symmetry Index
BW	Birth Weight
CA	Conceptional Age
cEEG	conventional ElectroEncephaloGram
CSI	Channel Symmetry Index
cx-cx	cortico-cortical (pathways)

DTF	Directed Transfer Function
ECG	ElectroCardioGram
EEG	ElectroEncephaloGram
ETDF	Energy weighted Temporal Dependency Function
EV	Envelope Value
FD	Fractal Dimension
FFT	Fast Fourier Transform
FN	False Negative
FP	False Positive
GA	Gestational Age
GC	Granger Causality
GCSI	Global Channelwise Symmetry Index
GS	Global Synchrony
HI	Histogram Index
HVS	High Voltage Sleep
IBI	Interburst Interval
ICA	Independent Component Analysis
IHS	InterHemispheric Synchrony
IMC	Imaginary part of the Coherence Function
LL	Line Length
LS-SVM	Least Squares Support Vector Machine
MDI	Mental Developmental Index
MEG	MagnetoEncephaloGram
MI	Mutual Information
MIF	Mutual Information Function
MSC	Magnitude part of the Coherence function
MSD	Mean Squared Difference
MST	Minimum Spanning Tree
NICU	Neonatal Intensive Care Unit
NIRS	Near-InfraRed Spectroscopy
NLEO	Non-Linear Energy Operator
PCA	Principal Component Analysis
PDC	Partial Directed Coherence
PDI	Psychomotor Developmental Index
PMA	PostMenstrual Age
PSD	Power Spectral Density
Q	Quantization
QPC	Quadratic Phase Coupling
QS	Quiet Sleep
r	correlation coefficient
ROC curve	Receiver Operating Characteristic curve

SAT	Spontaneous Activity Transient
SAT%	Proportion of SATs in the EEG signal
SC	Suppression Curve
SNR	Signal-to-Noise Ratio
SVM	Support Vector Machine
SWC	Sleep Wake Cycling
TA	Tracé Alternant
TD	Tracé Discontinue
TN	True Negative
TP	True Positive

Contents

Abstract v

Nomenclature ix

Contents xiii

List of Figures xix

List of Tables xxix

1 Introduction 1

1.1 Problem statement 1

1.2 Thesis Outline 2

2 Physiological interpretation of the preterm EEG 5

2.1 Premature neonates 5

2.2 Electroencephalography 8

2.2.1 Neuronal activity in the brain 8

2.2.2 Scalp EEG 10

2.2.3 Amplitude integrated EEG (aEEG) versus conventional EEG 10

2.2.4 Dataset 13

2.3 What to extract from the EEG? 14
2.3.1 Level of discontinuity 14
2.3.2 Connectivity of the brain 19
2.3.3 Other EEG characteristics 22

3 Methods for automated preterm EEG background analysis 25

3.1 Level of discontinuity 25
3.1.1 State of the art for burst detection 25
3.1.2 Quantification of the global change of discontinuity . . . 31
3.2 Brain connectivity by means of interhemispheric symmetry and synchrony 32
3.2.1 Methods for symmetry classification 32
3.2.2 Methods for synchrony maturation and classification . . 34
3.3 Handling of artefacts 38

4 Line Length as a Robust Method to Detect High-Activity Events: Automated Burst Detection in Premature EEG Recordings 41

4.1 Introduction: Towards improving preterm prognosis 43
4.2 Methods: automatically reading EEG recordings 45
4.2.1 Data acquisition 45
4.2.2 Burst Detection 46
4.2.3 Performance Evaluation 52
4.3 Results: detection characteristics applying real-world data . . . 54
4.3.1 Comparing burst detection methods 54
4.3.2 Prognostic features 56
4.3.3 Statistical significance 58
4.3.4 Detection on a variable number of channels 59
4.4 Discussion 61

4.5 Conclusion 62

5 The suppression curve as a quantitative approach for measuring brain maturation in preterm infants 65

5.1 Introduction 67

5.2 Methods 68

5.2.1 Data Acquisition 68

5.2.2 EEG monitoring 69

5.2.3 Automated analyses 69

5.2.4 Statistical analyses 70

5.3 Results 71

5.4 Discussion 75

6 Data-driven metric representing the maturation of preterm EEG 79

6.1 Introduction 80

6.2 Methodology 81

6.2.1 Data Acquisition 81

6.2.2 Line Length Calculation 82

6.2.3 Histogram Distribution 82

6.2.4 Feature Relevance 83

6.3 Results and Discussion 84

6.3.1 Line Length Histogram Evolution 84

6.3.2 Feature Relevance 86

6.3.3 Accuracy 86

6.4 Conclusion 88

7 Development of an interhemispheric symmetry measurement in the neonatal brain 89

7.1 Introduction 90

7.2 Data acquisition 91
7.3 Methodology 92
7.3.1 Channel Symmetry Index 92
7.3.2 Outcome dependent features 94
7.3.3 One-class SVM classification 94
7.4 Results and Discussion 97
7.5 Conclusions 98

8 Interhemispheric synchrony in the neonatal EEG revisited: Activation Synchrony Index as a promising classifier 101

8.1 Introduction 103
8.2 Materials and methods 104
8.2.1 Subjects and EEG recordings 104
8.2.2 Activation Synchrony Index 106
8.2.3 Parameter Optimization 107
8.2.4 Classification 109
8.2.5 Age dependence of ASI 109
8.3 Results 110
8.3.1 Optimal parameters for ASI stabilization 110
8.3.2 Classification 110
8.3.3 Age dependence of ASI 114
8.4 Discussion 114
8.4.1 Intra-individual stability and measurement stability: selection of small epochs 116
8.4.2 Channel pair combination and cut-off value 117
8.4.3 Age independency of ASI 117
8.4.4 Future directions 118

9 Early development of synchrony in cortical activations in the human 121

9.1 Introduction . . . 123

9.2 Methodology . . . 124

9.2.1 Data acquisition . . . 124

9.2.2 Analysis of synchrony . . . 125

9.3 Results . . . 128

9.4 Discussion . . . 135

10 Summary and future research lines 139

10.1 Summary of chapters . . . 139

10.2 General afterthoughts . . . 143

10.3 Future directions . . . 145

10.3.1 Influence of medication (propofol) on the EEG . . . 146

10.3.2 EEG growth charts . . . 149

10.3.3 Neurodevelopmental outcome prediction based on EEG features . . . 155

10.3.4 Combining modalities into one maturational model . . . 160

A Patient Data Sets 163

B Supplementary Material: The suppression curve as a quantitative approach for measuring brain maturation in preterm infants 165

C Supplementary material: Interhemispheric synchrony in the neonatal EEG revisited: Activation Synchrony Index as a promising classifier 167

C.1 Supplementary table: Detailed overview of the selected patients 167

Bibliography 177

Curriculum 199

Publication list **201**

List of Figures

1.1 Overview of the different chapters, including the two main thesis contributions to unravel premature brain maturation: quantification of the level of discontinuity and the brain connectivity. 4

2.1 Estimated distribution of neonatal deaths in 193 countries in 2010. As adapted from (March of Dimes Geneva, 2012). 6

2.2 Preterm birth. (A) Increasing trend of preterm birth rate. (B) Preterm babies are born too early (1-4 months), and therefore, the brain still has to develop during extra-uterine life towards term age. 7

2.3 A. Neurotransmission: a neuron sends an electrical impulse through a neuronal pathway, followed by a transmission of chemicals across the synapse, to the neighbouring neuron (Daylan & Abbott 2005). B. The electrodes measure an electric field created by the sum of many stimulated cells. The EEG signal is a potential difference between two electrodes, which should be amplified due to the resistance of the cerebrospinal fluid, the skull and the scalp surrounding the brain. 9

2.4 The international 10-20 EEG system seen from the left side (A) and above the head (B). Nomenclature of the electrodes is given according to the position on the scalp. EEG waveforms differ according to the bipolar montage (C) or the unipolar montage set-up (D). 11

2.5 Current state in the NICU, conventional EEG signals of the patient are monitored in the incubator and an expert will read the EEG on the screen. 12

2.6 Evaluation of EEG monitoring systems: amplitude integrated EEG (aEEG) versus conventional EEG (cEEG). 13

2.7 Maturational changes regarding patterns and sleep states in the premature EEG (Cherian et al. 2009): a shift from tracé discontinu to tracé continu (André et al. 2010). 15

2.8 Discontinuous EEG pattern consists of bursts (spontaneous activity transients) interrupted by quiet periods (interburst intervals). An example of a burst and an IBI is depicted. . . . 16

2.9 Schematic overview of the maturation of bursts and IBIs from early preterm to fullterm, concerning the number of bursts/IBIs, their amplitude, as well as their synchrony. Figure adapted from Vanhatalo & Kaila 2006 17

2.10 The influence of propofol administration on the discontinuity level on (a) the aEEG, (b) the suppression curve. 19

2.11 Synchrony and symmetry between both hemispheres. Comparing T4-O2 and T3-O1, bursts start simultaneously (synchronous) and no significant difference in amplitude can be noticed (symmetric). (A) Longitudinal montage (B) Transversal montage. As adapted from Selton et al. (2000). 21

2.12 EEG patterns representing different sleep states: (a) Active sleep (AS), (b) Quiet sleep (QS). As adapted from André et al. (2010). 24

3.1 Flow chart of a burst detection algorithm. A-D present the consecutive methodological steps of the algorithm. 26

3.2 Overlapping windows for EEG segmentation with fixed-window length of 1 second, presuming quasi-stationary EEG in each window. 29

3.3 The ASI algorithm. (A) Neonatal EEG recording with an EEG cap. The synchrony can be calculated between any pair of signals. (B) Different steps of the ASI paradigm (Ch= channel, FFT= Fast Fourier Transform, Q = quantization, ETDF = energy weighted temporal dependency function). (C) Different stages of the ASI calculation: EEG signals from two hemispheres (left=red, right=blue), pre-emphasized and temporally smoothed energy envelopes, quantized energy envelopes. (D) ETDFs illustration of synchronous signals (left) and asynchronous signals (right). Asynchrony is represented by a flat dependency distribution function or peaks at a time delay $\tau \neq 0$. Figure adapted from Räsänen et al. (2013). 36

4.1 (a) Example of 65 s 9-channel EEG recording with reference electrode Cz, (b) Burst detection: by 2 clinicians and by algorithm, (c) Black curve: median $L_n(i)$ as calculated in step 2, gray line: threshold for detection of bursts (Thr_Det), diamonds: detected burst segments after step 3. 49

4.2 ROC curve of the burst detection algorithm, F is adapted to get different Thr_Det. 49

4.3 Comparison of the line length curve, for a discontinuous pattern (a) and a more continuous pattern (b). Median of the curve is shown by a gray line; mean is shown by a dashed line. 50

4.4 Suppression curve of one patient. Discontinuities are revealed around the 6000th second and the 16000th second of the 5 h long measurement. 51

4.5 Box plots of sensitivity, specificity and accuracy for the three detection algorithms, all 13 measurements are included. 56

4.6 (a) clean EEG with clear burst transitions, which results into high accuracy values for all detection methods; (b) Unclear transitions between bursts and IBIs (lot of activity), leading to a low accuracy for the NLEO method. 56

4.7 The evolution of the premature brain leads to a change in the IBI duration histogram: histogram in Figure 4.7 b are derived from a measurement taken two weeks later than the measurement resulting in the histograms in Figure 4.7 a. The histogram has shifted to the left; including shorter IBIs. The median IBI length (gray line) decreased too. 57

4.8 Error in automatic detection by comparing to clinicians' scoring for three prognostic values (median IBI, maximum IBI and burst percentage). The box plots represent the differences for all patients calculated for three detection methods (1: line length based method, 2: envelope based method, 3: NLEO based method). 58

4.9 Detection accuracy by using a different number of channels as input for the line length detection method: 2 channels (C3-C4), 4 channels (C3-C4-O1-O2), 9 channels (C3-C4-O1-O2-T3-T4-Fp1-Fp2-Cz). 60

5.1 The suppression curve derived from a multiple-hour recording. The suppression curve is depicted for discontinuous (black) and more continuous (gray) parts of the EEG recording. 70

5.2 The overall decrease in mean SC values of 90 multichannel EEG recordings over the course of early development. (a) We defined 6 age groups according to postmenstrual age (PMA), covering two weeks difference in PMA age (red: PMA <28 weeks PMA, black: 28-30 weeks PMA, blue: 30-32 weeks PMA, green: 32-34 weeks PMA, pink: 34-36 weeks PMA, yellow: > 36 weeks PMA). (b) Boxplots representing the developmental changes of the mean SC over the different PMA groups. (c) Boxplots representing the developmental changes of the standard deviation of the SC over the different PMA groups. 72

5.3 The decrease in mean SC value over the course of early development. There is a linear correlation between the mean SC and PMA till 34 weeks (r= -0.8, p=$3.5*10^{-12}$). (a-d) The suppression curve from 4 hours multichannel EEG recording at different PMA in one patient. (a) High suppression values represent mainly discontinuous EEG. (b-c) When maturing, a more cyclic pattern is seen in the SC, representing alternating continuous and discontinuous EEG. (d) At term age, difference between discontinuous EEG and continuous EEG became smaller in the SC. 73

5.4 The IBI 95th percentiles of 90 multichannel EEG recordings, performed in 25 preterm infants. (a) The IBI 95th percentiles decrease with advancing postmenstrual age (r= -0.82, p<0.001). (b) Boxplots representing the 95th percentile over the different PMA groups. The median IBI 95th percentile group values are as follows: (<28 weeks PMA) 15.1s, (28-30 weeks PMA) 12.4s, (30-32 weeks PMA) 10.7s, (32-34 weeks PMA) 8.9s, (34-36 weeks PMA) 8.0s, (>36 weeks PMA) 6.5s. 74

5.5 The suppression curve of one patient at different PMA with variable EEG recording times. Mean SC values can be influenced by recording time. 75

5.6 Future work could focus on neurotherapeutic treatments. For example, the suppression curve of two patients (black) is influenced by receiving fentanyl during the first EEG recording. Higher suppression curve values represent more discontinuous or suppressed EEG. Mean SC value is below 0.25 in preterm infants without sedative drugs (gray), even in the smallest age group (26-28 weeks PMA). In addition, intra-patient follow-up with multiple EEG recordings is possible. The follow-up curves of the presented population is shown by grey curves. 78

6.1 A schematic overview of the presented method. 81

6.2 A. Example of continuous EEG pattern, B. Example of discontinuous EEG pattern. 83

6.3 Concept of EEG content change by means of histogram change. A. Example histograms for one patient with 3 consecutive recordings, B. Schematic presentation of the trend change in the histogram shape, C. 20 defined bin heights (%) in function of the postmenstrual age (weeks) for channel C3, D. 8 defined statistical measurements in function of the postmenstrual age (weeks) for channel C3. 85

6.4 Feature relevance for maturation for the 28 predefined features. The grey features have been selected for further analysis. 86

7.1 Electrode placements for 9 channel EEG measurement, contralateral channels are given in white-black (O1-O2, C3-C4, T3-T4, Fp1-Fp2) 93

7.2 a. mean CSI values, averaged over frequency bands, shown for different channel pairs; b. box plot mean CSI. 93

7.3 Different features for a normal patient (patient 1) and a patient with hemimegalencephaly-haemorrhage (patient 2), measurements taken at comparable PMA. 94

7.4 Number of normal/abnormal patients, number of data excluded for analysis since artefacts are present in the data. 95

7.5 Principle of the quadratic problem of the one-class SVM (Fourie et al. 2011). 96

8.1 (A) Schematic overview of the presented method. (B) EEG tracks with Normal and Abnormal synchrony. (C) Schematic view of the ASI algorithm (Räsänen et al. 2013). (D) Two 10-min quiet sleep epochs are subdivided into shorter epochs of 2.5, 5, and 10 min for analysis which gives respectively *ASI2.5*, *ASI5* and *ASI10* values. 105

8.2 Difference in mean squared difference (MSD) between two analyzed periods of 10-min EEG, every dot representing a different patient. Results are shown for Frontal-Centro (Fp-C) and Centro-Occipital (C-O) derivations for different analyzing window lengths (2.5/10 min). Best result with lowest MSD is shown in the upper right plot, obtained for average ASI values over 4 x 2.5 min analysis on C-O derivations. 111

8.3 ASIs for subsequent 10-min epochs from the same quiet sleep period or for separate 10-min epochs from two different quiet sleep periods. 113

8.4 (A) $ASI2.5_1$ and $ASI2.5_2$ for both 10-min EEG segments from 31 patients for C-O derivation with the lowest MSD value. Two groups are specified: normal patients (black labels) and abnormal patients (gray labels). (B) Discrimination between normal and abnormal ASI taking the minimum ASI of $ASI2.5_1$ and $ASI2.5_2$ and thresholding (Th_ASI = 3.6). (C) ROC curve for classification, AUC = 0.971. 113

8.5 ROC curves for different ASI window lengths and different epoch lengths. 115

8.6 ASI value is independent of postmenstrual age of the term infant (PMA >36 weeks). Black labels represent healthy patients with synchronous patterns; gray labels are patients with asynchronous patterns. The mean ASI value is calculated for manually-selected 20-min periods (8 × 2.5min). 116

9.1 Comparison of ASI analysis settings with respect to developmental correlations. Left side graph shows correlation coefficient (r) between ASI and PMA in the same dataset when ASI is computed using different amount of data (x axis), different analysis windows (1min vs 2.5min), or different combinations of channels. A little increase in r-values is found when using longer EEG epochs. On the right side, PMA correlations are shown for 1 min and 2.5 min ASI windows. Both correlations are significant, however use of 2.5 minute ASI windows gave clearly steeper developmental trends and higher correlation values. 126

9.2 Intra-individual ASI stability and its development. (A) Connectivity matrices derived from subsequent EEG epochs of 2.5 minutes, (B) Temporal variability of global synchrony values (see also Fig 9.3 A), (C) Spatial variability of all 28 channel combinations for each individual without significant developmental trend, (D) similar interquartile variability for each channel pair combination. 129

9.3 Spatial ASI Analysis and its development. (A) In addition to the temporal variability seen as the interquartile range of GS values in successive epochs, there was also an overall increase in GS values with increasing PMA, (B) Graphs depicting the developmental change in the mean ASI of each EEG channel compared to the other 7 channels, which have all significant correlations, (C) Graphs representing the developmental change in the mean ASI over the given spatial subgroup as schematically shown in the topoplots. The right most plot depicts developmental change of the first component of principal component analysis (PCA). Significance of the correlation is depicted with an asterisk after correlation coefficient 'r'. The value 'a' depicts the slope of linear regression computed for the given graph. 131

9.4 Validation of findings using both the original data set (black labels) and the validation dataset (grey labels). The validation dataset showed more variability, especially in the lower age range, however the developmental correlations were significant: GS (r = 0.64, p = 2.0*10-9, a = 0.25) and interhemispheric synch (r = 0.70, p = 1.2*10-11, a = 0.32). 132

9.5 Developmental change of graph metrics, MST mean and algebraic connectivity, both of which showed a significant correlation with PMA. 133

9.6 ASI in bipolar derivations. (A) Developmental changes in ASI computed from bipolar derivations for both interhemispheric and intrahemispheric channel combinations. Note that the correlation is often not significant and its strength (r) is smaller as compared to monopolar derivations (Figure 9.3). (B) Hemispheric and anterior-posterior comparisons reveal significant asymmetries. Comparison of frontal and posterior interhemispheric connections shows frontal dominance in 20 out of 22 cases, while the left side shows stronger ASI in 16 out of 22 cases. 134

10.1 Effect of propofol administration on the suppression curve. In the lower plot, the 1-hour average of the SC after propofol is shown, with an increased suppression value during the first hour (dashed line). 147

10.2 Statistical descriptive SC values (median, interquartile range) for each age group. Number of patients between brackets. SC values are decreasing towards baseline values, with faster propofol clearance in the older neonates. 148

10.3 Impact of birth weight and gestational age on survival probability for female and male preterm babies, as adapted from Shah et al. (2012). 151

10.4 Histogram Index Growth Curve obtained by categorical regression on the predicted Q factor scores, with 95% confidence intervals. 152

10.5 Developmental features obtained by applying the burst detection algorithm (Chapter 4) and estimation of the histogram index (HI) (Chapter 6) for a healthy patient group (Bayley score > 85 at 9 months). Maximum interburst interval lengths are depicted, with the 95th percentile being more robust to outliers/artefacts, because the maximum is just a single value. The HI is calculated by including all LL values (full EEG recording) and by including the LL values from only the discontinuous EEG parts. 154

10.6 A correlation (r=0.73, p<0.01) was found between the mode of the lognormal distribution ($\exp(\mu - \sigma^2)$ and the postconceptional age (PCA). The mode is associated with the discontinuity of the EEG (μ) and the asymmetry of the distribution (σ). Figure adapted from Saji et al. (2015). 155

10.7 (A) Distribution of abnormal and normal patients according to different age groups, (B) Linear regression between PMA and HI (in disc. EEG) is shown. Difference in postmenstrual age correlations between the normal (r_norm) and abnormal (r_ab) class, (C) small difference a is found in the real situation because the age range of normal patients is centered around a younger PMA, whereas in an ideal situation a difference b can be found for both classes centered around a similar age range. 158

List of Tables

2.1 Maturational changes in background EEG variables describing the level of discontinuity, adapted from Palmu (2015) 18

2.2 Changes of descriptive features in the young preterm. 20

3.1 Relevant algorithms to detect bursts, adapted from Palmu 2015 27

3.2 Symmetry indexes. 33

3.3 Methods for synchrony analysis 35

4.1 Sensitivity, specificity and accuracy of three detection methods for both the training and validation set. Detection methods are based on line length, based on envelope calculation and based on NLEO. 57

4.2 Statistical performance t-test on statistical measurements – accuracy, sensitivity and specificity – (see boxplots in Figure 4.5). Two detection methods are compared each line; m1, line length based method; m2, envelope based method; m3, NLEO based method. In the table, the differences between the mean values of these statistical measurements are given. Thereby, a significant difference is presented as *($p < 0.05$), **($p < 0.01$), ***($p<0.001$). 59

4.3 Statistical performance t-test on three prognostic features: median IBI length, maximum IBI length and the burst percentage. Two detection methods are compared each line; m1, line length based method; m2, envelope based method; m3, NLEO based method. In the table, the differences between errors on the prognostic features are given. Thereby, significant difference is presented as *($p < 0.05$), **($p < 0.01$), ***($p < 0.001$). 60

6.1 Mean residual error using the 6 relevant features, averaged over the consecutive recordings for different regions of the brain. . . 87

7.1 Specificity (%) of the four trained one-class SVMs with 10-fold cross-validation. Sensitivity (%) on detecting the abnormal EEG patterns. For this small sample, we would go for $\nu = 0.15$ in case of the C3C4 classifier and $\nu = 0.1$ for the three other classifiers. 99

8.1 Mean squared difference (MSD) for different channel pairs and different ASI analyzing window lengths shown as anaverage for all 31 patients. Grand averages of the MSD values over all channel pair combinations and window lengths are shown as well. Examples shown in Figure 8.2 are underlined in this table. . . . 112

10.1 Outcome prediction based on synchrony assessment at 9 months using the Bayley score. Interhemispheric synchrony normality was obtained using ASI values (Koolen et al. 2014c, Chapter 8) 145

10.2 Performance measures using EEG features to predict the neurodevelopmental outcome at 9 months obtained using support vector machines. Sensitivity, specificity, accuracy are calculated based on the TP (true positive), TN (true negative), FP (false positive) and FN (false negative) numbers. 159

A.1 Patient data sets: overview per chapter 164

B.1 Demographic and clinical data of the study population. Values are expressed as n (%), mean ± SD, range. BPD: need for supplemental oxygen/ventilation at 36 weeks PMA. Sepsis: positive blood culture or highly suspected with antibiotic treatment > 72h. 166

C.1 Detailed overview of the selected patients 168

Chapter 1

Introduction

1.1 Problem statement

The brain is a very complex network of neurons. Through electrical and chemical signals, these neurons send all the information in our body around. They coordinate the organs in the body, the sensory systems, movements, behavior and the homeostatic body functions such as respiration and blood pressure. To non-invasively register all these processes on the scalp, electroencephalography (EEG) is commonly used. This method measures the electrical potential differences in the brain that have arisen by forwarding information. In case of comorbidities, the EEG explains both the nature and location of the abnormality. EEG is already widely used in the measurement of brain signal activity, for example in epilepsy patients (Snead 2001, Jaseja 2009). However, (semi-)automated monitoring of quantitative EEG variables and its validated use is nearly non-existent in neonates, whereas a high demand exists in the hospitals in which EEG is registered. In this PhD research, the goal was to develop supporting software for the automatic analysis of premature EEG. In this group of patients, it is very important to monitor the brain activity in the weeks after birth to make an accurate diagnosis about the maturation and an accurate prognosis for survival. In this way, objective evaluation on long-term monitoring would improve the neonatal assessment a lot, in addition to reducing the workload of the clinicians. Moreover, there would be more evidence to start neuro-protective therapies.

Seizures in the neonatal EEG are important clinical phenomena (Legido et al. 1991, Mellits et al. 1982), for which medical treatments have been described in

several studies (Azzopardi et al. 2000, van den Broek et al. 2011). However, the duration of a registered seizure is short compared to the recording time of the entire EEG. Clearly, there is much more information in the EEG, called 'EEG background activity' (Menache et al. 2002, André et al. 2010). Therefore, it is important to quantify the entire EEG signal to make a reliable neurological assessment. Critical factors for the diagnosis are both the amplitude of the background EEG, and the degree of the (dis-)continuities (Monod et al. 1972, Vanhatalo & Kaila 2006, Niemarkt et al. 2010). Namely, a discontinuous pattern consists of periods containing high amplitude and frequency bursts interrupted by low voltage EEG. The level of discontinuity will decrease parallel to maturation. We will investigate this deeper in the rest of the thesis. In the literature, it is generally believed that long periods of low-voltage EEG lead to an increased risk of brain dysfunction (Lombroso 1985, Le Bihannic et al. 2012). Early detection makes treatment possible, and thus significantly reduces the risk of brain damage. Nevertheless, normal brain development is expected when an originally discontinuous EEG pattern evolves into a continuous EEG pattern at term age. In addition, neural networks are formed and stronger connection is found parallel to maturation of the brain. Based on the evolution of the most discriminatory features over time, we set up trend profiles in function of the postmenstrual age. The objective and automatic quantification based on these EEG characteristics is as yet commercially non-existent and, therefore, we express the importance of this research.

1.2 Thesis Outline

This thesis contributes to automated EEG quantification and consists of two main parts: namely, maturation of the preterm brain can be quantified by

- the level of discontinuity
- the level of brain connectivity

The outline of this thesis is depicted in Figure 1.1.

Chapters 2 and 3 are organized by explaining the quantifications of the brain development, with emphasis on EEG discontinuity and interhemispheric connectivity. A general introduction will be given for the physiological background of the phenomena appearing in the preterm EEG, as well as an overview of the algorithms to process and extract these interesting EEG patterns. We present a review of the recent literature, whereas methodologies and results will be explained in the next chapters, based on full research publications in

peer-reviewed international scientific conference proceedings and peer-reviewed international academic journals.

Level of discontinuity

In chapters 4, 5 and 6, three publications on the level of discontinuity are presented. First, we developed a burst detection algorithm, based on the easily interpretable feature 'line length' (LL). In a next step, the 'suppression curve' was extracted, which is a curve expressing the level of discontinuity in the EEG. It is promising to quantitatively measure the brain development with respect to the change in continuity. Moreover, quiet sleep epochs can be extracted in order to perform further maturational feature calculation. In addition, based on the same line length curve, we built up histograms representing the preterm EEG content. The shifting shape of the histogram resembles the maturational process of the brain.

Brain connectivity

Three publications about connectivity of the brain are incorporated (chapters 7, 8, and 9). First, we have looked at the interhemispheric symmetry, i.e. the amplitude difference between EEG signals of the left and right hemisphere. In this way, we could detect patients with abnormalities. We have also performed interhemispheric synchrony classification with the Activation Synchrony Index (ASI) feature, between normal/abnormal patients selected on holistic, conventional visual criteria. Moreover, a maturational trend was discovered using ASI with multichannel information.

In chapter 10, a summary of the main findings of each chapter is given. Some thoughts on the results are discussed. The extracted features are very promising to set up 'preterm EEG growth charts'. Furthermore, future lines are considered including recent work as a first step towards the implementation of these ideas. These objectives incorporate, among others, the influence of medication on the EEG, the preterm growth charts and the correlation of the neurodevelopmental outcome with the extracted EEG features.

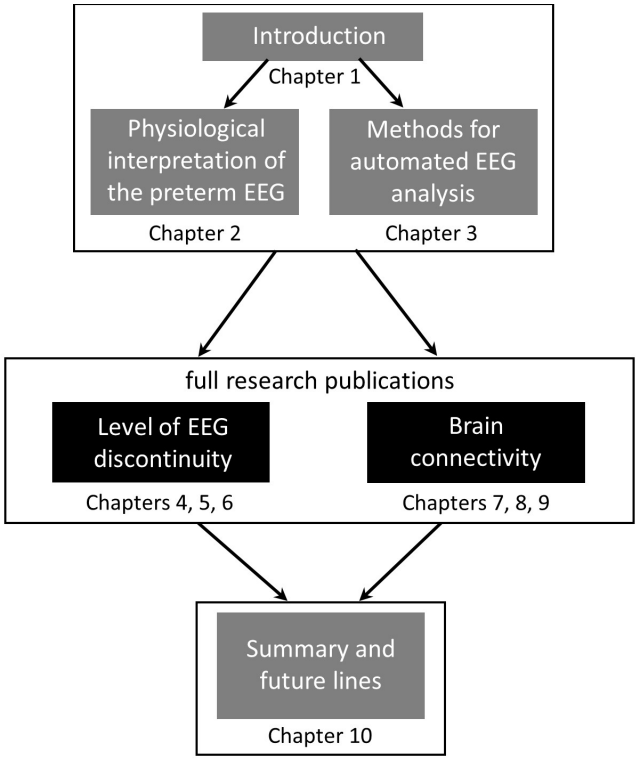

Figure 1.1: Overview of the different chapters, including the two main thesis contributions to unravel premature brain maturation: quantification of the level of discontinuity and the brain connectivity.

Chapter 2

Physiological interpretation of the preterm EEG

With annually 15 million babies born prematurely, it is important to assess the state of the brain development as early as possible to reduce the risk of neurological abnormalities and ultimately the cost for society. Modern technologies allow us to measure the EEG of these premature babies. By analyzing the data, we can determine the maturation level of the premature brain. In particular, the discontinuity in the EEG pattern but also the symmetry and synchrony between the hemispheres provide a sound indication for the state of development. With healthy aging, a more continuous EEG pattern and stronger connectivity would suggest a good prognosis for the brain's maturation; abnormalities then can be spotted from deviating EEG characteristics.

2.1 Premature neonates

Around 10 percent of babies are born prematurely (Beck et al. 2010), which is about 15 million babies each year. This group causes 33.2% of admissions to the neonatal intensive or special care in Flanders (Cammu et al. 2009). 1 million babies die due to complications of preterm birth (March of Dimes Geneva, 2012, Blencowe et al. 2012). 44% of the child deaths (< 5 years) were in the neonatal period (Liu et al. 2012). Prematurity is even the most common cause of neonatal deaths, followed by intrapartum-related events, such as birth asphyxia (Liu et al. 2012, March of Dimes Geneva, 2012) (Figure 2.1). The proportion of

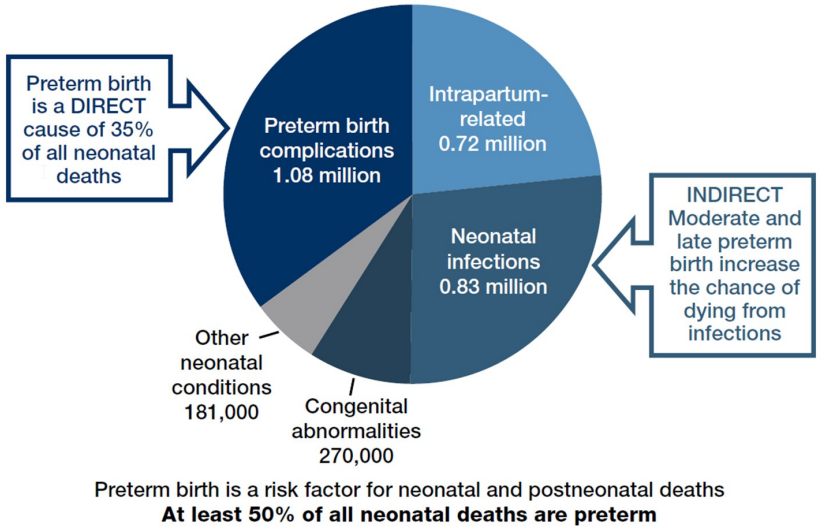

Figure 2.1: Estimated distribution of neonatal deaths in 193 countries in 2010. As adapted from (March of Dimes Geneva, 2012).

preterm births worldwide has an upward trend, and thereby increasing costs for society. In Figure 2.2A, a prediction curve is shown for premature birth rate until 2025 (March of Dimes Geneva, 2012).

Prematurity is defined as birth before 37 completed weeks of gestation, instead of the normal 40 gestational weeks (figure 2.2B). Survival chances are about 50% with special neonatal intensive care for extremely preterm infants, i.e. born between 22-28 weeks of gestation (Blencowe et al. 2012), with higher chances for respectively older gestational age (GA). More than 80% of preterm births occur at late preterm gestational age, 32-36 weeks, from which most patients survive provided special care is given in the Neonatal Intensive Care Units (NICU). In general, premature and immature babies have a high risk for neurological abnormalities. The brain not only has to grow but also has to mature, both in size and in complexity (Figure 2.2B). In particular, the physical connection between neurons will grow during the time when youngest preterm infants are already born and treated in the NICU (Kostović & Judas 2010). Even though improved health care has increased the survival chances of these neonates, one out of three patients has neurocognitive disabilities during later life (Mwaniki et al. 2012). Early preterm babies are very prone to brain damage such

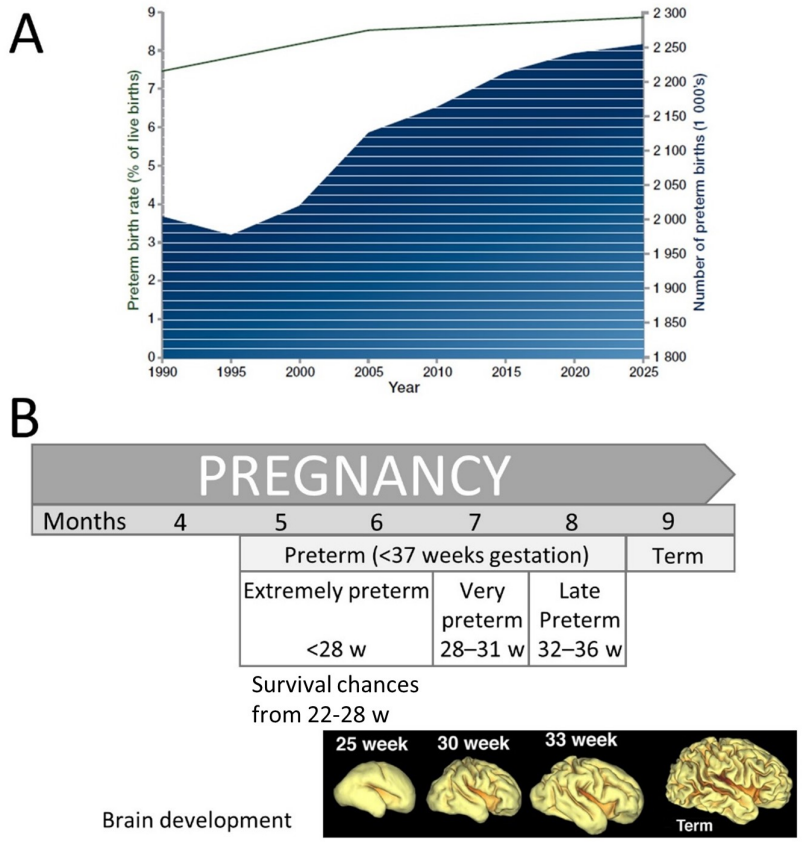

Figure 2.2: Preterm birth. (A) Increasing trend of preterm birth rate. (B) Preterm babies are born too early (1-4 months), and therefore, the brain still has to develop during extra-uterine life towards term age.

as intraventricular bleeding and ensuing white matter lesions. Consequently, learning disabilities and visual and hearing problems could arise. Lifelong disabilities cause a high toll on individuals born preterm, their families and the communities in which they live (Institute of Medicine 2007), and therefore, both for the clinicians as for the parents, it is important to make an accurate diagnosis and prognosis by means of assessing the electroencephalography.

2.2 Electroencephalography

-monitoring electrical activity of the brain-

2.2.1 Neuronal activity in the brain

What exactly are we measuring with the electroencephalography? The bioelectric current generated by neurons to transmit information around the body.

The largest concentration of neurons exists in our central nervous system, consisting of the brain and the spinal cord. A typical neuron is built by three important elements: a soma (a cell body), an axon and dendrites. The axon carries electrical signals away from the cell body to other neurons and it can be as long as 1 m in human beings. The electrical signal is not able to pass the interface to the neighbouring neuron, since they are not physically connected. Therefore, dendrites receive the information through a chemical reaction across the synapse, the small space between the two membranes of the axon and the dendrite. The action potential arriving at the end of the axon opens voltage-dependent ion channels in the membrane of the axon, which produce an influx of Ca^{++}. As a result, a neurotransmitter is released (exocytose) and crosses the synapse (Figure 2.3A). These molecules bind to the receptors on the signal-receiving side. Different effects may occur; some neurotransmitters stimulate the activity of the neuron, whereas others inhibit the activity.

Neurons provide a rapid 'communication' through electrical signals around the neuronal network. Information is transmitted by firing sequences of spikes in various temporal patterns. The series of action potentials (spike trains) can be recorded by placing an electrode close to or inside the soma or axon of a neuron (Kostal et al. 2007). Non-invasively, we can record the electroencephalogram (EEG), which is generated by the summation of postsynaptic potentials in the cortex. The action potentials generated in the neurons do not contribute significantly to the scalp EEG, because they have a much smaller potential field distribution and are shorter in duration (1 ms versus 15-200 ms of postsynaptic potentials). Hence, the electrodes measure the potential changes in large cortical areas of pyramid cells, despite an amplitude reduction due to the intermediate cerebrospinal fluid, skull and scalp (Figure 2.3B).

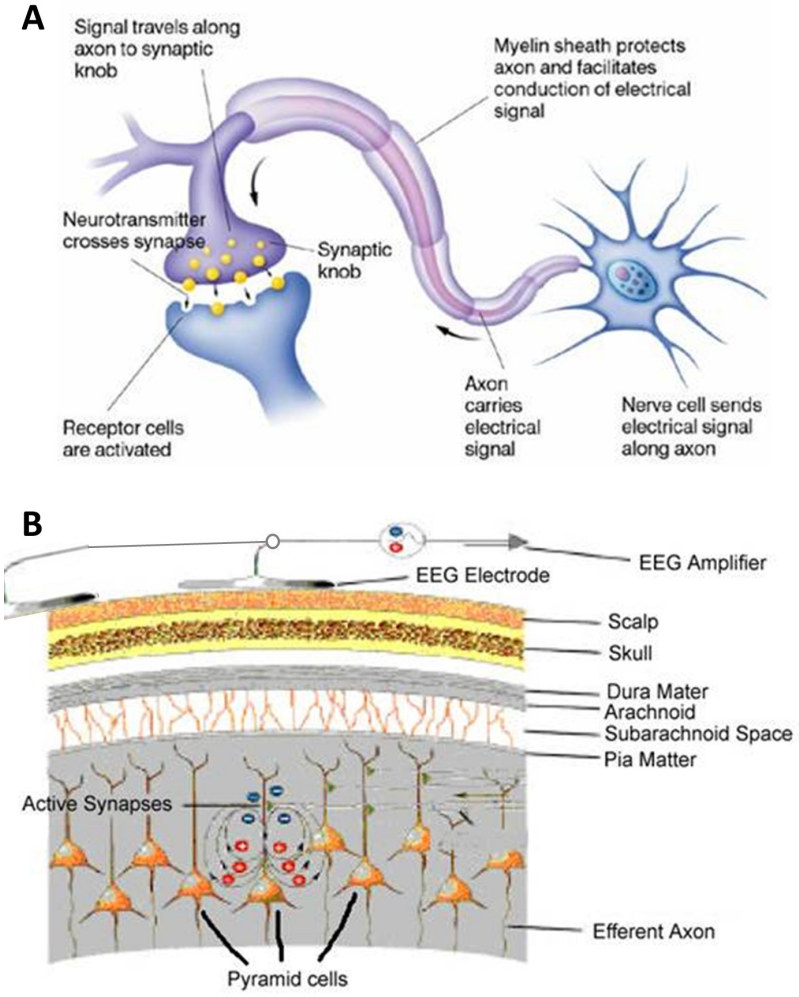

Figure 2.3: A. Neurotransmission: a neuron sends an electrical impulse through a neuronal pathway, followed by a transmission of chemicals across the synapse, to the neighbouring neuron (Daylan & Abbott 2005). B. The electrodes measure an electric field created by the sum of many stimulated cells. The EEG signal is a potential difference between two electrodes, which should be amplified due to the resistance of the cerebrospinal fluid, the skull and the scalp surrounding the brain.

2.2.2 Scalp EEG

During the hospitalization in the NICU, premature brain networks become organized during development. The electroencephalogram (EEG) noninvasively records the activity in the central nervous system. An EEG signal is the potential difference between two electrodes as a function of time. The EEG set-up is performed in a standardized way, that is, the Ag/AgCl electrodes are placed according to the 10-20 international system. This name is derived from the interelectrode distances, which are 10% or 20% of the total front-back or right-left distance of the scalp (Figure 2.4A-B). The names of the electrodes are derived from the underlying brain lobes: Fp (Frontal), C (Central), T (Temporal) and O (Occipital). Odd electrode numbers represent positions on the left hemisphere, whereas the even numbers represent positions on the right hemisphere. In this way, fixed electrode positions are obtained, from which we use a limited set of 9 electrodes due to the small circumference of the premature head. To visually assess the EEG, a bipolar or monopolar setup can be used. The former method measures the potential difference between pairs of electrodes, whereas the latter presents the potential differences between each electrode and the neutral electrode (for example Cz) (Figure 2.4C-D). The EEG waveforms depend on this montage mode.

In this way, the brain development can be monitored and pathological processes can be detected. This technique is already widely used to register epileptic seizures. However, it is only recorded in selected patients, and usually 1-2 lead amplitude integrated EEG (aEEG) for easy interpretation, whereas deeper insights could also be extracted from full-head conventional EEG (8 channel EEG)(Kato et al. 2011). Thereby, interpretation of the EEG can be quite challenging. For detection of pathological processes, it would be helpful to automatically quantify brain activities - in addition to the time-consuming visual EEG inspection by the clinical experts (figure 2.5). Moreover, doctors are not available 24/7.

2.2.3 Amplitude integrated EEG (aEEG) versus conventional EEG

aEEG is widely used, in secondary as well as in primary hospitals. Advantages include its fast assessment and its easy interpretability. In addition, aEEG is reliable to monitor the presence or absence of sleep-wake cycling and the severity of the background pattern for the selected central or parietal brain areas(Toet et al. 2002, de Vries & Toet 2006). However, the data provided by conventional EEG are more nuanced and allow detailed assessment of particular

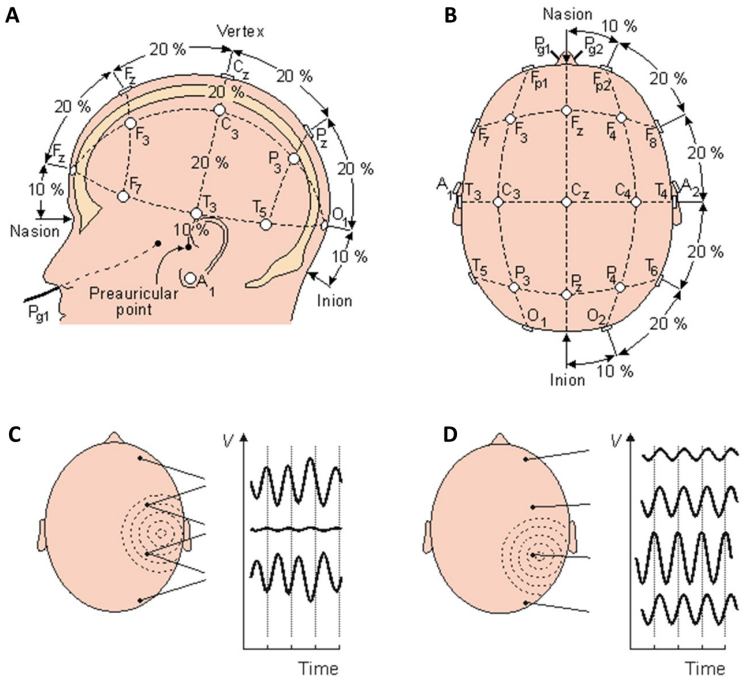

Figure 2.4: The international 10-20 EEG system seen from the left side (A) and above the head (B). Nomenclature of the electrodes is given according to the position on the scalp. EEG waveforms differ according to the bipolar montage (C) or the unipolar montage set-up (D).

brain areas (Shellhaas et al. 2011). That is, aEEG is less sensitive for neonatal seizure detection (Shah et al. 2008, Shellhaas et al. 2011). In addition, detailed information about relevant EEG events can be lost. Maturation has been proven to be better quantified with the conventional EEG (Kato et al. 2011). Multichannel information is lost with aEEG, and therefore conventional EEG is used to continuously monitor all brain regions because it is more sensitive to evaluate the functional connectivity (Figure 2.6).

Objective quantification of the EEG background is important for further prognosis of the neurodevelopmental outcome. The aim is to identify the most informative segments in the EEG which can describe reliable background activity of prematurity (e.g. bursts, interburst intervals, symmetry and synchrony between the bursts), and to quantitatively characterize these epochs. For these research purposes, discontinuous EEG epochs have been selected manually by



Figure 2.5: Current state in the NICU, conventional EEG signals of the patient are monitored in the incubator and an expert will read the EEG on the screen.

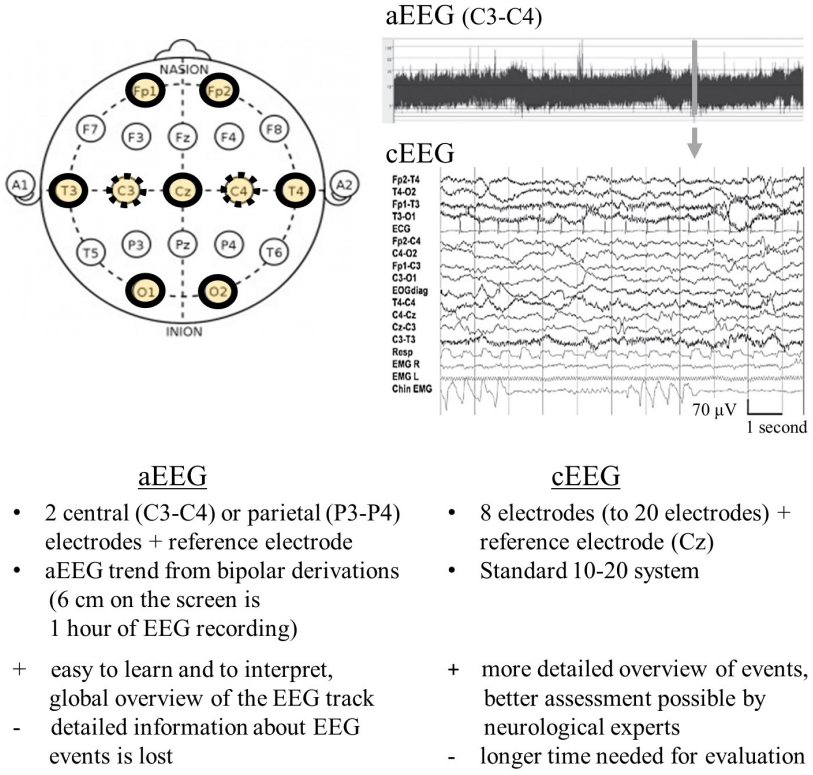

Figure 2.6: Evaluation of EEG monitoring systems: amplitude integrated EEG (aEEG) versus conventional EEG (cEEG).

a clinical expert possibly assisted by the aEEG or the developed suppression curve. Future research will focus on the automatic sleep stage classification, incorporating both aEEG and full-head EEG information. Vital features can be extracted from these quiet sleep segments in the young preterm babies, and from the tracé alternant segments in the mild preterm babies.

2.2.4 Dataset

Patients were recorded at postmenstrual age of 24-44 weeks. Conventional EEG registration was taken of 25 admitted patients during the period 2010-2012. We started the research on this relatively small set. In addition, around 240

patients have been monitored with an EEG device from 2013 onwards. All data was recorded at the Neonatal Intensive Care Unit of the University Hospitals of Leuven, Belgium. Preterm infants were consecutively enrolled in the study after informed parental consent. Data was obtained with a sampling frequency of 250 Hz, at 8 electrode positions (Fp1, Fp2, C3, C4, T3, T4, O1, O2) placed according to the 10-20 standard locations and reference electrode Cz (BRAIN RT, OSG equipment, Mechelen, Belgium). The EEG protocol was approved by the Ethics Committee of the University Hospitals of Leuven, Belgium.

The targeted recording time was 4 hours to include multiple vigilance states. The frequency band of 1-20 Hz is extracted, because this is the range of interest to obtain maturational information. For analytical purposes, EEGs without major artefacts were selected by experienced clinicians (AD and KJ). Clear inclusion criteria were used, which are described in detail in each publication chapter. An overview of the used datasets is given in Table A.1, Appendix A.

2.3 What to extract from the EEG?

From the EEG, different signal patterns are identified to assess the maturity and potential abnormalities in the given infant. Notably, the standard EEG analysis is based on visual recognition of waveforms and other signal properties, where standardized definitions are lacking to allow for a fully objective assessment. Notwithstanding, in the course of this study a number of clinically relevant characteristics have been objectively quantified in the automated analysis.

2.3.1 Level of discontinuity

In order to make a reliable neurological assessment, it is important to quantify the entire EEG signal. That is, to quantify the EEG background activity, which is the predominant ongoing physiological electrical activity during different vigilance states. Here, the background EEG pattern is typically characterized by the amplitude of the EEG, and the level of discontinuity (Monod et al. 1972, Vanhatalo & Kaila 2006, André et al. 2010, Niemarkt et al. 2010).

As maturation progresses, a discontinuous pattern with high activity epochs alternated by inactive intervals will shift to a more continuous pattern where the amplitude of the intervals is of higher voltage: tracé discontinu (TD) $\rightarrow$ tracé alternant (TA) $\rightarrow$ tracé continu (Cherian et al. 2009, Figure 2.7). The maturation is most often expressed in function of the postmenstrual age (PMA), the age counted from the first day of the last menstruation.

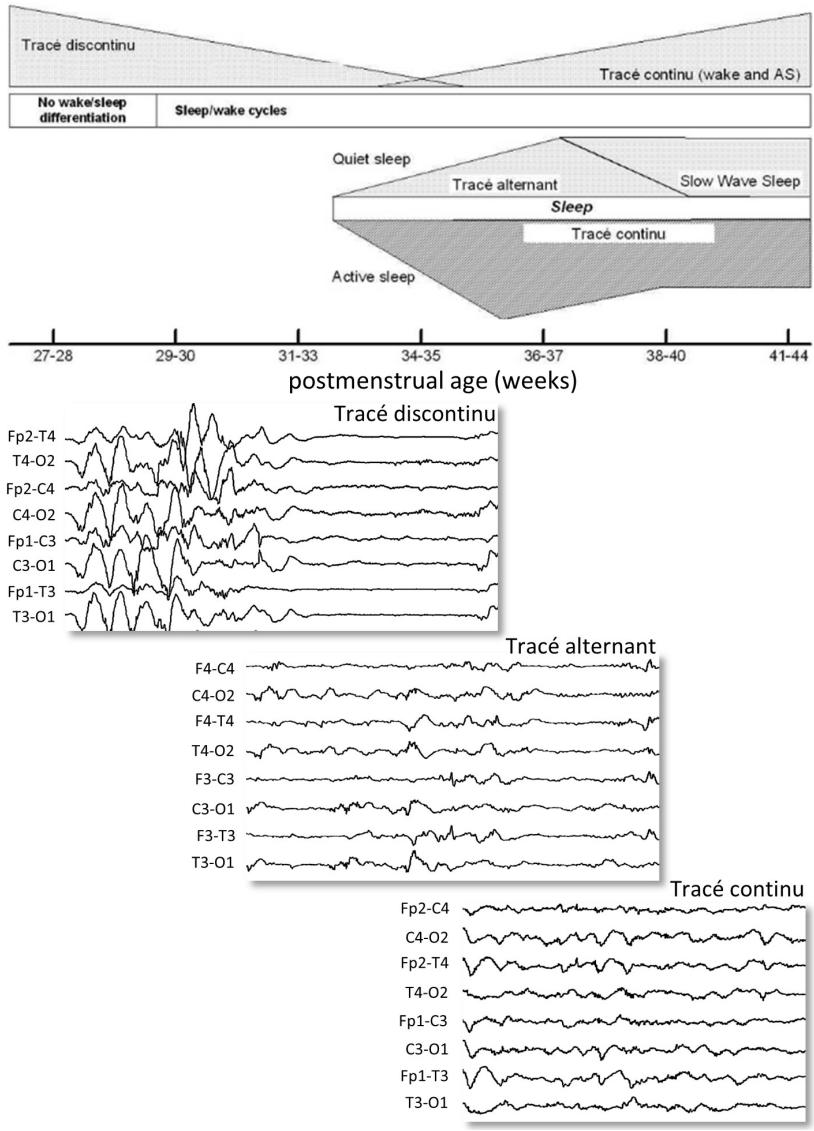

Figure 2.7: Maturational changes regarding patterns and sleep states in the premature EEG (Cherian et al. 2009): a shift from tracé discontinu to tracé continu (André et al. 2010).

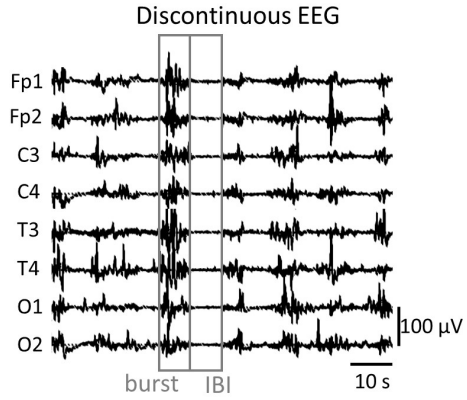

Figure 2.8: Discontinuous EEG pattern consists of bursts (spontaneous activity transients) interrupted by quiet periods (interburst intervals). An example of a burst and an IBI is depicted.

In the literature, the 'level of discontinuity' is well characterized by the following events: short transient activity (bursts) occur after relative quiet EEG activity (interburst intervals or IBIs) (Selton et al. 2000, Hayakawa et al. 2001, Vecchierini et al. 2007). A discontinuous EEG pattern, containing bursts and IBIs, is illustrated in Figure 2.8. Bursts are also called SATs (Spontaneous Activity Transients) or delta brushes (fast activity on delta waves). For convenience, we continue with the term 'bursts'.

Bursts are defined as cerebral activity with an amplitude (>100 µV), which can last from about 1 to several seconds in all EEG channels (Hayakawa et al. 2001). Tracé discontinue pattern consists of long periods (typically> 10 s) of suppressed EEG (voltage <5 µV), interrupted by shorter periods of burst activity with a relatively constant interburst interval (i.e., the absence of any variability in the signal) (Cherian et al. 2009). By lack of harmonized standards, Hayakawa et al. (2001) uses a slightly different definition: the suppressed interval has low amplitude (<30 µV) for more than 5 s.

The change of these events contains valuable information about the premature development (Table 2.1). in the early life stages of premature neonates, it has been shown that the length of the IBIs is related to the neurological maturation, i.e. the IBI length will become shorter with increasing PMA (Hellström-Westas & Rosén 2005). For example, the average IBI length decreases from 25.8 s at 21-22 weeks to 12.7 s at 25-26 weeks, while the maximum IBI also decreases from 126s at 21-22 weeks to 44.2s at 25-26 weeks (Hayakawa et al. 2001). This

decrease in maximum IBI length is correlated to the degree of cortical folding (Biagioni et al. 2007), and bursts will become more synchronous due to the intensive growth of cortico-cortical connections (as further explained in section 2.3.2). These findings are visually presented in Figure 2.9.

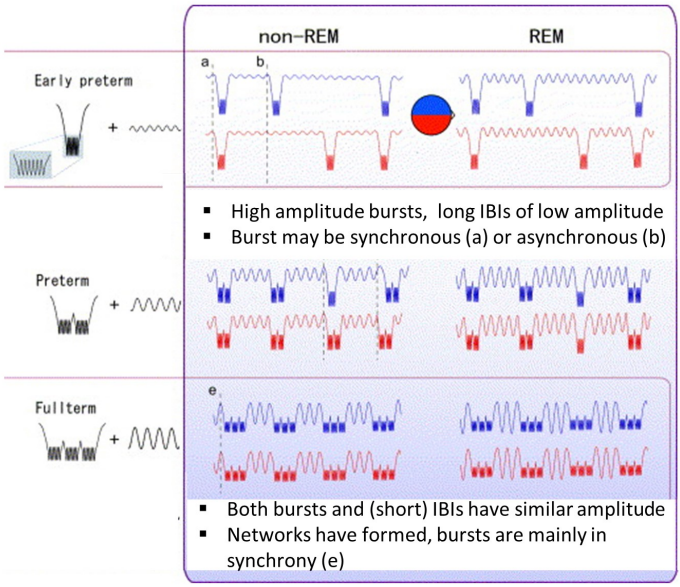

Figure 2.9: Schematic overview of the maturation of bursts and IBIs from early preterm to fullterm, concerning the number of bursts/IBIs, their amplitude, as well as their synchrony. Figure adapted from Vanhatalo & Kaila 2006

As bursts and IBIs provide valuable information about brain development, an accurate detection of the pattern characteristics becomes of great importance (Lombroso 1985, Douglass et al. 2002, Menache et al. 2002).

One example of the pattern characteristics is a decreasing discontinuity with respect to sleep states. During a full EEG recording, a patient will have fluctuating sleep states which are expressed by a different level of discontinuity. At premature age, we can distinguish a discontinuous from a continuous pattern, respectively representing quiet sleep and active sleep / awake. However, this distinction is more difficult at term age due to the higher level of activity, yet some discontinuity is still evident (Lamblin et al. 1999). In case of dysmaturity, more 'suppressed' EEG patterns are observed, which reflect abnormalities (Cherian et al. 2009). Also, poor prognosis is denoted by worsening of the background activity, that is, longer IBIs with respect to the postmenstrual age

Table 2.1: Maturational changes in background EEG variables describing the level of discontinuity, adapted from Palmu (2015)

variable	**measure**	**change**	**references**
IBI	mean/median duration	↓	Parmelee et al. 1969, Anderson et al. 1985, Connell et al. 1987, Hahn et al. 1989, Benda et al. 1989, Hayakawa et al. 2001, Victor et al. 2005b, Biagioni et al. 2007, Vecchierini et al. 2007, Niemarkt et al. 2010, Jennekens et al. 2011
IBI	max duration	↓	Connell et al. 1987, Anderson et al. 1985, Hahn et al. 1989, Benda et al. 1989, Selton et al. 2000, Hayakawa et al. 2001, Victor et al. 2005b, Conde et al. 2005, Biagioni et al. 2007, André et al. 2010
IBI	number	↓	Hahn et al. 1989
IBI	proportion of the signal	↓	Anderson et al. 1985, Hahn et al. 1989, Victor et al. 2005b, Niemarkt et al. 2010
IBI	RMS during quiet sleep	↑	Tolonen et al. 2007
burst	mean duration	↑	Parmelee et al. 1969, Hayakawa et al. 2001, Jennekens et al. 2011
burst	min duration	=	Biagioni et al. 2007
burst	number	↓	Vanhatalo et al. 2005
burst	spectrum: total power (1.5-25 Hz)	↑	Havlicek et al. 1975
burst	spectrum: total and band powers	↓	Jennekens et al. 2012
burst	RMS during active sleep	↓	Tolonen et al. 2007
discontinuous activity	proportion of the signal	↓	Van Sweden et al. 1991

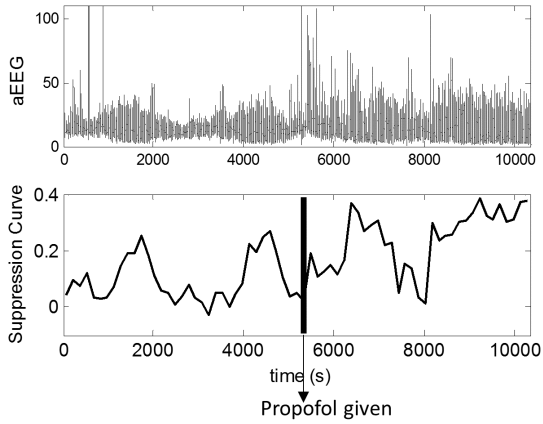

Figure 2.10: The influence of propofol administration on the discontinuity level on (a) the aEEG, (b) the suppression curve.

(Menache et al. 2002). More in general, table 2.2 shows changes of descriptive features in the young preterm.

Medication can affect these patterns. For example, it is known that after administration of propofol, the EEG will be more 'suppressed', including longer/more IBIs. This pattern change is captured by the developed *suppression curve* (Figure 2.10). A larger value of the suppression curve corresponds to a more discontinuous EEG pattern.

2.3.2 Connectivity of the brain

A long range of brain functions is sustained by neuronal networks (Bressler & Menon 2010, Uhlhaas et al. 2010, Palva & Palva 2011). Neuronal activity correlates with behavioral states (Raichle 2010, Palva & Palva 2011, Hutchison et al. 2013). Early neuronal dynamics emerge into structural networking of the preterm brain (Kostović & Jovanov-Milosević 2006, Kostović & Judas 2010). The underlying process of physiological development forming the cerebral connections, has been recently explored in histological studies (Kostović & Jovanov-Milosević 2006).

To capture the functional networking, multichannel EEG recordings are very advantageous. Too often these multichannel information is being ignored, considering that spatial 'integration' is mostly limited to the concatenating of the characteristics of different channels (Hunyadi et al. 2011). Here, spatial

Table 2.2: Changes of descriptive features in the young preterm.

	Postmenstrual Age (weeks)			
	24-25	*26-27*	*28-29*	*30-31*
Background activity	very discontinuous IBI $<$ 60 s ($<$ 25 µV)	very discontinuous brief periods of semi-continuous	IBI $<$ 20-25 s 70% synchronous	IBI $\leqslant$ 20 s 70% synchronous in QS
Organization of behavioral state	undifferentiated wake/sleep	undifferentiated wake/sleep periods with eye movement: less discontinuous (DC) and higher amplitudes	active wake, active sleep: REM less discontinuous quiet sleep: no REM, more DC and lower amplitudes	active wake active sleep: continuous/ semi-contnuous quiet sleep: DC

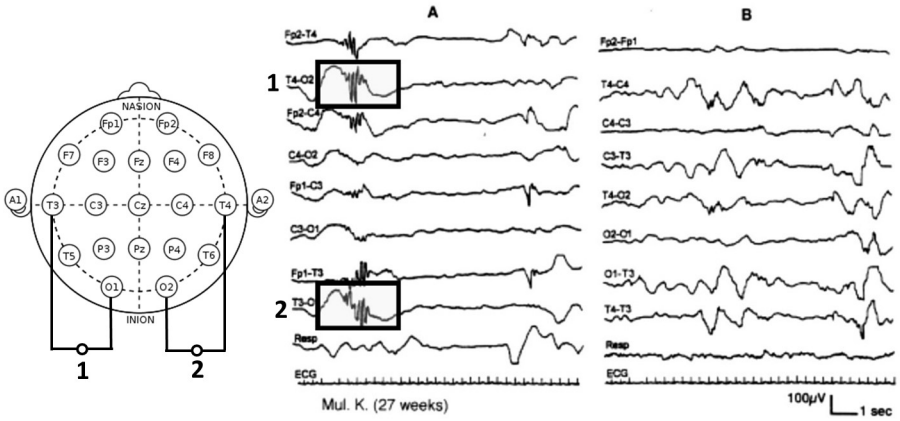

Figure 2.11: Synchrony and symmetry between both hemispheres. Comparing T4-O2 and T3-O1, bursts start simultaneously (synchronous) and no significant difference in amplitude can be noticed (symmetric). (A) Longitudinal montage (B) Transversal montage. As adapted from Selton et al. (2000).

information is used to quantify the interaction between different brain areas using connectivity analysis. Such connectivity values may become relevant for the prognosis of premature infants' maturation and outcome. The connectivity values are the mathematical translation of the degree of connectedness between different brain regions. Indeed, it is generally assumed that the regions of the brain in very young babies are barely connected, and a refined network is being formed during brain development, guided by spontaneous interaction (Vanhatalo & Kaila 2006, Smyser et al. 2010).

As a measure of connectedness, we investigated both symmetry and synchrony between the two hemispheres. Interhemispheric symmetry of two contralateral EEG traces implies that amplitude and frequency content is comparable among the homologous brain regions. Asymmetry represents a possible remarkable difference in activity levels (>50%) between the two hemispheres and is related to adverse outcome (Cherian et al. 2009, Selton et al. 2000). Underlying sources consist of strokes, intraventricular haemorrhage, sinus thrombosis and abscess (Volpe 1998, Cherian et al. 2009). Asymmetry should be evaluated over reasonably long EEG segments.

Synchrony, on the other hand, indicates the temporal co-occurence of bursts in both hemispheres. This is shown in (Figure 2.11). Synchrony is often associated with maturity. Synchronization between the bursts exists during quiet sleep in

the two hemispheres to 28 weeks PMA (start of bursts < 1.5 s apart), after which the synchrony decreases slightly (Lombroso 1979). However, from 31 weeks PMA, the interhemispheric synchrony increases is stable at full-term age (Cherian et al. 2009, André et al. 2010, Niemarkt et al. 2010). Poor outcome is associated with <25% of the bursts being synchronous (Anderson et al. 1985, Lombroso 1985).

The degree of connectivity could be an important predictive parameter. Up till now, this has always been based on subjective visual assessment. An accurate quantification through automated analysis therefore becomes of great interest.

2.3.3 Other EEG characteristics

Seizures

Although seizures do not occur in all babies, their presence in combination with abnormal background EEG can provide accurate prognostic information. Seizures can disturb the vital processes of cell division, cell migration, myelination or stabilization of synapses (Deburchgraeve 2010). Consequently, seizures are often associated with poor prognosis (Monod et al. 1972, Legido et al. 1991, Scher et al. 1993). Neonatal seizures have a very variable morphology, topography and frequency, even in the same patient. Visually, a clear change of these events relative to the background and their repetitive behavior make them relative easy to distinguish. However, artefacts can have a similar pattern or different clinical centers can have a different cutoff to designate seizures. There are two distinctive types of seizures: pulse train (discontinuous) and oscillating seizures (continuous) (Deburchgraeve et al. 2008). Seizures have been characterized to distinguish mild and severe abnormalities based on different characteristics, such as the number of attacks, the length of an attack(s), frequency content, etc. (Cherian et al. 2011). Automatic algorithms to detect seizures have already been developed; heuristical detection of the two seizure types (or combination of them) (Deburchgraeve 2010) and a feature-based machine learning classifier (Temko et al. 2011). For this reason, seizure detection was out of our scope and the main focus was to objectively quantify the background EEG. Moreover, seizures are mainly present during the first days after premature birth in about 5-6% of the patients and then gradually diminish. During prematurity, only a small percentage is effectively treated for seizures in the hospital.

Sleep states

During continuous monitoring of EEG, additional information can be extracted about the fluctuation of vigilance states, or the so-called sleep-wake cycling (Weisman et al. 2011, Palmu et al. 2013). The content of the bursts change during the different vigilance states. In the conventional EEG reading, sleep cycles are only recognized after 30 weeks of PMA (Grigg-Damberger et al. 2007, André et al. 2010), although the aEEG already shows some cycling between presumably vigilance states (Hellström-Westas et al. 2006, Olischar et al. 2007, Wikström et al. 2012). Proper cycling could even be related to a healthy developing distributed brain network (Olischar et al. 2007, Weisman et al. 2011). Early presence of cycling has been associated with neurodevelopmental outcomes (Wikström et al. 2012, Klebermass et al. 2011, Kidokoro et al. 2012, Natalucci et al. 2013).

Sleep states can be recognized by the specific EEG patterns. In addition to the awake state, a distinction between two sleep states can be made:

- Active sleep (AS) (Figure 2.12a)
- Quiet sleep (QS) (Figure 2.12b)

The content and length of the different states also changes with maturation (see Table 2.2). The percentage of discontinuous activity decreases with PMA increasing, being higher in quiet sleep than in active sleep and wakefulness (André et al. 2010). However, all studies have been based on clinical scoring and are, therefore, subjective and dependent on the hospital settings and training. For this purpose, network activity is quantified by the SAT% (percentage of bursts in the EEG pattern) (Palmu et al. 2013). Using the SAT%, cyclicity has been objectively quantified by the BAC (Brain Activity Cycling) score (Stevenson et al. 2014).

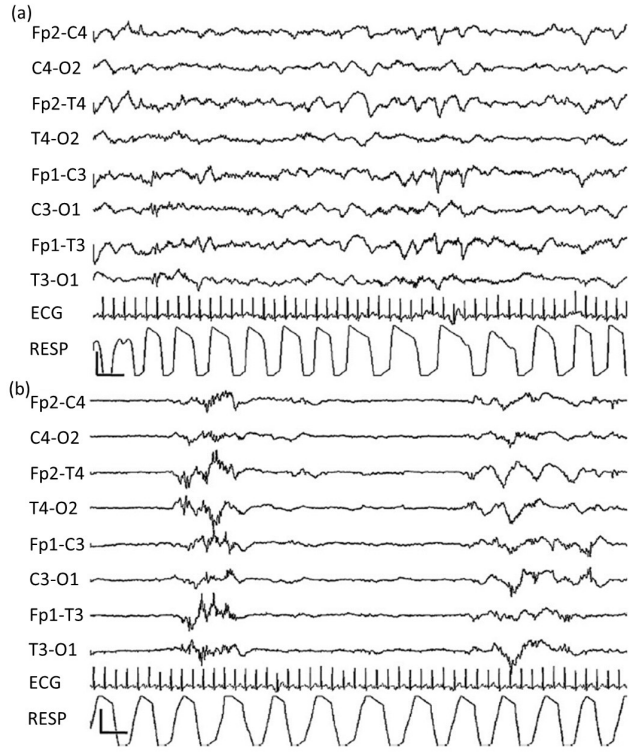

Figure 2.12: EEG patterns representing different sleep states: (a) Active sleep (AS), (b) Quiet sleep (QS). As adapted from André et al. (2010).

Chapter 3

Methods for automated preterm EEG background analysis

The algorithms used for the analysis of premature EEG characteristics, in particular the level of discontinuity and the level of brain connectivity, are based on a wide variety of underlying features. We give an overview of different published methods to extract valuable information from the EEG. This is followed by a description of the methods used in this thesis. An elaborate description of the algorithms and results is given in the next chapters in the form of publications.

3.1 Level of discontinuity

3.1.1 State of the art for burst detection

We lack technology in the hospitals to measure neuronal processes over longer timescales. Hence, several algorithms have already been developed: segmentation by means of an autoregressive model to approximate stationary segments (Praetorius et al. 1977), segmentation on the basis of temporal profiles to identify the EEG pattern (Paul et al. 2003), algorithm on the basis of Nonlinear Energy Operator (Palmu et al. 2010a,b). Adult EEG patterns have different characteristics compared to neonatal EEG, therefore, we

mainly summarized relevant algorithms handling the neonatal EEG to detect suppression differences by means of IBIs and bursts in Table 3.1. One should note that there is a difference in EEG change over time between preterm babies and term babies with hypoxic-ischemic injury. The latter ones show a change (recovery) in function of hours, whereas preterm babies develop over the time course of weeks. Nevertheless, certain algorithms can be adapted to detect for example EEG suppression.

Own contribution to burst detection

We have developed a burst detection algorithm based on the line length (Koolen et al. 2014b, chap. 4). This feature Line Length (LL) has successful applications for seizure detections (Esteller et al. 2001a, Logesparan et al. 2012). An overview of the consecutive steps of the algorithm is given in Figure 3.1.

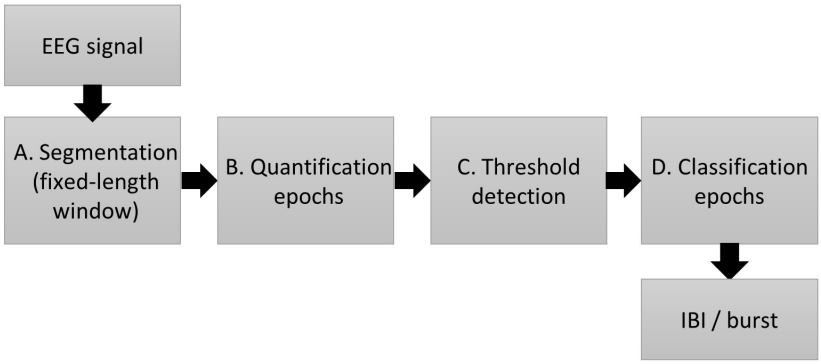

Figure 3.1: Flow chart of a burst detection algorithm. A-D present the consecutive methodological steps of the algorithm.

Analysis with variable or fixed window length (Figure 3.1A)

Due to random firing of neurons, the EEG is a non-stationary signal; i.e. the amplitude- and frequency content change over time. In particular, the content between burst and IBI epochs will change as well (Selton et al. 2000, Palmu et al. 2010a,b). However, the burst and suppression segments can be considered as stationary. To make a partition between these two epochs, segmentation techniques with fixed-length segments and with variable-length segments can be applied. For the latter one, the length of the segment is adapted to the

Table 3.1: Relevant algorithms to detect bursts, adapted from Palmu 2015

Referrences	**Patient group**	**Detecting**	**Classifier design**
Barlow 1985	fullterm	burst and interburst periods in manually selected epoch of trace alternant	adaptive segmentation based on thresholding, clustering of segmentation results by hierarchical clustering
Krajca et al. 1991	adult	clusters of similar EEG graphoelements	fuzzy c-means clustering of segments found by adaptive segmentation
Wertheim et al. 1991	preterm	low amplitude intervals (amount of discontinuity)	amplitude threshold with time constraint
Arnold et al. 1996	fullterm and preterm	burst onsets during manually selected periods of quiet sleep	neural network with adaptive preprocessing unit
Griessbach et al. 1997	neonates	a) burst onset	a) neural network with adaptive preprocessing unit
		b) burst ending	b) thresholding
Sherman et al. 1997	piglet model of hypoxic-ischemic injury in neonates	bursts	thresholding
Atit et al. 1999	piglet model of hypoxic-ischemic injury in neonates	bursts	thresholding
Leistritz et al. 1999	adult burst-suppression	a) suppression	a) neural network
		b) burst, suppression and remaining EEG	b) neural network
Pan & Ogawa 1999	preterm (CA=30-39w)	a) discontinuity	a) amplitude threshold
		b) sleep stage (active sleep, quiet sleep, wakefulness)	b) multivariate discriminant analysis
Särkelä et al. 2002	adult burst-suppression	burst, suppression and artefacts	sequential thresholds
Vanhatalo et al. 2005	preterm	multiband activity transients	sequential thresholds
West et al. 2006	preterm	high amplitude intervals (amount of continuity)	threshold
Wong & Abdulla 2006	neonate	stationary segments	3 different methods tested. Design for SEM and GLR thresholding, for NLEO peak detection.
Wang & Agarwal 2007	neonate	suppression in burst-suppression pattern	sequential thresholds
Wong & Abdulla 2008	preterm	continuous and discontinuous segments	linear discriminant analysis
Pfurtscheller et al. 2008	preterm	burst "peaks"	thresholding and peak detection
Krajča et al. 2009	preterm and fullterm	a) clusters of similar EEG graphoelements	a) k-means clustering of segments found by adaptive segmentation
		b) sleep stages (AS vs. QS)	b) thresholding

Table 3.1 cont.

Referrences	Patient group	Detecting	Classifier design
Vairavan et al. 2009	fetuses and fullterm	a) discontinuous MEG patterns	a) sequential threshold
	neonates (MEG)	b) bursts (and IBI) in segments of discontinuous MEG	b) sequential threshold
Niemarkt et al. 2010	preterm	a) bursts, interburst-intervals	a) Description in deviates from the technical description by the vendor (NicOne). See Palmu et al. 2010b, original algorithm.
		b) periods of discontinuous activity	b) threshold
Palmu et al. 2010a	preterm	burst, IBI, (continuous EEG/artifact)	sequential thresholds
Palmu et al. 2010b	preterm	SAT, inter-SAT	sequential thresholds
Jennekens et al. 2011	preterm	bursts, interburst-intervals and continuous patterns	sequential thresholds
Bhattacharyya et al. 2011	fullterm	bursts and normal (nonburst) EEG	support vector machine (SVM)
Hartley et al. 2012	preterm	bursts of nested oscillations	threshold
Matic et al. 2012	fullterm	IBIs in burst-suppression	adaptive segmentation (Krajča et al. 2009), classification of segments based on sequential thresholds
Mitchell et al. 2013	preterm	delta waves (divided into delta brushes and smooth delta waves) and interburst intervals	detection of patterns based on wave morphology utilizing Bayesian probability theory
Koolen et al. 2014b	preterm	bursts (and interbursts)	sequential thresholds
Murphy et al. 2014	preterm	bursts (and interbursts)	sequential thresholds
Iyer et al. 2015	preterm	bursts	sequential thresholds, statistic metrics

signal characteristics (adaptive segmentation). Thereby, a sliding window is used, for which the window length increases until the feature calculated in that segment exceeds a certain threshold. For example, Krajca et al. (1991) used the mean amplitude and mean frequency, whereas Agarwal et al. (1998) used the non-linear energy operator (NLEO).

For fixed-length segments, we suppose that the EEG is 'quasi-stationary' during the length of the segment (Wong & Abdulla 2006). For that reason, the length of the segments is heuristically chosen as 1 second. Thereby, the accuracy of a burst length is limited to 1 second, however, with overlapping windows improvement is reached (Figure 3.2). We have applied an overlap of 0.12 second (model of Cabukovski et al. 1993, Accardo et al. 1997). Improvements on the overlap could be made, although the current settings are considered to be sufficient for burst/IBI detection. That is, the minimum length of the transients bursts are near 1 second (Palmu et al. 2010b) and an IBI is clinically not expected to be

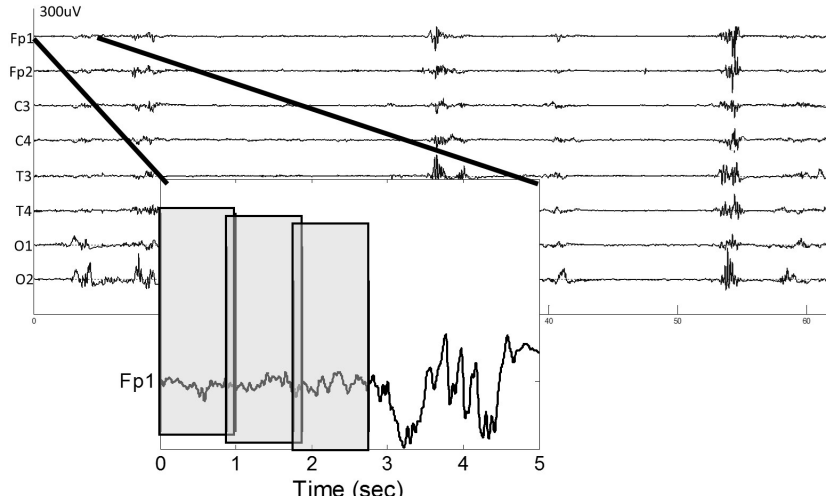

Figure 3.2: Overlapping windows for EEG segmentation with fixed-window length of 1 second, presuming quasi-stationary EEG in each window.

shorter than 2 seconds.

Quantification epochs with Line Length (Figure 3.1B)

The Line Length (LL) is a simplified version derived from the fractal dimension, which has been shown to be very successful for transient event detection. It consists of estimating the dimension of a time-varying signal directly in the time domain (Esteller et al. 2001b). The LL has the advantage of fast computation and is easy to understand in clinical practice. The Line Length L is calculated as the running sum of the absolute difference between the values of 250 consecutive samples x_j within a 1 second sliding window (formula 3.1), after which it is normalized through dividing the L by the total sum of all L in that channel ch (for the selected epoch) (Accardo et al. 1997). This is done in order to exclude large differences in the amplitude range as a consequence of different electrode placement or thickness of the skull (formula 3.2).

$$LL = \sum_{j=1}^{250-1} |x_{j+1} - x_j| \tag{3.1}$$

$$L_{n,ch} = \frac{L}{\sum_i L(i)} \tag{3.2}$$

with $L(i)$ every LL in the selected epoch

The line length will increase as the data magnitude or frequency increases, performing as an amplitude and frequency demodulator, analogous to the NLEO feature (Palmu et al. 2010b, Kaiser 1990). This has been tested for sinusoids with constant and chirp frequencies (Esteller et al. 2001a). Burst detection has been performed on the median line length curve, defined by taking the median of all the channel line length curves. It describes the 'trend' of the selected epoch', and burst detection can be performed by using a threshold.

Adaptive or fixed threshold (Figure 3.1C)

After segmentation and calculating the LL, a threshold is applied for detection. Hence, the question arises whether the threshold should be adaptive interpatient/intrapatient. For instance, often a fixed threshold is used (Palmu et al. 2010b, Jennekens et al. 2011). Once a certain feature is above a predefined threshold, it will be classified into the according class, e.g. a burst. However, medication can alter the amplitude range of the EEG amplitudes (Leistritz et al. 1999, Särkelä et al. 2002). For example, sedative medication could suppress the EEG background activity (Bell et al. 1993). In addition, EEG amplitudes can change according to the electrode placement and thickness of the scalp. Therefore, we have preferred to work with an adaptive threshold, which changes every 2.5 minute, and is based on the level of background activity.

No gold standard to classify epochs (Figure 3.1D)

There is no gold standard available to objectively quantify the performance of the detection algorithm. Therefore, it is important to have labeling/scores from at least two clinical experts. Namely, disagreement sometimes exists among clinical EEG readers on the precise terms used to describe these patterns. Inter-rater agreements tend to be low when multiple neurophysiologists interpret the EEG while making a determination of normal versus abnormal (Mani et al. 2012). Precise terminology of the EEG patterns would allow for consistency among raters, and as a result, meaningful algorithms can be pursued. As a matter of fact, the algorithm will overfit the subjective scoring if it is based on only one clinical expert. Palmu et al. (2010b) has three independent ratings to

optimize the burst detection algorithm, and a 84.5% inter-rater agreement was reached. There existed full agreement on 77% amount of data, which were used for the evaluation of the algorithm. However, we used all the data available for performance testing by averaging single rater-algorithm agreements.

3.1.2 Quantification of the global change of discontinuity

During continuous monitoring of EEG, additional information can be extracted about the fluctuation of vigilance states. However, all studies have been based on clinical scoring and are, therefore, subjective and dependent on the hospital settings and training. For this purpose, the BAC score (brain activity cycling) has been developed. The main challenge is to automate this time-varying sleep-wake cycling (SWC), because its nature is not sinusoidal, rather pseudo-periodical. The length of the sleep cycles change during the recording. As a result, the developed BAC score is a trend measure. The measures of BAC were summary statistics computed on a frequency domain representation of the proportional duration of the SAT% derived from the EEG. The presence of preterm sleep-wake cycling in the aEEG is related to a high BAC score and vice versa (Stevenson et al. 2014).

We have also looked at the different EEG vigilance states using the 'suppression curve', with the line length as the fundamental feature (Koolen et al. 2014b, Dereymaeker et al. 2015, Chap. 4 and 5). Application is found by searching for the most discontinuous segments, identified as the quiet sleep epochs. In addition, we have used the average as a new metric for maturational premature trend and for follow-up intrapatient development. Furthermore, the suppression curves are used to look at the influence of administration of propofol. After the medication is given, we know the global EEG trend will include more suppression for a certain timespan.

Finally, we proposed a new data-driven metric for maturation, the histogram-index, after creating the line length curve over the whole EEG recording (few hours - more than 12 hours) (Koolen et al. 2015b, Chap. 6). Rather than detecting IBIs and bursts on the LL curve, all LL information is used to create a histogram, which represents the distribution of activity in the brain. Hence, instead of simply reporting the mean or median changes of the parameters, a quantitative evaluation of the entire distribution is appropriate. Only through the quantification of the entire distribution, and its changes over time, one can gain accurate insights in structural and functional maturational changes (Buzsáki & Mizuseki 2014). That is, the division between 'strong' and 'weak', and 'fast' and 'slow' neuronal firing is not absolute, but should be seen as a continuous distribution to characterize the anatomical structure and brain

activity (Buzsáki & Mizuseki 2014). The connectivity profile is best constructed by a log-normal distribution, because it consists of a majority of weak inputs and just few strong afferents. Next, 28 features to describe the change of the distribution were defined. The ones which correlate the best with the maturational trend were selected and finally combined in a histogram index.

3.2 Brain connectivity by means of interhemispheric symmetry and synchrony

Brain development and future neurocognitive outcome do crucially depend on how well the brain circuitries connect during pre- and perinatal period. Symmetry and synchrony reflect the underlying neuronal interactions between the brain regions, and thus, our next path was to investigate the corresponding measures.

3.2.1 Methods for symmetry classification

To detect neural dysfunction in time, automated interhemispheric symmetry analysis can be relevant for premature EEG assessment in the NICU. Through classification of symmetric patterns in each brain region, our objective was to make a distinction between pathologic asymmetry and physiologic (a)symmetry. Multiple symmetry indexes have been developed, a summary can be found in Table 3.2. We decided to apply the channel symmetry index (CSI), which takes the difference in predefined power spectral bands $[F_{min}, F_{max}]$ of the contralateral channel signals (measuring homologous areas on opposite sites of the brain), characterized by both amplitude and frequency content (formula 3.3). *ch* is a chosen EEG channel and *opp* its contralateral channel.

$$CSI(ch, F) = \sum_{f=F_{min}}^{F_{max}} \frac{|PSD_{f,ch} - PSD_{f,opp}|}{PSD_{f,ch} + PSD_{f,opp}} \tag{3.3}$$

Only few outliers

The goal was to make a classification between two classes, with or without any comorbidities. Knowing that there will only exist a small percentage of outliers, unsupervised learning is not preferred. The misclassification rates

Table 3.2: Symmetry indexes.

Symmetry Measure	**References**
• brain symmetry index (BSI): measure for amount of ischemic damage: absolute difference between hemispheres in 1-25 Hz power • relative power of certain frequency bands and spectral ratios	van Putten & Tavy 2004, van Putten 2007, Sheorajpanday et al. 2009, Korotchikova et al. 2009
• channel symmetry index (CSI): power asymmetry in the predefined frequency bands between contralateral channel pairs • global channelwise symmetry index (GCSI): spectral power of the actual channel compared to all the other channels	Hunyadi et al. 2010
• bilateral brain symmetry index (BBSI): quantity discrepancy between the right and the left channels for the spectral densities in the range 1-20Hz	Yan et al. 2011

of this small group will be very high when the sample size ratio is around 10:90 (abnormal:normal), or even in general when the sample sizes of the two groups are of unequal size (Finch & Schneider 2006). Based on labeled data, supervised learning algorithms can be applied. In our dataset, we have only few abnormal asymmetric hemispheres and a majority of normal symmetric hemispheres (90%). Moreover, outliers do not have the same properties, but are of different nature. Therefore, one-class Support Vector Machines (SVM) offer the solution to this classification problem (Schölkopf et al. 2001). Analogously to the two-class SVM, feature vectors are mapped into a higher dimensional space with a kernel transformation function. In one-class SVM, the large group containing the normal samples will be as much separated from the origin of the high dimensional projections. In this research, different features derived from the channel symmetry index (CSI), are used as an input to this classifier (Koolen et al. 2014a, Chap. 7).

3.2.2 Methods for synchrony maturation and classification

In neural network structures of the premature brain, symmetry is not the only relevant feature to detect abnormalities. Even more important, because less sensitive to artefacts, was the interhemispheric synchrony. Analysis methods exist from easy linear correlation and coherence functions to more complicated models, searching for the direction of connectivity, e.g. directed transfer function. Blinowska and Quiroga reported an overview of the performance of different synchrony measures (Blinowska 2011, Quiroga et al. 2002). A subdivision into 4 technical groups can be made (Table 3.3).

Activation Synchrony Index

With first the aim of abnormal interhemispheric synchrony detection, and later finding a trend in synchrony maturation, we have opted to apply the Activation Synchrony Index (ASI). An overview of the ASI paradigm can be found in Figure 3.3. Special attention is paid to the dependency of high-energetic events (bursts) in the signals, whereas simultaneous occurrence of low-energy background epochs serves no clinical purpose (Räsänen et al. 2013).

In order to measure the degree of coupling between the two signals using probabilistic methods, both signal envelopes are first quantized into eight discrete amplitude levels (Räsänen et al. 2013). Quantization is performed by estimating the eight levels using a standard k-means clustering algorithm. The smoothed envelopes served as inputs and each amplitude envelope sample is then assigned to the nearest cluster (indexed from 1 to 8). As a result, both channels A and B

Table 3.3: Methods for synchrony analysis

Analysis method	Synchrony Measure	References
1. Time domain analysis		
Burst time analysis	Amplitude thresholding on the envelope	Zwanenburg et al. 2012
2. Coherence		
Adaptive coherence analysis	coherence	Bullock et al. 1997, Eiselt et al. 2001, Grieve et al. 2008
Coherence function	magnitude (MSC) and the imaginary part (IMC), phase synchronization	González et al. 2011
Coherence analysis to sensory-evoked brain activity	conventional and wavelet coherence	Klein et al. 2006
3. Phase synchronization		
Phase locking value	Phase synchrony between band-specific amplitude envelopes	Tokariev et al. 2012
Phase synchrony	Bivariate empirical mode decomposition and Hilbert transformation to detect the phase, which serves as input to calculate the mean phase coherence	Zheng et al. 2014
Phase synchrony	Phase difference with the phase estimation based on Rihaczek distribution, instead of Hilbert or wavelet transformation	Aviyente & Mutlu 2011
Quadratic phase coupling (QPC)	Time-variant bispectral analysis: Biamplitude, bicoherence and phase-coherence	Witte et al. 2000, Schack et al. 2001, Schwab et al. 2004
4. Directed connectivity		
Neural mass model	Granger causality (GC), Directed transfer function (DTF), Partial Directed Coherence (PDC)	Blinowska 2011, Faes et al. 2012, Sartori 2013
Information transfer	Mutual information	Schreiber 2000, Räsänen et al. 2013

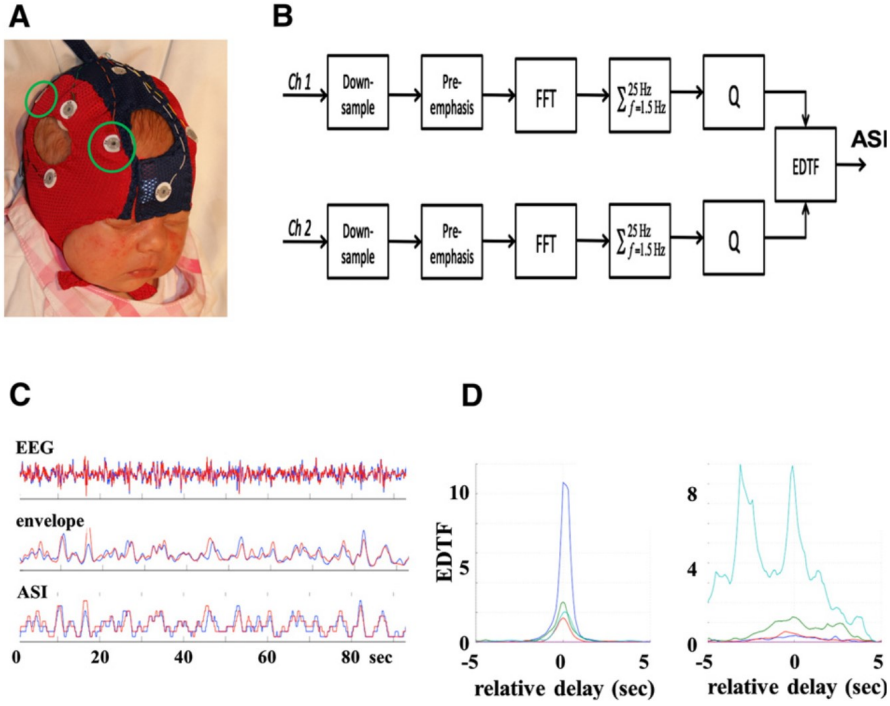

Figure 3.3: The ASI algorithm. (A) Neonatal EEG recording with an EEG cap. The synchrony can be calculated between any pair of signals. (B) Different steps of the ASI paradigm (Ch= channel, FFT= Fast Fourier Transform, Q = quantization, ETDF = energy weighted temporal dependency function). (C) Different stages of the ASI calculation: EEG signals from two hemispheres (left=red, right=blue), pre-emphasized and temporally smoothed energy envelopes, quantized energy envelopes. (D) ETDFs illustration of synchronous signals (left) and asynchronous signals (right). Asynchrony is represented by a flat dependency distribution function or peaks at a time delay $\tau \neq 0$. Figure adapted from Räsänen et al. (2013).

are described as discrete sequences $X_A = a_1, a_2, \ldots, a_N$ and $X_B = b_1, b_2, \ldots, b_N$ with subscripts denoting the time index. Each $a_i, b_j \in 1, 2, \ldots, 8$ and one element occurring every 100 ms.

The mutual information function is used to quantify the information overlap between two signals. However, it does not contain any dynamic or directional information (Schreiber 2000). It is calculated after the model of the Kull-back entropy, as the ratio of joint probability of the two states over the independent probabilities of these states. Therefore, a time delayed mutual information function is introduced MIF(τ) as function of a certain temporal delay τ (formula 3.4). In that way, a velocity of information transport can be obtained. Also, in the sense of synchrony, useful information about time delays can be extracted.

$$\begin{aligned} \mathrm{MIF}(\tau) &= \sum_{i,j} p(X_A(t) = a_i, X_B(t+\tau) = b_j) log_2 \left(\frac{p(X_A(t) = a_i, X_B(t+\tau) = b_j)}{p(X_A(t) = a_i) p(X_B(t+\tau) = b_j)} \right) \\ &= \sum_{i,j} p_\tau(a_i, b_j) log_2 \left(\frac{p_\tau(a_i, b_j)}{p(a_i) p(b_j)} \right) \end{aligned} \tag{3.4}$$

with τ elements in between a_i and b_j, denoted by subscript τ. Probabilities can be estimated by the number of occurrence of each state a_i or b_j or state pairs $\{a_i, b_j\}$ divided by the total frequency count.

Next, the so-called energy weighted temporal dependency function (EDTF) is computed between the two quantized envelopes. The logarithm in the mutual information function is omitted, because we are interested in the overal linear dependency between the signal state pairs, not in the bits of information (Räsänen 2012). In order to measure the dependency of signal energy instead of purely abstract states, we weight each state pair by the product of the amplitude values corresponding to the given states ($AMP(a)$ and $AMP(b)$). This leads to so-called energy weighted temporal dependency function (ETDF) (formula 3.5) (Räsänen et al. 2013).

$$ETDF(\tau) = \sum_{a,b} AMP(a) AMP(b) \frac{p_\tau(a, b)^2}{p(a) p(b)} \tag{3.5}$$

In the equation, a and b denote the quantization levels in the two channels respectively. $p_\tau(a, b)$ is the probability of observing level a in first channel and level b in second channel when the second channel is delayed by τ units, $p(a)$ is the probability of observing level a in the first channel and $p(b)$ for

level b in the second channel. $AMP(a)$ and $AMP(b)$ are the mean amplitudes corresponding to quantization levels a and b. All probabilities are computed by simply counting the relative frequencies of lagged state pairs a, b and individual states across the entire ASI analysis time window. In a next step, the ETDF curve is normalized (formula 3.6). The final ASI value can be derived from the normalized ETDF curve as the ratio of the ETDF value at zero lag ($\tau = 0$) over the expected (mean) value of the ETDF across the analyzed 10 s range [-5, 5] (formula 3.7).

$$ETDF_n(\tau) = ETDF(\tau) - min(EDTF(x), x \in [-5, 5\ s]) \tag{3.6}$$

$$ASI = \frac{EDTF_n(\tau = 0)}{E\{EDTF_n(\tau) \mid \tau \in [-5, 5\ s]\}} \tag{3.7}$$

As long as the energy envelopes are coupled properly and show typical transient behavior, their dependency is highest at the zero lag and diminishes with increasing relative lag between the two channels, thereby leading to a high ASI value. Conversely, low synchrony or synchrony at a non-zero lag (delayed coupling between the hemispheres) will result in low ASI since the mean of the ETDF is proportionally larger than the ETDF at zero lag (Räsänen et al. 2013).

We found a significant discrimination between high and low ASI values, with respect to normal versus abnormal physiological synchrony states (Koolen et al. 2014c, Chap. 8). Increasing ASI values are obtained for increasing synchrony parallel to maturation (Koolen et al. 2015c, Chap. 9).

3.3 Handling of artefacts

We should note here that preselected EEG data is used for the analysis, which is almost artefact-free. In present studies, visual and manual extraction is well-accepted in order to develop and extract different premature EEG features. Artefact removal should be taken into account in future processing. Using Independent Component Analysis (ICA), artefacts caused by ECG, pulsation and respiration can be removed if the simultaneously recorded polygraphy signals are available to identify the underlying sources (De Vos et al. 2011). In addition, canonical correlation analysis can be applied to remove muscle artefacts (De Clercq et al. 2006). Empirical Mode Decomposition can be applied as well, for example to remove the action potential influence on local field potentials (Loncar-Turukalo et al. 2012). Nevertheless, as previously been mentioned, the source signals themselves (like ECG, respiration) should be noise-free to use

them for continuous artefact removal. This is often not the case. Another way to remove high amplitude 'spike'-artefacts, is by thresholding the EEG with the standard deviation multiplied by a predefined factor (Dolan et al. 2009, Stevenson et al. 2014).

Chapter 4

Line Length as a Robust Method to Detect High-Activity Events

Automated Burst Detection in Premature EEG Recordings

Ninah Koolen[1,2], Katrien Jansen[3], Jan Vervisch[3], Vladimir Matic[1,2], Maarten De Vos[1,4], Gunnar Naulaers[3], Sabine Van Huffel[1,2]

[1] Division STADIUS, Department of Electrical Engineering (ESAT), University of Leuven, Leuven, Belgium

[2] iMinds-KU Leuven Medical IT Department, Leuven, Belgium

[3] Department of Development and Regeneration, University of Leuven, Leuven, Belgium

[4] Cluster of Excellence 'Hearing4all' & Methods in neurocognitive Psychology, University of Oldenburg, Oldenburg, Germany

As adapted from *Clinical Neurophysiology*, vol. 125 (10), pp. 1985-1994, 2014

Highlights

- We present a novel method for automated burst detection in premature EEG recordings, using a single feature Line Length based on both the amplitude and frequency content of the signal.
- The accuracy of the burst detection method is within the range of 79.54%-89.82%, resulting from both high sensitivity and high specificity and a comparable inter-rater agreement.
- The implemented algorithm combines the knowledge of multiple neurologists, thereby objectively assessing premature brain function and reducing the costs for the labor intensive visual analysis.

Abstract

Objective: EEG is a valuable tool for evaluation of brain maturation in preterm babies. Preterm EEG constitutes of high voltage burst activities and more suppressed episodes, called interburst intervals (IBIs). Evolution of background characteristics provides information on brain maturation and helps in prediction of neurological outcome. The aim is to develop a method for automated burst detection.

Methods: Thirteen polysomnography recordings were used, collected at preterm postmenstrual age of 31.4 (26.1-34.4) weeks. We developed a burst detection algorithm based on the feature Line Length and compared it with manual scorings of clinical experts and other published methods.

Results: The line length–based algorithm is robust (84.27% accuracy, 84.00% sensitivity, 85.70% specificity). It is not critically dependent on the number of measurement channels, because two channels still provide 82% accuracy. Furthermore, it approximates well clinically relevant features, such as median IBI duration 5.45 (4.00-7.11) seconds, maximum IBI duration 14.02 (8.73-18.80) seconds and burst percentage 48.89 (35.45-60.12) %, with a median deviation of respectively 0.65s, 1.96s and 6.55%.

Conclusion: Automated assessment of long-term preterm EEG is possible and its use will optimize EEG interpretation in the NICU.

Significance: This study takes a first step towards fully automatic analysis of the preterm brain.

Keywords

Preterm; Brain monitoring; Background EEG; Brain maturation; Automated detection; Bursts; Interburst intervals; Line length

4.1 Introduction: Towards improving preterm prognosis

Each year, more than 15 million babies are born preterm worldwide. Over 1 million babies die each year due to complications of early birth (March of Dimes Geneva, 2012). Two principal brain lesions that result in neurological problems for premature infants are periventricular hemorrhagic infarction and periventricular leukomalacia (Volpe 1998). As a consequence, premature newborns risk to develop disabilities, including learning impairments, motor and cognitive problems (Institute of Medicine 2007). These disabilities exert pressure and raise cost on society and on families. Therefore, it is important that preterm born babies are diagnosed, prognosed and treated as quickly and as accurately as possible.

In large hospitals, the diagnosis and special care after birth is provided by the Neonatal Intensive Care Unit (NICU). Recording of long term EEG can help in evaluating brain function in a non-invasive way. EEG recordings are interpreted by experts through visual analysis. However, interpretation of the EEG has several important limitations. For instance, the analysis of relevant features varies across reviewers and quantification is very restricted due to visual analysis. Moreover, it is very labor intensive and thus expensive. In small hospitals, the expertise is often not available. The analysis of the evolution of the EEG over time requires long term monitoring and thus significant effort for clinicians. Hence, the automatic analysis of the preterm EEG would be a welcome addition in the tool set of hospitals.

Currently, algorithms developed for automatic EEG analysis in newborns are limited. Neonatal seizures are an important clinical phenomenon (Legido et al. 1991), and as many seizures have only very subtle or no clinical manifestations, there is a need for monitoring of seizures with long term EEG. Solutions have been proposed for seizure detection (Deburchgraeve et al. 2009, Cherian et al. 2011, Temko et al. 2011), but have not yet been extended to preterm babies. However, we believe much more information can be found within the background EEG on brain functionality and maturation (Menache et al. 2002, André et al. 2010, Cherian et al. 2009, Niemarkt et al. 2010). Quantification of parameters within the background EEG will make it possible to objectively assess brain

function and detect abnormalities. For preterm babies, the EEG of the first week provides a good basis for prediction, even though more information about the evolution can be obtained from sequential EEG measurements. In this way, brain maturation can be evaluated and patients at risk for abnormal neurological development can be identified.

Long term prognosis is based on background EEG analysis. That means, clinically relevant information is visually extracted from the EEG background pattern, to discover acute and chronic abnormalities. The background parameters change in function of postmenstrual age and parallel brain maturation. Abnormal background characteristics can predict adverse neurological outcome (Le Bihannic et al. 2012). Critical factors, describing this pattern, are degree of (dis-)continuities, amplitude and frequency content (Vanhatalo & Kaila 2006, Löfhede et al. 2010). The best studied parameter in preterm EEG is continuity. Discontinuous activity is the characteristic EEG pattern below 30 weeks of gestational age. A discontinuous EEG pattern, or the so-called tracé discontinue, consists of high amplitude and frequency periods (bursts) interrupted by periods of low brain activity with low-voltage EEG, defined as the interburst intervals (IBIs). A good neurological outcome can be expected, if the duration of the interburst intervals decrease gradually and the EEG evolves to a continuous pattern. At the same time, the burst length and the activity within the burst increases with age (Vecchierini et al. 2007). Furthermore, the time continuous tracings are observed over the EEG measurement, increases with age, as Niemarkt demonstrated using the interburst/burst ratio in preterm babies with normal neurological outcome (Niemarkt et al. 2010). However, amplitude depression and increased discontinuity give rise to an increased risk of brain dysfunctions (Hellström-Westas & Rosén 2005, Le Bihannic et al. 2012).

Many people have been correlating the EEG pattern to a prognosis or outcome (Menache et al. 2002, Vanhatalo & Kaila 2006, Niemarkt et al. 2010, Le Bihannic et al. 2012, Hayashi-Kurahashi et al. 2012), but so far the research in automatically detecting these patterns has been restricted. For this purpose, we want to extract the bursts and IBIs from the preterm EEG in an automated and novel way. Commercial algorithms and algorithms published earlier in literature only make use of the amplitude content of the bursts to detect them (Hayakawa et al. 2001, Niemarkt et al. 2010). However, accuracy can be enhanced by taking frequency content into account. In this way, less false positives will be introduced by moving artefacts, while medication and filter settings will have less influence on the detection system. Some recent studies already make use of both amplitude and frequency content to detect the bursts in the background EEG, such as the non-linear energy operator (NLEO) (Särkelä et al. 2002, Palmu et al. 2010b) and threshold detection on the envelope of the EEG (Jennekens et

al., 2011). However, the clinical aim is to maximize both detection sensitivity and specificity above 80% (Mani et al. 2012), since respectively both burst and IBI derived parameters are of prognostic importance.

In this paper, we present a novel method by using a single feature, Line Length, to accurately detect bursts and to find suppressed parts (IBIs) in long EEG recordings. In addition, this feature has already been proven to detect the onset of high frequency activity in the EEG, such as seizures (Esteller et al. 2001a, Logesparan et al. 2012, Paz et al. 2013). Furthermore, we applied a variable detection threshold, which automatically adapts to changing amplitude levels, e.g. when medication is administrated. We estimated prognostic maturational features and their manifestation. We also investigated whether there is an influence of the number of input EEG channels on burst detection. As such, we decreased the number of channels from 9 to 2 and 4 channels. Using fewer channels has the advantage that it is applicable in a broader field, easier to apply and to interpret and hence helpful in secondary and tertiary care, but obviously less information will become available. Our goal was to get accuracy, sensitivity and specificity above 80% or as close as possible to inter-rater agreement. High values are not easily obtained for the inter-rater agreement, because there is no golden standard for the description of bursts in literature. However, it is believed to be the best possible estimate combining the experiences and capacities of all assessors/neurologists involved.

4.2 Methods: automatically reading EEG recordings

4.2.1 Data acquisition

EEG data were recorded between Jan 2011 and November 2012 at the Neonatal Intensive Care Unit of the University Hospitals of Leuven, Belgium. In this large hospital, 2400 babies are delivered each year with approximately 350 born prematurely. The study recruited only preterm infants, of which a polysomnographic dataset is available including long-term video-EEG recordings. No exclusion criteria were used. This resulted in a dataset of 10 subjects born with a postmenstrual age (PMA) of 24-32 weeks. Two subjects had a suspicion of convulsions, two suffered from mild peripartal asphyxia and three suffered from intracranial hemorrhage. Measurements were started on the preterm infants from a few hours to a few weeks after birth (26-34 weeks PMA) and were typically 3-12 hours long. If necessary, a second and a third measurement were taken, respectively at day 14 and on the day the patient was allowed to leave

the hospital. For two out of these ten patients, an evaluation of these three EEG recordings was carried out to see an evolution of the brain. OSG (Rumst, Belgium) equipment was used, with full head EEG recordings at 9 electrode locations (Fp1, Fp2, T3, T4, C3, C4, Cz, O1, O2) and sampling frequency of 250 Hz. The reference electrode was Cz, set up was in unipolar mode. Afterwards, a pre-processing step was performed consisting of a 50 and 100 Hz Notch filter followed by a 1-20 Hz band pass filter. The latter one was applied because most information about neurological processes is within this frequency band. Two experienced clinicians have scored twenty minutes of each EEG measurement into bursts and IBIs for further research. The study had full approval from the Clinical Ethics Committee of the University Hospitals of Leuven and written informed parental consent was obtained for all infants studied.

4.2.2 Burst Detection

Detection based on Line Length

Fractal dimension (FD) is a method for transient detection, requiring no prior knowledge of the transient characteristics (Accardo et al. 1997). Since a line and a plane have respectively the dimension of 1 and 2, the FD of an EEG signal will always lie within the interval [1, 2]. The more the line fluctuates, the more the plane is 'covered', thus increasing the FD. Line length, a simplified version of the FD, is reported as successful at detecting EEG transients, such as seizures (Esteller et al. 2001a). Line length is defined as the running sum of the absolute differences between all consecutive samples within a predefined window. The value of this feature will grow as the data sequence magnitude or signal variance increases. Line Length can be seen as an amplitude and frequency demodulator (Esteller et al. 2001a). We propose an efficient burst detection algorithm based on this feature, consisting of the following steps:

1. The firing of neurons is random, resulting in non-stationary EEG signals, i.e. statistical properties of the frequency and amplitude content change. Moreover, we can expect these differences in the content of epochs in the EEG, such as bursts and IBIs (Selton et al. 2000, Palmu et al. 2010a,b). Therefore, the signal is divided into smaller 'stationary' parts of fixed length with similar characteristics, to extract useful neural information (Wong & Abdulla (2006)). Here, we consecutively segmented each EEG channel for the duration of 1 second, with an overlap of 0.12 second (Accardo et al. 1997). Short duration segments are essential for reliable detection of transient events, such as bursts. For every segment, we want to decide whether it constitutes of bursts or suppressed EEG (IBIs).

2. Line length is calculated for each segment i as the sum of all absolute distances between the consecutive 250 sample points x_j. The total length of each segment is represented by $L(i)$ and calculated as in formula 4.1.

$$L(i) = \sum_{j=1}^{250-1} |x_{j+1} - x_j| \tag{4.1}$$

After computing line length $L(i)$ for each segment i in each EEG channel ch, normalization is achieved through dividing the line length by the total sum of all $L(i)$ values of the same channel (Accardo et al. 1997). This is defined in formula 4.2.

$$L_{n,ch}(i) = \frac{L(i)}{\sum_i L(i)} \tag{4.2}$$

Clinical experts define bursts as high activity on more than one or more than half of the EEG channels. Consequently, burst segments will have high line length values for several EEG channels in which a burst appears. In order to detect the burst segments, we determine the median value for each segment i over all channels ch:

$$Me_L_n(i) = median\Big(L_{n,ch}(i)\Big) \tag{4.3}$$

We take the median since this variable is more robust than the mean in the presence of outliers. For example, a moving electrode can cause an artefact on one channel resulting in high amplitude content, which would have a dominant unwanted influence on the mean. The median line length values are represented by the curve in Figure 4.1 c for an example of 65 seconds EEG recording.

3. In the last step, burst detection is performed. Bursts are detected when the amplitude of the curve Me_L_n is above a certain threshold, which we denote by Thr_Det. In order to find an optimal threshold, we divided the dataset into two sets: training and validation. First set includes 5 patients, of which 2 patients have had multiple EEG recordings, resulting in 8 recordings. The validation set consists of 5 patients. For each patient, two human EEG readers have scored 20 minutes data into bursts/IBIs. The threshold Thr_Det is adapted in the following way:

$$Thr_Det = F \cdot mean(Me_L_n) \tag{4.4}$$

Thereby, factor F runs from 0.5 to 1.1, in steps of 0.05. Thus, Thr_Det has 13 different values during the training phase. As a result, the ROC

curve in Figure 4.2 is obtained by comparing burst detected samples with samples clinically classified as bursts, as further explained in section 2.3a. Because we want to maximize both the sensitivity and the specificity of the algorithm, we deduct from this figure that $F = 0.8$ or $F = 0.85$ results in good detection rates for the comparison with both clinicians. Namely, for $F = 0.8$, it gives an averaged sensitivity of 85.49% and a specificity of 83.03%. Respectively, it provides for $F = 0.85$ a 82.85% sensitivity and a 85.75% specificity. Considering both are suitable, we decided to further work with a threshold $Thr_Det = 0.85 \cdot mean(Me_L_n)$. This threshold is applied in the validation set.

An additional condition for detection is that the difference in amplitude between a successive non-detected and detected point of the curve Me_L_n and vice versa should be large enough. That is to say, larger than $0.4 \cdot std(Me_L_n)$, so only pronounced peaks are detected. Furthermore, all IBIs shorter than 2 seconds are removed since they are not considered by clinical experts. An example of 65 seconds EEG partitioned into bursts and IBIs is shown in Figure 4.1. Each circle or diamond in Figure 4.1 c represent a segment EEG of 150 seconds. Segments detected as bursts are indicated by diamonds. In Figure 4.1 b, we compare the detected bursts with clinical labeling of high activity periods by two experienced clinicians.

Suppression curve

To make an objective validation, the original aim was to segment and detect the bursts in the last 10 minutes of every hour in a 4 hour EEG recording. However, neurologists are not looking into these same parts of the recording when they are interested in features to make a prognosis about the neurological outcome. Instead, they are searching for the most discontinuous parts within the EEG, because this is best related to the outcome of the patient (Menache et al. 2002). Consequently, we developed another part of the algorithm which indicates the 'suppression of the EEG', defined as the suppression curve.

This curve is deducted from the median curve, determined every 150 seconds, as defined in the previous section. We calculate the median and the mean of the curve Me_L_n, respectively shown by a grey and dashed line in Figure 4.3. Then, the difference between the mean and the median is taken as follows:

$$supp = 1 - \frac{median(Me_L_n)}{mean(Me_L_n)} \tag{4.5}$$

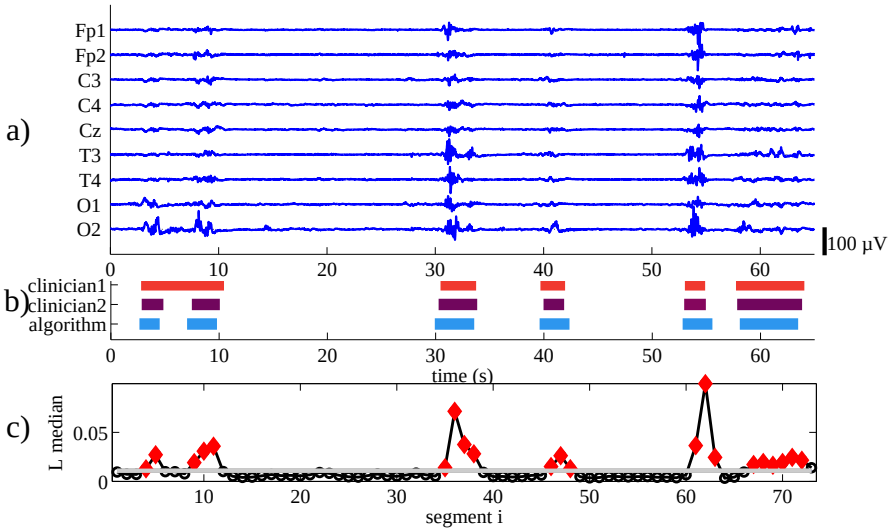

Figure 4.1: (a) Example of 65 s 9-channel EEG recording with reference electrode Cz, (b) Burst detection: by 2 clinicians and by algorithm, (c) Black curve: median $L_n(i)$ as calculated in step 2, gray line: threshold for detection of bursts (Thr_Det), diamonds: detected burst segments after step 3.

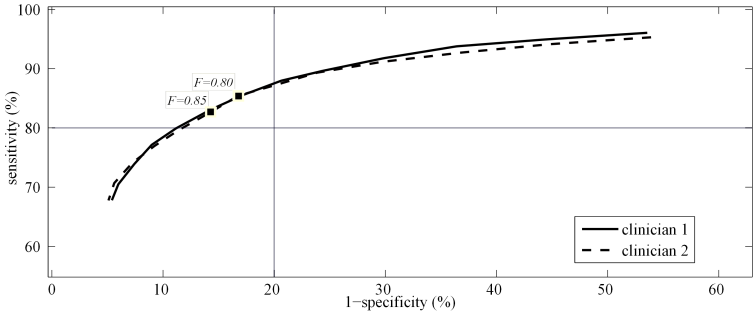

Figure 4.2: ROC curve of the burst detection algorithm, F is adapted to get different Thr_Det.

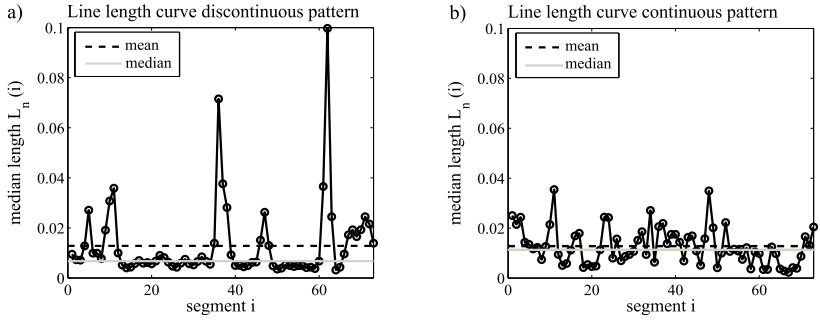

Figure 4.3: Comparison of the line length curve, for a discontinuous pattern (a) and a more continuous pattern (b). Median of the curve is shown by a gray line; mean is shown by a dashed line.

This difference, called *supp*, is depicted in the suppression curve in Figure 4.4 as a single point. Thus, every point of this curve represents the grade of suppression for an EEG segment of 150 seconds. Therefore, EEG parts with long IBIs resulted in high *supp* values, whereas continuous EEG with short or even no IBIs resulted in lower *supp* values. This is also shown in Figure 4.3, where the difference between mean and median is larger for a discontinuous pattern (a), compared to a more continuous pattern (b). An example of the suppression curve of one patient is shown in Figure 4.4, in which we can see that the EEG recording is more or less continuous (very low *supp* values), except two suppressed periods around the 6000th and the 16000th second of the measurement. In general, neurologists are scrolling through a measurement to find these suppressed periods to make a diagnosis. A suppression curve is created for every premature patient and visually verified by an expert human EEG reader. Isolated extreme peaks in the suppression curve are often due to artefacts, so discarded for the further analysis. For each patient, we have selected two periods of 10 minutes with consecutive high *supp* values, to be sure that we incorporate the most informative and practically artefact-free periods in the burst detection examination.

Comparison to other detection algorithms

Whereas most developed methods for burst detection only make use of the amplitude content of the EEG background pattern, a few methods exploit both the amplitude and the frequency content. One of these methods applies

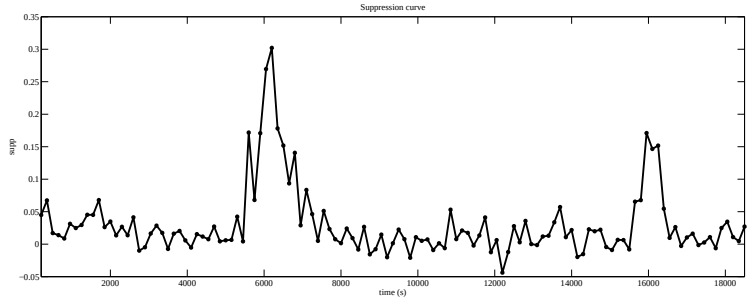

Figure 4.4: Suppression curve of one patient. Discontinuities are revealed around the 6000th second and the 16000th second of the 5 h long measurement.

threshold detection on the envelope of the EEG signals (Jennekens et al. 2011). This envelope EV_j is derived from the average signal power P_j:

$$EV_j = \sqrt{2 \cdot P_j} = \sqrt{\frac{2}{Nw} \sum_{j=1}^{Nw} x_j^2} \tag{4.6}$$

Thereby, x_j represents the amplitude of the EEG signal and Nw the number of samples within 1 second of data (250 samples). If two or more of the nine EEG channels have an envelope value EV_j higher than the predefined amplitude threshold, then sample x_j will be classified as burst. Otherwise it is an IBI sample. Similarly to the line length-based method, IBIs shorter than two seconds are removed and changed into burst samples.

Another non-linear method makes use of the non-linear energy operator (NLEO) (Palmu et al. 2010b), where x_j is the value at sample j (Palmu et al. 2010b):

$$NLEO\Big(x_j\Big) = |x_j \cdot x_{j-3} - x_{j-1} \cdot x_{j-2}| \tag{4.7}$$

This signal is smoothed by the average value of a 1.5 second sliding window centred around the time sample $NLEO\Big(x_j\Big)$. Next, a baseline correction is achieved by subtracting the minimum signal value within the second before the

current sample to remove continuous artefacts. Similar to the envelope-based method, a sample is classified as a burst if the processed signal is higher than a predefined amplitude on two or more channels.

Those two methods are compared to the developed line length-based method by statistical analysis, analyzing the discrepancies between automated and clinical detection of bursts. However, we should keep in mind that the line length algorithm has an adaptive threshold whereas the other two methods have a fixed threshold. Furthermore, it is not only important to have high sensitivity and specificity, it is even more crucial to get similar values for prognostic maturational features. In this paper, we present the median length of IBIs, the maximum length of IBIs (longest period of EEG inactivity) and the percentage of bursts (proportion of time covered by bursts). Although more features have been explored (Koolen et al. 2013), these three features are highly informative. For example, with a good development of the premature brain, the median and maximum IBI length will decrease when the PMA is increasing (André et al. 2010, Niemarkt et al. 2010). This means, there will be more EEG activity in the form of bursts due to more connectivity between neurons in the premature brain. In conclusion, we want these prognostic values to be well approximated to assess the evolution of the premature EEG pattern.

Comparison of a variable number of EEG channels

Small hospitals do not have the possibility and the equipment to measure a full head EEG. Therefore, we reduced the number of input channels of the line-length detection algorithm from 9 to only 2 and 4 EEG channels. We compared the detection accuracy to the full head clinical scoring of bursts and IBIs based on 9 channels. EEG channels recorded at C3 and C4 are taken as 2 input channels and C3,C4, O1 and O2 are used for 4 channels detection. In case that the accuracy would be similar, many hospitals could advantage considering that most hospitals in Europe only measure two channel EEG (C3 and C4), resulting in the so-called amplitude-integrated EEG (aEEG) (Hellström-Westas et al. 2006, Tao & Mathur 2010).

4.2.3 Performance Evaluation

Defining accuracy, sensitivity, specificity

Bursts are detected by the algorithm and are visually marked by two experienced clinicians (KJ and JV). Since there is no 'golden standard' available for burst detection, visual scoring of more than one rater is taken into account. Moreover,

raters often did not agree on the start and ending sample of a burst, resulting into a different number of bursts/IBIs. In addition, bursts should sometimes be merged together to get the same burst as the other rater marked. Therefore, statistical analysis of the detection accuracy is performed sample-by-sample (Palmu et al. 2010a,b). Confusion matrices are obtained by comparing the burst detection of the algorithm with the markings of the clinician. This matrix is composed for each clinician separately and consists of:

- Number of true positives (TP): samples detected as burst by the expert AND by the algorithm
- Number of false positives (FP): samples detected as burst by the algorithm, but not by the expert
- Number of true negatives (TN): samples classified as IBI by the algorithm and by the expert
- Number of false negatives (FN): samples marked as a burst by the expert, but missed by the algorithm

Based on these values, we can determine the robustness of the developed algorithm by calculating the sensitivity, the specificity and the accuracy:

$$sensitivity = \frac{TP}{TP + FN} \tag{4.8}$$

$$specificity = \frac{TN}{TN + FP} \tag{4.9}$$

$$accuracy = \frac{TP + TN}{TP + TN + FP + FN} \tag{4.10}$$

Some false positives are introduced by movement artefacts. We did not filter out these movement artefacts, because we have selected EEG segments practically free of artefacts based on the suppression curve. Movement artefacts are detected by thresholding the line length signal obtained from the tremor or respiratory signal. A false positive sample, caused by movements, is defined by the following three conditions: the data sample is detected as movement on the tremor or respiratory signal *and* it is detected by the algorithm as a burst *and* both clinicians did not label the sample as a burst. The number of false positives due to movements over the total number of false positives is calculated.

Relationship among statistical parameters

A high accuracy will be achieved through a high number of correctly classified samples: true positives (bursts) and true negatives (IBIs). However, it can be the case that a high number of only TP or TN can still result in a high accuracy. In other words, we can obtain high accuracy for the combination of low sensitivity and high specificity or vice versa. Nevertheless, the clinical aim is to maximize both the sensitivity and specificity, above 80% (Mani et al. 2012). Maximizing both values can be achieved for the applied thresholds, although increasing or decreasing the threshold will have an influence on both sensitivity and specificity. Therefore, it is of key importance to set patient specific and adapting thresholds. Maximization of both statistical parameters is crucial for clinical EEG examination to make an accurate prognosis about the brain's state of activity. That is, false negatives or false positives will affect prognostic values, such as the median IBI length, the maximum IBI length or the burst percentage.

Statistical analysis

Numerical values calculated for the statistical measurements – accuracy, sensitivity and specificity – and for the prognostic values – maximum IBI length, median IBI length and burst percentage – are compared between different detection methods to see whether there is one performing significantly better. Thereto, we first applied Anova test, to see whether there is a difference between the three detection algorithms. Next, we used Student's t-test. Each time two detection methods are compared. The null hypothesis states that the statistical measurement is similar for both detection methods. If the null hypothesis is rejected ($h = 1$), then the detection methods are performing significantly differently on this measurement with a p-value of $p<0.05$, $p<0.01$ or $p<0.001$.

4.3 Results: detection characteristics applying real-world data

4.3.1 Comparing burst detection methods

In a first step of the validation part, the suppression curves of all patients were manually verified by an experienced neurologist (KJ). It is confirmed that the peaks of all suppression curves represent the most discontinuous parts of the EEG measurements. Next, for both training and validation set, automatically

detected bursts are compared with the manual scoring of the bursts by two clinical experts (KJ and JV). In Table 4.1, we present the sensitivity, specificity and accuracy for both sets of the three detection algorithms: based on line length, envelope calculation and NLEO. These methods show respectively a mean accuracy of 84.27%, 80.58% and 82.04%, whereas the inter-rater agreement is 86.20%. There is no remarkable difference for the values of these statistical performance measurements between the training and validation set. The mean percentages of false positives introduced by movement artefacts over the total amount of false positives are respectively for the three methods 4.84%, 8.36% and 10.91%. Nevertheless, movement artefacts are rare in the selected and analyzed EEG segements.

All three algorithms can be used to reliably and accurately detect bursts. The boxplots, depicted in Figure 4.5, show the range of sensitivity, specificity and accuracy, including values of all 13 measurements (training and validation set). The accuracy of the line length method is within the range of 79.54%-89.82%, resulting from both high sensitivity and high specificity. For this data set, the accuracy values are good and comparable to clinician's inter-rater agreement. In addition, both sensitivity and specificity are above the aim of 80% predefined by clinical experts (Mani et al. 2012). Furthermore, we can see that the envelope based algorithm gives lower accuracy values within the range of 76.05-83.99% with two extremes of 70.3% and 91.53%. Overall, this method has lower accuracy due to false positives introduced by movement artefacts. The reason therefore is that only an amplitude threshold is used upon the envelope of the EEG signal (around 30 µV). Therefore, bursts are detected by the algorithm, but not by the expert. In addition, a training phase is needed to tune the different parameter values for the algorithm settings, which requires a broader dataset. The lower extreme value is caused by a low sensitivity of 61.84%, resulting in low accuracy. The other extreme has resulted in a very high accuracy for all three detection methods (89.63%-91.97%), because the transitions between bursts and IBIs were clearly pronounced (Figure 4.6 a), as the EEG was in the state of the so-called tracé discontinue (André et al. 2010).

The NLEO method has a high accuracy (above 80%), although this is due to the averaging of high sensitivity of 93.90% and low specificity of 70.38%. This lower specificity is not desirable, as the aim is to maximize both the sensitivity and specificity of the detection algorithm (>80%). For one in thirteen cases, the NLEO method clearly has a lower accuracy of 68.6%, due to a low specificity of 51.26% and high sensitivity of 96.85%. This patient's EEG contains more activity periods of higher voltage, which are not marked by clinicians as bursts (Figure 4.6 b). However, these periods are detected by the algorithm, because this high activity is smoothed out. This smoothing step results into more detected burst samples due to a fixed amplitude threshold in the algorithm.

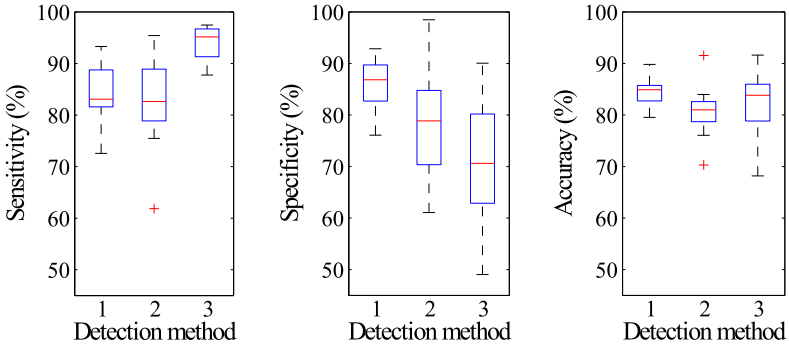

Figure 4.5: Box plots of sensitivity, specificity and accuracy for the three detection algorithms, all 13 measurements are included.

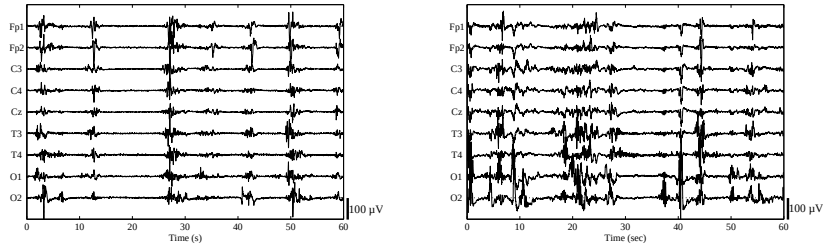

Figure 4.6: (a) clean EEG with clear burst transitions, which results into high accuracy values for all detection methods; (b) Unclear transitions between bursts and IBIs (lot of activity), leading to a low accuracy for the NLEO method.

4.3.2 Prognostic features

It is not only important to have the highest detection accuracy, in addition prognostic features should be well approximated after automated burst detection. Especially, the evolution of these maturational EEG features is of great importance for diagnosis and prognosis. A good prognosis can be expected, in case that the median IBI length decreases (Le Bihannic et al. 2012). An example is presented in Figure 4.7, where the median IBI length decreased over 14 days. That is, the grey line shifted to the left comparing the histograms in Figure 4.7 a and 4.7 b. Moreover, the whole histogram shifted to the left, thus including shorter detected IBIs. Hence, more EEG discontinuities are interrupted by bursts, resulting in shorter IBIs. This is also shown by the increase of the

Table 4.1: Sensitivity, specificity and accuracy of three detection methods for both the training and validation set. Detection methods are based on line length, based on envelope calculation and based on NLEO.

	Training set (8 measurements)			
	LL	*envelope*	*NLEO*	*inter-rater*
Sensitivity (%)	85.49	81.33	93.38	
Specificity (%)	83.49	77.79	68.16	
Accuracy (%)	84.02	79.07	80.22	86.56

	Validation set (5 measurements)			
	LL	*envelope*	*NLEO*	*inter-rater*
Sensitivity (%)	81.63	84.62	94.73	
Specificity (%)	89.23	79.97	73.96	
Accuracy (%)	84.70	83.00	84.95	85.63

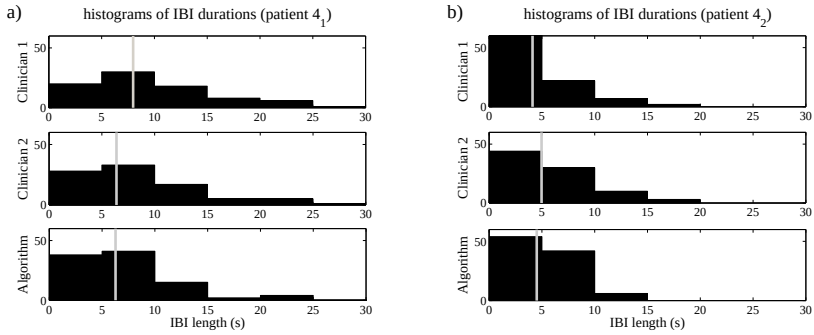

Figure 4.7: The evolution of the premature brain leads to a change in the IBI duration histogram: histogram in Figure 4.7 b are derived from a measurement taken two weeks later than the measurement resulting in the histograms in Figure 4.7 a. The histogram has shifted to the left; including shorter IBIs. The median IBI length (gray line) decreased too.

burst percentage in these EEGs: from 42.55% to 57.82% two weeks later (after automated detection of the bursts). These results are in accordance with a normal evolution of the brain maturation.

In Figure 4.8, boxplots are provided which represent the error between automated and manual detection for three prognostic values: median IBI length, maximum IBI length and the percentage of bursts in the EEG. Mean

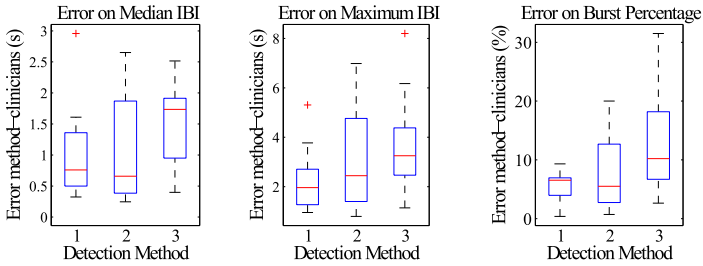

Figure 4.8: Error in automatic detection by comparing to clinicians' scoring for three prognostic values (median IBI, maximum IBI and burst percentage). The box plots represent the differences for all patients calculated for three detection methods (1: line length based method, 2: envelope based method, 3: NLEO based method).

values over all 13 measurements are respectively 5.45 (4.00-7.11) seconds, 14.02 (8.73-18.80) seconds and 48.89 (35.45-60.12) %. In Figure 4.8, the errors on clinical values are shown, instead of the real values, since we try to approximate the clinical features as good as possible. In this way, we want the error to be minimized. For median IBI, the error for automated detection is small for all three detection methods; the median error ranges between 0.65-1.75 seconds. The error on the maximum IBI length is larger (1.96 - 3.25 seconds), because this variable varies more within the EEG data. Namely, over all measurements, clinicians found a maximum IBI length between 3.93 and 66.61 seconds. For all 3 methods, the burst percentage deviates respectively 6.55%, 5.50% and 10.22% from the clinical values. For the NLEO detection method, it deviates the most (2.63%-31.49%). The statistical significance is described in the next section.

4.3.3 Statistical significance

We tested whether one of the detection methods was performing significantly better for burst detection. Therefore, we first applied ANOVA tests, because we have values obtained by three groups (detection methods). The ANOVA tests have revealed the variability between the means of the three groups, for values of all statistical measurements and all prognostic features ($p<0.05$). Then, we compared the detection methods in pairs using two-group t-tests. We applied t-tests with an input of two vectors, both sized 26x1. For example, one vector includes the accuracy values of method 1 compared to clinician 1 (13 values for 13 EEG measurements), and the accuracy values of method 1 compared to clinician 2 (also 13 values). The second vector is analogously constructed,

*Table 4.2: Statistical performance t-test on statistical measurements – accuracy, sensitivity and specificity – (see boxplots in Figure 4.5). Two detection methods are compared each line; m1, line length based method; m2, envelope based method; m3, NLEO based method. In the table, the differences between the mean values of these statistical measurements are given. Thereby, a significant difference is presented as *($p < 0.05$), **($p < 0.01$), ***($p<0.001$).*

	Difference in mean accuracy (%)	**Difference in mean sensitivity (%)**	**Difference in mean specificity (%)**
m1-m2	3,7 ***	1,41	7,07 **
m1-m3	2,24	-9,9 ***	15,31 ***
m2-m3	-1,46	-11,31 ***	8,24 ***

but contains the accuracy of method 2. In a similar way, we have built all other input vectors containing the statistical measurements and prognostic features. The results can be found in Table 4.2 and Table 4.3 for t-tests on respectively statistical measurements and most prognostic features. For the accuracy, the null hypothesis is rejected by comparing the line length method with the envelope method. Based on numerical values, we can conclude that the former one is better. In addition, this method's specificity is better too, since the null hypothesis is rejected twice for both t-tests where the line length was compared with the other two methods ($p<0.01$). However, the sensitivity of the NLEO based method was the best (null hypothesis rejected twice for the analysis with the two other methods). Nevertheless, the line length method performs good as well for the statistical analysis of the prognostic values (Table 4.3). Namely, the error of these IBI lengths is small for the line length method, as well as for the envelope method. There is even a significant difference with the NLEO method. In fact, the null hypothesis is rejected twice by comparison of the line length method with the NLEO method ($p<0.05$).

4.3.4 Detection on a variable number of channels

The investigation of the developed line-length detection algorithm with fewer input EEG channels showed only a minor difference in accuracy. As expected, the accuracy will increase when information of more channels is included (Figure 4.9). In fact, the accuracy only increases a few percent (3-5%), respectively for comparison with scoring of clinician 1 and clinician 2. More concretely, when using the the two most informative EEG channels (C3 and C4), the accuracy is still around 82%.

*Table 4.3: Statistical performance t-test on three prognostic features: median IBI length, maximum IBI length and the burst percentage. Two detection methods are compared each line; m1, line length based method; m2, envelope based method; m3, NLEO based method. In the table, the differences between errors on the prognostic features are given. Thereby, significant difference is presented as *($p < 0.05$), **($p < 0.01$), ***($p < 0.001$).*

	Difference in error on median IBI (s)	**Difference in error on max IBI (s)**	**Difference in error on burst percentage (%)**
m1-m2	0,1	-0,48	1,04
m1-m3	-0,98	-1,29*	-3,67**
m2-m3	-1,08*	-0,81	-4,72*

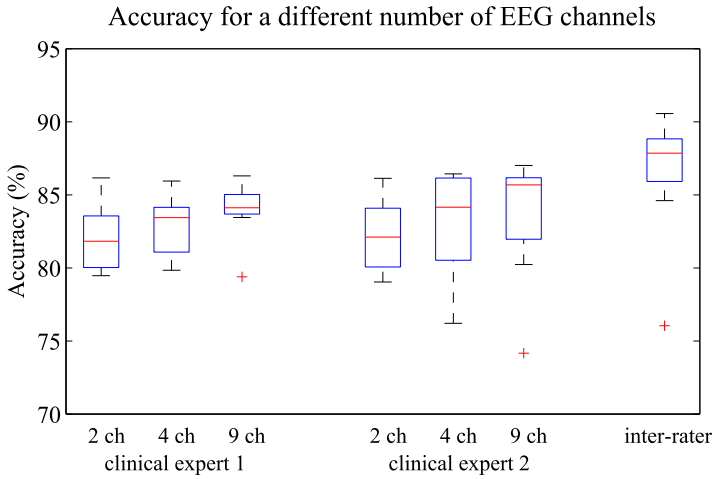

Figure 4.9: Detection accuracy by using a different number of channels as input for the line length detection method: 2 channels (C3-C4), 4 channels (C3-C4-O1-O2), 9 channels (C3-C4-O1-O2-T3-T4-Fp1-Fp2-Cz).

A higher accuracy can be achieved for two channels when the neurologists manually put an amplitude threshold (14-18 µV). Notwithstanding, this higher accuracy can never be achieved in an automatic way by setting a fixed amplitude threshold, since the threshold is patient dependent and should be adapted visually to the patient's EEG pattern.

4.4 Discussion

EEG in preterms shows dynamic changes parallel to brain maturation (André et al. 2010). The aim of this study was to automatically detect the bursts in the background EEG, which will be used to calculate these maturational features. In this way, normal brain maturation can be assessed and abnormal EEG patterns can be detected identifying patients at risk for abnormal neurological outcome (Hellström-Westas & Rosén 2005). Moreover, influences of different treatment options can be studied and an accurate prognosis and early counseling can be achieved. In the future this can help in identifying preterm babies that could benefit from neuroprotective measures.

Mimicking the way clinicians observe phenomena in the EEG signals, we have introduced the suppression curve, so that the most discontinuous parts can be examined and used as the input of the burst detection algorithm. The overall results show that the feature line length in the detection algorithm catches the high-frequency phenomena, the bursts, in an accurate way. The accuracy of this line length detection method is in general good and comparable to clinician's inter-rater agreement. In addition, both sensitivity and specificity are above the aim of 80% predefined by clinical experts (Mani et al. 2012). Moreover, the detection threshold is adapted every 150 seconds for each patient, because the EEG could be attenuated when medication is provided and the pattern is corresponding to the age. Only using the two most informative channels, as in aEEG, the detection accuracy resembles the high accuracy already obtained for 'full head' EEG. These findings result in usability for the secondary care as well, where only two channels are measured instead of a 'full head' EEG. Therefore, not only hospitals doing research, but every hospital can benefit from the use of this method for automatic detection and analysis of the background EEG.

Assessment of the evolution over time of the unique characteristics of the EEG is very valuable and beneficial for better understanding of the preterm brain development. Consequently, good approximation of clinical features is of high importance. Discontinuity is a normal pattern in the very preterm infant. It is an alternating pattern of bursts of high amplitude slow waves and sharp transients, with intervals of low amplitude activity (interburst interval). Increased discontinuity increases the risk of brain dysfunction and abnormal neurological outcome. Dysmaturity of the EEG pattern, with prolonged IBI as the most important feature, is the predominant EEG pattern found in infants who later develop moderate or severe neurological sequelae (Le Bihannic et al. 2012). Conde et al. showed that in preterm babies with major ultrasound brain lesions, the interburst interval was prolonged and the burst duration was shorter when compared to preterm babies without major brain lesions at 2 and 4 weeks

postnatal life (Conde et al. 2005). Predictive EEG characteristics, describing the severity of the discontinuity, are the length of the consecutive interburst intervals, but also the amplitude and duration of bursts (Biagioni et al. 1994). IBI and burst lengths, as well as burst interburst ratio, are dependent on postconceptional age (Niemarkt et al. 2010). Burst percentage was considered as the statistically most significant parameter for correlations between all raters (Palmu et al. 2010a). The line length just give small deviations from clinical values for this parameter. Not only the burst percentage is informative, even more the IBI lengths are indicative for normal maturation of the brains. By using the developed technique, the median and maximum IBI length are well approximated too. Using these parameters, normal maturation can be assessed and abnormal background EEG patterns can be easily identified. The line length and NLEO methods have a significantly higher accuracy than the envelope method, for which many false positives were introduced. Whereas the NLEO method reached the highest sensitivity in detecting bursts, our goal was to maximize both sensitivity and specificity. Therefore, the line length method was performing significantly better at the approach of the three selected prognostic features (median IBI length, maximum IBI length and burst percentage). For these prognostic features, the errors between algorithm and clinical values were minimized. Nevertheless, the threshold of the other two detection methods can be made adaptive as well.

Some limitations should be included. The validation is only carried out on a small patient database (13 measurements), further research would need to include more patients. In addition, no artefact removal is applied on these signals to remove artefacts introduced by ECG, respiration or movements (De Vos et al. 2011). In fact, automated artefact removal cannot be easily applied, since the ECG and respiration signal should be clear and continuous signals, with a high SNR, which is often not the case for these preterm measurements. Furthermore, a first step towards finding the most discontinuous parts in the EEG has been made, by introducing the suppression curve. Nevertheless, automation of selecting the largest peaks in the suppression curve could be incorporated, since they are yet manually chosen. Future work will focus on fine-tuning the algorithm, based on a larger dataset of validated EEG segments. In addition, more features and their clinical relevance require exploration.

4.5 Conclusion

The EEG provides vital information about the state of the brains of premature babies and their evolution prognosis. However, it is generally difficult and time-consuming work to analyse the recordings and requires the trained eye of one

or more specialized neonatologists. This paper shows that it is possible to read the EEG and accurately analyse the pattern by a computer. The implemented algorithm combines the knowledge and expertise of several neurologists and automatically adapts to specific conditions of the individual patient. The accuracy of the analysis is generally equivalent to that of clinical experts in the NICU. It shows that access to all patient data coupled with an automated analysis is a very useful tool to assess the evolution of the EEG pattern over longer periods of time and to plan immediate treatment. Furthermore, the detection method works accurately with only 2 or 4 measurement channels allowing it to be used in small hospitals, significantly enhancing their capabilities.

Acknowledgements

Research supported by Research Council KUL: GOA MaNet, PFV/10/002 (OPTEC), IDO 08/013 Autism, several PhD/postdoc & fellow grants; Flemish Government: FWO: PhD/postdoc grants, projects: G.0427.10N (Integrated EEG-fMRI), G.0108.11 (Compressed Sensing), G.0869.12N (Tumor imaging) G.0A5513N (Deep brain stimulation); IWT: TBM070713-Accelero, TBM080658-MRI (EEG-fMRI), TBM110697-NeoGuard, Ph.D. Grants; iMinds 2013; Flanders Care: Demonstratieproject Tele-Rehab III (2012-2014); Belgian Federal Science Policy Office: IUAP P719/ (DYSCO, 'Dynamical systems, control and optimization', 2012-2017); ESA AO-PGPF-01, PRODEX (CardioControl) C4000103224; EU: RECAP 209G within INTERREG IVB NWE programme, EU HIP Trial FP7-HEALTH/ 2007-2013 (n 260777), EU MC ITN Transact 2012 # 316679.

Chapter 5

The suppression curve as a quantitative approach for measuring brain maturation in preterm infants

Anneleen Dereymaeker[1,†], Ninah Koolen[2,3,†], Jan Vervisch[1,4], Els Ortibus[4], Katrien Jansen[1,4], Maarten De Vos[5], Sabine Van Huffel[2,3], Gunnar Naulaers[1]

[1] Department of Development and Regeneration, University Hospital, Neonatology , University of Leuven, Leuven, Belgium

[2] Division STADIUS, Department of Electrical Engineering (ESAT), University of Leuven, Leuven, Belgium

[3] iMinds-KU Leuven Medical IT Department, Leuven, Belgium

[4] Department of Development and Regeneration, Child Neurology, University of Leuven, Belgium

[5] Institute of Biomedical Engineering, Department of Engineering Science, University of Oxford, Oxford, UK

[†] These authors are joint first authors.

As adapted from a submission to *Clinical Neurophysiology*, Oct. 2015

Highlights

- Automated detection of maturational changes in multichannel preterm EEG.
- The Suppression curve reflects the decrease in EEG discontinuity with advancing postmenstrual age in healthy preterm infants.
- Interburst Intervals values are calculated automatically and correlated with postmenstrual age.

Abstract

Objectives: We introduce the suppression curve (SC) as an automated approach to describe the maturational change in EEG discontinuity in preterm infants. This method allows to define normative values of interburst intervals (IBIs) at different postmenstrual ages (PMA).

Methods: Ninety multichannel EEG recordings from 25 preterm infants (born $\leq$ 32 weeks) with normal developmental outcome at 9 months, were first analyzed using the Line Length method, an established method for burst detection. Subsequently, the SC was defined as the 'level of EEG discontinuity'. The mean and the standard deviation of the SC, as well as the IBIs from each recording were calculated and correlated with PMA.

Results: Over the course of development, there is a decrease in EEG discontinuity with a linear correlation between the mean SC and PMA till 34 weeks (r= -0.8 p=$3.5*10^{-12}$). From 30 weeks PMA, differences between discontinuous and continuous EEG become smaller, which is reflected by the decrease of the standard deviation of the SC. IBIs are found to have a significant correlation with PMA.

Conclusions: Automated detection of maturational changes in EEG discontinuity is possible with the SC. These changes include more continuous tracing, less amplitude differences and shorter suppression periods, reflecting development of the vigilance states.

Significance: The suppression curve facilitates automated assessment of EEG maturation. Clinical applicability is straightforward since values for IBIs according to PMA are generated automatically.

Keywords

EEG; Preterm infant; Brain monitoring; EEG discontinuity; Interburst intervals; Automated analysis; Line Length; Suppression Curve

5.1 Introduction

Despite cardiorespiratory advances in perinatal and neonatal intensive care, premature infants are still at high risk for neurological disabilities (Larroque et al. 2008, Aarnoudse-Moens et al. 2009, Mwaniki et al. 2012, Back & Miller 2014). Early identification of at risk infants can improve short-term neuroprotective measures, and can ameliorate supportive measures in future life. Intensive brain monitoring in this vulnerable period of care, can help to identify the influence of various endogenous and exogenous disturbances on cortical activity and maturation (Victor et al. 2005b, Kostović & Jovanov-Milosević 2006, Kostović & Judas 2010, Wikström et al. 2008, Chau et al. 2013).

Early cortical brain activity alternates between two activity modes. Periods of relative quiescence (interburst intervals) are interrupted by spontaneous activity transients (SATS or bursts (Vanhatalo & Kaila 2006, Tolonen et al. 2007). Bursts and interburst intervals (IBIs) will change with development and are influenced by medication as well as brain lesions (Hellström-Westas & Rosén 2005, Malk et al. 2014, Iyer et al. 2015). Discontinuous activity (tracé discontinue) is the characteristic EEG pattern below 30 weeks postmenstrual age. Gradually, the electroencephalographic patterns evolve into a more continuous pattern (tracé continue) as a marker of maturation towards term age (Scher 1996, Vecchierini et al. 2003, Hayakawa et al. 2001, André et al. 2010). Abnormal discontinuity for age (also referred as IBI duration) is the most studied feature in the preterm infant, associated with cerebral pathology, immaturity and adverse neurological outcome (Holmes & Lombroso 1993, Biagioni et al. 1994, Menache et al. 2002, Conde et al. 2005, Wikström et al. 2012). However, accurate outcome prediction based on one single parameter may not be robust enough due to both physiological and technical shortcomings, and therefore, additional objective maturational parameters would fill the gap. Brain function can be transiently or permanently disturbed by various factors. To understand better physiological and pathological maturational processes in the preterm brain, continuous, consecutive and multichannel EEG measurements are essential. However, visual EEG interpretation requires expertise, and there are no standardized classification methods. A quantitative analysis of EEG activity, including

automated analysis of selected maturational features of cortical function, would create a more objective and accurate classification scheme for preterm EEG.

Different burst detection algorithms for multichannel EEG are described in the literature (Palmu et al. 2010a, Jennekens et al. 2011, Koolen et al. 2014b, Murphy et al. 2014). These studies were intended to improve algorithm performance and compared with interobserver agreement. Based on these automated algorithms, a possibility has been opened to study the developmental changes in the level of EEG discontinuity, and this without human intervention. Niemarkt et al. (2010) tested the maturational trend with an interburst/burst ratio algorithm in 18 healthy preterms, however this study used only one bipolar EEG signal (C3-C4). No further studies have been performed on a larger dataset with consecutive, multichannel EEG recordings to verify the performance of any of these algorithms to assess global maturational changes in the discontinuous EEG pattern.

We present a method, which quantitatively describes the maturational changes in EEG discontinuity in preterm infants with normal neurodevelopmental outcome at the corrected age of 9 months. This quantitative metric, the suppression curve, uses a single feature, the Line Length (LL). It has been shown in previous work to accurately detect high activity epochs (burst) and suppressed parts (IBIs) in long EEG recordings (Koolen et al. 2014b). In the present study, we want to assess whether the global developmental changes in the level of discontinuity, detected by the suppression curve, are robust enough to use it as a maturational feature. Second, we will improve the clinical applicability by presenting age-specific values for interburst intervals.

5.2 Methods

5.2.1 Data Acquisition

The main dataset consisted of 149 recordings in 41 infants (gestational age 24 $\leq$ 32 weeks), recorded at a postmenstrual age (PMA) of 27 to 42 weeks. All infants had at least 2 consecutive recordings to assess brain development. The study was performed at the Neonatal Intensive Care Unit of the University Hospitals of Leuven, Belgium during the period from February 2013 to September 2014. The study was approved by the Ethics Committee of the University Hospitals of Leuven, Belgium. All preterm infants with gestational age (GA) $\leq$ 32 weeks were eligible to enter this study. Preterm infants were consecutively enrolled in the study after informed parental consent. Measurements were started as soon as the infant was clinically stable. All infants born $\leq$ 32 weeks or birthweight <1500g

underwent standardized neurodevelopmental testing at 9 months corrected age with the Bayley Scales of Infant Development, version II. The BSID-II provides developmental scores for cognition (Mental Developmental Index, MDI) and motor skills (Psychomotor Developmental Index, PDI). From this larger dataset, 25 premature infants with GA $\leq$ 32 weeks were retrospectively selected based on strict inclusion criteria: 1. normal neurodevelopmental outcome score (BSID-II MDI and PDI) $>$ 85, 2. no use of any sedative or anti-epileptic medication during EEG registration and 3. normal cerebral ultrasonography (intraventricular hemorrhage grade $\leq$ II, no periventricular leukomalacia or ventricular dilatation$>$ p97). All infants were treated with caffeine.

5.2.2 EEG monitoring

All EEG measurements were recorded at 250 Hz, with 8 electrodes (Fp1, Fp2, C3, C4, T3, T4, O1, O2) placed according to the 10-20 standard locations and reference electrode Cz (BRAIN RT, OSG equipment, Mechelen, Belgium). The targeted recording time was 4 hours to record multiple vigilance states. No artefact correction was performed on these recordings.

Preprocessing the data involved applying a 50 Notch filter and a 1-20 Hz band pass filter to capture the interesting burst information present in this frequency range.

5.2.3 Automated analyses

Multichannel EEG recordings were analyzed using the Line Length method, which includes the characteristics of both amplitude and frequency content, and serves for automatic burst detection (Koolen et al. 2014b). In the first part of the algorithm, each EEG channel is divided into consecutive segments of 1 second (with an overlap of 0.12 second). Next, the Line Length value is calculated for each segment and normalized in 150 seconds windows by dividing through the total line length of each window. Normalization is necessary to average out the effect of amplitude differences between EEG channels due to different electrode placement. After normalization, the median value over all 8 EEG channels is obtained for each segment: Me_L_n.

In the second part of the algorithm, the suppression curve (SC) is derived, which represents the level of discontinuity in the EEG (different EEG states: discontinuous or continuous EEG). Each sample of the SC is calculated as the difference between the mean and the median of the median curve (Me_L_n). In this way, the level of discontinuity is described for every EEG segment of 150

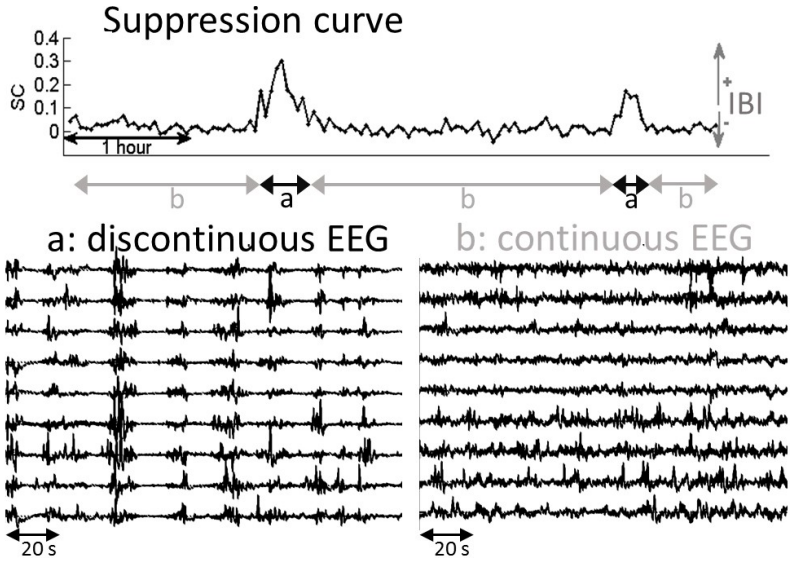

Figure 5.1: The suppression curve derived from a multiple-hour recording. The suppression curve is depicted for discontinuous (black) and more continuous (gray) parts of the EEG recording.

seconds, resulting in the suppression curve over time (derived from a multiple-hour recording). EEG parts with long IBI lengths resulted in high suppression values (larger difference between mean and median), whereas continuous EEG with short or even no IBIs resulted in lower suppression values. In this case, the mean and median of the Me_L_n have comparable values. This is shown in Figure 5.1, in which the suppression curve is depicted for discontinuous and more continuous parts of the EEG recording.

Based on the same metric Line Length, we developed an accurate burst and IBI detection algorithm (Koolen et al. 2014b). All interburst intervals are extracted from the full EEG recording.

5.2.4 Statistical analyses

The mean and the standard deviation (SD) of the suppression curve from each recording were calculated and correlated with postmenstrual age (regression analysis). An analysis of variance (ANOVA) was used to test whether changes in the mean or the SD of the SC were significant between subsequent age groups

and could be associated with PMA. The IBI 95th percentile was calculated for all recordings. This reflects the maximum IBI length, since the maximum IBI itself is too sensitive for outliers as it is just one single value (Victor et al. 2005a, Niemarkt et al. 2010). The median of the IBI 95th percentile was calculated for every age group.

5.3 Results

Twenty-five infants (mean GA 28w 5/7 (24w5/7-32w), birth weight 1277g (540g-2540g), F/M ratio 64%) with normal neurodevelopmental follow-up at a corrected age of 9 months were selected for further analysis. There is a wide range of illness severity in the study population. The demographics of the cohort and clinical details of the data are summarized in Appendix B, Table B.1. All infants underwent two to six EEG recordings, resulting in 90 recordings. There is variability in PMA, ranging from 27 weeks to 41 weeks. All infants had at least one EEG recording $<$ 34 weeks and one EEG recording at $\geq$ 36 weeks PMA. We defined 6 age groups according to postmenstrual age (PMA), covering two weeks difference in PMA age (see Figure 5.2 group 1: PMA $<$28 weeks PMA, group 2: 28-30 weeks PMA, group 3: 30-32 weeks PMA, group 4: 32-34 weeks PMA, group 5: 34-36 weeks PMA, group 6: $>$ 36 weeks PMA).

There is a clear overall decrease in mean SC values of all infant's recordings over the course of early development. As shown in Figure 5.3, there is a highly significant linear correlation between the mean SC and PMA till 34 weeks (r=-0.8 p=$3.5*10^{-12}$). Mean SC value is below 0.25 even in the smallest age group (26-28 weeks PMA). From 34 weeks onwards, mean SC was below 0.05, reflecting the presence of more continuous EEG (Figure 5.2).

The largest developmental change in EEG discontinuity is observed around 30 weeks (boxplots of the mean SC: median value for 28-30 weeks: 0.17, 30-32 weeks: 0.10 and 32-34 weeks: 0.05, ANOVA p $<$0.05, all groups ANOVA p= $1.2*10^{-22}$) (Figure 5.2b). When maturing, a more cyclic pattern is seen in the SC, representing alternating continuous and discontinuous EEG (Figure 5.3a-d). However, near term age, difference between discontinuous EEG and continuous EEG became smaller in the SC. This is represented in the decrease of the standard deviations of the SC as depicted in Figure 5.2c (all groups ANOVA p= $7*10^{-9}$). The largest differences were found around 32 weeks PMA and 36 weeks PMA (p$<$ 0.05).

The overall decrease in discontinuity is further reflected in the evolution of the interburst intervals. The IBI 95th percentiles decreased with advancing postmenstrual age (r= -0.82, p$<$0.001) (Figure 5.4a). The median IBI 95th

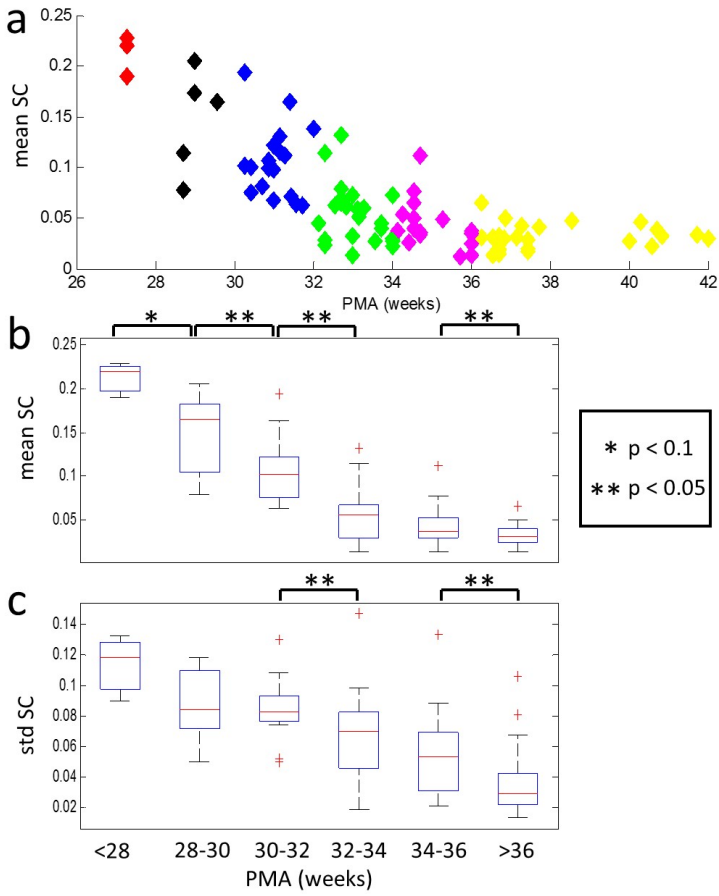

Figure 5.2: The overall decrease in mean SC values of 90 multichannel EEG recordings over the course of early development. (a) We defined 6 age groups according to postmenstrual age (PMA), covering two weeks difference in PMA age (red: PMA <28 weeks PMA, black: 28-30 weeks PMA, blue: 30-32 weeks PMA, green: 32-34 weeks PMA, pink: 34-36 weeks PMA, yellow: > 36 weeks PMA). (b) Boxplots representing the developmental changes of the mean SC over the different PMA groups. (c) Boxplots representing the developmental changes of the standard deviation of the SC over the different PMA groups.

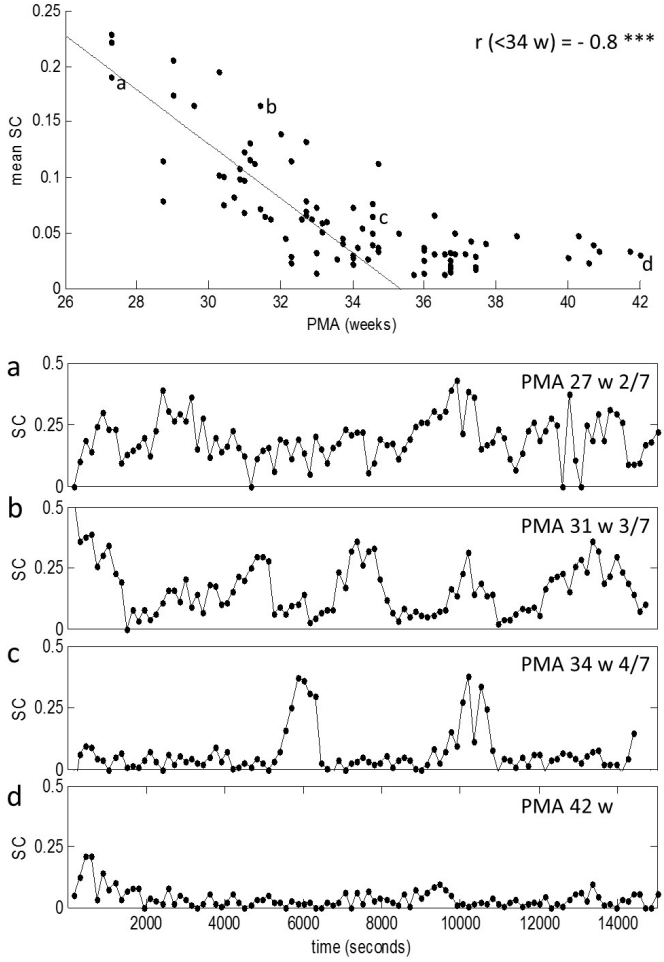

Figure 5.3: The decrease in mean SC value over the course of early development. There is a linear correlation between the mean SC and PMA till 34 weeks (r= -0.8, p=3.5∗10^{-12}). (a-d) The suppression curve from 4 hours multichannel EEG recording at different PMA in one patient. (a) High suppression values represent mainly discontinuous EEG. (b-c) When maturing, a more cyclic pattern is seen in the SC, representing alternating continuous and discontinuous EEG. (d) At term age, difference between discontinuous EEG and continuous EEG became smaller in the SC.

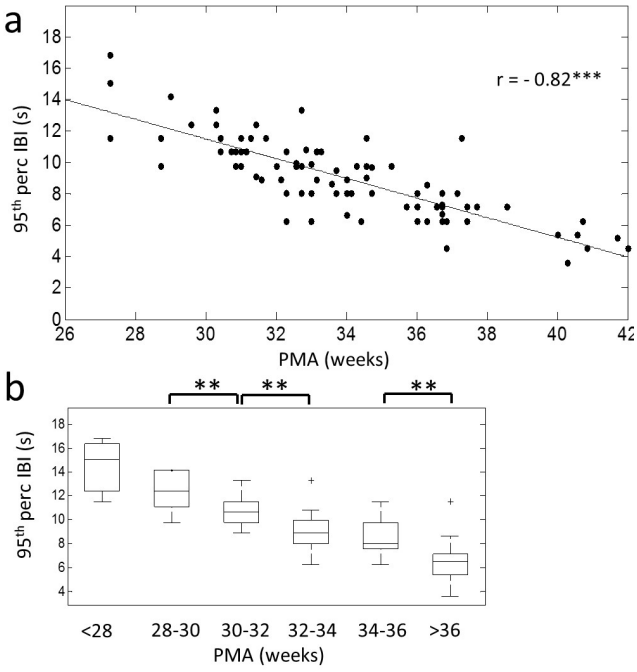

Figure 5.4: The IBI 95th percentiles of 90 multichannel EEG recordings, performed in 25 preterm infants. (a) The IBI 95th percentiles decrease with advancing postmenstrual age (r= -0.82, p<0.001). (b) Boxplots representing the 95th percentile over the different PMA groups. The median IBI 95th percentile group values are as follows: (<28 weeks PMA) 15.1s, (28-30 weeks PMA) 12.4s, (30-32 weeks PMA) 10.7s, (32-34 weeks PMA) 8.9s, (34-36 weeks PMA) 8.0s, (>36 weeks PMA) 6.5s.

percentile group values are as follows: (<28 weeks PMA) 15.1s, (28-30 weeks PMA) 12.4s, (30-32 weeks PMA) 10.7s, (32-34 weeks PMA) 8.9s, (34-36 weeks PMA) 8.0s, (>36 weeks PMA) 6.5s (Figure 5.4b).

Four EEG recordings had higher mean SC values as compared with the group results. These results were affected by reduction in EEG data (2.5 to 3h instead of 4h, stopped after second QS period), with relatively more discontinuous EEG (Figure 5.2b and Figure 5.5).

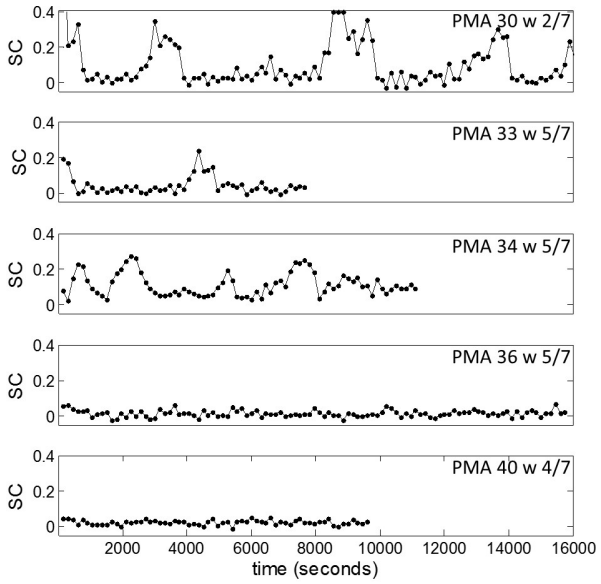

Figure 5.5: The suppression curve of one patient at different PMA with variable EEG recording times. Mean SC values can be influenced by recording time.

5.4 Discussion

Assessment of consecutive multichannel EEG of preterm infants without major brain lesions who develop normally, is generally accepted as the closest approximation of normal brain maturation (Hellström-Westas & Rosén 2005, Victor et al. 2005a, André et al. 2010, Niemarkt et al. 2010). This study shows that automated analysis of the 'level of discontinuity', an important marker of brain maturation in preterm multichannel EEG, is feasible with the suppression curve. Moreover, this study is clinically relevant as it adds automated, objective and normative values of interburst intervals at different postmenstrual ages, considered as a valuable prognostic feature in the literature (Holmes & Lombroso 1993, Menache et al. 2002, Vecchierini et al. 2003, Wikström et al. 2012).

This work extends prior work as no other studies used automated analysis on multichannel EEG records to describe the maturational trend of EEG discontinuity. Niemarkt et al. (2010) assessed brain maturation based on automated analysis of a single channel. Although single channel EEG is easier to analyse, algorithm performance may not be a realistic estimate of its expected performance on multichannel EEG recordings (Jennekens et al. 2011, Koolen

et al. 2014b, Murphy et al. 2014). Furthermore, quantitative definitions of burst and interburst intervals differ in the literature, however IBIs in EEG are mostly defined as inactivity in more than one channel (Victor et al. 2005a, Biagioni et al. 2007, André et al. 2010). As proven by Kato et al. (2011), the evaluation of brain maturation was much more accurate on continuous, multichannel EEG than on amplitude-integrated EEG (aEEG) based on one or two channels.

This study demonstrates that the highest decrease in the suppression curve is before 30-32 weeks PMA, reflecting the overall discontinuous EEG activity typically observed in preterm ages of 24-30 weeks PMA (Scher 1996, Vecchierini et al. 2003, André et al. 2010). As the preterm infant matures, differences between discontinuous EEG and continuous EEG become smaller, which is reflected by the decrease of the standard deviation of the SC. These observations include more continuous tracing, shorter suppressions (IBIs) in the discontinuous EEG periods, and less amplitude difference between different EEG periods. These early changes in EEG continuity reflect functional brain maturation with maturing of different vigilance states as sleep and wakefulness. Interburst intervals of respectively 8 and 6 seconds from 34 weeks onwards, together with less amplitude differences between continuous and discontinuous EEG at 36 weeks, reflect the transition to tracé alternant in quiet sleep. All these findings from the fully automated, objective suppression curve measures are in line with the visual interpretation of normal premature and neonatal EEG, associated with good neurodevelopmental outcome reported in literature (Holmes & Lombroso 1993, Scher et al. 2005b, Wikström et al. 2012, Shellhaas et al. 2014).

The strength of this method is its good performance at different age groups (Murphy et al. 2014). In addition, the present study is an extra validation of our algorithm presented in previous work in a different preterm cohort (Koolen et al. 2014b). Previous data set included infants with confounding conditions such as suspected seizures or intracranial haemorrhage, representing potentially more suppressed EEG patterns. For this study, we applied strict selection criteria, resulting in a small cohort. However, this study population is clinically representative due to a wide range of illness severity in the cohort.

Another major advantage of this method is that the technical applicability of this method is straightforward since no preprocessing or artefact removal is applied on these signals, such as published by (De Vos et al. 2011). This may facilitate further work to implement the algorithm on larger datasets in clinical NICU settings.

There are some technical and methodological considerations that may limit the accuracy of this study. First, two technical considerations: EEG recordings containing repetitive artefacts will result in lower SC values as expected for age. The SC allows more global assessment by integrating over longer time periods,

however it relies on continuous temporal behavior, such as vigilance state cyclicity, which is another challenge to handle (Iyer et al. 2015). Fluctuations of brain state can alter mean SC value. We found higher mean SC values in 4 EEG recordings which had EEG data reduced in time due to measurement conditions. In these infants, EEG was interrupted promptly with relatively more discontinuous EEG (Figure 5.5). Therefore, EEG epochs should be long enough and of the same duration to overcome technical artefacts and subtle differences in vigilance state. Hence, one can speculate that consecutive measurements will overcome these shortcomings as the global maturational trend of intra-patient development is more important.

Second, we correlated mean SC only with PMA and not with GA or other confounding factors (e.g. intrauterine growth restriction) (Niemarkt et al. 2010, Yerushalmy-Feler et al. 2014). Preterm EEG patterns may change as a function of gestational age and postmenstrual age. Changes in EEG discontinuity are most pronounced before 34 weeks, as shown in the results. As a consequence, there may be some variability in mean SC on a certain PMA due to GA. However, electro-cortical and anatomical maturation in 'healthy' preterm infants can be estimated within ± 2 weeks PMA (Biagioni et al. 2007, André et al. 2010, Kato et al. 2011) We assume to find no deviations more than two weeks due to GA, since all infants under study had normal developmental outcome. Recent reports show that EEG dynamics changes substantially over the first 72h after birth (Victor et al. 2005a, West et al. 2006, Schumacher et al. 2014). In this study, EEG measurements were performed after the first 72h in order to have stable brain dynamics at the respective age groups.

Although most prior studies have focused on predicting long-term neurodevelopment based on measuring different features of brain activity during the first 72h of life, other studies have correlated EEG maturation with neurodevelopmental outcome (Hayashi-Kurahashi et al. 2012, Le Bihannic et al. 2012). However, there is still no consensus in the literature which age is the correct moment to assess 'abnormal brain maturation'. As early brain activity relates to subsequent brain growth (Benders et al. 2014), differences in preterm brain maturation, measured with mean SC slopes, may reflect altered brain organization. Further studies are warranted to test whether this is a potential feature for predicting neurodevelopmental outcome with longer follow-up data. Potential value of this method is its usefulness in EEG which represent various changes in infant alertness. Further work may include to test how endogenous (brain lesions, intrauterine growth restriction) and exogenous (medication, kangaroo care) factors may influence the suppression curve (Figure 5.6).

To conclude, this detection algorithm improves the expertise and time consuming EEG assessment in preterm infants. Promising maturational features (IBI and burst characteristics, interhemispheric synchrony (Koolen et al. 2014c) are

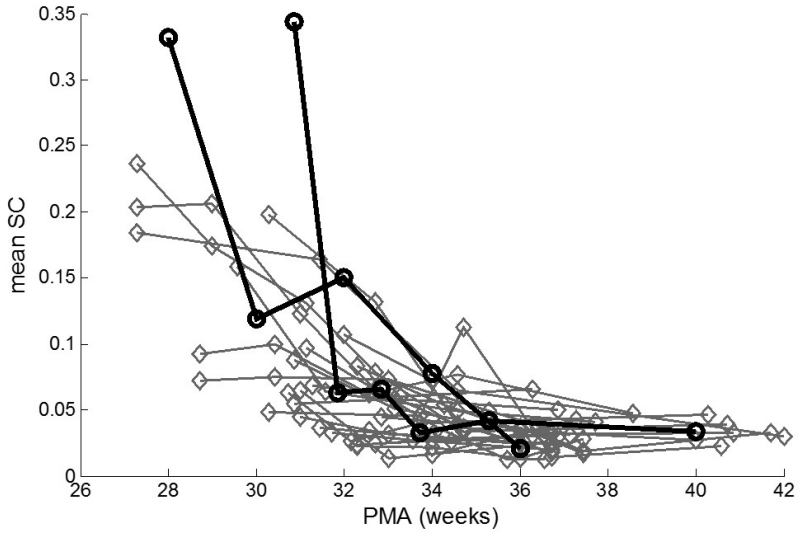

Figure 5.6: Future work could focus on neurotherapeutic treatments. For example, the suppression curve of two patients (black) is influenced by receiving fentanyl during the first EEG recording. Higher suppression curve values represent more discontinuous or suppressed EEG. Mean SC value is below 0.25 in preterm infants without sedative drugs (gray), even in the smallest age group (26-28 weeks PMA). In addition, intra-patient follow-up with multiple EEG recordings is possible. The follow-up curves of the presented population is shown by grey curves.

extracted from the most discontinuous periods. Hence, detection of these discontinuous periods by using the suppression curve opens the way for further automated assessment of EEG maturation. Automated detection of normative values of interburst intervals can facilitate clinical practice.

Acknowledgements

Research supported by FWO, IWT: A. Dereymaeker supported by IWT PhD grant: TBM 110697-NeoGuard; N. Koolen supported by IWT PhD grant 111480. Research supported by Research Council KUL: GOA/10/09 MaNet, CoE PFV/10/002 (OPTEC); BELSPO: IUAP P7/19/ (DYSCO, 2012-2017), ERC Advanced Grant, n° 339804 BIOTENSORS.

Chapter 6

Data-driven metric representing the maturation of preterm EEG

Ninah Koolen[1,2], Anneleen Dereymaeker[3], Okko Räsänen[4], Katrien Jansen[3], Jan Vervisch[3], Vladimir Matic[1,2], Maarten De Vos[5], Gunnar Naulaers[3], Sabine Van Huffel[1,2], Sampsa Vanhatalo[6]

[1] Division STADIUS, Department of Electrical Engineering (ESAT), University of Leuven, Leuven, Belgium

[2] iMinds-KU Leuven Medical IT Department, Leuven, Belgium

[3] Department of Development and Regeneration, University of Leuven, Leuven, Belgium

[4] Department of Signal Processing and Acoustics, Aalto University, Espoo, Finland

[5] Institute of Biomedical Engineering, Department of Engineering Science, University of Oxford, Oxford, UK

[6] BABA center and Department of Children's Clinical Neurophysiology, HUS Medical Imaging Center and Children's Hospital, Helsinki University Central Hospital and University of Helsinki, Helsinki, Finland

As adapted from *Proceedings of the 37th Annual International Conference of the IEEE EMBS*, Milan, Italy, pp., Aug. 2015

Abstract

Essential information about early brain maturation can be retrieved from the preterm human electroencephalogram (EEG). This study proposes a new set of quantitative features that correlate with early maturation. We exploit the known early trend in EEG content from intermittent to continuous activity, which changes the line length content of the EEG. The developmental shift can be captured in the line length histogram, which we use to obtain 28 features; 20 histogram bins and 8 other statistical measurements. Using the mutual information, we select 6 features with high correlation to the infant's age. This subset appears promising to detect deviances from normal brain maturation. The presented data-driven index holds promise for developing into a computational EEG index of maturation that is highly needed for overall assessment in the Neonatal Intensive Care Units.

6.1 Introduction

Premature babies are at high risk to develop mental or physical disabilities. Electroencephalogram (EEG) allows early diagnostics of neurological disorders, and a means for monitoring maturation of the preterm brain. However, the conventional clinical EEG inspection by visual reading is subjective, variable and time-consuming, which calls for development of automated and objective tools in EEG assessment. Due to the recent shift in attention in neonatal care from cardiorespiratory functions to neurological care, there has been a rapidly increasing need to incorporate EEG assessment into neonatal intensive care units, especially when supported by automated quantification methods that adapt to different maturational stages. Some EEG features are developed and used in the hospital environment (André et al. 2010).

Diagnosis of premature neurological adversities and hence, prognosis of neurological outcome is based on the information in the background EEG activity. The amount of EEG activity changes parallel to brain maturation which is reflected in both amplitude and frequency content (Vanhatalo & Kaila 2006, Tolonen et al. 2007, André et al. 2010). Specific patterns related to the postmenstrual age (PMA) are observed: normal maturation is characterized by an initially very discontinuous pattern that evolves into a more continuous pattern towards term age. In the intermittent pattern, also known as discontinuous pattern, very low voltage EEG is interrupted by high frequency bursts of activity, and the maturation of the baby is reflected as an increase in amplitude content during low voltage intervals (a.k.a. interburst

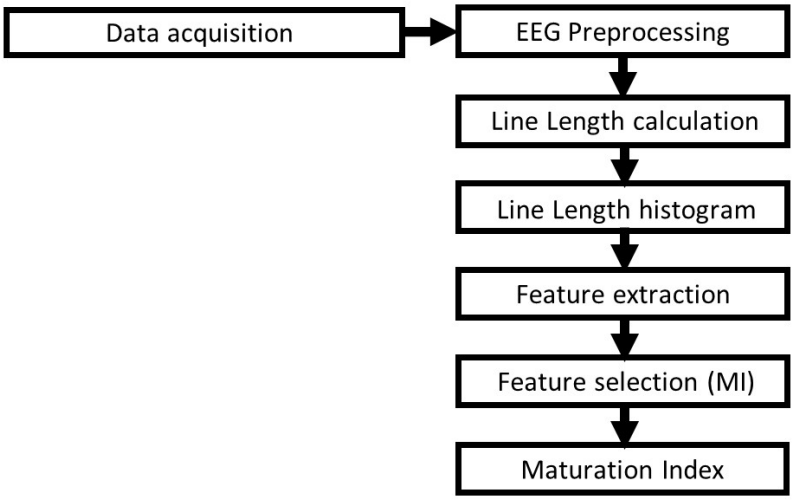

Figure 6.1: A schematic overview of the presented method.

intervals). Adverse neurodevelopmental outcome is often related to very low early activity, seen as long low-voltage periods (Biagioni et al. 1994, Le Bihannic et al. 2012, Benders et al. 2014). For that reason, recent studies have focused on detection of the high-activity bursts (Palmu et al. 2010b, Jennekens et al. 2011, Koolen et al. 2014b, Murphy et al. 2014) to be used for subsequent quantitative indices. Notably, no gold standard describing this specific EEG event is available, so the detection algorithms are commonly compared to multiple clinical raters (Palmu et al. 2010a), but no larger scale validation or systematic comparisons have been published. To circumvent the challenges inherent to event detection, we propose a more data-driven feature that is able to index the maturation by exploiting the raw statistical properties of the feature line length that we had previously used for the purpose of burst detection (Koolen et al. 2014b). A schematic overview of the presented method can be found in Figure 6.1.

6.2 Methodology

6.2.1 Data Acquisition

EEG signals were recorded at eight standard electrode locations (Fp1, Fp2, C3, C4, T3, T4, O1, O2) and reference electrode placed at Cz, with OSG

equipment (Rumst, Belgium). The sampling frequency was 250 Hz. The data set included 22 patients. They all had 2 to 6 subsequent recordings in order to see maturational brain processes, with on average two weeks in between the recordings, which gave in total 84 EEG recordings. They had a median postmenstrual age of 33.57 weeks (27-40 weeks). The protocol was approved by the ethics committee of the University Hospitals of Leuven, Belgium. First, a pre-processing step is performed; a 50 and 100 Notch filter and a 1-20 Hz band pass filter are applied before visual selection of two hours of EEG without major artefacts. Two hours long EEG epochs were used to include different sleep states that minimizes bias due to differences in histograms between them.

6.2.2 Line Length Calculation

Line length (LL) is a simplified form of the fractal dimension, reflecting the complexity of the signal. The more signal activity, the more of the time-amplitude plane is covered, and as a consequence the line length will increase. The line length is the running absolute sum between samples j in 1 second segments i, with sampling frequency 250 Hz (formula 6.1).

$$L_i = \sum_{j=1}^{250-1} |x_{j+1} - x_j| \tag{6.1}$$

Every 2.5 minutes, LLs are normalized by the total sum of LLs in that window, to average out baseline effects (Koolen et al. 2014b). For every single channel, we calculate the LL for the whole 2 hours of EEG recording.

LL will have large values for active periods as can be seen in continuous EEG patterns (Figure 6.2A). In contrast, in the discontinuous pattern both small values (inactive periods) and large values (bursts) for LL are found (Figure 6.2B). In a next step, we take the decimal logarithm of the LL curve to enlarge differences between small and large LL values.

6.2.3 Histogram Distribution

We decide to graphically summarize the distributions in histograms in order to capture the information about the log LL distributions at different ages. We calculate a histogram of log LLs with 20 predefined centers of the histogram bins [-3.1:0.1:-1.2]. In that way, we can compare the patients among each other to discover a shift in EEG content in function of the PMA. The number of data points in each bin has been used for describing this shift in the

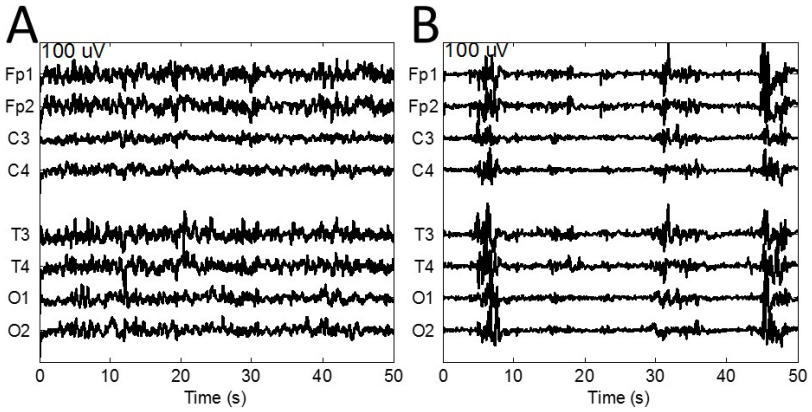

Figure 6.2: A. Example of continuous EEG pattern, B. Example of discontinuous EEG pattern.

histogram distribution. In addition, we added several statistical measurements to characterize the LL histogram: mean, median, standard deviation, interquartile range, skewness, kurtosis and the 5th and 95th percentile values. We assume that rare outliers with long LL will not significantly influence the shape of the histogram.

6.2.4 Feature Relevance

After observing several developmental correlations between our features and the postmenstrual age, we were interested in exploring systematically whether each single feature could be used as a maturational feature. To measure the dependence between two variables (PMA and feature), we can use the correlation function or the mutual information (MI). However, we decide to continue using the MI (formula 6.2), since it is well known that the MI captures the general dependence, while the correlation function estimates the linear dependence (Li 1990).

Amplitudes of the features and age values are quantized first in 8 quantization levels, after which the joint and individual probabilities of the amplitude levels are calculated. The MI is relative to the ratio of joint over individual probabilities, in which a_i is always the age and a_j the histogram-based signal feature.

$$MI(a_i, a_j) = \sum_{i,j} p(a_i, a_j) log_2 \left(\frac{p(a_i, a_j)}{p(a_i)p(a_j)} \right) \tag{6.2}$$

6.3 Results and Discussion

Since no objective gold standard exists for correlating EEG to postmenstrual age, we decided to compare our data-driven features to postmenstrual age without further EEG correlations. The strength in our approach is that the method is fully ignorant to specific features or vigilance states. We do not preselect epochs or EEG events based on their intermittent features such as burst occurrence or length of interburst intervals.

6.3.1 Line Length Histogram Evolution

During early development, the EEG content transforms from a discontinuous pattern (where brain connections are still scarce and immature), towards a continuous active pattern (when brain connections are physically established). Line length catches their EEG reflections in a global way without being based on event detection. It is not necessary to pick up quick activity changes, though amplitude and frequency content is captured with the line length. As shown in Figure 6.3A, we can see that in 5 weeks' time the histogram has shifted towards the right side, which includes the longer line lengths. This means concretely, more bursting activity is present. The overall trend of this shift is represented in Figure 6.3B. For all 84 EEG selections (2 hours), the 28 defined features have been calculated in every channel. In certain histogram bins, we cannot find any maturation, whereas others correlate with the postmenstrual age, and hence parallel with brain development (Figure 6.3C). On the other side, we can describe the shape change with global measurements (Figure 6.3D). We see that the mean / median is increasing, which is analogously to our previous findings. The interquartile range is decreasing, which means that the EEG content is more concentrated in the same range of amplitudes and range of frequencies. The 95th percentile of the histogram is also found to correlate with maturation, however the change (shift to the left) in the histogram may be counterintuitive at first sight. This is made more understandable by the idea that the bursting activity in the young preterm infants is of very high amplitude. The amplitudes of the bursts typically decrease parallel to the maturation. However, it implies they will have higher entropy and random organization.

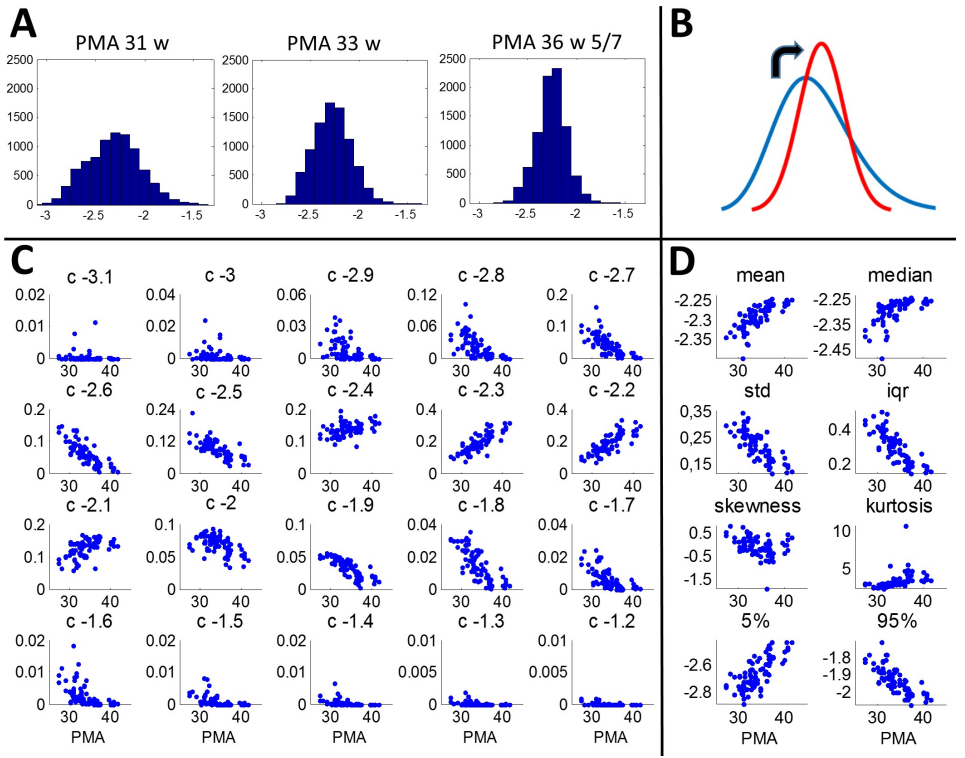

Figure 6.3: Concept of EEG content change by means of histogram change. A. Example histograms for one patient with 3 consecutive recordings, B. Schematic presentation of the trend change in the histogram shape, C. 20 defined bin heights (%) in function of the postmenstrual age (weeks) for channel C3, D. 8 defined statistical measurements in function of the postmenstrual age (weeks) for channel C3.

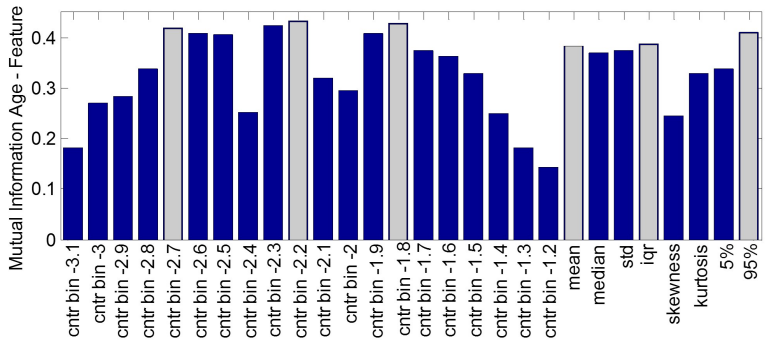

Figure 6.4: Feature relevance for maturation for the 28 predefined features. The grey features have been selected for further analysis.

6.3.2 Feature Relevance

The mutual information represents in a statistical way the relevance of the feature to predict the postmenstrual age. The information MI is zero if two variables are independent, and in case of strong dependence the MI is large. To build a maturational index, six relevant features have been selected based on the output of the feature relevance averaged over all EEG channels (Figure 6.4). The selection includes three bins with centers -2.7, -2.2 and -1.8 (two bins decreasing and the middle one increasing), and 3 global measures (mean, interquartile range and 95% percentile).

6.3.3 Accuracy

For each of the six most descriptive features, the mean linear fit is determined through all the data points. Next, the residual error is calculated for each of the data points, which is the deviation from this curve in vertical direction; PMA will not change. After normalization - necessary to compare the errors the different features - the residual errors are averaged over the six features and subsequently over the consecutive EEG recordings of the same patient. In a last step, we took the mean over Fp1-Fp2, C3-C4, T3-T4 and O1-O2, to extract significant information about the different brain regions. The results for each individual patient can be found in Table 6.1. Outliers (>0.015) are in bold. EEG maturation was not appropriate for age by clinical labelling in patient 4, 8 and 22 and mildly abnormal in patient 7 and 21. We can distinct clearly patient 8 and 22 based on this method. Patient 4 had a very abnormal first recording,

however, with a good maturational trend towards term age. This is confirmed in the individual analysis of the histograms. Patient 14 is an outlier. It could be explained by the fact that the 3rd EEG selection contains continuous active sleep parts and some longer periods of high voltage slow wave sleep (continuous EEG). Therefore, it looks 'more mature' than his actually 37 weeks PMA.

Table 6.1: Mean residual error using the 6 relevant features, averaged over the consecutive recordings for different regions of the brain.

	Region of the brain			
	Frontal	*Central*	*Temporal*	*Occipital*
PT 1	0,011	0,01	0,011	0,013
PT 2	0,015	0,008	0,01	0,013
PT 3	0,008	0,012	0,01	0,01
PT 4	0,012	0,013	0,013	0,012
PT 5	0,008	0,01	0,012	0,012
PT 6	0,01	0,011	0,011	0,011
PT 7	**0,017**	**0,016**	**0,017**	**0,015**
PT 8	**0,014**	**0,015**	**0,016**	**0,015**
PT 9	0,009	0,006	0,008	0,007
PT 10	0,014	0,013	0,014	0,011
PT 11	0,009	0,006	0,005	0,009
PT 12	0,014	0,012	0,01	0,01
PT 13	0,015	0,013	0,014	0,013
PT 14	**0,019**	**0,017**	**0,018**	**0,015**
PT 15	0,007	0,007	0,007	0,009
PT 16	0,008	0,014	0,013	0,008
PT 17	0,009	0,009	0,009	0,006
PT 18	0,007	0,007	0,005	0,008
PT 19	0,015	0,012	0,011	0,011
PT 20	0,011	0,011	0,01	0,009
PT 21	**0,011**	**0,016**	**0,014**	**0,018**
PT 22	**0,015**	**0,02**	**0,018**	**0,018**

This new maturational index can be used in addition to other known maturational features, like the lengths of the interburst intervals, bursts, synchrony and frequency parameters (Koolen et al. 2014b,c). In addition, we were able to reduce the number of electrodes while maintaining the diagnostic power, using only central electrodes.

6.4 Conclusion

The developed algorithm reveals an interesting maturational parameter, in addition to the traditional heuristic features, such as the bursts / interburst intervals and the synchrony. No preselection of data epochs is required if no major artefacts are present, which simplifies analysis procedure and removes one key subjective step in the preprocessing. Our method would also allow more global assessment by integrating over longer time periods, which would be challenging if not impossible to evaluate visually as is done in the conventional clinical EEG reading. In addition, our approach would allow objective and quantitative follow-up of the individual maturation over time, which opens a more sensitive means for discovering relative dysmaturity and/or neurological morbidities.

Our method was using linear regression to assess accuracy in developmental assessment, however future work with nonlinear regression with the postmenstrual age might provide better accuracy as suggested by the partly non-linear evolution of many of our features (see Figure 6.3C). The residual error is calculated over the sequential recordings, some information about a single record can be lost. Therefore, a closer look to the individual histograms can add some information. We also want to acknowledge that LL may be sensitive to the choice of filter settings, which could be optimized for the purpose as recently described (Palmu et al. 2010b). Furthermore, we want to combine the retrieved maturational indexes in an EEG premature growth chart. Confidence bands, related to normality, with polynomial regression models will be defined. The EEG grow chart composed with the help of computer-aided analysis will reduce the costs for the time-consuming clinical assessment. In this way, automated analysis would be of high value in the clinic.

Acknowledgements

Research supported by Research Council KUL: GOA/10/09 MaNet, CoE PFV/10/002 (OPTEC); PhD/Postdoc grants; Flemish Government: FWO, IWT: projects: TBM 110697-NeoGuard; PhD/Postdoc grants; Belgian Federal Science Policy Office: IUAP P7/19/ (DYSCO); EU: ERC Advanced Grant: BIOTENSORS (n. 339804).

Chapter 7

Development of an interhemispheric symmetry measurement in the neonatal brain

Ninah Koolen[1,2], Anneleen Dereymaeker [3], Katrien Jansen[3], Jan Vervisch[3], Vladimir Matic[1,2], Maarten De Vos[1,2,4], Gunnar Naulaers[5], Sabine Van Huffel[1,2]

[1] Department of Electrical Engineering (ESAT), division SCD, University of Leuven, Leuven, Belgium

[2] iMinds-KU Leuven Future Health Department, Leuven, Belgium

[3] Department of Pediatrics, University Hospital Gasthuisberg, Leuven, Belgium

[4] Department of Psychology, University of Oldenburg, Oldenburg, Germany

[5] Neonatal Intensive Care Unit, University Hospital Gasthuisberg, Leuven, Belgium

As adapted from *Proceedings of the International Conference on Pattern Recognition Applications and Methods (ICPRAM)*, Angers, France, pp. 765-770, Mar. 2014

Abstract

The automated analysis of the EEG pattern of the preterm newborn would be a valuable tool in the neonatal intensive care units for the prognosis of neurological development. The analysis of the (a)symmetry between the two hemispheres can provide useful information about neuronal dysfunction in early stages. Consecutive and subgroup analyses of different brain regions will allow detecting physiologic asymmetry versus pathologic asymmetry. This can improve the assessment of the long-term neurodevelopmental outcome. We show that pathological asymmetry can be measured and detected using the channel symmetry index, which comprises the difference in power spectral density of contralateral EEG signals. To distinguish pathological from physiological normal EEG patterns, we make use of one-class SVM classifiers.

Keywords

preterm brain, symmetry, channel symmetry index, spectral power, EEG, one-class SVM, classification

7.1 Introduction

Electroencephalogram (EEG) is a non-invasive and sensitive tool for assessing cerebral function in premature infants. The chronological changes in EEG background with increasing postconceptional age reflect the central nervous system maturation. Standard values of maturational features in premature EEG are already well described (Hellström-Westas & Rosén 2005, Vecchierini et al. 2007, Hayashi-Kurahashi et al. 2012, Le Bihannic et al. 2012). Chronic EEG background abnormalities are strongly associated with adverse neurological outcome in both preterm and full-term infants (Hellström-Westas et al. 2001, Okumura et al. 2002). These abnormal patterns must be scored and interpreted visually and, thus, subjectively. However, analyses and interpretation of multichannel neonatal EEG is difficult, requires expertise and is time consuming.

Therefore, objective criteria for the assessment of EEG abnormalities have to be established and automated background EEG analysis may contribute to reliable interpretation (Palmu et al. 2010a). In previous research, we have defined features that can be calculated for each time signal, in other words, for each EEG channel independently (Koolen et al. 2013). However, EEG is a multichannel measurement, and all too often this spatial dimension is ignored.

Spatial 'integration' is usually limited to concatenate the characteristics of different channels (Hunyadi et al. 2011). Here, we intend to exploit the available spatial information to quantify the interaction between the various areas of the brain using connectivity analysis. Such connectivity values can be highly relevant to make an accurate prognosis of the neurological outcome of the premature babies, since they are the mathematical quantification of the degree of connectivity between different brain regions. After all, it is commonly assumed that brain areas in very young babies are barely connected, and that during brain development through spontaneous interaction a sophisticated network is formed (Vanhatalo & Kaila 2006, Smyser et al. 2010). In this paper, the interhemispheric symmetry is examined: can we detect pathological asymmetry in electrophysiological activity between two hemispheres.

Interhemispheric asymmetry in premature infants is defined as a persistent amplitude difference of 50% over homologous areas in one hemisphere and must be persistent to all behavioural states to be significant (Holmes & Lombroso 1993). In addition, abnormalities can be extracted from a difference in the power of the frequency domain. This abnormality in background pattern is frequently associated with lateralized pathology such as an underlying anatomical or acquired brain lesion (e.g. intraparenchymal haemorrhage, stroke, ischemic insults and congenital brain malformations) (Holmes & Lombroso 1993, van Putten & Tavy 2004).

Automated interhemispheric symmetry analysis in preterm and term infants can be a valuable tool to detect neuronal dysfunction in early stages. Consecutive and subgroup analyses of different brain regions (as detected in frontal, central, temporal and occipital electrophysiological activity) will allow detecting physiologic asymmetry versus pathologic asymmetry. Correlation of this pattern with long–term neurodevelopmental outcome has to be defined.

In order to detect those abnormal patterns in a classification process, we will use the channel symmetry index (CSI) (Hunyadi et al. 2010). Both amplitude and frequency content are taken into account, since the CSI is based on the difference in the power spectral bands of the contralateral channels. Derived features from the CSI curves will serve as input for the classification. Due to an unbalanced dataset, we will make use of a one class Support Vector Machine (SVM) (Schölkopf et al. 2000, 2001).

7.2 Data acquisition

The proposed method is tested on EEG measurements, obtained with OSG equipment (OSG, Belgium). The purpose is to observe the symmetry between

different brain areas. Therefore, we use multi-channel or 'full' EEG taken at 9 electrode locations (Fp1, Fp2, T3, T4, C3, C4, Cz, O1, O2). The sampling frequency is 250 Hz. The dataset contains EEG recordings of 47 newborns, born at a postmenstrual age (PMA) of 24-40 weeks, including patients with structural brain abnormalities (acquired or congenital) and clinical convulsions. To assess brain maturation, 20 preterm infants had several EEG measurements at consecutive moments with increasing PMA. This resulted in a total of 92 EEG measurements. In this way, we scored physiologic brain symmetry in the developing premature brain. On the other hand, we scored brain symmetry in both preterm and term infants with pathologic conditions. Data containing artefacts (>30% of the whole measurement) were excluded from this study. Contralateral signal pairs were excluded in case that one electrode was disturbed. However, not the whole EEG (8 channels) was excluded. The data was labelled into two categories: pathologic asymmetry and physiologic normal symmetry. The protocol was approved by the ethics committee of the University Hospitals of Leuven, Belgium. A pre-processing step including a 50 and 100 Hz Notch filter and a 1-20 Hz band pass filter was applied on the data.

7.3 Methodology

7.3.1 Channel Symmetry Index

First, we investigate detecting asymmetry between different EEG channels based on a feature called *channel symmetry index* (CSI) (Hunyadi et al. 2010). This feature is defined as the power asymmetry in predefined frequency bands and is calculated between two contralateral channel pairs presented in formula 7.1 (O1 vs. O2, C3 vs. C4, T3 vs. T4, Fp1 vs. Fp2).

$$CSI(ch, F) = \sum_{f=F_{min}}^{F_{max}} \frac{|PSD_{f,ch} - PSD_{f,opp}|}{PSD_{f,ch} + PSD_{f,opp}} \tag{7.1}$$

where *ch* is a chosen EEG channel and *opp* its contralateral channel as can be found in Figure 7.1.

The selected frequency bands correspond to the clinically relevant frequencies to monitor brain activity: delta band (1-4 Hz), theta band (4-8 Hz), alpha band (8-13 Hz) and beta band (13-21 Hz). A CSI value is calculated for each 150 seconds of the EEG measurement, for each channel pair and each frequency band. A mean value is obtained by averaging the CSI values of the different

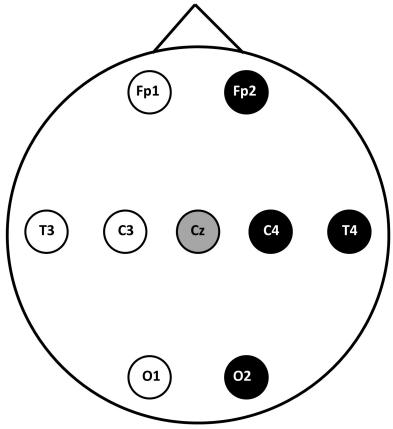

Figure 7.1: Electrode placements for 9 channel EEG measurement, contralateral channels are given in white-black (O1-O2, C3-C4, T3-T4, Fp1-Fp2)

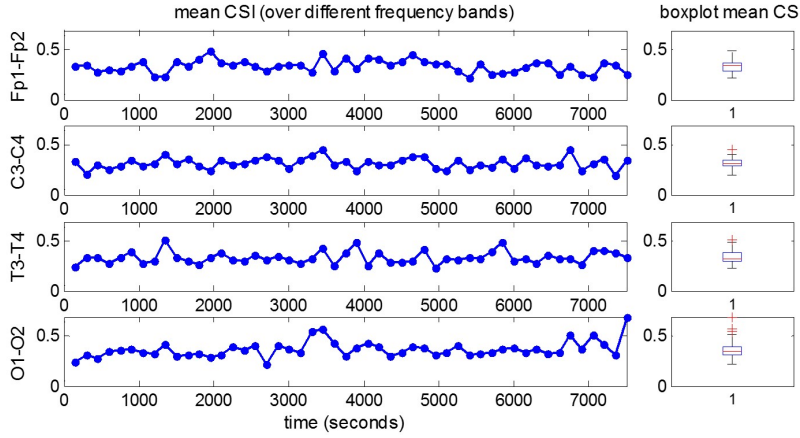

Figure 7.2: a. mean CSI values, averaged over frequency bands, shown for different channel pairs; b. box plot mean CSI.

frequency bands (Figure 7.2 a). Subsequently, a patient specific box plot of these values over the whole EEG measurement is determined (Figure 7.2 b).

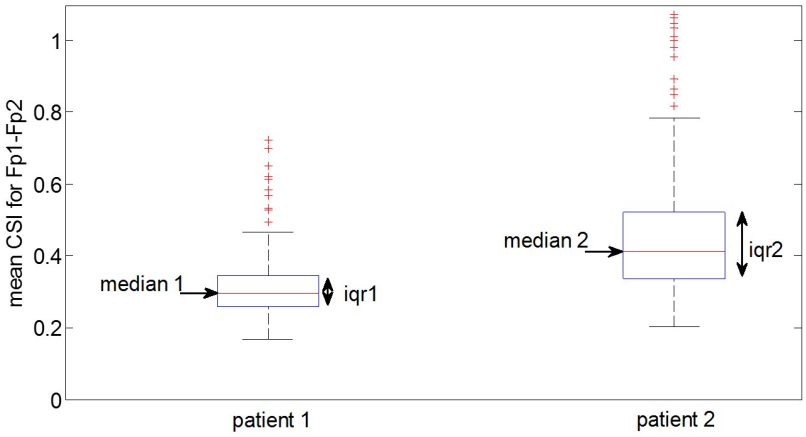

Figure 7.3: Different features for a normal patient (patient 1) and a patient with hemimegalencephaly-haemorrhage (patient 2), measurements taken at comparable PMA.

7.3.2 Outcome dependent features

For classification, we need features to distinguish normal and abnormal EEG patterns. Based on the box plots (Figure 7.3), we have worked with four features:

- Median box plot
- Interquartile range (iqr) of the box plot: a statistical measurement to describe the spread of the data. iqr is calculated as the difference between the upper and the lower quartiles. This feature is similar to the range, although it is less sensitive to outliers, e.g. the movement of an electrode.
- Standard deviation (std) of the boxplot: variation from the average.
- Postmenstrual age (PMA): brain maturation may have an influence on the median of the box plot. The hemispheres connection is still developing.

7.3.3 One-class SVM classification

A simple threshold on the median value of the patient box plots is not sensitive enough, leading to a lot of false positive detections. Therefore, we need to

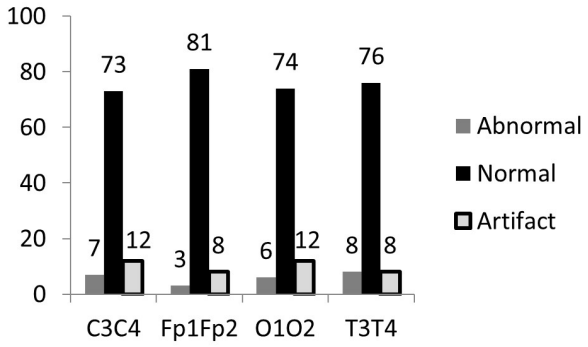

Figure 7.4: Number of normal/abnormal patients, number of data excluded for analysis since artefacts are present in the data.

incorporate the different features into a more complex classification system. Here, a classifier is constructed and trained for every channel pair, resulting in four classifiers. Unfortunately, one classifier incorporating all features is not enough, since pathologies can result in lateralization of only one region of the brain. This means, the hemisphere's symmetry elsewhere in the brain can be normal compared to patients of similar age. In addition, there is a huge imbalance between the number of normal and abnormal classes (Figure 7.4).

For this purpose, one-class SVM classifiers are applied. It will give the value +1 in a small region capturing the pathological class and -1 for all other data points (normal class). The data is mapped in the feature space corresponding to the radial basis kernel function and to separate them from the origin with maximum margin (Schölkopf et al. 2000). On which side of the hyperplane a new point will fall in feature space, will decide to which class this point will belong.

The quadratic problem to separate the data from the origin is solved (Scholkopf, 2001):

$$min_{w\in F,\varepsilon\in\mathbb{R}^l,\rho\in\mathbb{R}} \ \frac{1}{2}\left\|w\right\|^2 + \frac{1}{\nu^l}\sum_i \varepsilon_i - \rho \tag{7.2}$$

$$\text{subject to } (w\cdot\phi(x_i)) \geq \rho - \varepsilon_i,\ \varepsilon_i > 0 \tag{7.3}$$

Here, w and ρ are a weight vector and an offset to parameterize the hyperplane in feature space associated with the kernel (Schölkopf et al. 2000). Outliers are those points defined as points on the wrong side of the hyperplane (within

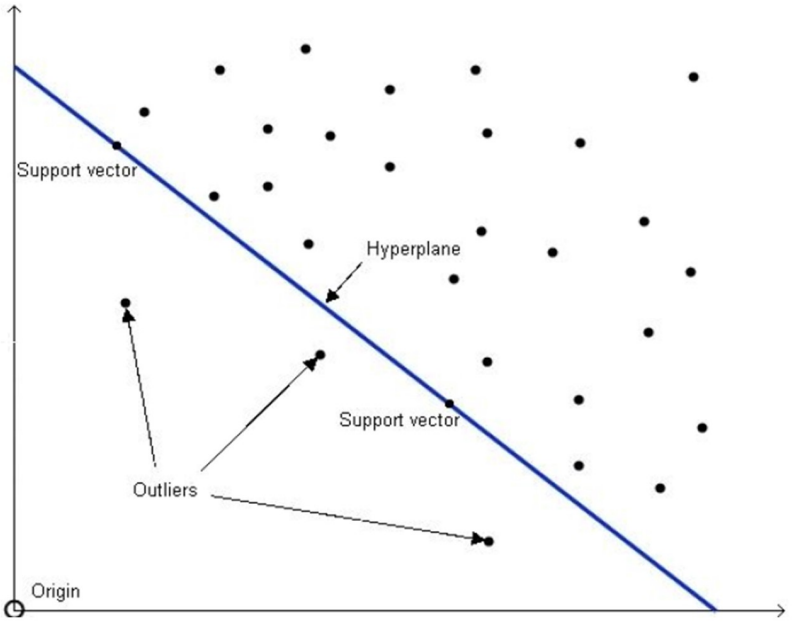

Figure 7.5: Principle of the quadratic problem of the one-class SVM (Fourie et al. 2011).

margin of the origin). ε_i are the outlier distances from the hyperplane (Figure 7.5).

In order to choose the best subset of model parameters, we have trained the hyper parameters of this classifier, namely ν and γ. ν is an upper bound on the fraction of training errors and a lower bound of the fraction of support vectors. When ν decreases, a misclassification will have a large impact on the objective. This can also result in overfitting of the data. First, ν is adapted from 0.05 to 0.2 in steps of 0.05, since it resembles how many outliers can be without the class. For the data (Figure 7.4), this is a percentage of around 10% for each group. γ is constrained to a default value by 1/number_features=0.25 (Chang & Lin 2011).

As we applied the RBF kernel, γ represents the width of the Gaussian kernel, representing the boundary to catch all the training data within the class. Therefore, in a next step ν and γ are adjusted simultaneously to find the optimal set of hyper parameters. ν (range 0.05 to 0.2) is adapted in steps of 0.05 and γ (range 0.1 to 0.7) in steps of 0.15.

We made use of leave-one-out 10-fold cross-validation (loo-cv) to optimize the model parameters. Thereby, a comparison of the accuracies of the models built on each subset is carried out. Due to the small sample at disposal, a result in terms of best loo-cv error is presented here, as a (necessarily small) test set would not be very informative. Moreover, within a small test set there is necessarily huge variability. The loo-cv error is called the specificity of the model (true negative rate). After the model is trained, we can define the sensitivity as the true positive rate. That is, the number of abnormalities correctly classified by the SVM model as abnormal.

7.4 Results and Discussion

Results of the optimization of the four one-class SVM classifiers are shown in Table 7.1. For the C3C4 classifier, $\nu = 0.15$ is chosen to be the optimal value. For the other 3 classifiers, $\nu = 0.1$ gives the highest sensitivity and specificity. Grid search for optimal combination of γ and ν by adapting them simultaneously resulted in the same optimal value for the model parameter γ (=0.25). Due to the relatively small sample size, both high sensitivity and specificity are difficult to obtain. Therefore, we set the minimum specificity on 70%, considering that not too many false alarms can be given in case there is no pathological pattern.

We want to emphasize that we want to detect patients with lateralized lesions; cases confirmed by clinical doctors through lesion(s) on MRI images. For example, lateralized lesions can be hemimegalencephaly or cases with convulsions. These cases were found by all four optimized one-class SVM classifiers. However, there are still some false negatives in the C3C4 classifier and T3T4 classifier. That is, there exists always three false negatives for the T3T4 classifier; abnormal patterns which are not detected (Table 7.1). Two of these false negatives are not detected by most T3T4 classifiers. An explanation could be that one patient has corpus collosum agenese, what affects more the asynchrony instead of the asymmetry. The other false negative has mainly asymmetry in only one frequency band (theta), which is presumably not picked up by the classifier as we work with the average over the different frequency bands (CSI). In fact, clinical doctors visually detected the lesion on the other hemisphere on the MRI than they did on the EEG measurement, indicating it is hard to specify the lateralization. In addition, one patient with pathologic asymmetry is never detected by the C3C4 classifier. The pathologic EEG pattern, comparing the C3 and the C4 channel, is very short compared to the length of the whole measurement. Moreover, the lesion is located in the thalamus (=sub cortical),

which is less pronounced in the cortical EEG signals. Overall, the Fp1Fp2 and the O1O2 classifiers are performing well, all pathologies are detected.

In future, other classification models can be applied to this problem, which also take the imbalance between classes into account. For example, weighted least squares-support vector machines (LS-SVM) can be trained (Cawley 2006). In general, weighted loss functions are appropriate to balance the contribution of classes that are not equally represented. Nevertheless, further improvement of the applied one-class SVM model is possible by adding more features into the training phase. Thereby, we think of asymmetry defined in clinical papers; a ratio of amplitude difference. Another possibility is to search more localized in time, in case of convulsions, instead of calculating features over the whole EEG measurement. However, this will probably lead to a higher rate of false positive detections introduced by short-time artifacts. In addition, more patients will be incorporated in future to refine and tune the model. In this way, normal values for the channel symmetry indexes can be established, dependent on the physiologic maturation.

7.5 Conclusions

By applying the developed algorithm, we could successfully detect abnormal lateralized lesions in the neonatal brain. Based on non-invasive EEG measurements, we can extract useful features to distinguish physiological from pathological asymmetry. Therefore, we have used characteristics derived from the channel symmetry index as input features for a classifier. Moreover, automated assessment creates possibilities to look over a longer period of time in an objective way including the experience of clinical doctors. Future work will focus on fine-tuning the algorithm based on a larger dataset, adding clinically relevant features to the classifier, and trying out other weighted SVMs. Measuring and analyzing connectivity in the neonatal brain is of added value and high interest for the overall assessment in the Neonatal Intensive Care Units for EEG diagnosis.

Acknowledgements

I want to thank M. Signoretto, B. Hunyadi and M. Milosevic for their valuable discussions.

Research supported by
Research Council KUL: GOA MaNet, PFV/10/002 (OPTEC), several

Table 7.1: Specificity (%) of the four trained one-class SVMs with 10-fold cross-validation. Sensitivity (%) on detecting the abnormal EEG patterns. For this small sample, we would go for $\nu = 0.15$ in case of the C3C4 classifier and $\nu = 0.1$ for the three other classifiers.

	C3C4		**Fp1Fp2**		**O1O2**		**T3T4**	
ν	*spec*	*sens*	*spec*	*sens*	*spec*	*sens*	*spec*	*sens*
0.05	67.12	42.86 (3/7)	61. 72	66.67 (2/3)	74.32	100 (6/6)	64.47	62.5 (5/8)
0.1	71.23	57.14 (4/7)	**71.60**	**100 (3/3)**	**75.67**	**100 (6/6)**	**73.68**	**62.5 (5/8)**
0.15	**76.71**	**71.43 (5/7)**	67.9	66.67 (2/3)	75.67	100 (6/6)	68.42	62.5 (5/8)
0.2	68.49	85.71 (6/7)	66.67	66.67 (2/3)	68.92	83.33 (5/6)	61.84	62.5 (5/8)

PhD/postdoc & fellow grants;
Flemish Government: FWO: Postdoc grants, projects: G.0427.10N (Integrated EEG-fMRI), G.0108.11 (Compressed Sensing) G.0869.12N (Tumor imaging) G.0A5513N (Deep brain stimulation)
IWT: PhD grants, projects: TBM 070713-Accelero, TBM 080658-MRI (EEG-fMRI), TBM 110697-NeoGuard
iMinds: SBO dotatie 2013, ICONs: NXT_Sleep, FallRisk
Flanders Care: Demonstratieproject Tele-Rehab III (2012-2014)
Belgian Federal Science Policy Office: IUAP P719/ (DYSCO, 'Dynamical systems, control and optimization', 2012-2017); ESA AO-PGPF-01, PRODEX (CardioControl) C4000103224
EU: RECAP 209G within INTERREG IVB NWE programme, EU HIP Trial FP7-HEALTH/ 2007-2013 (nº 260777), EU MC ITN TRANSACT 2012 (nº 16679), ERC Advanced Grant: BIOTENSORS (nº 39804), ERASMUS EQR: Community service engineer (nº 539642-LLP-1-2013)

Chapter 8

Interhemispheric synchrony in the neonatal EEG revisited: Activation Synchrony Index as a promising classifier

Ninah Koolen[1,2,†], Anneleen Dereymaeker[3,†], Okko Räsänen[4], Katrien Jansen[3], Jan Vervisch[3], Vladimir Matic[1,2], Maarten De Vos[5,6], Sabine Van Huffel[1,2], Gunnar Naulaers[3], Sampsa Vanhatalo[7]

[1] Division STADIUS, Department of Electrical Engineering (ESAT), University of Leuven, Leuven, Belgium

[2] iMinds-KU Leuven Medical IT Department, Leuven, Belgium

[3] Department of Development and Regeneration, University of Leuven, Leuven, Belgium

[4] Department of Signal Processing and Acoustics, Aalto University, Espoo, Finland

[5] Department of Psychology, University of Oldenburg, Oldenburg, Germany

[6] Institute of Biomedical Engineering, Department of Engineering Science, University of Oxford, Oxford, UK

[7] Department of Children's Clinical Neurophysiology, HUS Medical Imaging Center and Children's Hospital, Helsinki University Central Hospital and University of Helsinki, Helsinki, Finland

[†] These authors are joint first authors.

As adapted from *Frontiers in Human Neuroscience*, vol. 8, art.nr. 1030, Dec. 2014

Abstract

A key feature of normal neonatal EEG at term age is interhemispheric synchrony (IHS), which refers to the temporal co-incidence of bursting across hemispheres during trace alternant EEG activity. The assessment of IHS in both clinical and scientific work relies on visual, qualitative EEG assessment without clearly quantifiable definitions. A quantitative measure, activation synchrony index (ASI), was recently shown to perform well as compared to visual assessments. The present study set out to test whether IHS is stable enough for clinical use, and whether it could be an objective feature of EEG normality.

We analyzed 31 neonatal EEG recordings that had been clinically classified as normal (n=14) or abnormal (n=17) using holistic, conventional visual criteria including amplitude, focal differences, qualitative synchrony, and focal abnormalities. We selected 20-minute epochs of discontinuous background pattern. ASI values were computed separately for different channel pair combinations and window lengths to define the optimal ASI intra-individual stability. Finally, ROC curves were computed to find trade-offs related to compromised data lengths, a common challenge in neonatal EEG studies.

Using the average of four consecutive 2.5-minute epochs in the centro-occipital bipolar derivations gave ASI estimates that very accurately distinguished babies clinically classified as normal vs. abnormal. It was even possible to draw a cut-off limit (ASI 3.6) which correctly classified the EEGs in 97% of all cases. Finally, we showed that compromising the length of EEG segments from 20 minutes to 5 minutes leads to increased variability in ASI-based classification.

Our findings support the prior literature that IHS is an important feature of normal neonatal brain function. We show that ASI may provide diagnostic value even at individual level, which strongly supports its use in prospective clinical studies on neonatal EEG as well as in the feature set of upcoming EEG classifiers.

Keywords

interhemispheric synchrony, biomarker, preterm infant, brain monitoring, neonatal EEG

8.1 Introduction

Recent progress in basic neuroscience, neuroimaging, and neonatal care has raised interest in the understanding of physiological and pathological processes in the preterm and neonatal brain. Electroencephalography (EEG) is a non-invasive and sensitive tool for evaluating brain function in the neonatal period. A key component in early brain functional development is the emergence of functional networks, the long range connectivity between and within brain hemispheres, which lay the basis for the development of neurocognitive capabilities (Grieve et al. 2008, Uhlhaas et al. 2010, Lubsen et al. 2011). In this context, it is intriguing that synchrony between hemispheres has been considered as an important feature of normal neonatal brain function since the seminal studies in the late 1970s (Lombroso 1979).

Clinical classification of spontaneous neonatal EEG is traditionally based on visual assessment of multiple features: continuity, quality of sleep wake organization, interhemispheric synchrony (IHS), symmetry and amplitude. However, visual EEG interpretation requires expertise, and there are no objective standards for classification schemes, nor any other established method to yield appropriate diagnostic accuracy to support modern neuroscience or evidence based medicine. This has greatly compromised comparisons of results between different studies. A quantitative analysis of EEG activity, including automated analysis of selected features of cortical function, could create an objective and appropriate classification scheme for neonatal EEG. Moreover, it could also support and accelerate visual EEG analyses in treatment units without access to highly skilled EEG interpretation.

Visual estimation of IHS is based on observation of co-incidence of bursts in spontaneous background EEG activity during tracé alternant/discontinue (Holmes & Lombroso 1993). IHS is interpreted as a sign of connectivity or functional interaction between hemispheres and is hence considered an important feature of normal brain function, resulting from the development of callosal connections (Kostović & Jovanov-Milosević 2006, Dudink et al. 2008).

Despite the long and widespread clinical use of IHS, there is no physiologically plausible definition of IHS for visual EEG reading (for more details, please see Räsänen et al. 2013). A quantitative measure for IHS, the activation synchrony index (ASI), was recently developed by Räsänen et al. 2013. The ASI is based on statistically measuring the temporal delay between two signal energies, and was shown to correlate with visually rated IHS grades. It was also shown to clearly outperform other methods proposed for the same purpose in the recent literature (Räsänen et al. 2013).

Our ultimate aim is to use ASI more widely as a clinical biomarker or as a feature in EEG classifiers, which poses special requirements for individual stability. In addition, the analysis settings such as the epoch lengths need to be practical with respect to clinical reality, where obtaining longer high quality epochs is often challenging due to intermittent, trivial artifacts. The aim of this study was to test the ability of the ASI to distinguish normal and abnormal neonatal EEG recordings. Therefore we first defined the optimal ASI parameters to maximize its intra-individual and technical stability, and then tested ASI as an input for a classifier to identify abnormal EEG activity.

8.2 Materials and methods

The present study consisted of two discrete phases (see Figure 8.1). First, we optimized the intra-individual stability of ASI. The earlier development of ASI had aimed to optimize parameter settings for maximal distinction between asynchrony grades as well as robustness against artefacts. Our present study continued ASI optimization by searching for EEG epoch lengths and channel derivations that would strike a balance between technical reliability and clinical practice. For clinical practice, an important consideration is that the algorithm should work equally well on EEG samples either with longer continuous epochs or with multiple shorter epochs. In addition, we tested our optimized ASI protocol on a new EEG dataset that had been classified using conventional clinical criteria, with the aim of seeing how well ASI alone is able to distinguish normal and abnormal EEG recordings. This latter aim is also a rigorous test of the conventional, albeit quantitatively untested assumption, that interhemispheric asynchrony would be an essential property in the abnormal EEG near term age.

8.2.1 Subjects and EEG recordings

A total of 31 neonatal EEG traces (postmenstrual age (PMA) 36-42 weeks), were retrospectively selected to assess the spontaneous background EEG activity (A.D.). These EEG recordings were collected from a larger EEG dataset, recorded for clinical purposes. All EEG data were recorded at 250 Hz with a video-synchronized EEG device (BRAIN RT, OSG equipment, Mechelen, Belgium). After skin preparation (Nuprep Gel), 10-17 Ag/AgCl cup electrodes were placed according to the international 10-20 standard locations. The reference electrode was Cz. Electrode impedance was below 10 kΩ at the start, and the signal quality was monitored visually throughout the recording. The minimum recording time was 4 hours to record multiple vigilance states. The

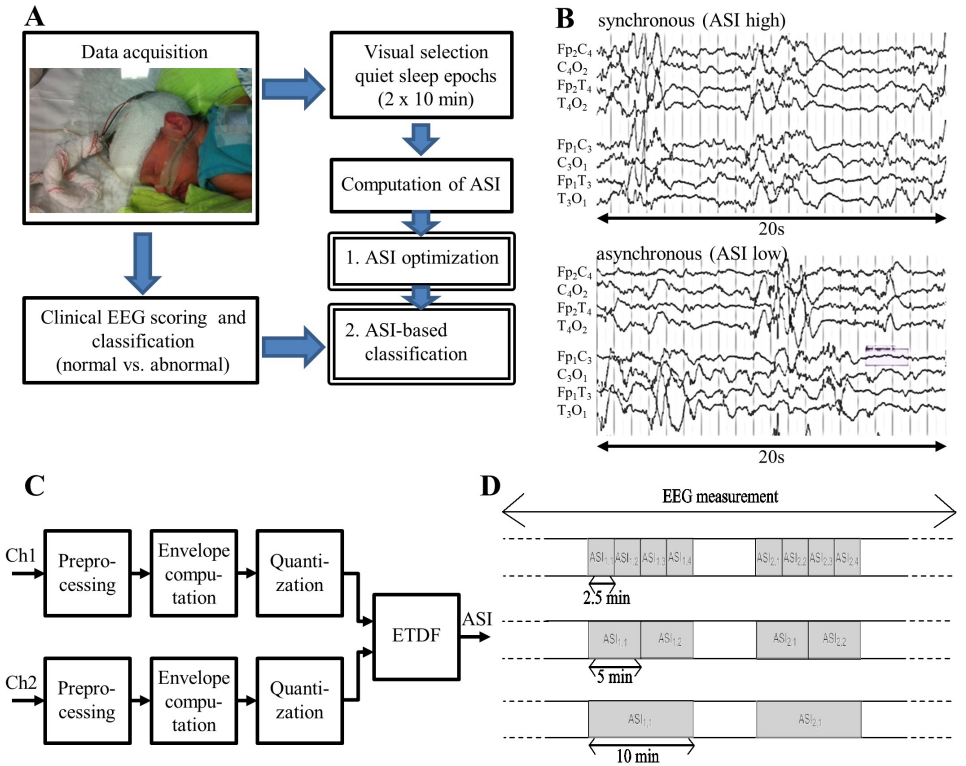

Figure 8.1: (A) Schematic overview of the presented method. (B) EEG tracks with Normal and Abnormal synchrony. (C) Schematic view of the ASI algorithm (Räsänen et al. 2013). (D) Two 10-min quiet sleep epochs are subdivided into shorter epochs of 2.5, 5, and 10 min for analysis which gives respectively ASI2.5, ASI5 and ASI10 values.

protocol was reviewed and approved by the relevant Ethics Committee of the University Hospitals of Leuven, Belgium.

The EEG records were reviewed for clinical purposes by two independent raters (A.D., K.J.) who were not aware of the later use of the EEG for this study. Hence, they were fully blinded to both the overall design as well as the numerical ASI results. The clinical assessment is based on holistic, conventional visual criteria (see Table C.1 in Appendix C). If there was any difference in the interpretation of an EEG, a consensus was reached after re-evaluation (2 patients, Table C.1 in Appendix C). The following parameters were assessed on the whole measurement, according to standard developmental features in preterm and term EEG (Scher et al. 2005b, André et al. 2010, Shellhaas et al. 2011, Hayashi-Kurahashi et al. 2012):

1. brain activity cycling as being normal or abnormal for the age
2. grade of continuity
3. age-specific landmarks: amplitude, disorganization and dysmaturation patterns
4. qualitative synchrony in quiet sleep

The overall clinical classification of the EEG recording as normal (n=14) vs. abnormal (n=17) was based on observing at least two features that were not appropriate for age.

8.2.2 Activation Synchrony Index

The ASI algorithm implemented in Matlab is described in full detail in the original publication (Räsänen et al. 2013). Technical details of the algorithm can be found in section 3.2.2 in Chapter 3. It takes two EEG-signals (e.g., bipolar derivations in left and right hemispheres respectively) as inputs to be processed through four main stages (Figure 8.1 C): 1) preprocessing; 2) computation of signal amplitude envelope; 3) quantization of the amplitude envelope; and 4) calculation of the ASI value, a single scalar value, from the temporal relationship of the two quantized signals. For as long as the peaks in energy envelopes are temporally co-incident (clinically perceived as 'synchronized'), their dependency is highest at zero lag and diminishes with increasing relative lag between the two channels, thereby leading to a high ASI value. On the other hand, lack of temporal co-incidence, the sign of low-synchrony, will result in low ASI (for example signals, see Figure 8.1 B or Räsänen et al. 2013).

8.2.3 Parameter Optimization

The prior work on ASI development defined the main parameter settings, the most important of which appeared to be the definition of the frequency band, and the weighting of higher frequencies (a.k.a. "pre-emphasis"). These yielded an ASI that can discriminate between different visually rated IHS grades, and which clearly outperforms the other methods proposed earlier in the literature (Räsänen et al. 2013). However it was not shown 1) how stable the ASI is technically and physiologically within an individual; 2) what window length would allow the most practical setting in clinical practice where selecting longer data epochs is always challenged by the intermittent, trivial artifacts; and 3) which of the bipolar EEG derivations would produce the best results.

Stability over time

It is commonly assumed by clinicians that IHS is a fairly stable property of a given brain function, at least at the scale of multiple hours. Thus the IHS measure should be comparable between successive sleep cycles, and at least between few-minute epochs within a given QS period. Theoretically and physiologically thinking, it is also possible, and may even be more likely, that subtle fluctuations occur in the IHS over time. The clinically required intra-individual stability of our measure by a test-retest paradigm is technically straightforward, but the differences to be seen in repeated measures are affected by multiple factors. First, there is a numerical uncertainty in the measure itself when recorded from typically noisy neonatal recordings. Second, the feature quantified by ASI may change due to subtle fluctuations in brain state at multi-minute scale. The former possibility is typically tackled by using longer data epochs, while the latter possibility is better assessed by looking at multiple shorter data epochs. Hence, we decided to study the whole range of epoch lengths and numbers that we felt could be practical in future clinical implementations.

To this end, we divided the original 10-minute data epochs into 10, 5 and 2.5-minute epochs, and examined ASI in each. The aim was to define the epoch length with the smallest possible intrapatient deviations. This was assessed by searching for the lowest mean-squared difference (MSD) between the (average) ASI value of the first 10-minute epoch (ASI_1) and the (average) ASI value of the second 10-minute epoch (ASI_2). In formula 8.1 this difference is squared, summed and averaged over all patients, with n representing the number of patients.

$$MSD = \frac{1}{n}\sum_{i=1}^{n}(ASI_{1,i} - ASI_{2,i})^2 \tag{8.1}$$

MSD measures the difference between the different ASI values within an individual. The optimal ASI parameters were expected to give the lowest MSD. In this way, a MSD minimization problem is solved as a function of different channel pair combinations and different ASI window lengths.

A further issue to investigate was the stability of ASI between different quiet sleep epochs. In clinical practice, it may not always be possible to find long epochs of undisturbed and good signal quality epochs of quiet sleep. Therefore, more data could be readily gathered from successive sleep cycles. Hence, we analyzed either continuous 20-minute epochs from one cycle or two 10-minute epochs from successive cycles.

ASI window length

ASI is a statistical estimate of synchrony, and its numerical accuracy ('technical reliability') will increase when the analysis epochs get longer. Our earlier work showed that an ASI estimate becomes more stable when the epochs grow longer than about two minutes (Räsänen et al. 2013). Longer EEG epochs are needed to statistically quantify temporal co-incidence of pseudoperiodic, intermittent cortical activity. In this work, we searched for the optimal window by calculating the ASI feature for window lengths of 2.5, 5 and 10 minutes. To have a fair comparison between different window lengths, we studied two manually-selected epochs of 10 minutes. First, we divided each epoch into 4 equal parts of 2.5 minutes from which we separately computed the ASI value (*ASI2.5*), and then averaged them (Figure 8.1 D upper part). Similarly, the 10-minute epoch was split into two equal parts of 5 minutes and the ASI values (*ASI5*) were estimated and averaged (Figure 8.1 D middle part). These average ASI values were compared to the single ASI value from the 10-minute analysis (*ASI10*) (Figure 8.1 D lower part).

Channel pair combination

Interhemispheric synchrony is traditionally analyzed from bipolar derivations (Lombroso 1979) rather than from individual EEG signals (Omidvarnia et al. 2014). To comply with this idea, we also analyzed ASI from symmetric bipolar derivations. We wanted to define the derivation with least intra-individual

variability. Hence, we computed ASI from the following symmetric combinations; Fp_1C_3-Fp_2C_4, C_3O_1-C_4O_2, Fp_1O_1-Fp_2O_2, Fp_1T_3-Fp_2T_4, T_3O_1-T_4O_2.

8.2.4 Classification

After optimization of the ASI parameters, we examined the ability of ASI to distinguish normal and abnormal EEG recordings classified by clinical criteria. To this end, we used 20 minutes of data, channel pair combination C_3O_1-C_4O_2, and 2.5-minute ASI analysis windows (*ASI2.5*). This gave us two average ASI estimates in each patient, derived from the two 10-minute epochs (Figure 8.1 D upper part). The lower of these was used to represent the lowest possible synchrony level in the given patient (ASI_{class}).

$$ASI_{class} = minimum(mean_1\ ASI2.5,\ mean_2\ ASI2.5) \tag{8.2}$$

Next, we searched for a threshold that could distinguish normal and abnormal EEG records. The optimal ASI settings were found to yield nearly non-overlapping distributions of ASI values in the two groups, so the ASI threshold can be readily drawn between the distributions. However, we then wanted to see how much ASI–based classification would be compromised if the user has only a limited amount of data available for the ASI computation. In this situation, distributions between ASI values in the two groups are overlapping. Hence, all thresholds will have their own classifier performance, i.e. levels sensitivity and specificity. Their dependence on the threshold can be readily visualized using receiver operating characteristic (ROC) curves that were computed to assess the classifier performance as a function of thresholds.

8.2.5 Age dependence of ASI

Finally, we studied the dependence of ASI on PMA to know whether it should be taken as a confound in babies near term age. It is known that both anatomical and electrical cortico-cortical connectivity increases towards term age (Kostović & Judas 2010, Omidvarnia et al. 2014). The previous study with ASI showed a modest age-dependence in a much younger group of preterm babies compared to our present group of fullterm newborns (Räsänen et al. 2013). This could be a biological confound when using ASI on babies with a wider age range. Hence, we wanted to see whether ASI exhibits significant changes around the term age.

8.3 Results

8.3.1 Optimal parameters for ASI stabilization

In Figure 8.2, we show the ASI comparison of 10-minute epochs for two clinically relevant channel pair combinations (Fp_1C_3- Fp_2C_4 and C_3O_1-C_4O_2). Visual inspection of the scatter plots shows that least scatter is found for C_3O_1-C_4O_2 in combination with smaller ASI windows (2.5 minutes). Quantization of the scatter with MSD is summarized in Table 8.1 for all channel pair combinations and ASI window lengths. Out of all channel pairs tested, C_3O_1-C_4O_2 yielded the lowest MSD values. Out of all combinations of ASI windows tested, the average over 4 windows of 2.5 minutes led to the lowest MSD.

Next, we tested how stable the ASI value is for different selections of epochs in the whole EEG recording. We could find uninterrupted 20-minute epochs of 'artefact-free' quiet sleep in only a few patients, while in most of them the EEG was interrupted by arousals, movements or care procedures. Therefore, a scatter plot is shown for the analysis of an epoch of the same quiet sleep period (20 minutes) and of two epochs of different quiet sleep periods (2 x 10 minutes) (Figure 3). There is no significant difference in the MSDs between the epochs taken from the same vs. different quiet sleep epochs (mean MSD_subsequent=1.061 and mean MSD_separated= 1.066, respectively; p=0.12; Mann-Whittney U test).

8.3.2 Classification

Using the two epochs of 10 minutes, we plotted the ASI values using the best channel pair (C3O1-C4O2) and window lengths (4 x 2.5 minutes), and labelled them according to clinical EEG judgements. As shown in Figure 8.4, the distributions of ASI values in the two groups are distinct. Comparison of the smaller of the two ASI values in each baby shows that the difference is highly significant ($p<0.001$, t-test). A tentative cut-off set at ASI=3.6 gives only one misclassified normal baby (pt #28) having an ASI below that limit, yielding a very high classification accuracy (96.77%). This patient was clinically classified as normal due to age-specific transients interpreted as 'borderline' for the PMA age of 37.6 weeks (i.e. 'immaturity'), which as a clinical finding does not need to be associated with globally abnormal function detected by ASI.

After observing such high classification accuracy using 2x10 minutes EEG epochs, we finally wanted to do a *post-hoc* analysis to see how the classification accuracy is affected by reduction in EEG data. This is important for clinical studies where the ideal 20 minutes of good quality EEG from quiet sleep is usually not

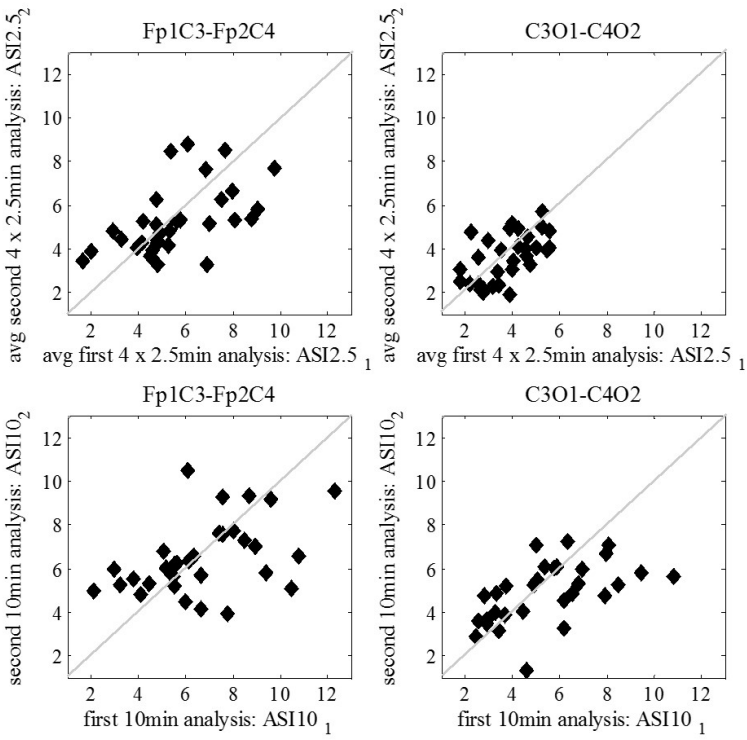

Figure 8.2: Difference in mean squared difference (MSD) between two analyzed periods of 10-min EEG, every dot representing a different patient. Results are shown for Frontal-Centro (Fp-C) and Centro-Occipital (C-O) derivations for different analyzing window lengths (2.5/10 min). Best result with lowest MSD is shown in the upper right plot, obtained for average ASI values over 4 x 2.5 min analysis on C-O derivations.

Table 8.1: Mean squared difference (MSD) for different channel pairs and different ASI analyzing window lengths shown as an average for all 31 patients. Grand averages of the MSD values over all channel pair combinations and window lengths are shown as well. Examples shown in Figure 8.2 are underlined in this table.

	Fp_1C_3-Fp_2C_4	**C_3O_1-C_4O_2**	**Fp_1O_1-Fp_2O_2**	**Fp_1T_3-Fp_2T_4**	**T_3O_1-T_4O_2**	**Mean MSD_ch**
ASI_10min	4,84	3,58	6,05	4,76	5,22	**4,89**
ASI avg_4x2.5min	2,99	1,06	1,63	1,15	2,02	**1,77**
ASI avg_2x5 min	9,9	4,23	8,6	5,51	5,25	**6,7**
ASI avg_2x2.5min	3,21	2,22	3,82	2,91	3,74	**3,18**
ASI_5min	7,59	4,71	5,71	5,38	9,05	**6,49**
Mean_MSD ASIwindows	**5,71**	**3,16**	**5,16**	**3,94**	**5,06**	

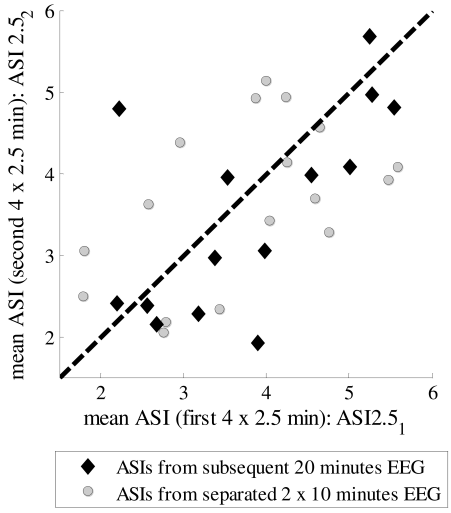

Figure 8.3: ASIs for subsequent 10-min epochs from the same quiet sleep period or for separate 10-min epochs from two different quiet sleep periods.

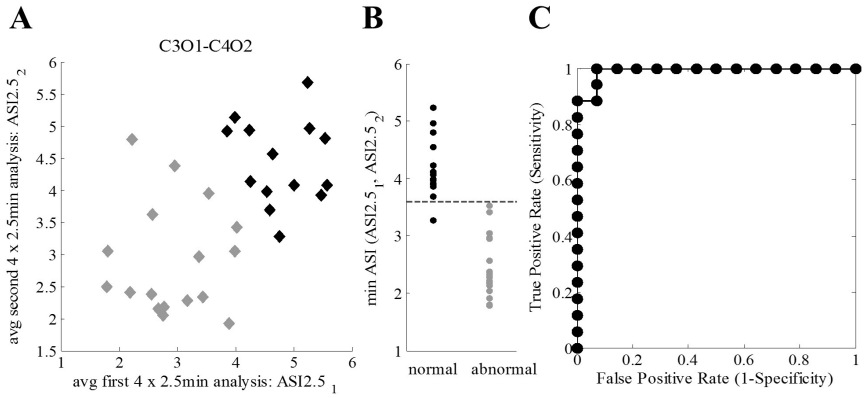

Figure 8.4: (A) $ASI2.5_1$ and $ASI2.5_2$ for both 10-min EEG segments from 31 patients for C-O derivation with the lowest MSD value. Two groups are specified: normal patients (black labels) and abnormal patients (gray labels). (B) Discrimination between normal and abnormal ASI taking the minimum ASI of $ASI2.5_1$ and $ASI2.5_2$ and thresholding (Th_ASI = 3.6). (C) ROC curve for classification, AUC = 0.971.

available. Hence, we systematically examined a range of EEG lengths (5, 10 or 20 minutes), ASI window lengths (2.5, 5 and 10 minutes), as well as the way of combining the ASI values from multiple windows. Instead of attempting formal statistical comparisons, we aimed to provide useful practical answers by visually analyzing trends in the changes of ROC curves when the data and analysis are changed. As an expected finding in the visual comparison of ROC curves, using more EEG data led to a generally better overall classification (Figure 8.5). We also observed that the length of the ASI window made a difference such that shorter ASI windows tended to yield higher classification accuracy. Moreover, the way of combining ASI estimates of multiple windows (mean vs. minimum vs. maximum) also appeared to affect the classification accuracy. Taking the mean ASI value from several windows seemed to produce more accurate classifications. However, qualitative comparison of ROC curves based on subsequent 5-minute epochs showed that the classification accuracy varies considerably.

8.3.3 Age dependence of ASI

ASI was not found to significantly correlate with PMA in infants near term age (PMA >36 weeks) (Figure 8.6), and the slopes of the linear regression lines are very small. Hence, the same cutoff limit can be applied to distinguish normal and abnormal EEG throughout this age range, and no PMA-dependent correction is needed.

8.4 Discussion

Our study shows that IHS is a very robust feature of normal neonatal EEG, and that it can be readily quantified by using the novel metric ASI. We further show that ASI is able to reach the same classification that has been traditionally reached by a skilled EEG clinician when combining multiple visually-identified signal features. To the best of our knowledge, this study provides the first quantitative evidence in support of the old clinical thinking that disturbance of neonatal brain function is readily reflected in the interaction between hemispheres. We extend the earlier work with ASI by providing detailed assessment of how ASI performance is affected by variations in data length or analysis settings. As a conclusion, the results provide guidance for future employment of ASI in clinical work and research as well as in the development of automated EEG classifiers.

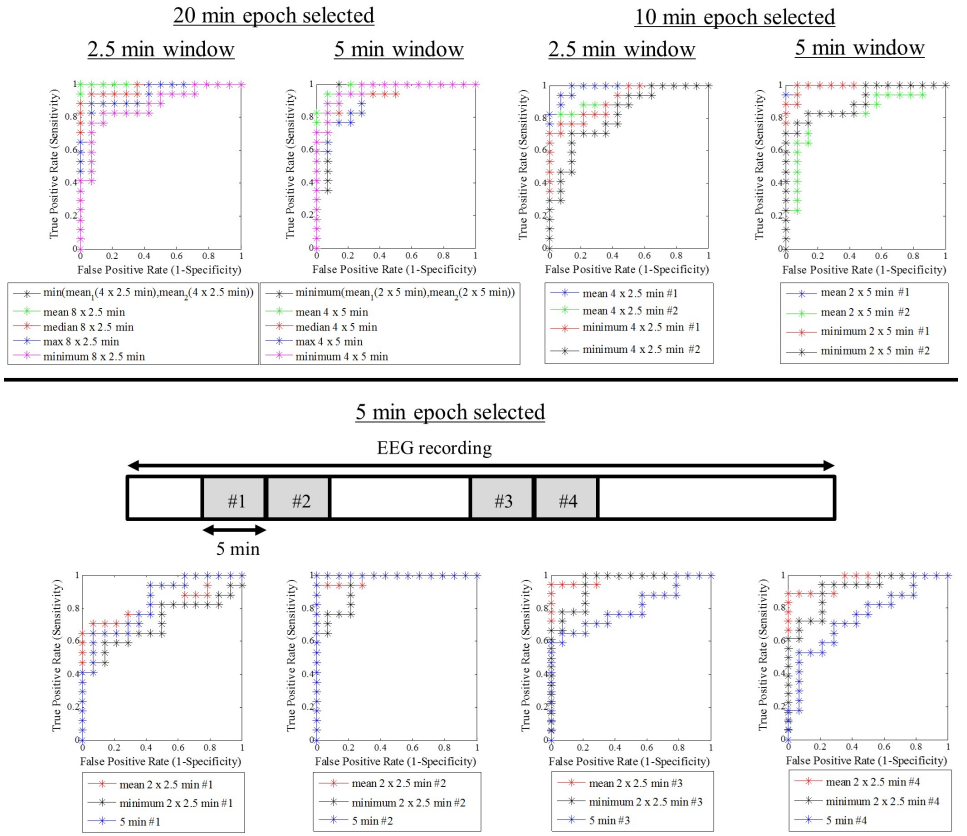

Figure 8.5: ROC curves for different ASI window lengths and different epoch lengths.

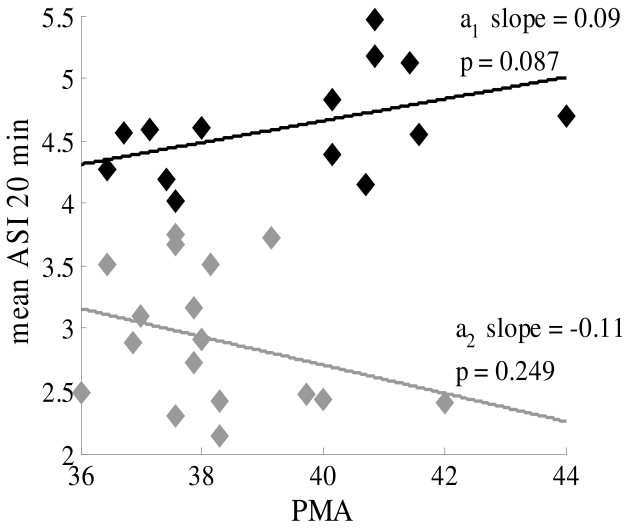

Figure 8.6: ASI value is independent of postmenstrual age of the term infant (PMA >36 weeks). Black labels represent healthy patients with synchronous patterns; gray labels are patients with asynchronous patterns. The mean ASI value is calculated for manually-selected 20-min periods (8 × 2.5min).

8.4.1 Intra-individual stability and measurement stability: selection of small epochs

We found that the most stable ASI value was obtained by using the mean of multiple short-term ASI values, each estimated from a 2.5-minute epoch. Physiologically, this observation suggests that the long-range temporal correlation in the synchrony of bursts between hemispheres is limited over time. Temporal correlations in amplitude fluctuations over several minutes have been shown in the adult brain (Linkenkaer-Hansen et al. 2001). Our recent observations in neonatal EEG datasets suggest, however, that only limited temporal correlations can be seen in the neonatal EEG signals (Matic et al. 2015), indirectly supporting the idea that ASI analyses may also best operate when using limited window lengths. Clinically and methodologically, using short segments offers several advantages in future studies and for possible implementation in brain monitoring algorithms. It is relatively easy to find several 2.5-minute long undisturbed and sufficiently high quality (cf. Räsänen et al. 2013) EEG segments from neonatal recordings, while requesting longer (e.g. 10 minutes) continuous and undisturbed EEG epochs would pose a serious

limitation in the future use of ASI. We suggest that the minimum duration of the recordings should be long enough to improve the statistical value and to overcome technical artefacts and subtle fluctuations in brain state at the multi-minute level. To this end, one should aim to collect a total of up to 20 minutes of quiet sleep data, which may come from successive sleep cycles. Reduction of the total data to 10 minutes will compromise individual diagnostic accuracy; however, it would only moderately decrease the utility of ASI at group level analyses (e.g. as an early biomarker).

8.4.2 Channel pair combination and cut-off value

We found that the best intra-individual stability is obtained from using central-occipital derivation. Despite decades of clinical visual assessment of IHS, there are no established practices as to which derivations should be used. A common clinical experience is that temporal co-incidence of activity bursts varies between brain areas, especially when the IHS is decreased in sick babies. It is also common to have disturbing movement and muscle artefacts in the frontal and temporal channels. Our finding suggests that ASI is optimally measured from a derivation that, by co-incidence, also happens to be usually clean of artefacts. This helps implementation of ASI in future studies. Physiologically, this finding is compatible with current knowledge of neonatal brain networks. It is well established that anatomical neonatal networks grow first in post-central regions (Kostović & Judas 2010), and that neonatal EEG activity mostly occurs in posterior regions (André et al. 2010). Hence, we chose this derivation to deliberately capture only post-central brain activity. It was also shown recently that there is a prominent posterior-parietal network in the newborn brain created by long-range amplitude correlations (Omidvarnia et al. 2014), which as a coupling mechanism comes close to what is measured by ASI. Taking these together, our observations suggest that the post-central networks may be the key driver of interhemispheric connectivity, and the traditionally observed loss of IHS in sick babies is probably due to changes in these posterior networks. Further studies are warranted to study whether different structural pathologies could give rise to altered IHS in a spatially selective manner.

8.4.3 Age independency of ASI

We found a clear cut-off across the whole age range of babies, which suggests that future ASI implementation can disregard PMA when studying babies near term age. The younger infants in our group (PMA 36-38 weeks) showed more interindividual variability, which may reflect the as yet poorly established brain

networks at that age. It has been shown that both the anatomical growth of callosal connections (Kostović & Judas 2010) and the appearance of visually observed IHS (Tharp et al. 1989, André et al. 2010) take place only a few weeks earlier, up to the 35th week of gestation. It is commonly seen in the clinic in these younger babies (data not shown) that the onset of quiet sleep may be markedly asynchronous and that synchrony increases within the quiet sleep period. Such dynamics could arise from functional instability in the young networks, which would readily explain a larger variability both within and between individuals.

8.4.4 Future directions

Finding a high correlation between ASI and the traditional clinical visual EEG classification suggests that ASI may provide an objective and quantified global biomarker for neonatal brain function. Its design makes it physiologically reasoned; our current work makes it clinically benchmarked; and its technical properties make it transparent and straightforward to implement. Hence, it holds promise for becoming a useful feature in future clinical work and research, as well as in the construction of automated classifiers of neonatal EEG. In this context, finding quiet sleep periods in an automated way would be beneficial.

This research has potential value, as prematurity-associated injury of the subplate, early extrauterine environmental stimulation, and acquired brain lesions may induce a structural adaptation of synapses and, consequently, alter the normal differentiation of cortical connectivity or even disruption of the cortical network development. These altered brain functions, expressed as levels of inter- and intrahemisperic synchrony, may reflect transiently or permanently disturbed connectivity of the cortico-cortical and cortico-basal ganglia connections, even in the absence of standard neuroimaging abnormalities. Further work for clinical research may include ASI as an outcome parameter in standardized neurodevelopment follow-up data and may also include quantitative analyses of synchrony in preterm and term infants, to identify normative and altered patterns of development.

Acknowledgements

Research supported by
Research Council KUL: GOA/10/09 MaNet, CoE PFV/10/002 (OPTEC); PhD/Postdoc grants;
Flemish Government: FWO, IWT: projects: TBM 110697-NeoGuard;

PhD/Postdoc grants; IWT project 110697;
Belgian Federal Science Policy Office: IUAP P7/19/ (DYSCO);
EU: ERC Advanced Grant: BIOTENSORS (nº 339804).
S.V. and O.R. were supported by the Academy of Finland.
S.V. was also supported by the European Community's Seventh Framework Programme European Community (FP7-PEOPLE-2009-IOF, grant agreement nº 254235, as well as FP7-HEALTH-2009-4 · 2-1, grant agreement nº 241479, The NEMO Project).

Chapter 9

Early development of synchrony in cortical activations in the human

Ninah Koolen[1,2], Anneleen Dereymaeker[3], Okko Räsänen[4], Katrien Jansen[3], Jan Vervisch[3], Vladimir Matic[1,2], Gunnar Naulaers[3], Maarten De Vos[5], Sabine Van Huffel[1,2], Sampsa Vanhatalo[6]

[1] Division STADIUS, Department of Electrical Engineering (ESAT), University of Leuven, Leuven, Belgium

[2] iMinds-KU Leuven Medical IT Department, Leuven, Belgium

[3] Department of Development and Regeneration, University of Leuven, Leuven, Belgium

[4] Department of Signal Processing and Acoustics, Aalto University, Espoo, Finland

[5] Institute of Biomedical Engineering, Department of Engineering Science, University of Oxford, Oxford, UK

[6] Department of Children's Clinical Neurophysiology, HUS Medical Imaging Center and Children's Hospital, Helsinki University Central Hospital and University of Helsinki, Helsinki, Finland

As adapted from a submission to *Neuroscience*, Aug. 2015

Highlights

- We study the developmental change in the synchrony between cortical activations during the last ten weeks of normal pregnancy.
- We show strong developmental correlation across all cortical areas.
- Interhemispheric synchrony shows stronger developmental increase than intrahemispheric synchrony.
- The present analytic method is applicable to invasive recordings in animal models, allowing direct translational comparisons.
- The measure, activation synchrony index, holds promise for becoming a developmental marker of early brain connectivity.

Abstract

Early intermittent cortical activity is thought to play a crucial role in the growth of neuronal network development, and large scale brain networks are known to provide the basis for higher brain functions. Yet, the early development of the large scale synchrony in cortical activations is unknown. Here, we tested the hypothesis that the early intermittent cortical activations seen in the human scalp EEG show a clear developmental course during the last trimester of pregnancy, the period of intensive growth of cortico-cortical connections. We recorded scalp EEG from altogether 42 premature infants at post-menstrual age between 30 to 44 weeks, and the early cortical synchrony was quantified using recently introduced activation synchrony index (ASI). The developmental correlations of ASI were computed for individual EEG signals as well as anatomically and mathematically defined spatial subgroups. We report two main findings. First, we observed a robust and statistically significant increase in ASI in all cortical areas. Second, there were significant spatial gradients in the synchrony in fronto-occipital and left-to-right directions. These findings provide evidence that early cortical activity is increasingly synchronized across the neocortex. The ASI-based metrics introduced in our work allow direct translational comparison to in vivo animal models, as well as hold promise for implementation as a functional developmental biomarker in future research on human neonates.

Keywords

neonatal EEG; brain connectivity; biomarker; early development; brain monitoring

9.1 Introduction

Large-scale spatio-temporal correlations in neuronal activity are considered to provide the functional basis for a range of brain functions in distributed networks (Bressler & Menon 2010, Uhlhaas et al. 2010, Palva & Palva 2011). These correlations are readily observed in the neuronal activity, as well as in the fluctuation of cerebral blood flow (Biswal et al. 1995, Jerbi et al. 2010), and they also correlate with behavioural states (Raichle 2010, Palva & Palva 2011, Hutchison et al. 2013).

Little is known about the early ontogenesis of functional communication in the human neuronal networks. Recent anatomical studies have disclosed an account of the microscopic development of structural networks in the human fetus (Kostović & Jovanov-Milosević 2006, Kostović & Judas 2010), which sets the physical frame to how the early neuronal dynamics may emerge during latter half of gestation. Some features of large-scale spatial coordination in the electrical activity of the brain have been reported in sleeping human newborns (Tokariev et al. 2012, Omidvarnia et al. 2014). It is known that two modes of brain activity (Vanhatalo & Kaila 2006) alternate in sub-second time scales between a relative quiescence and its interruptions by spontaneous activity transients (SAT, a.k.a. burst; Vanhatalo et al. 2005). These SATs are thought to provide the endogenous driver needed for activity-dependent wiring of the early brain networks, prior to onset of genuine sensory experience (Hanganu-Opatz 2010, Kilb et al. 2011, Colonnese & Khazipov 2012).

Early clinical studies on neonatal EEG established that the temporal co-incidence of these activity bursts between the hemispheres, commonly called 'interhemispheric synchrony' (IHS), is a good marker of normally developing EEG activity at term age. A developmental increase in IHS was found during the last trimester of pregnancy (Lombroso 1979), however, the existing literature is based on subjective and largely qualitative EEG assessment that compromises the validity of detailed findings. Moreover, there are no reports on spatial differences in the development of synchrony between cortical areas, yet histological studies have clearly established distinct developmental trajectories in the growth of long-range cortico-cortical (cx-cx) pathways (Judas et al. 2005, Kostović & Jovanov-Milosević 2006).

We have recently developed and validated a measure for IHS, called Activation Synchrony Index (ASI), which statistically quantifies the temporal coincidence of spontaneous activity transients in the cortical activity (Räsänen et al. 2013, Koolen et al. 2014c). This has opened the possibility to study how the synchrony between cortical activations evolves during prematurity. In the present study, we aimed to characterize the developmental correlations of cx-cx synchrony during the last ten weeks of pregnancy, which is characterized by the rapid development of long-range cx-cx connections. In particular, we wanted to disclose potential spatial gradients, as well as assess whether the developmental changes are robust enough to even allow using the ASI-based cx-cx synchrony as a maturational measure.

9.2 Methodology

9.2.1 Data acquisition

The main dataset consisted of 22 recordings in 20 infants, recorded at a postmenstrual age (PMA) of 30-44 weeks at the Neonatal Intensive Care Unit of the University Hospitals of Leuven, Belgium (Koolen et al. 2014b,c). Two infants had consecutive recordings to assess brain development. The lower age limit was set to 30 weeks postmenstrual age (PMA) to assess the developmental window when the majority of thalamocortical connections are established, while there is an intensive growth of cortical-cortical connections (Jovanov-Milosević et al. 2009, Kostović & Jovanov-Milosević 2006, Kostović & Judas 2010). One term infant was excluded because of missing tracé discontinue EEG patterns, the foundation of ASI analysis. The recording time was at minimum 4 hours, and a clinical expert (A.D.) selected the most discontinuous EEG, resembling quiet sleep in older patients, for 2 x 10 minutes in each recording. All EEG measurements were recorded at 250 Hz, with 8 electrodes (Fp1, Fp2, C3, C4, T3, T4, O1, O2) placed according to the 10-20 standard locations and reference electrode Cz (BRAIN RT, OSG equipment, Mechelen, Belgium). The protocol was approved by the Ethics Committee of the University Hospitals of Leuven, Belgium. Preprocessing the data involved applying a 50 and 100 Hz Notch filter and a 1-20 Hz band pass filter to capture the interesting burst information present in this frequency range.

In order to validate the finding of maturational changes, we studied an independent dataset that consisted of 67 EEG recordings from another set of 22 newborn infants. This dataset was collected during a later time window in the same hospital, and using the same recording specifications as detailed above. We selected 50 EEG recordings from this cohort based on finding sufficiently

discontinuous patterns using a threshold (>0.05) derived from the suppression curve (Koolen et al. 2014b).

9.2.2 Analysis of synchrony

We estimated synchrony between cortical areas by using the recently developed measure Activation Synchrony Index (ASI), which estimates the temporal relationships between newborn cortical events (for further details, see Räsänen et al. 2013). Our primary aim was to study the development of ASI from prematurity to term age. In addition, we also studied spatial differences in ASI development, as well as the temporal fluctuations of ASI within each recording session in order to assess its methodological stability and potential use as a maturational measure of functional connectivity.

Computation of ASI

Temporal relationships between pairs of EEG signals were computed using a previously described measure ASI (Räsänen et al. 2013), which was recently shown to perform well in distinguishing normality in EEG traces from term patients (Koolen et al. 2014c). ASI provides a statistical measure for the temporal coincidence of two quantized EEG amplitudes so that it increases as the temporal dependence of the signal pair approaches its maximum value around the zero time lag.

For the present study, ASI was initially computed for EEG epochs (or ASI windows) of 1 minute and 2.5 minutes. It was originally shown (Räsänen et al. 2013), that ASI is more stable with longer (> 2min) window lengths. However, we have later shown that averaging over shorter windows may be preferred (Koolen et al. 2014c), perhaps due to limited long-range temporal correlations in the newborn EEG. Using multiple shorter windows is also better suited for the analysis of older neonates with shorter quiet sleep epochs. As a compromise of the above considerations, we decided to use the median ASI value over all EEG epochs as the representative ASI measure for the given subject. Additional analyses were performed for ASI values of each single EEG epoch.

Assessment of ASI stability

The underlying general assumption in IHS is temporal stability, hence ASI would be ideally expected to yield relatively stable values regardless of the data length used for its computation. In order to test whether ASI estimates

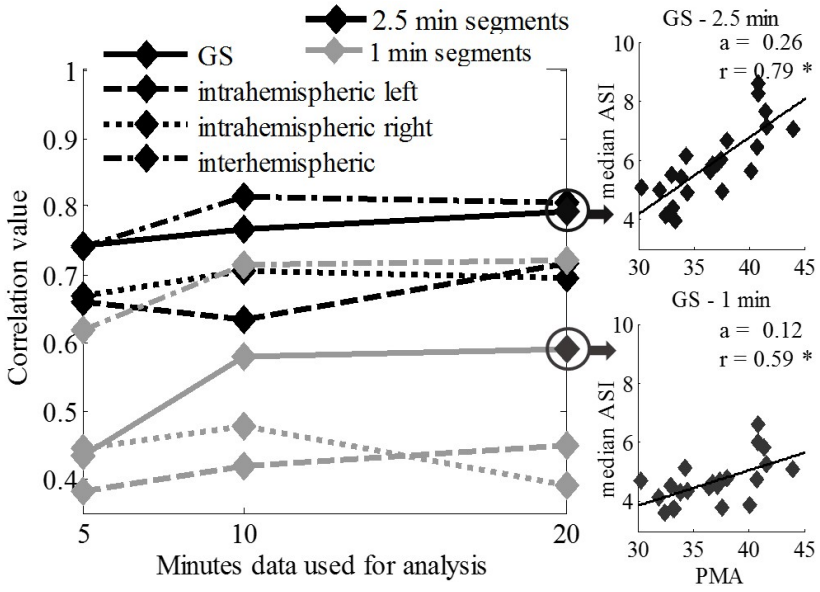

Figure 9.1: Comparison of ASI analysis settings with respect to developmental correlations. Left side graph shows correlation coefficient (r) between ASI and PMA in the same dataset when ASI is computed using different amount of data (x axis), different analysis windows (1min vs 2.5min), or different combinations of channels. A little increase in r-values is found when using longer EEG epochs. On the right side, PMA correlations are shown for 1 min and 2.5 min ASI windows. Both correlations are significant, however use of 2.5 minute ASI windows gave clearly steeper developmental trends and higher correlation values.

are really so stable, we first analyzed how the length of EEG epoch would affect the findings, and whether the choice of ASI analysis window influences the observed correlations to PMA. We found that significant developmental increase in ASI is seen with all tested amounts of EEG data, however, there was a slight increase in correlation coefficients when more EEG data was used (Figure 9.1). In addition, increasing the ASI window length from 1 min to 2.5 minutes resulted in ASI vs PMA correlations with both stronger correlation coefficients and steeper slopes (1min: r=0.59, slope a=0.12; 2.5min: r=0.79, slope a=0.26) (Figure 9.1). Based on these observations, all later analysis was performed using 2.5 minute ASI windows.

Spatial analysis of ASI

We computed ASI estimates between all monopolar channel combinations. In addition, ASI estimates for bipolar derivations in both hemispheres were obtained for Fp-C, Fp-T, Fp-O, C-O, T-O, C-T. Then, we formed the following groups of signal pairs to study spatially specific developmental correlations: i) Global Synchrony (GS) was computed as the average of all 28 pairwise ASI values to characterize global connectivity, ii) Interhemispheric synchrony was computed as the average of symmetric channel combinations between hemispheres, iii) Intrahemispheric Synchrony was computed by taking the average of all six channel combinations in each hemisphere (for the left hemisphere: Fp1-C3, Fp1-T3, Fp1-O1, C3-O1, T3-O1 and C3-T3; for the right hemisphere Fp2-C4, Fp2-T4, Fp2-O2, C4-O2, T4-O2 and C4-T4), iv) Synchrony in the anterior and posterior areas were computed as the average of all 8 channel combinations in the respective areas. A scheme of these spatial subgroups is shown in Figure 9.3. In addition, we assessed another possibility to reduce the number of pairwise ASI estimates by extracting the first component in principal component analysis.

Network measures

The pairwise connectivity matrix reflects interactions in the network that can also be quantified using graph metrics where each individual EEG signal can be considered as the node, the signal pair is the edge, and the connectivity measure, here ASI, can be considered the weight of this edge. The commonly used graph theoretical metrics (Bullmore & Sporns 2009, Stam & van Straaten 2012) may have limited utility in very sparse graphs, or graphs with highly varying edge levels (for see more details, see Stam et al. 2014), which characterize our present situation. Hence, we decided to quantify the global network properties with two alternative graph measures: Minimum spanning tree (MST) and Algebraic connectivity (AC).

The minimum spanning tree (MST) is an acyclic sub-network between nodes (here, EEG signals) that allows quantitative assessment and comparison of networks with presumably low bias as compared to more traditional graph metrics (Stam et al. 2014, Tewarie et al. 2015). We computed the metric MST mean using the freely available program BrainWave (http://home.kpn.nl/stam7883/brainwave.html; Stam et al. 2014). This returns the mean value of all edges selected for the MST of the given individual recording. In contrast to the mean over all 28 pairwise channel connections (measure GS above), MST mean will only take a subset of the strongest connections, which may reduce sensitivity to random variability.

Algebraic connectivity (AC) is a metric often used to quantify the connectivity; a low AC means that its cost to cut the connectivity graph in approximately two parts is low (cfr. smaller weights between nodes). For maturing babies, edges between the brain regions would be expected to become stronger, leading to more costly graph cuts and, consequently, higher AC values. AC is obtained as the second-smallest eigenvalue of the Laplacian matrix L of the original connectivity matrix, and it is strictly positive (under the assumption of a connected graph) and increasing if more links are added to L. (Bertrand & Moonen 2013).

9.3 Results

Intra-individual stability

We first examined the temporal and spatial variability of ASI by computing interquartile range (iqr) of all ASI values within each connectivity matrix (spatial variability), and by computing iqr of the GS in successive ASI windows (temporal variability, Figure 9.2 B). Our findings show that spatial variability is large (Figure 9.2 C), in the order of 1 to 6 ASI units within an individual, but without significant developmental trend. There were also no significant differences between specific channel combinations (Anova test: p=0.96; Figure 9.2 D). Temporal variability of the GS was expectedly lower, in the order of one ASI unit, and it showed no significant developmental change (Figure 9.2 B). These findings suggest that the search of developmental correlations is likely more reliable after spatial averaging over regional groups.

Spatial ASI analysis

We observed a clear overall increase in GS values over the course of early development (Figure 9.3 A). To see whether this was systematically related to specific EEG signal combinations, we assessed the mean ASI of each EEG signal compared to the other seven EEG signals. As shown in Figure 9.3 B, each of the eight EEG signals showed a significant developmental increase in their mean connectivity, and there were relatively minor differences between individual channels in the slopes of ASI vs. PMA.

The above findings together suggested that the development of activation synchrony is global, and a spatial combination across wider channel groups is possible. We hence computed the median ASI across spatial groups (Figure 9.3 C), and we found significant developmental correlations for all groups. There

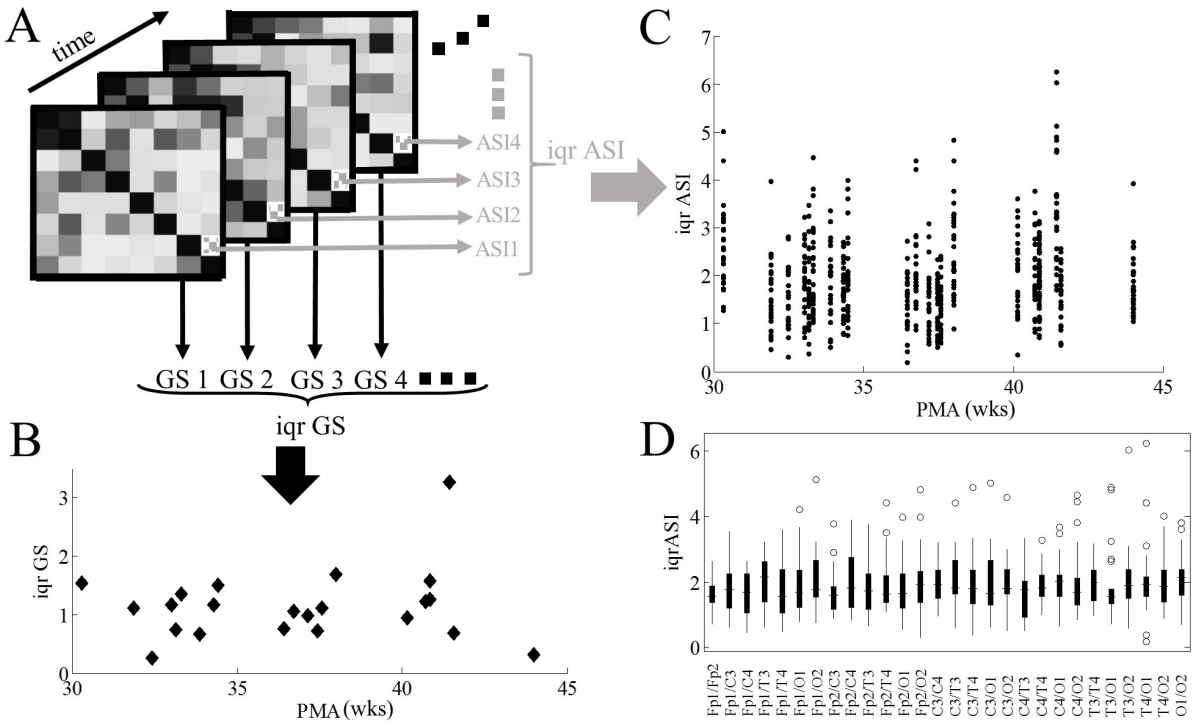

Figure 9.2: Intra-individual ASI stability and its development. (A) Connectivity matrices derived from subsequent EEG epochs of 2.5 minutes, (B) Temporal variability of global synchrony values (see also Fig 9.3 A), (C) Spatial variability of all 28 channel combinations for each individual without significant developmental trend, (D) similar interquartile variability for each channel pair combination.

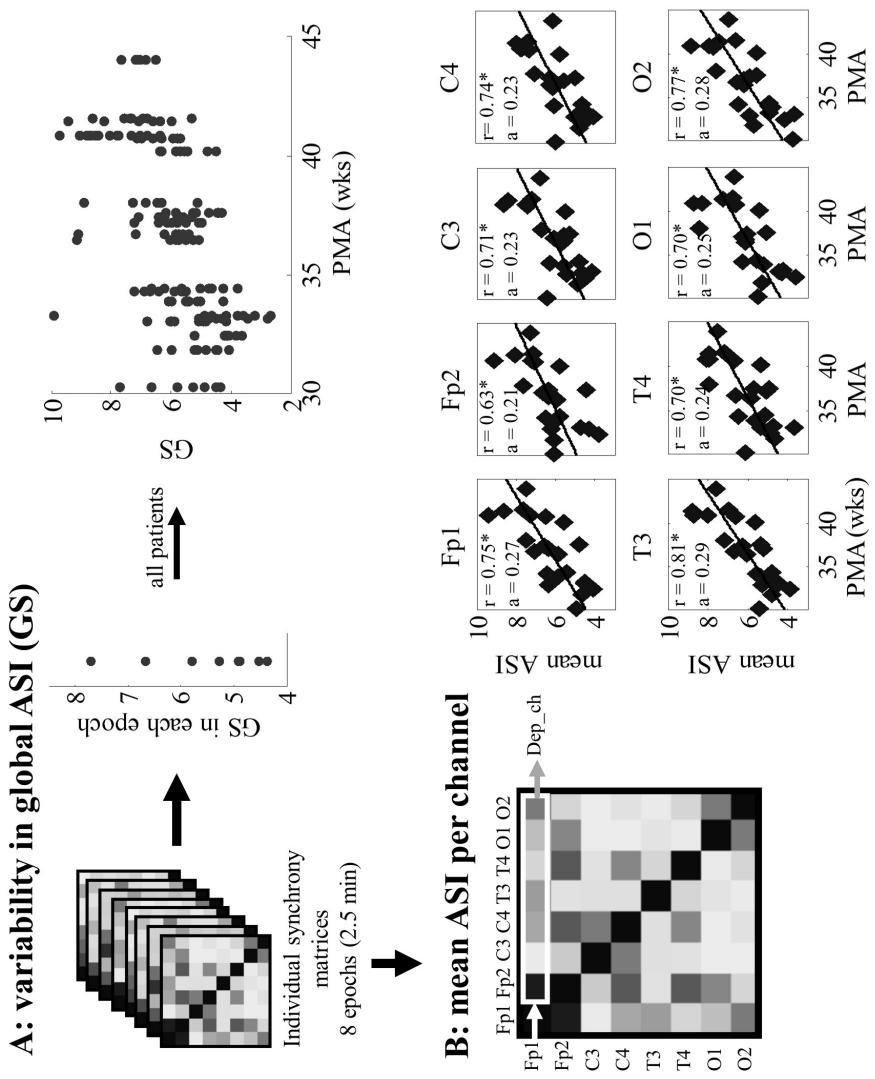
A: variability in global ASI (GS)
Individual synchrony matrices
8 epochs (2.5 min)
GS in each epoch
all patients
GS
PMA (wks)
B: mean ASI per channel
Fp1 Fp2 C3 C4 T3 T4 O1 O2
Dep_ch
mean ASI
PMA (wks)
PMA
Fp1
Fp2
C3
C4
T3
T4
O1
O2
r = 0.75*
a = 0.27
r = 0.63*
a = 0.21
r = 0.71*
a = 0.23
r= 0.74*
a = 0.23
r = 0.81*
a = 0.29
r = 0.70*
a = 0.24
r = 0.70*
a = 0.25
r = 0.77*
a = 0.28

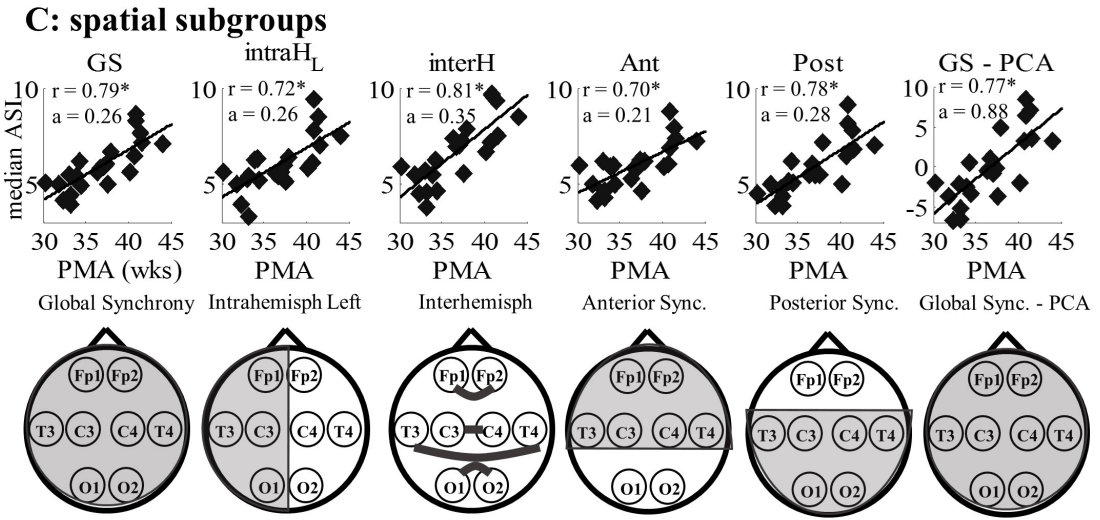

Figure 9.3: Spatial ASI Analysis and its development. (A) In addition to the temporal variability seen as the interquartile range of GS values in successive epochs, there was also an overall increase in GS values with increasing PMA, (B) Graphs depicting the developmental change in the mean ASI of each EEG channel compared to the other 7 channels, which have all significant correlations, (C) Graphs representing the developmental change in the mean ASI over the given spatial subgroup as schematically shown in the topoplots. The right most plot depicts developmental change of the first component of principal component analysis (PCA). Significance of the correlation is depicted with an asterisk after correlation coefficient 'r'. The value 'a' depicts the slope of linear regression computed for the given graph.

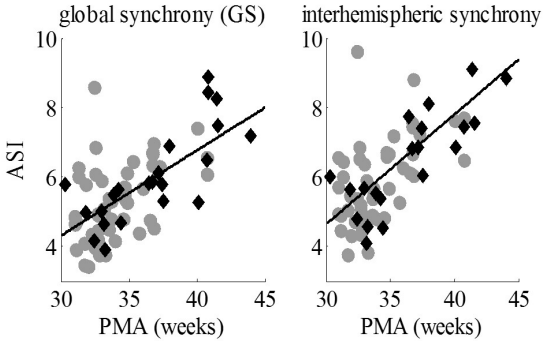

*Figure 9.4: Validation of findings using both the original data set (black labels) and the validation dataset (grey labels). The validation dataset showed more variability, especially in the lower age range, however the developmental correlations were significant: GS (r = 0.64, p = 2.0*10-9, a = 0.25) and interhemispheric synch (r = 0.70, p = 1.2*10-11, a = 0.32).*

were, however, clear differences between spatial groups: The interhemispheric ASI was highest (r=0.81, slope a=0.35), followed by GS (r=0.79, a=0.26), while the intrahemispheric ASI was the lowest (r=0.72, a=0.26 and r=0.69, a=0.18 for left and right hemispheres, respectively). By extending the original data set with the validation set, the following correlations were found: GS (r = 0.64, p = 2.0*10-9, a = 0.25) and interhemispheric synch (r = 0.70, p = 1.2*10-11, a = 0.32) (Figure 9.4).

Global metrics of ASI-based connectivity

We first tested reduction of analytic dimensions and spatial variability by using principal component analysis. Its first component was found to have a highly significant correlation (r=0.77, p= $2.62*10^{-5}$), as well as a steep relationship to PMA (slope a=0.88), suggesting that global properties of the connectivity might also reveal robust developmental correlations. Indeed, both measures of global graphs, the mean MST and AC, were found to correlate significantly to PMA (mean MST: r = 0.74, p = $7.2*10^{-5}$; AC: r = 0.82, p = $3.3*10^{-6}$) (Figure 9.5).

Finally, we examined the mutual correlations in the three global measures - GS, mean MST and AC – which all had shown significant developmental change. As expected, we observed high correlations for respectively MST mean–AC, MST

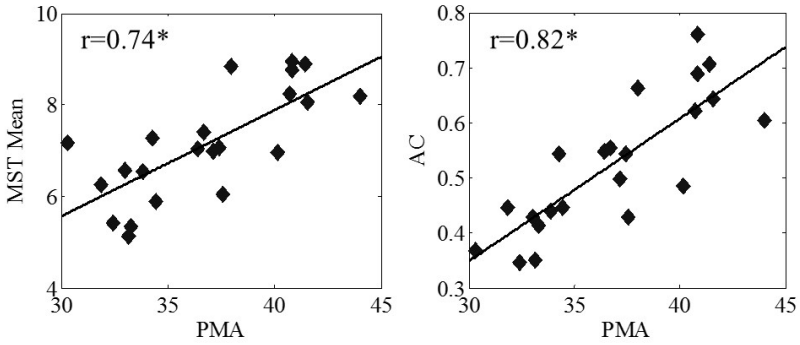

Figure 9.5: Developmental change of graph metrics, MST mean and algebraic connectivity, both of which showed a significant correlation with PMA.

mean–GS, GS–AC: r = 0.93, p = $5.2*10^{-10}$ and r = 0.94, p = $1*10^{-10}$ and r = 0.94, p = $3.8*10^{-11}$.

ASI in bipolar derivations

In order to provide an additional, clinically familiar benchmark, we computed ASI between bipolar signals, the preferred montage in the clinical EEG reading (André 2010). We have shown earlier that different bipolar derivations are not directly comparable in terms of their temporal stability (Koolen et al. 2014c) or sensitivity to therapeutic maneuvers (Vanhatalo, unpublished observations), hence they may also exhibit different developmental correlations. We found that frontal interhemispheric connections are stronger correlated to PMA compared to posterior brain regions (Figure 9.6). Indeed, no significant correlations are found between PMA and bipolar derivations in the posterior region or in the intrahemispheric channel combinations (r < 0.3 in all cases).

Finally, we wanted to see if there is a systematic spatial asymmetry in the bipolar derivations. Intra-individual comparison of anterior and posterior interhemispheric ASI showed that 20 out of 22 infants had stronger ASI in their anterior areas, which was statistically highly significant (p< 6*10-5; binomial statistics). In addition, intra-individual comparisons of left and right intrahemispheric derivations showed that 16 out of 22 infants had stronger ASI on their left hemisphere, which was statistically significant (p<0.03; binomial statistics).

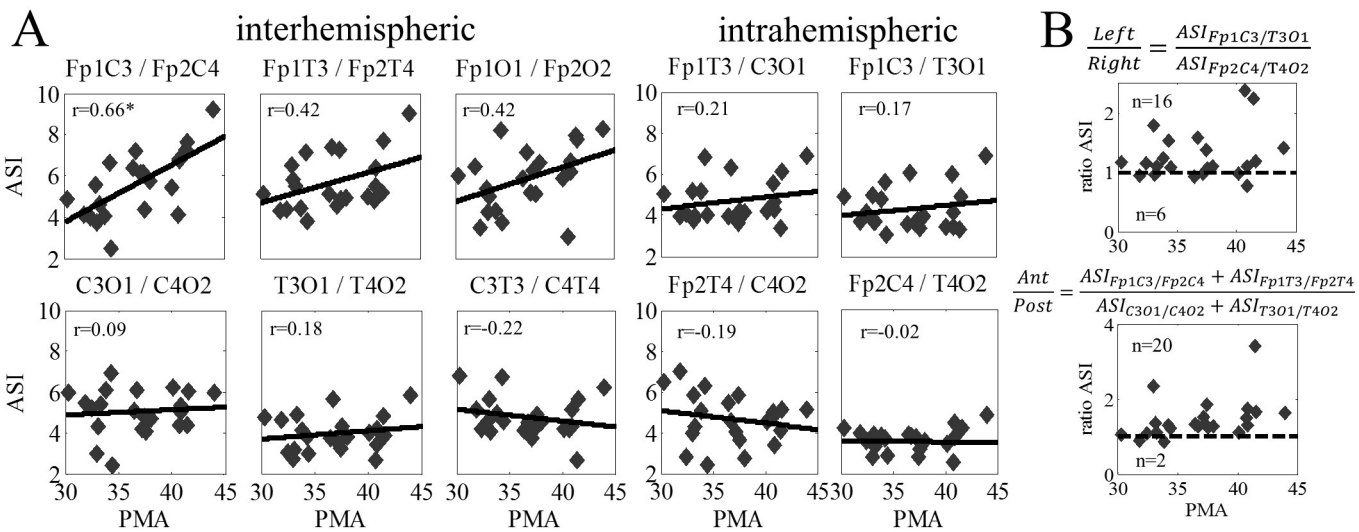

Figure 9.6: ASI in bipolar derivations. (A) Developmental changes in ASI computed from bipolar derivations for both interhemispheric and intrahemispheric channel combinations. Note that the correlation is often not significant and its strength (r) is smaller as compared to monopolar derivations (Figure 9.3). (B) Hemispheric and anterior-posterior comparisons reveal significant asymmetries. Comparison of frontal and posterior interhemispheric connections shows frontal dominance in 20 out of 22 cases, while the left side shows stronger ASI in 16 out of 22 cases.

9.4 Discussion

We show that the synchrony between cortical activations correlates strongly with development during the last two months before normal birth in the human. The present quantitative findings are fully compatible with the earlier, mainly qualitative visual EEG observations (Lombroso 1979). Our work extends prior knowledge by presenting how the developmental change is global, and it reflects the recently shown histological maturation of the corresponding cortico-cortical networks.

Comparison of brain regions showed that the ASI-based connectivity develops in a global manner, with relatively minor differences between cortical areas. This was somewhat surprising, given the spatial gradients in the development of structural long range cx-cx connections (Judas et al. 2005, Jovanov-Milošević et al. 2014). Our spatial findings cannot be directly compared to prior studies, because cortical activations comparable to ASI have been studied in central areas only (Meyerson 1968, Lombroso 1979, Marcano-Reik et al. 2010). However, recent work on spatial amplitude relationships suggested that the high cortical activity mode shows developmental gradients and an emergence of frontal and posterior groups towards late gestation (Omidvarnia et al. 2014). Our present findings show an anterior-posterior gradient in ASI without apparent developmental trajectory. This is compatible with the idea that stronger anterior IHS cx-cx correlations may reflect more global functional connectivity in the precentral areas as compared to the more spatially segregated postcentral areas that consist of sensory and association cortices.

Our group level hemispheric comparison revealed a significant asymmetry with left hemisphere showing relatively higher ASI levels in a majority of infants. This ASI asymmetry was computed between two bipolar derivations within the given hemisphere, so it reflects hemisphere level temporal coordination of spontaneous activations. Prior studies have shown consistently that functional and structural hemispheric lateralization begins very early in development (reviewed by Behrmann & Plaut 2015), however we are not aware of prior EEG studies showing hemispheric differences in connectivity measures in human preterm infants. We find it reasonable to speculate that the ASI asymmetry found in our work reflects the recently reported relative advance in the left side structural connectivity (Ratnarajah et al. 2013).

In addition to spatial averaging of ASI over channel combinations, we showed that graph metrics may disclose similar, significant developmental correlations. However, the limited number of (eight) electrodes available in our dataset did not allow pertinent assessment of graph measures at the hemispheric or lobar level. Yet the observations support prior studies (Omidvarnia et al. 2014, 2015)

in that graph measures may provide a useful tool for developmental indexing of functional connectivity. Future studies with many more EEG channels for pertinent developmental graph analysis are warranted.

While our findings are readily explained in the context of other physiological and anatomical literature, there are some technical considerations that limit the quantitative accuracy of our results. First, the spatial comparisons may be influenced by the number of electrodes and montages. The present dataset consists of eight channel recordings, which is the standard clinical practice (André et al. 2010), but limited with respect to spatial resolution available in the neonatal scalp EEG (Grieve et al. 2004, Odabaee et al. 2014, Tokariev et al. 2015). We computed most spatial analysis with monopolar montage (Cz reference), which is not fully neutral but likely the best compromise. This may bias findings towards less differences between electrodes, which is likely given the findings from our further assessment with bipolar derivations that showed spatial gradients in both anterior-posterior and left-right direction. The interelectrode distance between monopolar reference and the 'recording electrode' should not have much influence, because of the high spatial specificity shown in the newborn scalp EEG (Odabaee et al. 2013, 2014). Second, more EEG data available for the ASI analysis per patient could reduce the amount of random temporal variability. The amount of high quality EEG data available from human newborn infants is always limited, and our prior work (Koolen et al. 2014c) has shown 5-10 minutes to yield reasonably stable values. The possible bias from such technical variability would lead to the underestimation of correlations between ASI and development, which was already found to be highly significant with this data.

In addition to the physiological implications, our work does also suggest that ASI-based quantitation of functional cortical synchrony might offer a useful developmental measure in clinical studies. The recordings used in our present work are available in all medical centers doing routine neurophysiological service for neonates, and we demonstrate here the optimized analysis settings for such datasets. This opens a novel possibility to perform retrospective studies of brain functional connectivity in any developmental disorders that were recorded for clinical reasons during neonatal period. A particular extension of clinical research interest is the possibility to construct developmental indices from the ASI measures. Our work reports many ASI-based measures holding promise as a feature in developmental growth charts, which can be constructed using a well characterized, prospectively collected control population. Such growth charts would provide functional biomarkers that are very much needed in future studies on early development or in association with therapeutic interventions.

Acknowledgements

Research supported by Research Council KUL: GOA/10/09 MaNet, CoE PFV/10/002 (OPTEC); PhD/Postdoc grants; Flemish Government: FWO, IWT: projects: TBM 110697-NeoGuard; PhD/Postdoc grants; Belgian Federal Science Policy Office: IUAP P7/19/ (DYSCO); EU: ERC Advanced Grant: BIOTENSORS (nº339804). N.K. was supported by IWT PhD grant nº111480, and two FWO grants for a long stay in Helsinki. M.DV. was supported by Wellcome Trust through a Centre Grant No. 098461/Z/12/Z, 'The University of Oxford Sleep and Circadian Neuroscience Institute (SCNi)'. S.V. and O.R. were supported by the Academy of Finland and in addition, S.V. was supported by the Juselius Foundation.

Chapter 10

Summary and future research lines

10.1 Summary of chapters

The EEG of prematurely newborn provides critical information about the status of their brain development. Assessment of evolving EEG characteristics over both short and long periods of time provides relevant information about the maturation. Nevertheless, the analysis of long EEG recordings requires the trained eye of a clinical expert and is very time-consuming. Hence, the research question was whether we could extract descriptive EEG features by automated computer analysis, whether we could objectively quantify premature maturation and predict neurodevelopmental outcome. Therefore, we divided the research into two main parts: (**1**) Chapters 4, 5 and 6 investigated the ability to extract maturational features describing the change in the level of discontinuity, (**2**) Chapters 7, 8 and 9 explored the functional brain connectivity in patients with and without developmental disorders. We present an overview of the main findings per chapter.

Level of discontinuity

Chapter 4 outlined the development and results of a burst detection algorithm. It mimics the way how clinical experts observe the background EEG phenomena, using the interpretable feature Line Length. First, the

suppression curve is derived to get an idea of the level of discontinuity and to extract the most discontinuous epochs. These discontinuous EEG epochs served as an input for the burst detector, with an adaptable person-specific detection threshold. The study was performed on a small 10 patient dataset, born between 24-32 weeks, of which some patients had follow-up recordings. It has been shown to be very successful in detecting high-frequency and high-amplitude transient events (accuracy 84.27%), and comparable to inter-rater agreement (86.20%), including abnormal EEG patterns as well. The algorithm was compared to two other existing methods characterized by the NLEO feature and envelope derivation, and outperformed the latter one. Whereas NLEO showed higher sensitivity, we aimed to maximize both sensitivity and specificity. High sensitivity and high specificity rates were obtained (above 80%), necessary for both accurate burst and interburst interval extraction, since features of both phenomena show dynamic changes parallel to brain maturation. In addition, using less EEG channels only minimally influenced the accuracy rate, and therefore its applicability is enlarged to more hospitals. Normal maturation can be assessed over longer time intervals and patients at risk can be identified.

Chapter 5 outlined the results of an automated, multichannel approach to describe the maturational change in EEG discontinuity in healthy preterm infants. For this study, a dataset consisting of 90 multichannel EEG recordings of 25 preterm infants with gestational age $\leq$32 weeks was selected. All patients under study had normal Bayley-II scores (MDI and PDI >85) at 9 months of corrected age (based on the babies' due date). The suppression curve (SC), based on the LL characteristics, was introduced to quantify the level of discontinuity. In addition, the burst detection algorithm was applied to extract the interburst intervals (IBIs) in a fully automatic way. A significant decrease in EEG discontinuity (mean SC values) is found over the course of early development till 34 weeks postmenstrual age. Maturation of vigilance states includes more continuous tracing, less amplitude differences and shorter suppression periods. From 34 weeks onwards, mean SC was below 0.05, reflecting the presence of more continuous EEG. Furthermore, the shortening of the IBIs towards term age reflects the decrease in discontinuity as well. The burst detection algorithm has been shown to perform well on the new data set. The presented algorithm can further facilitate automated analysis based on the detection of specific EEG epochs.

Chapter 6 outlined the results of a study proposing a new data-driven metric to derive a set of quantitative features that correlate with maturation. The study was performed on a dataset of 84 EEG recordings, by sequential measuring 22 patients at 27-40 weeks PMA. The line length content changes equivalent to the change in EEG from discontinuous to continuous

activity (brain connections are physically established). As a result, the histogram representing the line length distribution, shifts corresponding to the developmental trend. That is, the histogram shifts to the right side, including longer line lengths. This change is captured in 28 histogram features; 20 histogram bins and 8 other statistical measurements. Using the mutual information function, 6 features with high predictive value on the infant's age were selected; three bins and 3 global statistical measures, namely the mean, interquartile range and 95th percentile. Through averaging the residual errors from the linear fits through the PMA-feature plots in the different brain regions, we could distinguish between normal patients and patients with comorbidities. The presented data-driven index is able to capture the maturation by exploiting the statistical properties of the LL feature, previously used for burst detection, and this index is notably not subjective to challenges inherent to these event detections.

Brain connectivity

Chapter 7 outlined the results of a study distinguishing between physiologic (a)symmetry and pathologic asymmetry between the two hemispheres of the brain. Interhemispheric asymmetry is clinically defined as a persistent amplitude difference (more than 50%) over homologous areas. An underlying or acquired brain lesion (e.g. hemorrhage, stroke) can be the source for this abnormal EEG pattern. Consequently, the available spatial information is explored, by using multichannel EEG signals recorded at frontal, central, temporal and occipital areas. To quantify the symmetric behavior, we opted for the channel symmetry index (CSI), which is the difference in the power spectral bands of contralateral channels. We extracted four features from the CSI curve, used to solve the classification problem. Due to the relatively small sample size including only few abnormal patterns, one-class SVM classifiers are applied. A classifier is trained for each brain region. Through mapping the data in a so-called feature space, the normal data is separated from the origin with maximum margin. We could detect most of the outliers within this way, that is, the following sensitivities are obtained: central 71.43%, frontal 100%, occipital 100% and temporal 62.5%, and always a specificity above 70%. These results can provide useful information about neuronal dysfunction in early stage, and therefore improve assessment of the neurodevelopmental outcome.

Chapter 8 outlined the results of a study proposing a new feature to quantify normal neonatal brain maturation, based on the interhemispheric synchrony (IHS). This feature is associated with the temporal co-incidence of bursting processes in spontaneous background EEG activity during tracé alternant

or discontinue. Yet, the IHS assessment relies on visual observation without any gold standard definitions. For this study, we used a dataset of 31 EEG recordings, which were classified as normal/ abnormal based on conventional visual criteria. As IHS is interpreted as a connectivity measure between hemispheres, we quantified it with a recently shown reliable metric compared to visual assessment; the activation synchrony index (ASI). The ASI is based on statistically measuring the temporal delay between two signal energies, and outperformed other methods to quantify the synchrony in these settings. Using centro-occipital bipolar derivations for ASI estimates, we found good classification (97%) at term age by averaging ASI estimates of consecutive 2.5 minute epochs in 20 minutes data. Reducing the EEG data to 5 minutes led to more variability in the ASI estimates and hence in the classification. Our results support the hypothesis that ASI is a clinically relevant feature to describe normal neonatal brain function at the level of functional interaction between hemispheres.

Chapter 9 outlined the results of a study quantifying the functional cortical synchrony, which could be a valuable metric in developmental assessment during the last trimester of prematurity. In analogy with the previous chapter, we used the measure ASI again to estimate the temporal relationships between newborn cortical events. The dataset consisted of 42 preterm infants born between 30-44 weeks. Maturational changes of ASI were computed for both individual EEG signals as for defined subgroups. First, we found only minor differences between the developmental increases of individual channels, which supports the idea of a global maturation. Across spatial subgroups, highest correlations were found for the interhemispheric synchrony (4 contralateral channel pair combinations between the two hemispheres), followed by the global synchrony (average of 28 pairwise ASI values). Moreover, using the first principal component of the 28 ASI values, high significant correlation and steep slope related to PMA were found. In addition, the change in the cortico-cortical network was quantified using network measures, the minimum spanning tree and the algebraic connectivity, which also showed significant developmental correlations. Applying ASI calculations on bipolar derivations, revealed a significant asymmetry with stronger ASI on the left hemisphere. The findings are compatible with visual observations, and are promising to be included in developmental models.

In conclusion, neurological maturation can be assessed over longer time intervals and patients at risk can be identified. The implemented algorithms aggregate the knowledge and expertise of several medical experts and automatically adapt to specific conditions of the individual patient. Our work reports many functional EEG indeces which hold promise to construct developmental growth charts by simultaneously collecting a larger normal control population. Moreover,

our work opens up possibilities towards objective quantification of therapeutic interventions. An outline is given for successful computer-aided maturational feature extraction from background EEG signals, paving the way for a significant step in the enhancement of the overall assessment capability of the NICU.

10.2 General afterthoughts

The aim was to develop white box models for which background knowledge of the clinical expert is still required to understand the patient's trends. This can be expanded to grey box models, for which parameters are trained based on the available data. However, the advantage of a white/grey box model is that it is easy to apply in practice in hospitals, that is, every subsystem of the model is easy to understand and parameters in the model are physically interpretable. Added value of the grey box model is here that the parameter estimation has taken into account uncertainty of the parameters. In general, we succeeded to develop understandable and applicable algorithms, although several barriers still exist.

The use of the burst detection algorithm is subject to several limitations. The adaptive threshold is developed for patterns which exist of both bursts and interburst intervals. However, towards term age, the EEG patterns will be affected by developmental changes of the brain activity (Lamblin et al. 1999, Vanhatalo & Kaila 2006). This means, the interburst intervals disappear and patterns become continuous. Consequently, the developed algorithm will achieve good results for premature EEG (24-36 weeks PMA), but once the EEG becomes too continuous, the accuracy will decrease. One solution could include the setting of an adaptive threshold depending on the age. However, larger datasets would be needed for this optimization. Moreover, it would be interesting to check accuracy performance of the developed algorithms using a lower number of channels. The use of aEEG is more common due to its usability, despite less available detailed background information. IBI detection using less channels still shows good performance by combining only the central EEG channels. Nevertheless, lateralized patterns or anomalies in a specific part of the brain, such as hemorrhages, will be missed. Unlike in one EEG channel, a suppressed background pattern in eight channels is more informative about the patient's health, because it could distinguish severe global brain activity.

Besides exploring the level of discontinuity, we have looked at normal brain maturation by means of interhemispheric connectivity. Normal brain activity gives rise to a symmetric EEG pattern between the two hemispheres. There are two facets of background symmetry; amplitude and waveform composition

(Ebersole & Pedley 2003); asymmetry is only clinically defined as an amplitude difference. By using the channel symmetry index, we have also taken into account the latter facet, i.e. frequency content is compared between contralateral EEG signals. Nevertheless, the physical, physiological and clinical meaning of this feature symmetry is still open to discussion. Symmetry is known to be very sensitive to technical factors such as little variation in electrode placement, a shift of electrodes due to sweating or interhemispheric difference in head shape. Notwithstanding, increasing awareness to apply symmetric quantification on continuous EEG monitoring exists, that is, to detect neurological deficits in acute hemispheric stroke patients (van Putten & Tavy 2004).

Synchrony between hemispheres is traditionally assessed by visually comparing the simultaneity of burst events at time scale (Uhlhaas et al. 2010, Bressler & Menon 2010, Vanhatalo & Palva 2011). To obtain synchrony relations among the developing brain network, we have used the ASI algorithm because it has been very promising in quantifying this synchrony at an event-level in neonatal EEG. Previous studies have discussed the pitfalls around existing methods, such as the cross-correlation, the coherence function, and phase synchrony (Tokariev et al. 2012, Räsänen et al. 2013). Firstly, the cross-correlations between raw signals (Varner et al. 1978, Korotchikova et al. 2009) were not able to differentiate between asynchrony levels (Räsänen et al. 2013). Secondly, the coherence (Kuks et al. 1988, Grieve et al. 2008, Witte et al. 2011) is a product of both phase and amplitude of the oscillations, for which high amplitude variability will lead to a more amplitude driven measure (Tokariev et al. 2012). In addition, some limitations exist as well for phase synchrony on event-level, i.e. the need for surrogate testing, its sensitivity to the noise level and the burst frequency content (Räsänen et al. 2013).

Whereas the ASI was already successfully applied to distinguish abnormal from normal patterns based on visual assessment at the moment of recording (Koolen et al. 2014c, Chapter 8), we also compared the ASI scores with the Bayley MDI-PDI scores (psychomotoric evaluation) at a corrected age of 9 months which data became available at a later date. A development index >85 is clinically considered as normal. Three patients were lost for follow-up at 9 months. The results are given in Table 10.1. An acceptable sensitivity of 80% is reached, however, low specificity is obtained (55%). An explanation for these results could be due to 'transient' abnormal synchrony (Koolen et al. 2014c). While these are early results, the estimates based on this small sample may indicate clinical relevance of the interhemispheric synchrony measure.

We always used preselected EEG data, almost free of artefacts. While this is a common way in recent literature, one could focus in the future on artefact removal (De Vos et al. 2011). Nonetheless, as previously been mentioned, source signals (such as ECG, respiration) should be noise-free by themselves to be

Table 10.1: Outcome prediction based on synchrony assessment at 9 months using the Bayley score. Interhemispheric synchrony normality was obtained using ASI values (Koolen et al. 2014c, Chapter 8)

	Abnormal Outcome	**Normal Outcome**
ASI abnormal	8	8
ASI normal	2	10
	sensitivity 0.8	**specificity** 0.55

able to use them for continuous artefact removal. Other developed algorithms used only a certain percentage of the data where unanimous detections of all human raters agreed. As a result, noisy and ambiguous EEG data is excluded. The detection accuracy is artificially increased in this way. If labelling is not available, we should look for automated artefact detection followed by rejection of these EEG segments.

Furthermore, the algorithms in this thesis were developed using data from the NICU in the University Hospital Gasthuisberg, Leuven, Belgium. The data had a sampling frequency of 250 Hz and other specific recording settings which are different from hospital to hospital. The used electrode set and Cz reference electrode varies as well in other NICUs. Electrode locations and interelectrode distances can influence the EEG amplitudes (Lamblin et al. 1999, Quigg & Leiner 2009, (Palmu et al. 2010b)). By applying normalization, it is possible to compare patients from a data set with the same filter settings. In multicenter studies, thresholds and other filter settings may need to be modified. The LL is sensitive to the selected frequency band, and therefore parameters should be optimized, such as the threshold for burst detection. The shape of the histogram can also look slightly different, even though the maturational shift will still be found. Therefore, we suggest to implement the same filter settings for future research. We already optimized settings to obtain stable ASI estimation, including preprocessing filters and the length of the analysis window/ length of the EEG epoch. It seems to be promising to apply on a large normal population.

10.3 Future directions

The methods developed in this thesis have been already shown to be useful for the clinical analysis of premature brain development. It addresses IBI/ burst detection and in addition, the general change of EEG discontinuity. Furthermore, changes in interhemispheric connectivity have been analyzed, which relates to

functional and structural connectivity. There exist several ways to continue this research, of which some have been initially explored. In the next sections, a first step has been taken towards testing the influence of medication on brain development, EEG growth charts for premature brain assessment and prediction of the neurodevelopmental outcome. Finally, algorithms should be validated using larger (multicenter) datasets. General considerations on combining modalities and multichannel data are given.

10.3.1 Influence of medication (propofol) on the EEG

Sick preterm infants need intensive care during the period of a rapid developing central nervous system. Analgesic or sedative drugs can possibly have side-effects on the cerebral activity or cause hypertension (van Alfen-van der Velden et al. 2006, Welzing et al. 2010, Norman et al. 2011). These effects can be measured, using aEEG (Bell et al. 1993, Shany et al. 2008) or near-infrared spectroscopy (NIRS) (van Bel et al. 2008). Prolonged aEEG depression and delayed onset of sleep wake cycling during follow-up have been noticed for premedication by morphine, which could give rise to adverse neurological effect (Norman et al. 2011, 2013). In contrast to morphine, propofol has been shown to give quick and effective sedation for (semi-)elective intubation (Ghanta et al. 2007, Smits 2014). However, no standard dosing regimens have been defined and therefore, effects are uncontrolled. Desirable conditions are fast recovery of the sedative reaction and no adverse effect on long term maturation. Yet, controversy exists about the safety of propofol to recommend it as the standard procedure for neonatal sedation. Hence, the aim of this study was to describe the effect of propofol administration on the aEEG. Other vital signs were analysed as well, such as the cerebral oxygenation, but these were out of the scope of this work.

The dataset consisted of 49 neonates with median (range) postmenstrual age of 30 (25-38) weeks, which got a median (range) dose of propofol (Diprivan 1%, AstraZeneca) of 1.5 (0.5-4.5) mg/kg to obtain successful intubation. They were all recorded at the NICU in the University Hospital of Leuven, Gasthuisberg, and written informed parental consent was obtained for all infants under study. Eight patients were excluded for further processing by exceeding the impedance of 10 kOhm. This threshold indicates inadequate signal quality due to poor contact with the electrodes. In addition, artefacts were removed in the beginning of the recording caused by electrode needles, which were not yet correctly in place. Neonates included in this study were stratified according to PMA [group 1: $<$28 weeks, group 2: 28-31 weeks, group 3: 32-36 weeks and group 4: $\geq$ 37 weeks], since PMA is seen as a major covariate of propofol clearance.

The grade of discontinuity gives important information about the effect of

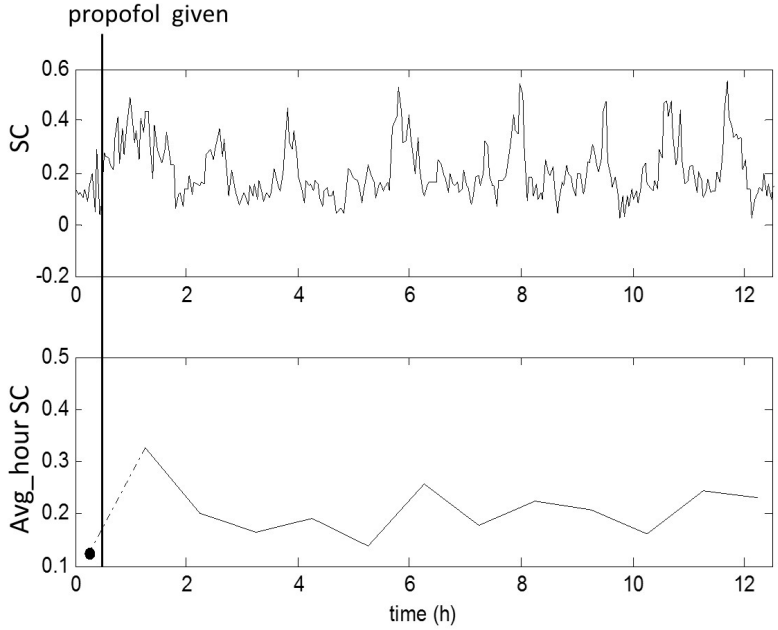

Figure 10.1: Effect of propofol administration on the suppression curve. In the lower plot, the 1-hour average of the SC after propofol is shown, with an increased suppression value during the first hour (dashed line).

propofol administration. We expect an increase in discontinuity relative to the baseline activity after premedication of propofol. To quantify this change, we considered the previously defined suppression curve (SC), which is a 'measure of discontinuity' (Chapter 5, Koolen et al. 2014b, Dereymaeker et al. 2015). It was calculated on one-channel EEG (no conventional EEG available), and a SC value was obtained for every window of 2.5 minutes. The SC values were averaged in 1 hour windows, since we were interested in the effect at longer time scales. Baseline values were obtained by averaging the SC values before the time instant of propofol administration.

A decrease of aEEG amplitude was visually observed (see Chapter 2, Figure 2.5). The effect on the SC is shown for one patient in Figure 10.1; the SC increases after propofol is given. In other words, an increase in EEG discontinuity is revealed. For this patient, the sedative effect seems to be diminished after 2 hours and normal vigilance states occur again (Figure 10.1b). In Figure 10.2, the median and interquartile range of the averaged SC are shown for each age

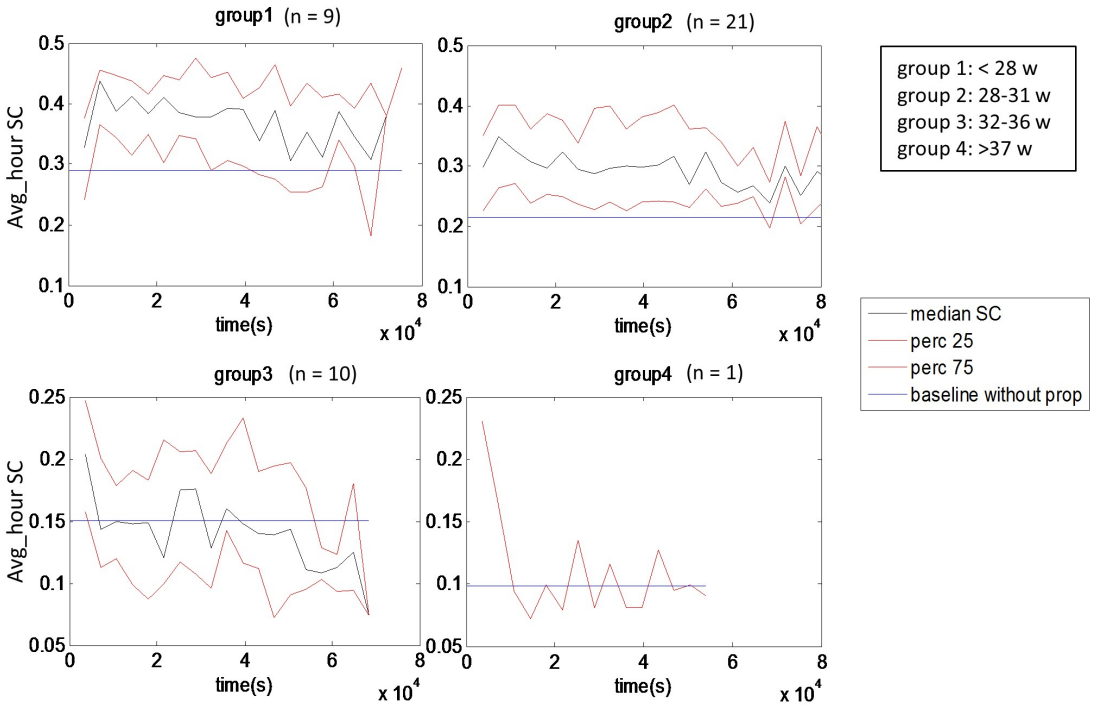

Figure 10.2: Statistical descriptive SC values (median, interquartile range) for each age group. Number of patients between brackets. SC values are decreasing towards baseline values, with faster propofol clearance in the older neonates.

group.

To use only high-quality EEG, segments with an impedance higher than 10 kOhm are excluded for further analysis. As a result, only few minutes were available for baseline calculation, with a median of 10 (2.5-97.5) minutes. This setting is not optimal, because the patient's state is hard to capture within this time interval. Nevertheless, a decrease in SC values towards baseline values is observed (Figure 10.2). In groups 3 and 4, this propofol clearance is more obvious due to a steep decline in SC. On the other hand, the suppression curve has already 'high values' for discontinuous EEG, which is a common pattern in the young preterm infants (groups 1 and 2). Hence, an increase in discontinuity is more complicated to assess in these groups with this measure. However, there is an option available to address this obstacle. One could look at the change in the histogram bins with a small bin center value, which could be associated with discontinuous activity (Chapter 6, Koolen et al. 2015b). Another possibility would be to look at the change of IBI lengths (Chapter 5, Dereymaeker et al. 2015). This study opens the way for further research to quantify the effect of treatment with medication, and herewith the effect on brain development.

This study opens the way for launching new studies to test the influence of medication on brain development or the occurrence of neonatal stress. Such studies should be planned carefully including the research questions, the underlying hypotheses as well as other critical conditions such as for instance the background noise or light settings in the NICU. In that way, it can be assured that labeling of medication administration will be more focused to solve the research question.

10.3.2 EEG growth charts

We have explored and extracted features from the EEG which describe the maturation (IBIs, bursts, suppression curve, HI and ASI). The goal is to set up "growth charts" for premature babies. They can be similar to the growth charts of a newborn baby, i.e. weight, length and head size. We can build these growth curves for each EEG feature separately, which reflects the maturation of the preterm brain. A graphical tool would provide an improved and easy interpretable method to predict survival for preterm babies. Analogously, a model has been recently developed for the prediction of survival without major morbidities for infants born at a gestational age under 33 weeks, which shows the impact of gestational age (GA) and birth weight (BW) (Shah et al. 2012) (figure 10.3). The gestational age is defined as the time between the first day of the last menstrual period and the day of delivery. The BW and GA both

reflect maturity. In general, given the patient sample size, it is impossible to develop models based on individual morbidities (Shah et al. 2012).

In Chapter 6, we introduced a purely data-driven metric able to follow preterm EEG maturation, i.e. the LL histogram changes with increasing postmenstrual age parallel to brain development. In order to make a first step towards the premature EEG growth charts, we introduce a preliminary growth chart based on the histogram index (HI).

The dataset consisted of 84 EEG recordings from 22 neonates, recorded at postmenstrual age (PMA) of 27-40 weeks. We used two hours of EEG data including active and quiet sleep, measured at 250Hz at nine standard electrode locations.

The line length signal is obtained for the two hour EEG epochs. Next, we designed a purely data-driven approach for the maturational index based on features derived from the LL histogram distribution (Chapter 6). The histogram is split into bins with 20 predefined bin centres. The 28 features consist of 20 histogram bin counts and 8 statistical distribution features (mean, median, standard deviation, interquartile range, skewness, kurtosis, 5th percentile and 95th percentile). Age correlation of these 28 features are obtained using the mutual information function (MIF). Finally, we created an 'EEG growth chart' based on these features, after performing dimensionality reduction by factor analysis. Factor analysis is an explorative analysis, searching for underlying but unobserved factors that define the correlation among a set of random variables measured for each individual (e.g. EEG recording) of a group (Jvreskog 1996, Johnson & Wichern 2015). Unlike principal component analysis (PCA), the factor model does not depend on the scale of the variables (Fodor 2002), since scale differences are present between histogram bin features and statistical histogram features. This technique analyses 'subject scores' by searching correlations between subjects (in the predefined age groups) across a sample of variables, instead of searching for correlations between the variables across subjects (i.e. PCA). The number of common factors should be smaller than the number of variables (Khosla 2004). In this way, one factor is derived for each EEG recording in this model. Categorical regression analysis was applied to define the prediction intervals, resulting in transformed factor scores (Q-scores). A categorical variable is a variable, which has a value assigned to each of the fixed categories, i.e. age ranges. This resulted in the following categories related to postmenstrual age (weeks) (n=number of patients in each group): 26-27 (n=6), 28-29 (n=7), 30 (n=9), 31 (n=17), 32 (n=18), 33 (n=17), 34 (n=15), 35-36 (n=27), 37-43 (n=40 at term age). Limited to a relative small amount of data, we have applied a range of multiple weeks in the young and old extremes. Therefore, the Q-scores are age and model dependent scaled factor scores. In regression analysis, these independent variables should be included as

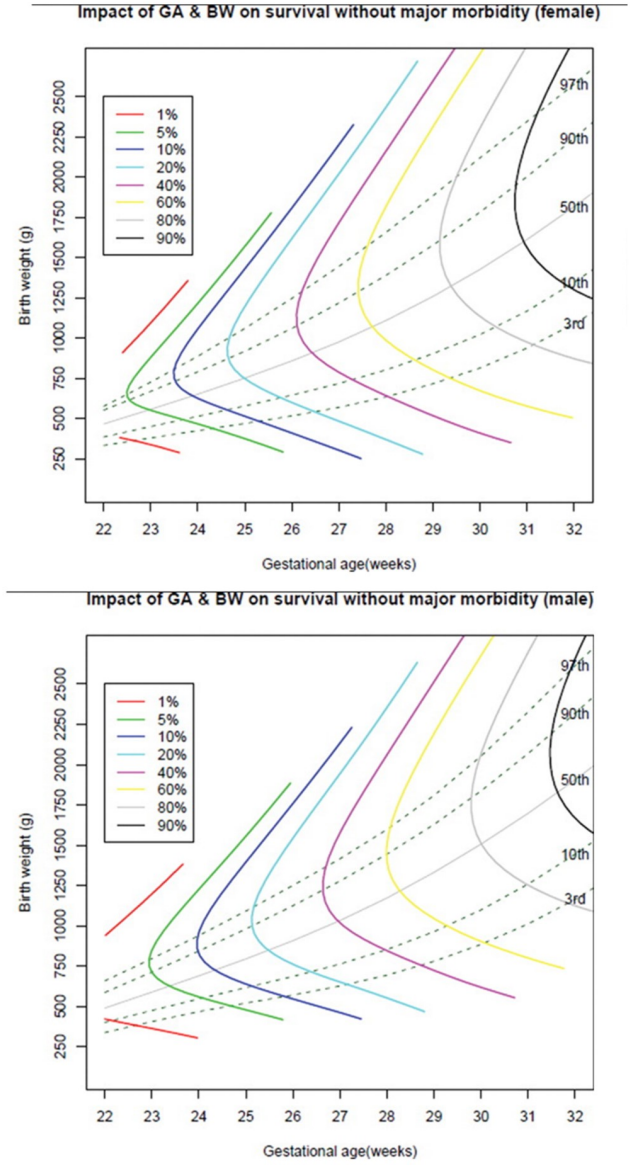

Figure 10.3: Impact of birth weight and gestational age on survival probability for female and male preterm babies, as adapted from Shah et al. (2012).

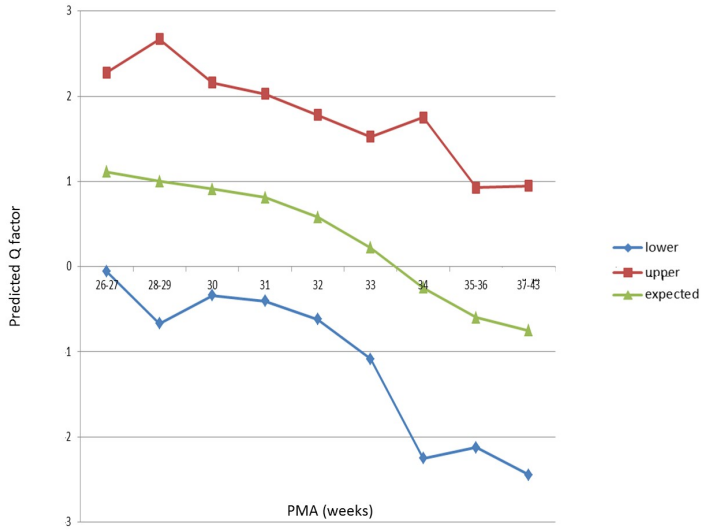

Figure 10.4: Histogram Index Growth Curve obtained by categorical regression on the predicted Q factor scores, with 95% confidence intervals.

quantitative data in order to evaluate group differences and to build a prediction model. Thereby, we used 95% confidence intervals for prediction estimated on the population in each category.

A shift in the histogram shape is found during maturation (Chapter 6). Consequently, 12 out of 28 histogram features showed a steep developmental correlation to PMA ($r>0.7$; $p<0.001$). Six features were selected based on the MIF (>0.37): 3 histogram bins and 3 global statistical features: mean, interquartile range, 95th percentile. Dimensionality reduction was performed by factor analysis. We found a nonlinear S-shape developmental trend, with steepest maturation between 31-36 weeks (Figure 10.4).

As an initial step to obtain confidence intervals, a normal distribution of babies was assumed for each age group, whereas other distributions could be closer to reality. Prediction intervals could be optimized by using an exponential distribution, because of long tails in the distributions of the youngest and oldest patient groups. Nevertheless, a larger data set is needed to test such a hypothesis. Another possibility could exist of interpolating distribution percentiles of age classes, for example the 5th, 50th and 95th percentile as presented by the next example.

For the same data set as used in Chapter 5 (patients with normal outcome at 9 months), we applied the burst detection algorithm and the HI estimation. Steep correlations were found for IBI 95th percentile and HI (including all LL), with respective correlation values of $r = -0.82$ and $r = -0.87$ (see Figure 10.5). Growth curves can be derived by connecting boxplots in age spans of two weeks, since within this time span 'healthy' maturation of electrocortical and anatomical structures can be evaluated (Biagioni et al. 2007, André et al. 2010).

Our findings show a strong maturational shift in the EEG complexity measured by LL, and we demonstrate how this can be used in a purely data driven manner to yield a maturational histogram index (HI). This index has potential to be used across different EEG systems and recording constellations, which opens also possibilities to collect normative data in multicenter settings. Based on a larger normative group, prediction intervals in the EEG growth charts will be narrowed. One could estimate a z-score per patient related to its health as compared to the healthy population's distribution at its specific age.

We introduced the histogram index to describe a global change from a discontinuous to continuous EEG pattern. Similarly, Saji et al. (2015) introduced the histogram of EEG envelopes, of which the asymmetry of the probability distribution gradually changes with brain maturation (PMA 26–44 weeks) (Figure 10.6). A transition from lognormal process in the preterm period to a gamma process in the late neonatal period was suggested. However, they just include 20 patients with only few patients in the extreme groups. We combined more features describing the maturational shift in the LL histogram, which could deliver a more robust functional biomarker.

More features and their clinical relevance require exploration. In this thesis, we have addressed some of the most relevant features for short-term neurological assessment. Nevertheless, one should not be retained to develop further data-driven maturational metrics. Preterm brain growth charts could be based on the following EEG features:

- Maturational histogram index
- IBI (interburst intervals) parameters
- ASI (synchrony index)
- (Symmetry)
- Suppression curve/ cyclicity
- Time frequency parameters
- Energy bursts

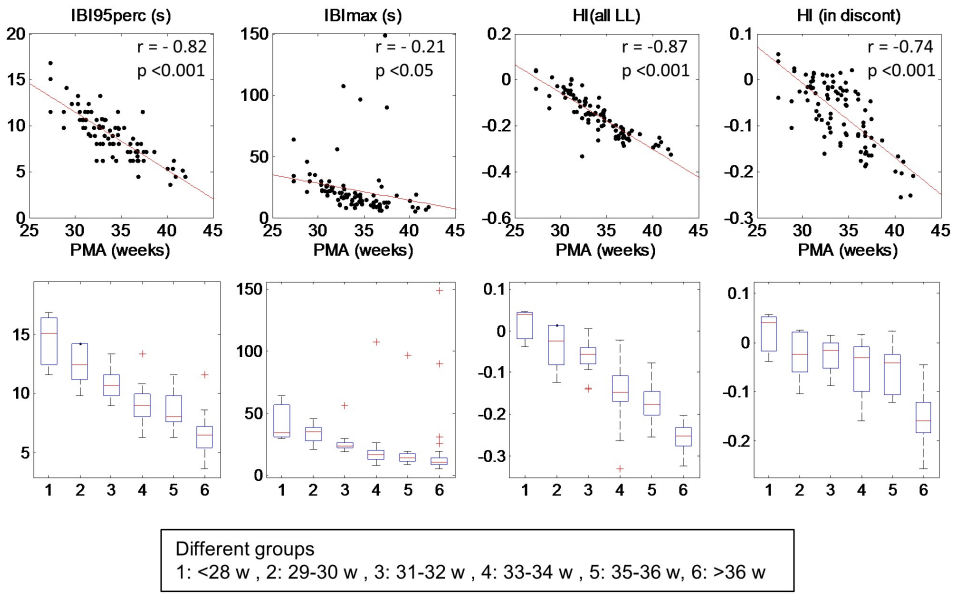

Figure 10.5: Developmental features obtained by applying the burst detection algorithm (Chapter 4) and estimation of the histogram index (HI) (Chapter 6) for a healthy patient group (Bayley score > 85 at 9 months). Maximum interburst interval lengths are depicted, with the 95th percentile being more robust to outliers/artefacts, because the maximum is just a single value. The HI is calculated by including all LL values (full EEG recording) and by including the LL values from only the discontinuous EEG parts.

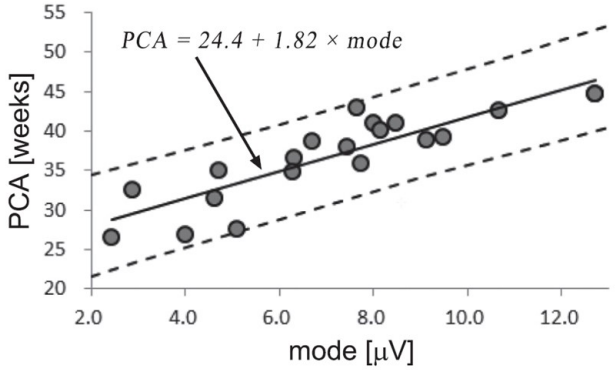

Figure 10.6: A correlation (r=0.73, p<0.01) was found between the mode of the lognormal distribution ($exp(\mu - \sigma^2)$ and the postconceptional age (PCA). The mode is associated with the discontinuity of the EEG (μ) and the asymmetry of the distribution (σ). Figure adapted from Saji et al. (2015).

The energy of the bursts (Koolen et al. 2013) should be further examined to detect abnormalities, such as atypical burst patterns. It is possible that these patients still have a normal ASI value and normal lengths of the bursts/IBIs, in spite of abnormal burst content. In addition, the power in certain frequency bands could reveal further insight. Also the speed of the change in maturational features extracted from one patient's consecutive recordings could provide valuable information, however, one should keep in mind that the administration of medication can have an impact on single recordings. In addition, lot of data is needed to test such hypothesis, because comparison should be available to normative maturational slopes in a similar age range.

10.3.3 Neurodevelopmental outcome prediction based on EEG features

In order to find maturational trends, we have developed methods for feature extraction, with the purpose of immediate/short term assessment. In a final stage of this research, we wanted to explore feature correlation with the long term neurodevelopmental outcome, associated with the following research question:

What lesson can we take home from the EEG at moment of discharge?

We have used the Bayley score at 9 months, since further outcome at 2 years

is not yet available for this population. The Bayley score is a scale which represents the Infant Development, based on a series of measurements assessing both the motor and mental (cognitive and language) development (Albers & Grieve 2007, Weiss et al. 2010, Greene et al. 2012). These derived scores can be compared to the normal range at their respective age.

The data was collected in 2013-2014, with a total of 351 preterm infants born under 34 weeks of gestational age. From this population, 116 preterm infants had a polysomnography at discharge. The neurodevelopmental Bayley score at 9 months was available for 107 patients, because a small number of patients was lost from follow-up. Other inclusion criteria consisted of relative 'artefact free' EEG and enough tracé discontinue or tracé alternant available (>15 minutes). The latter periods were selected by clinical experts A.D. and J.V. As a result, 96 patients were included in the study with a given dichotomous outcome (n=79 with good outcome, n=17 with poor outcome). This clinical outcome was obtained by a composite classification; poor outcome was assigned in case of one or more adverse outcomes (Mental Developmental Index <70, Psychomotor Developmental Index <70, cerebral palsy, blindness, deafness, or death) (Iyer et al. 2015).

Background EEG features were extracted from the EEGs of these 96 patients, at moment of discharge (term age). No further artefact correction was performed on the EEG recordings. We have selected eight features, based on previous research:

1. IBI length: median, 75th percentile, 90th percentile, maximum (see Chapter 4 for detection of IBIs)
2. Histogram index (HI): derived from all LL and derived from the LL in the selected tracé discontinue or alternant (see Chapter 6 and section 10.3.2)
3. ASI: 25th percentile and median (see Chapter 8)

IBIs, ASI and HI were estimated in the most discontinuous periods (visually labeled), whereas HI was additionally calculated based on the whole EEG measurement. Based on descriptive statistics, we could distinguish the most predictable features, as further used. Only linear regression models were considered, due to the relative small number of abnormal labeled patients. Both univariate and multivariate linear regression models were tested to extract the relative importance of the features. In addition, lasso shrinkage was applied for feature selection (formula 10.1) . This lasso shrinkage fits the multivariate linear model, but adds a penalty on overfitting (formula 10.2).

$$\hat{y} = \beta_1 x_1 + \beta_2 x_2 + \ldots + \beta_n x_n + \epsilon \tag{10.1}$$

$$\text{minimize} \sum (y - \hat{y})^2 \;\; \text{subject to} \sum_i |\beta_i| \leq s \tag{10.2}$$

As shown in Figure 10.7A, an influence of PMA at discharge related to outcome is expected. That is, patients which are developing according to 'normal ranges', are not kept longer in the hospital once they have reached term age (36 weeks). Nevertheless, if a baby is born at low GA, maturation can take few more weeks, but still normal outcome is possible. Over all, there is no influence of PMA on the abnormal group; i.e. the number of patients in each age group is constant. After descriptive statistics, we selected 3 features to reduce the number of parameters to estimate based on a, although minor, difference in median between classes: IBI length 75th perc, HI (in discont. EEG) and ASI 25th perc. The class difference for HI is depicted in Figure 10.7B. Only an influence of PMA was found by testing the univariate models (feature – outcome). Using a multivariate linear regression model (formula 10.3) with lasso shrinkage, two features remained in the model: HI in discont. EEG and PMA.

$$\hat{y} = \beta_1 \text{ PMA} + \beta_2 \text{ HI} + \beta_3 \text{ IBI75} + \beta_4 \text{ ASI25} + \epsilon \tag{10.3}$$

However, further research is necessary to confirm that HI is a valuable parameter to predict the neurodevelopmental outcome on a long term. As presented in Figure 10.7C, we observed a (small) difference in classes considering that the mean age range of normal patients is spread around a lower PMA than the mean age range of abnormal patients. This gave a difference a in the HI. In a more ideal situation, the age spread is centered around the same PMA for both classes to counter out the influence of PMA. In this case, a larger difference b might be found (Figure 10.7C). This would mean that in a prospective study, all patients should be recorded at the same moment. However, the moment of discharge, inherently connected to the clinical work flow, cannot change as there is no fixed time point at which the patients are clinically allowed to go home.

In addition, we also trained Support Vector Machine classifiers with a linear kernel. The choice of kernel was due to the relative small data set. Cross-validation with leave-one-out is applied. Results are presented in Table 10.2. Using all the features gave a sensitivity of 63%. This could be little improved by using another smaller feature list (to 68%). By including only the feature PMA to train the classifier, the sensitivity dropped to 42%. An additional 5 abnormal patients were classified as normal, which might mean that the effect of the features should not be underestimated. However, one cannot extract the impact on the outcome of a single feature by using support vector machines (black box model). For this reason, we would prefer the multivariate regression model as an interpretable clinical decision support model.

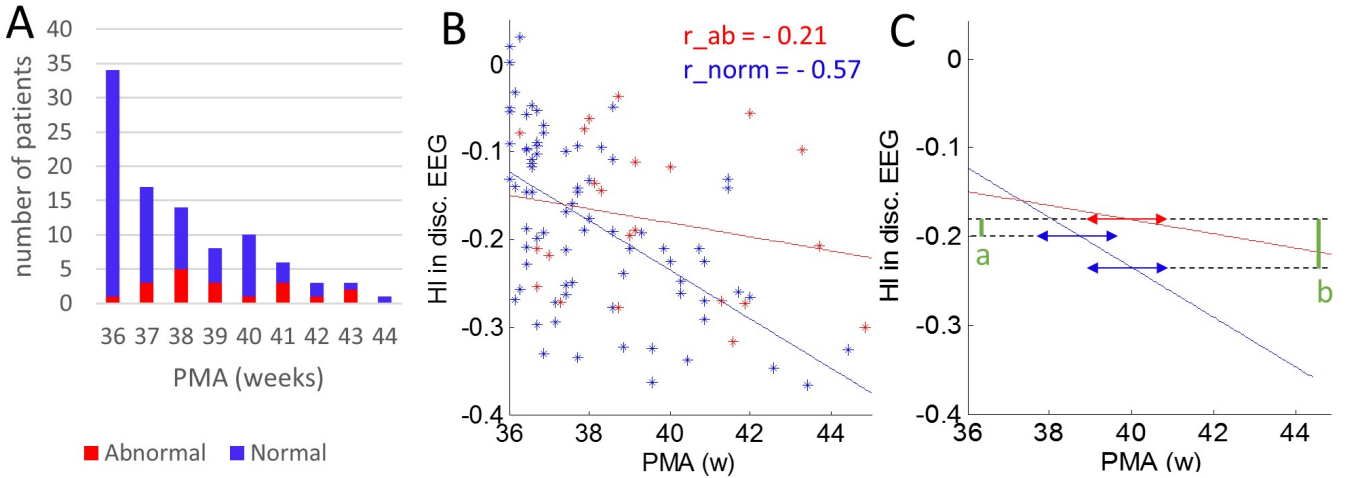

Figure 10.7: (A) Distribution of abnormal and normal patients according to different age groups, (B) Linear regression between PMA and HI (in disc. EEG) is shown. Difference in postmenstrual age correlations between the normal (r_norm) and abnormal (r_ab) class, (C) small difference a is found in the real situation because the age range of normal patients is centered around a younger PMA, whereas in an ideal situation a difference b can be found for both classes centered around a similar age range.

Table 10.2: Performance measures using EEG features to predict the neurodevelopmental outcome at 9 months obtained using support vector machines. Sensitivity, specificity, accuracy are calculated based on the TP (true positive), TN (true negative), FP (false positive) and FN (false negative) numbers.

	Sens.	**Spec.**	**Acc.**
SVM: all 8 features + PMA	0,63	0,73	0,71
SVM: IBI75, HI (disc EEG), ASI25 + PMA	0,63	0,73	0,71
SVM: IBI90, HI (disc EEG), ASI median + PMA	0,68	0,74	0,73
SVM: PMA	0,42	0,74	0,68

	TP	**TN**	**FP**	**FN**
SVM: all 8 features + PMA	12	56	21	7
SVM: IBI75, HI (disc EEG), ASI25 + PMA	12	56	21	7
SVM: IBI90, HI (disc EEG), ASI median + PMA	13	57	20	6
SVM: PMA	8	57	20	11

Due to its preliminary results, one should be careful to draw any conclusions. An overview of several limitations of the current study are given:

1. Other population: older neonates were included, i.e. at term age associated with more mature EEG patterns. Therefore, IBI detection performed less on high voltage sleep or, in general, high voltage activity. Moreover, IBIs are not expected in a normal term infant.

2. Features are estimated in a different way as a consequence of the different set up: IBI and HI feature extraction algorithms were developed to fit the best maturational trend, with a dataset of patients recorded at premature age (Chapters 4 and 6). In other words, the aim of the study was different. For ASI calculation, the age range of the data set was similar, however, in Chapter 8 we tested whether 10 minutes/ 20 minutes of EEG was enough to address the classification problem. In the current research, we had a variable amount of discontinuous EEG available (median: 52.5 minutes), which led to the ASI 25th percentile as a feature resembling the idea of Chapter 8.

3. The outcome is defined in another way: for the current study we used the outcome at 9 months, whereas classification / labeling was previously based on visual scoring the EEG at the moment of recording (for example Chapter 8).

Moreover, it has been shown that it is still a complicated issue to predict the patient's neurodevelopmental progress at examinations at 9 months – 1 year – 2 years. Social and biological risk factors, and their additive effects, are important aspects for developmental risk prognosis (Aylward 1992). That is, next to prematurity, infants could have medical risk factors such as asphyxia, or social risk factors, such as low socioeconomic status, low maternal education, or teenage parenting (DeGraw et al. 1988, Msall et al. 1991, Thompson et al. 1997). In addition to social factors and medical risk factors, there is the physical recovery from the neonatal hospitalization and the resilience of the infant, which affects the trajectory of developmental outcome (Leonard et al. 2001).

10.3.4 Combining modalities into one maturational model

More data is necessary to validate the developed algorithms and the usability of the features extracted in this thesis. It would be beneficial to set up multicenter studies, because applicability could differ among hospitals depending on recording devices and environmental conditions.

Kato et al. (2011) have analyzed the number of EEG electrodes necessary to accurately quantify preterm brain maturation. Both aEEG and cEEG are good tools for the evaluation of the maturation, although conventional EEG showed higher accuracy to estimate the postconceptional age from stable preterm infants. IBIs can be extracted from 1 or more channels, but connectivity metrics can only be applied by using more channels. Regarding channel reduction, a suppression in all EEG channels is still more informative about the global brain activity and severity. Nevertheless, reading aEEG is a first step towards visual cyclicity detection, i.e. discontinuous periods can be roughly annotated. More detailed information about the sleep stages can be extracted by looking at the conventional EEG. In this thesis, we regularly used visually labelled quiet sleep borders for feature extraction, but a next step towards automating this QS detection should not be far away. In order to extract the most discontinuous periods and changes between vigilance states (Scher et al. 2005a, Shellhaas et al. 2014), we have defined the suppression curve. An exploratory step was taken by applying a heuristically chosen threshold on the suppression curve. Yet, further research is necessary to validate or to develop quiet sleep detection algorithms, which would be very valuable (as a preprocessing step) for feature extraction in maturation assessment. Hereby, challenges related to a changing

sleep pattern with increasing age remain. At first, features related to interburst intervals have predictive value for quiet sleep classification in the young preterm infants, however, IBIs disappear when the pattern becomes more continuous (trace alternant/ high voltage sleep). In fact, this change in cyclicity parallel to maturation is worthwhile exploring by itself.

Changes between quiet sleep, active sleep or awake are not only detectable on EEG, but could be worthwhile to explore further in combination with other modalities. In the NICU, vital signals such as the heart rate, blood oxygenation, blood pressure and respiratory rate are measured. Incorporating this information could optimize cyclicity assessment and quiet sleep extraction. In the interest of the neonatal comfort, we have also worked on noncontact respiration monitoring (Koolen et al. 2015a). The goal was to extract the respiration rate from video data included in a polysomnography. After amplifying the respiration movements by Eulerian video magnification, the optical flow algorithm was applied to obtain the respiration rate during quiet sleep stages (Koolen et al. 2015a). Respiration monitoring, or even heart rate monitoring, through video analysis could be very beneficial to improve the patient's comfort in the NICU or to monitor in a home environment.

To combine multichannel EEG data or all these data obtained from different modalities into one structure, tensor structures could be implemented (Matic et al. 2014). Representing information dependencies in more than two dimensions is possible with a tensor structure, which is an extension of matrix (2D) and vector (1D) structures. A possible tensor could have the dimensions *time x EEG channels x extracted feature.* In this way, the topography of the electrodes could be included. A further dimension could be sequential recordings at longer time scale. The aim would be to extract information by using an optimal tensor-decomposition, with the Canonical Polyadic model or decomposition in blockterms. This information could be further used in a classification model (to detect abnormalities) or for dimensionality reduction, as an alternative for two-dimensional decomposition with factor scores or Principal Component Analysis. However, there is a huge unbalance in 'normal'/ 'abnormal' sample sizes. Moreover, abnormal patterns do not have similar background anomalies, and therefore it will be challenging to distinguish this class. Another way could be to define the classes with respect to different age ranges. In this way, one could extract an expected state of maturation relative to the age class. Nevertheless, changes by reduction in EEG leads will necessarily lead to new training steps. Supervised learning algorithms which are trained on the full set of EEG signals have to be adapted, such as support vector machines or tensor methods. In conclusion, the aim should be well defined to take advantage of tensor models to extract the interaction between synchronizing events and to identify relevant maturational components.

Appendix A

Patient Data Sets

Table A.1: Patient data sets: overview per chapter

	when rec	GA (w)	PMA (w)	# patients	# EEGs	# norm – # abn patients	reason abnnormalities
Chapter 4 Line Length	Jan 2011 - Nov 2012	24 - 32	26 - 34	10	13	3 – 7	**EEG definition (based on visual classification)** 2 subjects had a suspicion of convulsions, 2 suffered from mild peripartal asphyxia and 3 suffered from intracranial hemorrhage. **based on outcome**: 3 subjects abnormal
Chapter 5 Suppression Curve	Feb 2013 - Sep 2014	24 - 32	27 - 42	25	90	25 – 0	**all normal patients based on 9 months outcome**
Chapter 6 Histogram Index	June 2013 - Sep 2014	25 - 31	27 - 40	22	84	17 – 5	**EEG definition (based on visual classification)** 3 patients delayed maturation, 2 patients mildly abn.
Chapter 7 Symmmetry Classification	Jul 2010 - Oct 2013	24 - 40	26 - 43	47	92	According to brain region central: 73 – 7 – (12 artef) frontal: 81 – 3 – (8 artef) occipital: 74 – 6 – (12 artef) temporal: 76 – 8 – (8 artef)	**EEG definition (based on visual classification)** structural brain abnormalities (acquired or congenital), clinical convulsions
Chapter 8 Synchrony Classification	Mar 2013 - Aug 2014	25 - 42	36 - 42	31	31	14 – 17	**EEG definition (based on visual classification)** Abnormality based on clinical scoring of 1. brain activity cycling 2. grade of continuity 3. age-spec landmarks: ampl., disorganization and dysmaturation 4. qualitative synchrony in quiet sleep
Chapter 9 Synchrony Maturation	Jan 2011 - June 2014	24 - 40	30 - 44	20	22	15 – 5	**EEG definition (based on visual classification)** 1 subject extremely premature + grade III hemorrhage, 2 patients peripartal asphyxia at premature age, 2 patients hemorrhage

Appendix B

Supplementary material: The suppression curve as a quantitative approach for measuring brain maturation in preterm infants (Chapter 5)

Table B.1: Demographic and clinical data of the study population. Values are expressed as n (%), mean ± SD, range. BPD: need for supplemental oxygen/ventilation at 36 weeks PMA. Sepsis: positive blood culture or highly suspected with antibiotic treatment > 72h.

Characteristics	**patients (N=25)**
Gestational age (weeks+days)	28 5/7 ± 2 2/7 (range: 24 4/7-32)
Man:Female	9:16 (36%:64%)
Birth weight, g	1277 ± 451 (range: 540-2540)
Respiratory support	
• Conventional mechanical ventilation (SIMV)	9 (range: 1 - 28 days)
• High-frequency oscillation ventilation	3 (range: 8 - 13 days)
• Nasal continuous positive airway pressure	24 (range: 1 - 63 days)
Patent Ductus Arteriosus (PDA)	
• Drug (Ibuprofen)	6 (24%)
• Surgical ligation	2 (8%)
Postnatal Corticosteroids (Hydrocortisone)	3 (12%)
Sepsis/ Antibiotics > 72h	15 (60%)
Necrotizing Enterocolitis (NEC)	2 (8%)
Cranial Ultrasound	
• Normal	15 (60%)
• Grade I Intraventricular haemorrhage (IVH)	3 (12%)
• Grade II Intraventricular haemorrhage (IVH)	2 (8%)
• Flaring < 14d	5 (20%)
Retinopathy of prematurity (ROP) with laser therapy	3 (12%)
Bronchopulmonary dysplasia (BPD)	2 (8%)
Developmental outcome at corrected age of 9 months	
• Bayley Mental - II (MDI)	109 ± 12
• Bayley Motor - II (PDI)	113 ± 15

Appendix C

Supplementary material: Interhemispheric synchrony in the neonatal EEG revisited: Activation Synchrony Index as a promising classifier (Chapter 8)

C.1 Supplementary table: Detailed overview of the selected patients

With the following specifications: PMA = postmenstrual age

GLOBAL ASSESSMENT: 1= ABNORMAL : at least 2 abnormal features 0= NORMAL: no more than 1 abnormal feature

FEATURE: continuity, symmetry, synchrony, voltage, sleep, variability, dysmaturity, normal age transients, abnormal patterns

NORMAL CONTINUITY = continuous EEG in AS and AW, TA $>$ 38 weeks, 36-38 weeks TA or DC with IBI $<$10 sec,

SLEEP STAGE = sleep stage: QS (Quiet Sleep), AS (Active Sleep), AW (Active Wake), QS: DC (discontinuous pattern) or TA (tracé alternant)

AGE SPECIFIC TRANSIENTS: presence of different sleep stages: AS I, AS II en QS, specific transient: frontal ant dysrythmia, frontal sharps, occipital delta brushes, QS/AS

Table C.1: Detailed overview of the selected patients

	PMA	**FEATURE: continuity, symmetry, synchrony, voltage, sleep, variability, dysmaturity, normal age transients, abnormal patterns**		**GLOBAL ASSESSMENT**
PT 1	37 6/7	continuity, synchrony, abnormal patterns	discontinuity in QS, no TA, a clearly percentage of EEG bursts occur asynchronously (greater than 1.5 seconds between onset of activity in each hemisphere) during DC EEG, excessive sharp wave transients	1
PT 2	37 4/7	continuity, synchrony, sleep, abnormal patterns	discontinuity in QS, no TA , a clearly percentage of EEG bursts occur asynchronously (greater than 1.5 seconds between onset of activity in each hemisphere) during DC EEG, preponderance of QS, excessive sharp wave transients	1
PT 3	37 4/7	continuity, synchrony, dysmaturity	discontinuity in QS no TA, a clearly excessive percentage of EEG bursts occur asynchronously (greater than 1.5 seconds between onset of activity in each hemisphere) during DC EEG, EEG that would be normal for an infant at least two weeks younger than the PMA, abundance of temporal theta	1

	PMA	FEATURE: continuity, symmetry, synchrony, voltage, sleep, variability, dysmaturity, normal age transients, abnormal patterns		GLOBAL ASSESSMENT
PT 4	37	continuity, synchrony, voltage, sleep, age transients, abnormal patterns	excessive discontinuity in all states, a clearly percentage of EEG bursts occur asynchronously (greater than 1.5 seconds between onset of activity in each hemisphere) during DC EEG, global voltage depression, lack of normal SWC, lack of normal transients, excessive sharp wave transients	1
PT 5	36 6/7	continuity, synchrony, variability, age transients, abnormal patterns	excessive discontinuity in all states, a clearly percentage of EEG bursts occur asynchronously (greater than 1.5 seconds between onset of activity in each hemisphere) during DC EEG, variability but no SWC , excessive sharp wave transients	1
PT 6	38	continuity, synchrony, variability, age transients, abnormal patterns	excessive discontinuity in all states, a clearly percentage of EEG bursts occur asynchronously (greater than 1.5 seconds between onset of activity in each hemisphere) during DC EEG, variability but no SWC , excessive sharp wave transients	1
PT 7	40 1/7	continuity, synchrony, sleep, age transients	normal continuity, normal synchrony, normal SWC, normal transients for age	0

	PMA	**FEATURE: continuity, symmetry, synchrony, voltage, sleep, variability, dysmaturity, normal age transients, abnormal patterns**		**GLOBAL ASSESSMENT**
PT 8	36	continuity, synchrony, dysmaturity	excessive discontinuity in QS, a clearly excessive percentage of EEG bursts occur asynchronously (greater than 1.5 seconds between onset of activity in each hemisphere) during DC EEG, EEG that would be normal for an infant at least two weeks younger than the PMA	1
PT 9	37 4/7	continuity, synchrony, abnormal patterns	discontinuity in QS, no TA, a clearly percentage of EEG bursts occur asynchronously (greater than 1.5 seconds between onset of activity in each hemisphere) during DC EEG, excessive sharp wave transients	1
PT 10	44	continuity, synchrony, sleep, age transients	normal continuity, normal synchrony, normal SWC, normal transients for age, some sharp wave transients	0
PT 11	40 6/7	continuity, synchrony, variability, age transients, abnormal patterns	excessive discontinuity in all states, a clearly percentage of EEG bursts occur asynchronously (greater than 1.5 seconds between onset of activity in each hemisphere) during DC EEG, variability but no SWC , excessive sharp wave transients	1

	PMA	FEATURE: continuity, symmetry, synchrony, voltage, sleep, variability, dysmaturity, normal age transients, abnormal patterns		GLOBAL ASSESSMENT
PT 12	40 6/7	continuity, synchrony, sleep, age transients	normal continuity, normal synchrony, normal SWC, normal transients for age	0
PT 13	36 5/7	continuity, synchrony, age transients	trace discontinue/TA in QS, normal synchrony, normal transients	0
PT 14	38	continuity, synchrony, sleep, age transients	normal continuity, normal synchrony, normal SWC, borderline transients for age: proportion of delta brushes in all states (rater 1: 1, rater 2:0)	0
PT 15	37 1/7	continuity, synchrony, sleep, age transients	normal continuity, normal synchrony, normal SWC, normal transients for age	0
PT 16	38 2/7	continuity, synchrony, dysmaturity	trace discontinue in QS, a clearly excessive percentage of EEG bursts occur asynchronously (greater than 1.5 seconds between onset of activity in each hemisphere) during DC EEG, EEG that would be normal for an infant at least two weeks younger than the PMA	1

	PMA	**FEATURE: continuity, symmetry, synchrony, voltage, sleep, variability, dysmaturity, normal age transients, abnormal patterns**		**GLOBAL ASSESSMENT**
PT 17	42	continuity, synchrony, sleep, age transients, abnormal patterns	trace discontinue in QS, a clearly percentage of EEG bursts occur asynchronously (greater than 1.5 seconds between onset of activity in each hemisphere) during DC EEG, global voltage depression, lack of normal transients, excessive occipital delta	1
PT 18	37 1/7	continuity, synchrony, age transients	trace discontinue/TA in QS, normal synchrony, normal transients	0
PT 19	40 5/7	continuity, synchrony, sleep, age transients	normal continuity, normal synchrony, normal SWC, normal transients for age	0
PT 20	40 1/7	continuity, synchrony, sleep, age transients	normal continuity, normal synchrony, normal SWC, normal transients for age	0
PT 21	38 2/7	continuity, synchrony, symmetry, abnormal patterns	trace discontinue in QS, no TA, a clearly percentage of EEG bursts occur asynchronously (greater than 1.5 seconds between onset of activity in each hemisphere) during DC EEG, 2:1 difference in voltages and a clear disparity of background features between homologous regions of the two hemispheres, excessive sharp transients	1

	PMA	FEATURE: continuity, symmetry, synchrony, voltage, sleep, variability, dysmaturity, normal age transients, abnormal patterns		GLOBAL ASSESSMENT
PT 22	36 3/7	continuity, synchrony, dysmaturity	trace discontinue in QS, a clearly excessive percentage of EEG bursts occur asynchronously (greater than 1.5 seconds between onset of activity in each hemisphere) during DC EEG, EEG that would be normal for an infant at least two weeks younger than the PMA	1
PT 23	38 1/7	continuity, synchrony, sleep, abnormal patterns	discontinuity in all states, a clearly percentage of EEG bursts occur asynchronously (greater than 1.5 seconds between onset of activity in each hemisphere) during DC EEG, lack of normal SWC, excessive sharp wave transients	1
PT 24	41 3/7	continuity, synchrony, sleep, age transients	normal continuity, normal synchrony, normal SWC, borderline sharp wave transients	0
PT 25	39 5/7	continuity, synchrony, dysmaturity	trace discontinue in QS, a clearly excessive percentage of EEG bursts occur asynchronously (greater than 1.5 seconds between onset of activity in each hemisphere) during DC EEG, EEG that would be normal for an infant at least two weeks younger than the PMA	1

	PMA	**FEATURE: continuity, symmetry, synchrony, voltage, sleep, variability, dysmaturity, normal age transients, abnormal patterns**		**GLOBAL ASSESSMENT**
PT 26	37 6/7	continuity, synchrony, symmetry, variability, age transients, abnormal patterns	trace discontinue in all states, a clearly percentage of EEG bursts occur asynchronously (greater than 1.5 seconds between onset of activity in each hemisphere) during DC EEG, 2:1 difference in voltages and a clear disparity of background features between homologous regions of the two hemispheres, excessive sharp transients	1
PT 27	40 6/7	continuity, synchrony, sleep, age transients	normal continuity, normal synchrony, normal SWC, normal transients for age	0
PT 28	37 4/7	continuity, synchrony, dysmaturity	trace discontinue/TA in QS, normal synchrony, borderline dysmaturity: EEG that would be normal for an infant at least 1 week younger than the PMA	0
PT 29	36 3/7	continuity, synchrony, sleep, age transients	normal continuity, normal synchrony, normal SWC, normal transients for age	0
PT 30	41 6/7	continuity, synchrony, sleep, age transients	normal continuity, normal synchrony, normal SWC, normal transients for age	0

	PMA	FEATURE: continuity, symmetry, synchrony, voltage, sleep, variability, dysmaturity, normal age transients, abnormal patterns		GLOBAL ASSESSMENT
PT 31	39 1/7	continuity, synchrony, dysmaturity, abnormal patterns	trace discontinue in QS, a clearly excessive percentage of EEG bursts occur asynchronously (greater than 1.5 seconds between onset of activity in each hemisphere) during DC EEG, EEG that would be normal for an infant at least two weeks younger than the PMA, borderline sharp wave transients (rater 1: 1, rater 2:0)	1

Bibliography

Aarnoudse-Moens, C. S. H., Weisglas-Kuperus, N., van Goudoever, J. B. & Oosterlaan, J. (2009), 'Meta-analysis of neurobehavioral outcomes in very preterm and/or very low birth weight children.', *Pediatrics* **124**(2), 717–728.

Accardo, A., Affinito, M., Carrozzi, M. & Bouquet, F. (1997), 'Use of the fractal dimension for the analysis of electroencephalographic time series.', *Biol Cybern* **77**(5), 339–350.

Agarwal, R., Gotman, J., Flanagan, D. & Rosenblatt, B. (1998), 'Automatic eeg analysis during long-term monitoring in the icu.', *Electroencephalogr Clin Neurophysiol* **107**(1), 44–58.

Albers, C. A. & Grieve, A. J. (2007), 'Review of bayley scales of infant and toddler development–'.

Anderson, C. M., Torres, F. & Faoro, A. (1985), 'The eeg of the early premature.', *Electroencephalogr Clin Neurophysiol* **60**(2), 95–105.

André, M., Lamblin, M.-D., d'Allest, A. M., Curzi-Dascalova, L., Moussalli-Salefranque, F., S Nguyen The, T., Vecchierini-Blineau, M.-F., Wallois, F., Walls-Esquivel, E. & Plouin, P. (2010), 'Electroencephalography in premature and full-term infants. developmental features and glossary.', *Neurophysiol Clin* **40**(2), 59–124.

Arnold, M., Doering, A., Witte, H., Dörschel, J. & Eisel, M. (1996), 'Use of adaptive hilbert transformation for eeg segmentation and calculation of instantaneous respiration rate in neonates.', *J Clin Monit* **12**(1), 43–60.

Atit, M., Hagan, J., Bansal, S., Ichord, R., Geocadin, R., Hansen, C., Sherman, D. & Thakor, N. (1999), EEG burst detection: performance evaluation, *in* '[Engineering in Medicine and Biology, 1999. 21st Annual Conference and the 1999 Annual Fall Meetring of the Biomedical Engineering Society] BMES/EMBS Conference, 1999. Proceedings of the First Joint', Vol. 1.

Aviyente, S. & Mutlu, A. Y. (2011), 'A time-frequency-based approach to phase and phase synchrony estimation', **59**(7), 3086–3098.

Aylward, G. P. (1992), 'The relationship between environmental risk and developmental outcome.', *J Dev Behav Pediatr* **13**(3), 222–229.

Azzopardi, D., Robertson, N. J., Cowan, F. M., Rutherford, M. A., Rampling, M. & Edwards, A. D. (2000), 'Pilot study of treatment with whole body hypothermia for neonatal encephalopathy.', *Pediatrics* **106**(4), 684–694.

Back, S. A. & Miller, S. P. (2014), 'Brain injury in premature neonates: A primary cerebral dysmaturation disorder?', *Ann Neurol* **75**(4), 469–486.

Barlow, J. S. (1985), 'Computer characterization of tracé alternant and rem sleep patterns in the neonatal eeg by adaptive segmentation–an exploratory study.', *Electroencephalogr Clin Neurophysiol* **60**(2), 163–173.

Beck, S., Wojdyla, D., Say, L., Betran, A. P., Merialdi, M., Requejo, J. H., Rubens, C., Menon, R. & Van Look, P. F. A. (2010), 'The worldwide incidence of preterm birth: a systematic review of maternal mortality and morbidity.', *Bull World Health Organ* **88**(1), 31–38.

Behrmann, M. & Plaut, D. C. (2015), 'A vision of graded hemispheric specialization', *Annals of the New York Academy of Sciences* .

Bell, A. H., Greisen, G. & Pryds, O. (1993), 'Comparison of the effects of phenobarbitone and morphine administration on eeg activity in preterm babies.', *Acta Paediatr* **82**(1), 35–39.

Benda, G. I., Engel, R. C. & Zhang, Y. P. (1989), 'Prolonged inactive phases during the discontinuous pattern of prematurity in the electroencephalogram of very-low-birthweight infants.', *Electroencephalogr Clin Neurophysiol* **72**(3), 189–197.

Benders, M. J., Palmu, K., Menache, C., Borradori-Tolsa, C., Lazeyras, F., Sizonenko, S., Dubois, J., Vanhatalo, S. & Hüppi, P. S. (2014), 'Early brain activity relates to subsequent brain growth in premature infants.', *Cereb Cortex* .

Bertrand, A. & Moonen, M. (2013), 'Seeing the bigger picture: How nodes can learn their place within a complex ad hoc network topology', **30**(3), 71–82.

Bhattacharyya, S., Biswas, A., Mukherjee, J., Majumdar, A. K., Majumdar, B., Mukherjee, S. & Singh, A. K. (2011), 'Feature selection for automatic burst detection in neonatal electroencephalogram', *IEEE Journal on Emerging and Selected Topics in Circuits and Systems* **1**(4), 469–479.

Biagioni, E., Bartalena, L., Boldrini, A., Cioni, G., Giancola, S. & Ipata, A. E. (1994), 'Background eeg activity in preterm infants: correlation of outcome with selected maturational features.', *Electroencephalogr Clin Neurophysiol* **91**(3), 154–162.

Biagioni, E., Frisone, M. F., Laroche, S., Kapetanakis, B. A., Ricci, D., Adeyi-Obe, M., Lewis, H., Kennea, N., Cioni, G., Cowan, F., Rutherford, M., Azzopardi, D. & Mercuri, E. (2007), 'Maturation of cerebral electrical activity and development of cortical folding in young very preterm infants.', *Clin Neurophysiol* **118**(1), 53–59.

Biswal, B., Yetkin, F. Z., Haughton, V. M. & Hyde, J. S. (1995), 'Functional connectivity in the motor cortex of resting human brain using echo-planar mri.', *Magn Reson Med* **34**(4), 537–541.

Blencowe, H., Cousens, S., Oestergaard, M. Z., Chou, D., Moller, A.-B., Narwal, R., Adler, A., Vera Garcia, C., Rohde, S., Say, L. & Lawn, J. E. (2012), 'National, regional, and worldwide estimates of preterm birth rates in the year 2010 with time trends since 1990 for selected countries: a systematic analysis and implications.', *Lancet* **379**(9832), 2162–2172.

Blinowska, K. J. (2011), 'Review of the methods of determination of directed connectivity from multichannel data.', *Med Biol Eng Comput* **49**(5), 521–529.

Bressler, S. L. & Menon, V. (2010), 'Large-scale brain networks in cognition: emerging methods and principles.', *Trends Cogn Sci* **14**(6), 277–290.

Bullmore, E. & Sporns, O. (2009), 'Complex brain networks: graph theoretical analysis of structural and functional systems.', *Nat Rev Neurosci* **10**(3), 186–198.

Bullock, T. H., Achimowicz, J. Z., Duckrow, R. B., Spencer, S. S. & Iragui-Madoz, V. J. (1997), 'Bicoherence of intracranial eeg in sleep, wakefulness and seizures.', *Electroencephalogr Clin Neurophysiol* **103**(6), 661–678.

Buzsáki, G. & Mizuseki, K. (2014), 'The log-dynamic brain: how skewed distributions affect network operations', *Nature Reviews Neuroscience* **15**(4), 264–278.

Cabukovski, V., Rudolf, N. d. M. & Mahmood, N. (1993), 'Measuring the fractal dimension of eeg signals: selection and adaptation of method for real-time analysis', *Transactions on Biomedicine and Health* **1**, 285–292.

Cammu, H., Martens, G., Martens, E., Coen, K. & Defoort, P. (2009), 'Perinatale activiteiten in vlaanderen 2008.'.

Cawley, G. (2006), Leave-one-out cross-validation based model selection criteria for weighted LS-SVMs, *in* 'Neural Networks, 2006. IJCNN '06. International Joint Conference on', pp. 1661–1668.

Chang, C.-C. & Lin, C.-J. (2011), 'Libsvm: A library for support vector machines', *ACM Transactions on Intelligent Systems and Technology (TIST)* **2**(3), 27.

Chau, V., Synnes, A., Grunau, R. E., Poskitt, K. J., Brant, R. & Miller, S. P. (2013), 'Abnormal brain maturation in preterm neonates associated with adverse developmental outcomes.', *Neurology* **81**(24), 2082–2089.

Cherian, P. J., Deburchgraeve, W., Swarte, R. M., De Vos, M., Govaert, P., Van Huffel, S. & Visser, G. H. (2011), 'Validation of a new automated neonatal seizure detection system: a clinician's perspective.', *Clin Neurophysiol* **122**(8), 1490–1499.

Cherian, P. J., Swarte, R. M. & Visser, G. H. (2009), 'Technical standards for recording and interpretation of neonatal electroencephalogram in clinical practice.', *Ann Indian Acad Neurol* **12**(1), 58–70.

Colonnese, M. & Khazipov, R. (2012), 'Spontaneous activity in developing sensory circuits: Implications for resting state fmri.', *Neuroimage* **62**(4), 2212–2221.

Conde, J. R. C., de Hoyos, A. L. R., Martínez, E. D., Campo, C. G., Pérez, A. M. & Borges, A. A. H. (2005), 'Extrauterine life duration and ontogenic eeg parameters in preterm newborns with and without major ultrasound brain lesions.', *Clin Neurophysiol* **116**(12), 2796–2809.

Connell, J. A., Oozeer, R. & Dubowitz, V. (1987), 'Continuous 4-channel eeg monitoring: a guide to interpretation, with normal values, in preterm infants.', *Neuropediatrics* **18**(3), 138–145.

Daylan, P. & Abbott, L. (2005), *Theoratical Neuroscience: Computational and Mathematical Modeling of Neural Systems*, The MIT Press.

De Clercq, W., Vergult, A., Vanrumste, B., Van Paesschen, W. & Van Huffel, S. (2006), 'Canonical correlation analysis applied to remove muscle artifacts from the electroencephalogram.', *IEEE Trans Biomed Eng* **53**(12 Pt 1), 2583–2587.

De Vos, M., Deburchgraeve, W., Cherian, P. J., Matic, V., Swarte, R. M., Govaert, P., Visser, G. H. & Van Huffel, S. (2011), 'Automated artifact removal as preprocessing refines neonatal seizure detection.', *Clin Neurophysiol* **122**(12), 2345–2354.

de Vries, L. S. & Toet, M. C. (2006), 'Amplitude integrated electroencephalography in the full-term newborn.', *Clin Perinatol* **33**(3), 619–32, vi.

Deburchgraeve, W. (2010), Development of an automated neonatal EEG seizure monitor., PhD thesis, Department of Electrical Engineering, Katholieke Universiteit, Leuven.

Deburchgraeve, W., Cherian, P. J., De Vos, M., Swarte, R. M., Blok, J. H., Visser, G. H., Govaert, P. & Van Huffel, S. (2008), 'Automated neonatal seizure detection mimicking a human observer reading eeg.', *Clin Neurophysiol* **119**(11), 2447–2454.

Deburchgraeve, W., Cherian, P. J., De Vos, M., Swarte, R. M., Blok, J. H., Visser, G. H., Govaert, P. & Van Huffel, S. (2009), 'Neonatal seizure localization using parafac decomposition.', *Clin Neurophysiol* **120**(10), 1787–1796.

DeGraw, C., Edell, D., Ellers, B., Hillemeier, M., Liebman, J., Perry, C. & Palfrey, J. S. (1988), 'Public law 99-457: new opportunities to serve young children with special needs.', *J Pediatr* **113**(6), 971–974.

Dereymaeker, A., Koolen, N., Vervisch, J., Ortibus, E., Jansen, K., De Vos, M., Van Huffel, S. & Naulaers, G. (2015), The suppression curve as a quantitative approach for measuring brain maturation in preterm infants. submitted to Clinical Neurophysiology.

Dolan, K., Martens, H. C. F., Schuurman, P. R. & Bour, L. J. (2009), 'Automatic noise-level detection for extra-cellular micro-electrode recordings.', *Med Biol Eng Comput* **47**(7), 791–800.

Douglass, L. M., Wu, J. Y., Rosman, N. P. & Stafstrom, C. E. (2002), 'Burst suppression electroencephalogram pattern in the newborn: predicting the outcome.', *J Child Neurol* **17**(6), 403–408.

Dudink, J., Kerr, J. L., Paterson, K. & Counsell, S. J. (2008), 'Connecting the developing preterm brain.', *Early Hum Dev* **84**(12), 777–782.

Ebersole, J. S. & Pedley, T. A. (2003), *Current practice of clinical electroencephalography*, Lippincott Williams & Wilkins.

Eiselt, M., Schindler, J., Arnold, M., Witte, H., Zwiener, U. & Frenzel, J. (2001), 'Functional interactions within the newborn brain investigated by adaptive coherence analysis of eeg.', *Neurophysiol Clin* **31**(2), 104–113.

Esteller, R., Echauz, J., Tcheng, T., Litt, B. & Pless, B. (2001a), Line length: an efficient feature for seizure onset detection, *in* 'Engineering in Medicine and Biology Society, 2001. Proceedings of the 23rd Annual International Conference of the IEEE', Vol. 2, pp. 1707–1710.

Esteller, R., Vachtsevanos, G., Echauz, J. & Litt, B. (2001b), 'A comparison of waveform fractal dimension algorithms', **48**(2), 177–183.

Faes, L., Erla, S. & Nollo, G. (2012), 'Block partial directed coherence: a new tool for the structural analysis of brain networks.', *Int J Bioelectromag* **14**(4), 162–166.

Finch, W. H. & Schneider, M. K. (2006), 'Misclassification rates for four methods of group classification impact of predictor distribution, covariance inequality, effect size, sample size, and group size ratio', *Educational and Psychological Measurement* **66**(2), 240–257.

Fodor, I. (2002), A survey of dimension reduction techniques., Technical report, LLNL Technical Report, UCRL-ID-148494.

Fourie, C., Van Niekerk, A. & Mucina, L. (2011), Optimising a one-class svm for geographic object-based novelty detection, *in* 'Proceedings of the first AfricaGeo conference', pp. 1–25.

Ghanta, S., Abdel-Latif, M. E., Lui, K., Ravindranathan, H., Awad, J. & Oei, J. (2007), 'Propofol compared with the morphine, atropine, and suxamethonium regimen as induction agents for neonatal endotracheal intubation: a randomized, controlled trial.', *Pediatrics* **119**(6), e1248–e1255.

González, J. J., Mañas, S., De Vera, L., Méndez, L. D., López, S., Garrido, J. M. & Pereda, E. (2011), 'Assessment of electroencephalographic functional connectivity in term and preterm neonates.', *Clin Neurophysiol* **122**(4), 696–702.

Greene, M. M., Patra, K., Nelson, M. N. & Silvestri, J. M. (2012), 'Evaluating preterm infants with the bayley-iii: patterns and correlates of development', *Research in developmental disabilities* **33**(6), 1948–1956.

Griessbach, G., Eiselt, M., Dörschel, J., Witte, H. & Galicki, M. (1997), 'Common optimization of adaptive preprocessing units and a neural network during the learning period. application in eeg pattern recognition.', *Neural Netw* **10**(6), 1153–1163.

Grieve, P. G., Emerson, R. G., Isler, J. R. & Stark, R. I. (2004), 'Quantitative analysis of spatial sampling error in the infant and adult electroencephalogram.', *Neuroimage* **21**(4), 1260–1274.

Grieve, P. G., Isler, J. R., Izraelit, A., Peterson, B. S., Fifer, W. P., Myers, M. M. & Stark, R. I. (2008), 'Eeg functional connectivity in term age extremely low birth weight infants.', *Clin Neurophysiol* **119**(12), 2712–2720.

Grigg-Damberger, M., Gozal, D., Marcus, C. L., Quan, S. F., Rosen, C. L., Chervin, R. D., Wise, M., Picchietti, D. L., Sheldon, S. H. & Iber, C. (2007), 'The visual scoring of sleep and arousal in infants and children.', *J Clin Sleep Med* **3**(2), 201–240.

Hahn, J. S., Monyer, H. & Tharp, B. R. (1989), 'Interburst interval measurements in the eegs of premature infants with normal neurological outcome.', *Electroencephalogr Clin Neurophysiol* **73**(5), 410–418.

Hanganu-Opatz, I. L. (2010), 'Between molecules and experience: role of early patterns of coordinated activity for the development of cortical maps and sensory abilities.', *Brain Res Rev* **64**(1), 160–176.

Hartley, C., Berthouze, L., Mathieson, S. R., Boylan, G. B., Rennie, J. M., Marlow, N. & Farmer, S. F. (2012), 'Long-range temporal correlations in the eeg bursts of human preterm babies.', *PLoS One* **7**(2), e31543.

Havlicek, V., Childiaeva, R. & Chernick, V. (1975), 'Ontogeny of eeg power characteristics of quiet sleep periodic cerebral rhythm in preterm infants', *Neuropaediatrie* **6**(02), 151–161.

Hayakawa, M., Okumura, A., Hayakawa, F., Watanabe, K., Ohshiro, M., Kato, Y., Takahashi, R. & Tauchi, N. (2001), 'Background electroencephalographic (eeg) activities of very preterm infants born at less than 27 weeks gestation: a study on the degree of continuity.', *Arch Dis Child Fetal Neonatal Ed* **84**(3), F163–F167.

Hayashi-Kurahashi, N., Kidokoro, H., Kubota, T., Maruyama, K., Kato, Y., Kato, T., Natsume, J., Hayakawa, F., Watanabe, K. & Okumura, A. (2012), 'Eeg for predicting early neurodevelopment in preterm infants: an observational cohort study.', *Pediatrics* **130**(4), e891–e897.

Hellström-Westas, L., Klette, H., Thorngren-Jerneck, K. & Rosén, I. (2001), 'Early prediction of outcome with aeeg in preterm infants with large intraventricular hemorrhages.', *Neuropediatrics* **32**(6), 319–324.

Hellström-Westas, L. & Rosén, I. (2005), 'Electroencephalography and brain damage in preterm infants.', *Early Hum Dev* **81**(3), 255–261.

Hellström-Westas, L., Rosén, I., De Vries, L. & Greisen, G. (2006), 'Amplitude-integrated eeg classification and interpretation in preterm and term infants', *NeoReviews* **7**(2), e76–e87.

Holmes, G. L. & Lombroso, C. T. (1993), 'Prognostic value of background patterns in the neonatal eeg.', *J Clin Neurophysiol* **10**(3), 323–352.

Hunyadi, B., De Vos, M., Signoretto, M., Suykens, J. A., Van Paesschen, W. & Van Huffel, S. (2011), Automatic seizure detection incorporating structural information, *in* 'Artificial Neural Networks and Machine Learning–ICANN 2011', Springer, pp. 233–240.

Hunyadi, B., De Vos, M., Van Paesschen, W. & Van Huffel, S. (2010), 'A mimicking approach for human epileptic seizure detection', *Proc. of the International Biosignal Processing Conference* pp. 1–4.

Hutchison, R. M., Womelsdorf, T., Allen, E. A., Bandettini, P. A., Calhoun, V. D., Corbetta, M., Della Penna, S., Duyn, J. H., Glover, G. H., Gonzalez-Castillo, J., Handwerker, D. A., Keilholz, S., Kiviniemi, V., Leopold, D. A., de Pasquale, F., Sporns, O., Walter, M. & Chang, C. (2013), 'Dynamic functional connectivity: promise, issues, and interpretations.', *Neuroimage* **80**, 360–378.

Institute of Medicine (2007), 'Preterm birth: Causes, consequences, and prevention.', Washington, D.C.: National Academy Press.

Iyer, K. K., Roberts, J. A., Hellström-Westas, L., Wikström, S., Hansen Pupp, I., Ley, D., Vanhatalo, S. & Breakspear, M. (2015), 'Cortical burst dynamics predict clinical outcome early in extremely preterm infants.', *Brain* **138**(Pt 8), 2206–2218.

Jaseja, H. (2009), 'Significance of the eeg in the decision to initiate antiepileptic treatment in patients with epilepsy: a perspective on recent evidence.', *Epilepsy Behav* **16**(2), 345–346.

Jennekens, W., Niemarkt, H. J., Engels, M., Pasman, J. W., van Pul, C. & Andriessen, P. (2012), 'Topography of maturational changes in eeg burst spectral power of the preterm infant with a normal follow-up at 2 years of age.', *Clin Neurophysiol* **123**(11), 2130–2138.

Jennekens, W., Ruijs, L. S., Lommen, C. M. L., Niemarkt, H. J., Pasman, J. W., van Kranen-Mastenbroek, V. H. J. M., Wijn, P. F. F., van Pul, C. & Andriessen, P. (2011), 'Automatic burst detection for the eeg of the preterm infant.', *Physiol Meas* **32**(10), 1623–1637.

Jerbi, K., Vidal, J. R., Ossandon, T., Dalal, S. S., Jung, J., Hoffmann, D., Minotti, L., Bertrand, O., Kahane, P. & Lachaux, J.-P. (2010), 'Exploring the electrophysiological correlates of the default-mode network with intracerebral eeg.', *Front Syst Neurosci* **4**, 27.

Johnson, R. A. & Wichern, D. V. (2015), 'Applied multivariate statistical analysis', *Statistics* **6215**(10), 10.

Jovanov-Milosević, N., Culjat, M. & Kostović, I. (2009), 'Growth of the human corpus callosum: modular and laminar morphogenetic zones.', *Front Neuroanat* **3**, 6.

Jovanov-Milošević, N., Judaš, M., Aronica, E. & Kostovic, I. (2014), 'Neural ecm in laminar organization and connectivity development in healthy and diseased human brain.', *Prog Brain Res* **214**, 159–178.

Judas, M., Rados, M., Jovanov-Milosevic, N., Hrabac, P., Stern-Padovan, R. & Kostovic, I. (2005), 'Structural, immunocytochemical, and mr imaging properties of periventricular crossroads of growing cortical pathways in preterm infants.', *AJNR Am J Neuroradiol* **26**(10), 2671–2684.

Jvreskog, K. (1996), *Applied factor analysis in the natural sciences*, Cambridge University Press.

Kaiser, J. (1990), On a simple algorithm to calculate the 'energy' of a signal, *in* 'Acoustics, Speech, and Signal Processing, 1990. ICASSP-90., 1990 International Conference on', pp. 381–384.

Kato, T., Okumura, A., Hayakawa, F., Tsuji, T., Natsume, J. & Watanabe, K. (2011), 'Evaluation of brain maturation in pre-term infants using conventional and amplitude-integrated electroencephalograms.', *Clin Neurophysiol* **122**(10), 1967–1972.

Khosla, N. (2004), Dimensionality Reduction Using Factor Analysis., PhD thesis, Griffith University, Australia.

Kidokoro, H., Inder, T., Okumura, A. & Watanabe, K. (2012), 'What does cyclicity on amplitude-integrated eeg mean?', *J Perinatol* **32**(8), 565–569.

Kilb, W., Kirischuk, S. & Luhmann, H. J. (2011), 'Electrical activity patterns and the functional maturation of the neocortex.', *Eur J Neurosci* **34**(10), 1677–1686.

Klebermass, K., Olischar, M., Waldhoer, T., Fuiko, R., Pollak, A. & Weninger, M. (2011), 'Amplitude-integrated eeg pattern predicts further outcome in preterm infants.', *Pediatr Res* **70**(1), 102–108.

Klein, A., Sauer, T., Jedynak, A. & Skrandies, W. (2006), 'Conventional and wavelet coherence applied to sensory-evoked electrical brain activity.', *IEEE Trans Biomed Eng* **53**(2), 266–272.

Koolen, N., Decroupet, O., Dereymaeker, A., Jansen, K., Vervisch, J., Matic, V., Vanrumste, B., Naulaers, G., Van Huffel, S. & De Vos, M. (2015a), Automated respiration detection from neonatal video data, *in* 'Proceedings of the 4rd

International Conference on Pattern Recognition Applications and Methods', pp. 164–169.

Koolen, N., Dereymaeker, A., Jansen, K., Vervisch, J., Matic, V., Vos, M. D., Naulaers, G. & Huffel, S. V. (2014a), Development of an interhemispheric symmetry measurement in the neonatal brain, *in* 'Proceedings of the 3rd International Conference on Pattern Recognition Applications and Methods', pp. 765–770.

Koolen, N., Dereymaeker, A., Räsänen, O., Jansen, K., Vervisch, J., Matic, V., De Vos, M., Naulaers, G., Van Huffel, S. & Vanhatalo, S. (2015b), Data-driven metric representing the maturation of preterm eeg, *in* 'Proceedings of the 37th Annual International Conference of the IEEE Engineering in Medicine and Biology Society.', pp. 1492–1495.

Koolen, N., Dereymaeker, A., Räsänen, O., Jansen, K., Vervisch, J., Matic, V., De Vos, M., Van Huffel, S., Naulaers, G. & Vanhatalo, S. (2014c), 'Interhemispheric synchrony in the neonatal eeg revisited: activation synchrony index as a promising classifier.', *Front Hum Neurosci* **8**, art.nr. 1030.

Koolen, N., Dereymaeker, A., Räsänen, O., Jansen, K., Vervisch, J., Matic, V., Naulaers, G., De Vos, M., Van Huffel, S. & Vanhatalo, S. (2015c), Early development of synchrony in cortical activations in the human. submitted to Neuroscience.

Koolen, N., Jansen, K., Vervisch, J., Matic, V., De Vos, M., Naulaers, G. & Van Huffel, S. (2014b), 'Line length as a robust method to detect high-activity events: automated burst detection in premature eeg recordings.', *Clin Neurophysiol* **125**(10), 1985–1994.

Koolen, N., Jansen, K., Vervisch, J., Matic, V., Vos, M. D., Naulaers, G. & Huffel, S. V. (2013), Automatic burst detection based on line length in the premature eeg, *in* 'Proceedings of the International Conference on Bio-inspired Systems and Signal Processing', pp. 105–111.

Korotchikova, I., Connolly, S., Ryan, C. A., Murray, D. M., Temko, A., Greene, B. R. & Boylan, G. B. (2009), 'Eeg in the healthy term newborn within 12 hours of birth.', *Clin Neurophysiol* **120**(6), 1046–1053.

Kostal, L., Lansky, P. & Rospars, J.-P. (2007), 'Neuronal coding and spiking randomness.', *Eur J Neurosci* **26**(10), 2693–2701.

Kostović, I. & Jovanov-Milosević, N. (2006), 'The development of cerebral connections during the first 20-45 weeks' gestation.', *Semin Fetal Neonatal Med* **11**(6), 415–422.

Kostović, I. & Judas, M. (2010), 'The development of the subplate and thalamocortical connections in the human foetal brain.', *Acta Paediatr* **99**(8), 1119–1127.

Krajča, V., Petránek, S., Mohylová, J., Paul, K., Gerla, V. & Lhotská, L. (2009), Modeling the microstructure of neonatal eeg sleep stages by temporal profiles, *in* '13th International Conference on Biomedical Engineering', Springer, pp. 133–137.

Krajca, V., Petránek, S., Patáková, I. & Värri, A. (1991), 'Automatic identification of significant graphoelements in multichannel eeg recordings by adaptive segmentation and fuzzy clustering.', *Int J Biomed Comput* **28**(1-2), 71–89.

Kuks, J. B., Vos, J. E. & O'Brien, M. J. (1988), 'Eeg coherence functions for normal newborns in relation to their sleep state.', *Electroencephalogr Clin Neurophysiol* **69**(4), 295–302.

Lamblin, M. D., André, M., Challamel, M. J., Curzi-Dascalova, L., d'Allest, A. M., De Giovanni, E., Moussalli-Salefranque, F., Navelet, Y., Plouin, P., Radvanyi-Bouvet, M. F., Samson-Dollfus, D. & Vecchierini-Blineau, M. F. (1999), '[electroencephalography of the premature and term newborn. maturational aspects and glossary].', *Neurophysiol Clin* **29**(2), 123–219.

Larroque, B., Ancel, P.-Y., Marret, S., Marchand, L., André, M., Arnaud, C., Pierrat, V., Rozé, J.-C., Messer, J., Thiriez, G., Burguet, A., Picaud, J.-C., Bréart, G., Kaminski, M. & , E. P. I. P. A. G. E. S. g. (2008), 'Neurodevelopmental disabilities and special care of 5-year-old children born before 33 weeks of gestation (the epipage study): a longitudinal cohort study.', *Lancet* **371**(9615), 813–820.

Le Bihannic, A., Beauvais, K., Busnel, A., de Barace, C. & Furby, A. (2012), 'Prognostic value of eeg in very premature newborns.', *Arch Dis Child Fetal Neonatal Ed* **97**(2), F106–F109.

Legido, A., Clancy, R. R. & Berman, P. H. (1991), 'Neurologic outcome after electroencephalographically proven neonatal seizures.', *Pediatrics* **88**(3), 583–596.

Leistritz, L., Jäger, H., Schelenz, C., Witte, H., Putsche, P., Specht, M. & Reinhart, K. (1999), 'New approaches for the detection and analysis of electroencephalographic burst-suppression patterns in patients under sedation.', *J Clin Monit Comput* **15**(6), 357–367.

Leonard, C. H., Piecuch, R. E. & Cooper, B. A. (2001), 'Use of the bayley infant neurodevelopmental screener with low birth weight infants', *Journal of pediatric psychology* **26**(1), 33–40.

Li, W. (1990), 'Mutual information functions versus correlation functions', *Journal of statistical physics* **60**(5-6), 823–837.

Linkenkaer-Hansen, K., Nikouline, V. V., Palva, J. M. & Ilmoniemi, R. J. (2001), 'Long-range temporal correlations and scaling behavior in human brain oscillations.', *J Neurosci* **21**(4), 1370–1377.

Liu, L., Johnson, H. L., Cousens, S., Perin, J., Scott, S., Lawn, J. E., Rudan, I., Campbell, H., Cibulskis, R., Li, M., Mathers, C., Black, R. E., , C. H. E. R. G. o. W. H. O. & F., U. N. I. C. E. (2012), 'Global, regional, and national causes of child mortality: an updated systematic analysis for 2010 with time trends since 2000.', *Lancet* **379**(9832), 2151–2161.

Löfhede, J., Thordstein, M., Löfgren, N., Flisberg, A., Rosa-Zurera, M., Kjellmer, I. & Lindecrantz, K. (2010), 'Automatic classification of background eeg activity in healthy and sick neonates.', *J Neural Eng* **7**(1), 16007.

Logesparan, L., Casson, A. J. & Rodriguez-Villegas, E. (2012), 'Optimal features for online seizure detection.', *Med Biol Eng Comput* **50**(7), 659–669.

Lombroso, C. T. (1979), 'Quantified electrographic scales on 10 pre-term healthy newborns followed up to 40-43 weeks of conceptional age by serial polygraphic recordings.', *Electroencephalogr Clin Neurophysiol* **46**(4), 460–474.

Lombroso, C. T. (1985), 'Neonatal polygraphy in full-term and premature infants: a review of normal and abnormal findings.', *J Clin Neurophysiol* **2**(2), 105–155.

Loncar-Turukalo, T., Bozanic, N., Negyessy, L., Baszo, F., Procyk, E. & Bajic, D. (2012), 'Removal of action potential influence on local field potentials using empirical mode decomposition', *Int J Bioelectromag* **14**(4), 204–210.

Lubsen, J., Vohr, B., Myers, E., Hampson, M., Lacadie, C., Schneider, K. C., Katz, K. H., Constable, R. T. & Ment, L. R. (2011), 'Microstructural and functional connectivity in the developing preterm brain.', *Semin Perinatol* **35**(1), 34–43.

Malk, K., Metsäranta, M. & Vanhatalo, S. (2014), 'Drug effects on endogenous brain activity in preterm babies.', *Brain Dev* **36**(2), 116–123.

Mani, R., Arif, H., Hirsch, L. J., Gerard, E. E. & LaRoche, S. M. (2012), 'Interrater reliability of icu eeg research terminology.', *J Clin Neurophysiol* **29**(3), 203–212.

Marcano-Reik, A. J., Prasad, T., Weiner, J. A. & Blumberg, M. S. (2010), 'An abrupt developmental shift in callosal modulation of sleep-related spindle

bursts coincides with the emergence of excitatory-inhibitory balance and a reduction of somatosensory cortical plasticity.', *Behav Neurosci* **124**(5), 600–611.

March of Dimes, PMNCH, S. t. C. W. (Geneva, 2012), 'Born too soon: The global action report on preterm birth.', Eds CP Howson, MV Kinney, JE Lawn. World Health Organization.

Matic, V., Cherian, P. J., Jansen, K., Koolen, N., Naulaers, G., Swarte, R. M., Govaert, P., Visser, G. H., Van Huffel, S. & De Vos, M. (2012), 'Automated eeg inter-burst interval detection in neonates with mild to moderate postasphyxial encephalopathy.', *Conf Proc IEEE Eng Med Biol Soc* **2012**, 17–20.

Matic, V., Cherian, P. J., Koolen, N., Ansari, A. H., Naulaers, G., Govaert, P., Van Huffel, S., De Vos, M. & Vanhatalo, S. (2015), 'Objective differentiation of neonatal eeg background grades using detrended fluctuation analysis.', *Front Hum Neurosci* **9**, 189.

Matic, V., Cherian, P. J., Koolen, N., Naulaers, G., Swarte, R. M., Govaert, P., Van Huffel, S. & De Vos, M. (2014), 'Holistic approach for automated background eeg assessment in asphyxiated full-term infants.', *J Neural Eng* **11**(6), 066007.

Mellits, E. D., Holden, K. R. & Freeman, J. M. (1982), 'Neonatal seizures. ii. a multivariate analysis of factors associated with outcome.', *Pediatrics* **70**(2), 177–185.

Menache, C. C., Bourgeois, B. F. D. & Volpe, J. J. (2002), 'Prognostic value of neonatal discontinuous eeg.', *Pediatr Neurol* **27**(2), 93–101.

Meyerson, B. A. (1968), 'Ontogeny of interhemispheric functions. an electrophysiological study in pre- and postnatal sheep.', *Acta Physiol Scand Suppl* **312**, 1–111.

Mitchell, T. J., Neil, J. J., Zempel, J. M., Thio, L. L., Inder, T. E. & Bretthorst, G. L. (2013), 'Automating the analysis of eeg recordings from prematurely-born infants: a bayesian approach.', *Clin Neurophysiol* **124**(3), 452–461.

Monod, N., Pajot, N. & Guidasci, S. (1972), 'The neonatal eeg: statistical studies and prognostic value in full-term and pre-term babies.', *Electroencephalogr Clin Neurophysiol* **32**(5), 529–544.

Msall, M. E., Buck, G. M., Rogers, B. T., Merke, D., Catanzaro, N. L. & Zorn, W. A. (1991), 'Risk factors for major neurodevelopmental impairments and need for special education resources in extremely premature infants.', *J Pediatr* **119**(4), 606–614.

Murphy, K., Stevenson, N. J., Goulding, R. M., Lloyd, R. O., Korotchikova, I., Livingstone, V. & Boylan, G. B. (2014), 'Automated analysis of multi-channel eeg in preterm infants.', *Clin Neurophysiol* .

Mwaniki, M. K., Atieno, M., Lawn, J. E. & Newton, C. R. J. C. (2012), 'Long-term neurodevelopmental outcomes after intrauterine and neonatal insults: a systematic review.', *Lancet* **379**(9814), 445–452.

Natalucci, G., Rousson, V., Bucher, H. U., Bernet, V., Hagmann, C. & Latal, B. (2013), 'Delayed cyclic activity development on early amplitude-integrated eeg in the preterm infant with brain lesions.', *Neonatology* **103**(2), 134–140.

Niemarkt, H. J., Andriessen, P., Peters, C. H. L., Pasman, J. W., Zimmermann, L. J. & Bambang Oetomo, S. (2010), 'Quantitative analysis of maturational changes in eeg background activity in very preterm infants with a normal neurodevelopment at 1 year of age.', *Early Hum Dev* **86**(4), 219–224.

Norman, E., Wikström, S., Hellström-Westas, L., Turpeinen, U., Hämäläinen, E. & Fellman, V. (2011), 'Rapid sequence induction is superior to morphine for intubation of preterm infants: a randomized controlled trial.', *J Pediatr* **159**(6), 893–9.e1.

Norman, E., Wikström, S., Rosén, I., Fellman, V. & Hellström-Westas, L. (2013), 'Premedication for intubation with morphine causes prolonged depression of electrocortical background activity in preterm infants.', *Pediatr Res* **73**(1), 87–94.

Odabaee, M., Freeman, W. J., Colditz, P. B., Ramon, C. & Vanhatalo, S. (2013), 'Spatial patterning of the neonatal eeg suggests a need for a high number of electrodes.', *Neuroimage* **68**, 229–235.

Odabaee, M., Tokariev, A., Layeghy, S., Mesbah, M., Colditz, P. B., Ramon, C. & Vanhatalo, S. (2014), 'Neonatal eeg at scalp is focal and implies high skull conductivity in realistic neonatal head models.', *Neuroimage* **96**, 73–80.

Okumura, A., Hayakawa, F., Kato, T., Kuno, K. & Watanabe, K. (2002), 'Developmental outcome and types of chronic-stage eeg abnormalities in preterm infants.', *Dev Med Child Neurol* **44**(11), 729–734.

Olischar, M., Klebermass, K., Waldhoer, T., Pollak, A. & Weninger, M. (2007), 'Background patterns and sleep-wake cycles on amplitude-integrated electroencephalography in preterms younger than 30 weeks gestational age with peri-/intraventricular haemorrhage.', *Acta Paediatr* **96**(12), 1743–1750.

Omidvarnia, A., Fransson, P., Metsäranta, M. & Vanhatalo, S. (2014), 'Functional bimodality in the brain networks of preterm and term human newborns.', *Cereb Cortex* **24**(10), 2657–2668.

Omidvarnia, A., Metsäranta, M., Lano, A. & Vanhatalo, S. (2015), 'Structural damage in early preterm brain changes the electric resting state networks.', *Neuroimage* **120**, 266–273.

Palmu, K. (2015), Event detection in preterm electroencephalography, PhD thesis, Aalto University, Helsinki, Finland.

Palmu, K., Kirjavainen, T., Stjerna, S., Salokivi, T. & Vanhatalo, S. (2013), 'Sleep wake cycling in early preterm infants: comparison of polysomnographic recordings with a novel eeg-based index.', *Clin Neurophysiol* **124**(9), 1807–1814.

Palmu, K., Stevenson, N., Wikström, S., Hellström-Westas, L., Vanhatalo, S. & Palva, J. M. (2010b), 'Optimization of an nleo-based algorithm for automated detection of spontaneous activity transients in early preterm eeg.', *Physiol Meas* **31**(11), N85–N93.

Palmu, K., Wikström, S., Hippeläinen, E., Boylan, G., Hellström-Westas, L. & Vanhatalo, S. (2010a), 'Detection of 'eeg bursts' in the early preterm eeg: visual vs. automated detection.', *Clin Neurophysiol* **121**(7), 1015–1022.

Palva, S. & Palva, J. M. (2011), 'Functional roles of alpha-band phase synchronization in local and large-scale cortical networks.', *Front Psychol* **2**, 204.

Pan, X. L. & Ogawa, T. (1999), 'Microstructure of longitudinal 24 hour electroencephalograms in healthy preterm infants.', *Pediatr Int* **41**(1), 18–27.

Parmelee, A. H., Akiyama, Y., Stern, E. & Harris, M. A. (1969), 'A periodic cerebral rhythm in newborn infants.', *Exp Neurol* **25**(4), 575–584.

Paul, K., Krajca, V., Roth, Z., Melichar, J. & Petránek, S. (2003), 'Comparison of quantitative eeg characteristics of quiet and active sleep in newborns.', *Sleep Med* **4**(6), 543–552.

Paz, J. T., Davidson, T. J., Frechette, E. S., Delord, B., Parada, I., Peng, K., Deisseroth, K. & Huguenard, J. R. (2013), 'Closed-loop optogenetic control of thalamus as a tool for interrupting seizures after cortical injury.', *Nat Neurosci* **16**(1), 64–70.

Pfurtscheller, K., Bauernfeind, G., Müller-Putz, G. R., NOOPurlesberger, B., Müller, W. & Pfurtscheller, G. (2008), 'Correlation between eeg burst-to-burst intervals and hr acceleration in preterm infants.', *Neurosci Lett* **437**(2), 103–106.

Praetorius, H. M., Bodenstein, G. & Creutzfeldt, O. D. (1977), 'Adaptive segmentation of eeg records: a new approach to automatic eeg analysis.', *Electroencephalogr Clin Neurophysiol* **42**(1), 84–94.

Quigg, M. & Leiner, D. (2009), 'Engineering aspects of the quantified amplitude-integrated electroencephalogram in neonatal cerebral monitoring.', *J Clin Neurophysiol* **26**(3), 145–149.

Quiroga, R. Q., Kraskov, A., Kreuz, T. & Grassberger, P. (2002), 'Performance of different synchronization measures in real data: a case study on electroencephalographic signals', *Physical Review E* **65**(4), 041903.

Raichle, M. E. (2010), 'Two views of brain function.', *Trends Cogn Sci* **14**(4), 180–190.

Räsänen, O. (2012), Average spectrotemporal structure of continuous speech matches with the frequency resolution of human hearing., *in* 'Proceedings of Interspeech', pp. 1–4.

Räsänen, O., Metsäranta, M. & Vanhatalo, S. (2013), 'Development of a novel robust measure for interhemispheric synchrony in the neonatal eeg: activation synchrony index (asi).', *Neuroimage* **69**, 256–266.

Ratnarajah, N., Rifkin-Graboi, A., Fortier, M. V., Chong, Y. S., Kwek, K., Saw, S.-M., Godfrey, K. M., Gluckman, P. D., Meaney, M. J. & Qiu, A. (2013), 'Structural connectivity asymmetry in the neonatal brain.', *Neuroimage* **75**, 187–194.

Saji, R., Hirasawa, K., Ito, M., Kusuda, S., Konishi, Y. & Taga, G. (2015), 'Probability distributions of the electroencephalogram envelope of preterm infants.', *Clin Neurophysiol* **126**(6), 1132–1140.

Särkelä, M., Mustola, S., Seppänen, T., Koskinen, M., Lepola, P., Suominen, K., Juvonen, T., Tolvanen-Laakso, H. & Jäntti, V. (2002), 'Automatic analysis and monitoring of burst suppression in anesthesia.', *J Clin Monit Comput* **17**(2), 125–134.

Sartori, E. (2013), Parametric connectivity analysis in time and frequency domain from in silico and EEG data., PhD thesis, Universita degli Studi di Padova, Dipartimento di Ingegneria dell'Informazione, Padova, Italy.

Schack, B., Witte, H., Helbig, M., Schelenz, C. & Specht, M. (2001), 'Time-variant non-linear phase-coupling analysis of eeg burst patterns in sedated patients during electroencephalic burst suppression period.', *Clin Neurophysiol* **112**(8), 1388–1399.

Scher, M. S. (1996), 'Normal electrographic-polysomnographic patterns in preterm and fullterm infants.', *Semin Pediatr Neurol* **3**(1), 2–12.

Scher, M. S., Hamid, M. Y., Steppe, D. A., Beggarly, M. E. & Painter, M. J. (1993), 'Ictal and interictal electrographic seizure durations in preterm and term neonates.', *Epilepsia* **34**(2), 284–288.

Scher, M. S., Johnson, M. W. & Holditch-Davis, D. (2005a), 'Cyclicity of neonatal sleep behaviors at 25 to 30 weeks' postconceptional age.', *Pediatr Res* **57**(6), 879–882.

Scher, M. S., Turnbull, J., Loparo, K. & Johnson, M. W. (2005b), 'Automated state analyses: proposed applications to neonatal neurointensive care.', *J Clin Neurophysiol* **22**(4), 256–270.

Schölkopf, B., Platt, J. C., Shawe-Taylor, J., Smola, A. J. & Williamson, R. C. (2001), 'Estimating the support of a high-dimensional distribution', *Neural computation* **13**(7), 1443–1471.

Schölkopf, B., Smola, A. J., Williamson, R. C. & Bartlett, P. L. (2000), 'New support vector algorithms', *Neural computation* **12**(5), 1207–1245.

Schreiber (2000), 'Measuring information transfer', *Phys Rev Lett* **85**(2), 461–464.

Schumacher, E. M., Larsson, P. G., Pripp, A. H. & Stiris, T. A. (2014), 'The effect of blood glucose and pco2 on spectral eeg of premature infants during the first three days of life.', *Neonatology* **105**(4), 297–305.

Schwab, K., Putsche, P., Eiselt, M., Helbig, M. & Witte, H. (2004), 'On the rhythmicity of quadratic phase coupling in the tracé alternant eeg in healthy neonates.', *Neurosci Lett* **369**(3), 179–182.

Selton, D., Andre, M. & Hascoët, J. M. (2000), 'Normal eeg in very premature infants: reference criteria.', *Clin Neurophysiol* **111**(12), 2116–2124.

Shah, D. K., Mackay, M. T., Lavery, S., Watson, S., Harvey, A. S., Zempel, J., Mathur, A. & Inder, T. E. (2008), 'Accuracy of bedside electroencephalographic monitoring in comparison with simultaneous continuous conventional electroencephalography for seizure detection in term infants.', *Pediatrics* **121**(6), 1146–1154.

Shah, P. S., Ye, X. Y., Synnes, A., Rouvinez-Bouali, N., Yee, W., Lee, S. K. & , C. N. N. (2012), 'Prediction of survival without morbidity for infants born at under 33 weeks gestational age: a user-friendly graphical tool.', *Arch Dis Child Fetal Neonatal Ed* **97**(2), F110–F115.

Shany, E., Benzaquen, O., Friger, M., Richardson, J. & Golan, A. (2008), 'Influence of antiepileptic drugs on amplitude-integrated electroencephalography.', *Pediatr Neurol* **39**(6), 387–391.

Shellhaas, R. A., Burns, J. W., Barks, J. D. E. & Chervin, R. D. (2014), 'Quantitative sleep stage analyses as a window to neonatal neurologic function.', *Neurology* **82**(5), 390–395.

Shellhaas, R. A., Chang, T., Tsuchida, T., Scher, M. S., Riviello, J. J., Abend, N. S., Nguyen, S., Wusthoff, C. J. & Clancy, R. R. (2011), 'The american clinical neurophysiology society's guideline on continuous electroencephalography monitoring in neonates.', *J Clin Neurophysiol* **28**(6), 611–617.

Sheorajpanday, R. V. A., Nagels, G., Weeren, A. J. T. M., van Putten, M. J. A. M. & De Deyn, P. P. (2009), 'Reproducibility and clinical relevance of quantitative eeg parameters in cerebral ischemia: a basic approach.', *Clin Neurophysiol* **120**(5), 845–855.

Sherman, D., Brambrink, A., Walterspacher, D., Dasika, V., Ichord, R. & Thakor, N. (1997), Detecting EEG bursts after hypoxic-ischemic injury using energy operators, *in* 'Engineering in Medicine and Biology Society, 1997. Proceedings of the 19th Annual International Conference of the IEEE', Vol. 3, pp. 1188–1190.

Smits, A. (2014), Neonatale farmacologie: naar een betere voorspelbaarheid., PhD thesis, University of Leuven, Leuven, Belgium.

Smyser, C. D., Inder, T. E., Shimony, J. S., Hill, J. E., Degnan, A. J., Snyder, A. Z. & Neil, J. J. (2010), 'Longitudinal analysis of neural network development in preterm infants.', *Cereb Cortex* **20**(12), 2852–2862.

Snead, 3rd, O. (2001), 'Surgical treatment of medically refractory epilepsy in childhood.', *Brain Dev* **23**(4), 199–207.

Stam, C. J., Tewarie, P., Van Dellen, E., van Straaten, E. C. W., Hillebrand, A. & Van Mieghem, P. (2014), 'The trees and the forest: Characterization of complex brain networks with minimum spanning trees.', *Int J Psychophysiol* **92**(3), 129–138.

Stam, C. J. & van Straaten, E. C. W. (2012), 'The organization of physiological brain networks.', *Clin Neurophysiol* **123**(6), 1067–1087.

Stevenson, N. J., Palmu, K., Wikström, S., Hellström-Westas, L. & Vanhatalo, S. (2014), 'Measuring brain activity cycling (bac) in long term eeg monitoring of preterm babies.', *Physiol Meas* **35**(7), 1493–1508.

Tao, J. D. & Mathur, A. M. (2010), 'Using amplitude-integrated eeg in neonatal intensive care.', *J Perinatol* **30 Suppl**, S73–S81.

Temko, A., Thomas, E., Marnane, W., Lightbody, G. & Boylan, G. (2011), 'Eeg-based neonatal seizure detection with support vector machines.', *Clin Neurophysiol* **122**(3), 464–473.

Tewarie, P., van Dellen, E., Hillebrand, A. & Stam, C. J. (2015), 'The minimum spanning tree: an unbiased method for brain network analysis.', *Neuroimage* **104**, 177–188.

Tharp, B. R., Scher, M. S. & Clancy, R. R. (1989), 'Serial eegs in normal and abnormal infants with birth weights less than 1200 grams–a prospective study with long term follow-up.', *Neuropediatrics* **20**(2), 64–72.

Thompson, Jr, R., Gustafson, K. E., Oehler, J. M., Catlett, A. T., Brazy, J. E. & Goldstein, R. F. (1997), 'Developmental outcome of very low birth weight infants at four years of age as a function of biological risk and psychosocial risk.', *J Dev Behav Pediatr* **18**(2), 91–96.

Toet, M. C., van der Meij, W., de Vries, L. S., Uiterwaal, C. S. P. M. & van Huffelen, K. C. (2002), 'Comparison between simultaneously recorded amplitude integrated electroencephalogram (cerebral function monitor) and standard electroencephalogram in neonates.', *Pediatrics* **109**(5), 772–779.

Tokariev, A., Palmu, K., Lano, A., Metsäranta, M. & Vanhatalo, S. (2012), 'Phase synchrony in the early preterm eeg: development of methods for estimating synchrony in both oscillations and events.', *Neuroimage* **60**(2), 1562–1573.

Tokariev, A., Vanhatalo, S. & Palva, J. M. (2015), 'Analysis of infant cortical synchrony is constrained by the number of recording electrodes and the recording montage.', *Clin Neurophysiol* .

Tolonen, M., Palva, J. M., Andersson, S. & Vanhatalo, S. (2007), 'Development of the spontaneous activity transients and ongoing cortical activity in human preterm babies.', *Neuroscience* **145**(3), 997–1006.

Uhlhaas, P. J., Roux, F., Rodriguez, E., Rotarska-Jagiela, A. & Singer, W. (2010), 'Neural synchrony and the development of cortical networks.', *Trends Cogn Sci* **14**(2), 72–80.

Vairavan, S., Eswaran, H., Haddad, N., Rose, D., Preissl, H., Wilson, J., Lowery, C. & Govindan, R. (2009), 'Detection of discontinuous patterns in spontaneous brain activity of neonates and fetuses', **56**(11), 2725–2729.

van Alfen-van der Velden, A. A. E. M., Hopman, J. C. W., Klaessens, J. H. G. M., Feuth, T., Sengers, R. C. A. & Liem, K. D. (2006), 'Effects of midazolam and morphine on cerebral oxygenation and hemodynamics in ventilated premature infants.', *Biol Neonate* **90**(3), 197–202.

van Bel, F., Lemmers, P. & Naulaers, G. (2008), 'Monitoring neonatal regional cerebral oxygen saturation in clinical practice: value and pitfalls.', *Neonatology* **94**(4), 237–244.

van den Broek, M. P. H., Huitema, A. D. R., van Hasselt, J. G. C., Groenendaal, F., Toet, M. C., Egberts, T. C. G., de Vries, L. S. & Rademaker, C. M. A. (2011), 'Lidocaine (lignocaine) dosing regimen based upon a population pharmacokinetic model for preterm and term neonates with seizures.', *Clin Pharmacokinet* **50**(7), 461–469.

van Putten, M. J. A. M. (2007), 'The revised brain symmetry index.', *Clin Neurophysiol* **118**(11), 2362–2367.

van Putten, M. J. A. M. & Tavy, D. L. J. (2004), 'Continuous quantitative eeg monitoring in hemispheric stroke patients using the brain symmetry index.', *Stroke* **35**(11), 2489–2492.

Van Sweden, B., Koenderink, M., Windau, G., Van de Bor, M., Van Bel, F., Van Dijk, J. G. & Wauquier, A. (1991), 'Long-term eeg monitoring in the early premature: developmental and chronobiological aspects.', *Electroencephalogr Clin Neurophysiol* **79**(2), 94–100.

Vanhatalo, S. & Kaila, K. (2006), 'Development of neonatal eeg activity: from phenomenology to physiology.', *Semin Fetal Neonatal Med* **11**(6), 471–478.

Vanhatalo, S. & Palva, J. M. (2011), 'Phase brings a new phase to the exploration of the elusive neonatal eeg.', *Clin Neurophysiol* **122**(4), 645–647.

Vanhatalo, S., Palva, J. M., Andersson, S., Rivera, C., Voipio, J. & Kaila, K. (2005), 'Slow endogenous activity transients and developmental expression of k+-cl- cotransporter 2 in the immature human cortex.', *Eur J Neurosci* **22**(11), 2799–2804.

Varner, J. L., Peters, J. F. & Ellingson, R. J. (1978), 'Interhemispheric synchrony in the eegs of full-term newborns.', *Electroencephalogr Clin Neurophysiol* **45**(5), 641–647.

Vecchierini, M.-F., André, M. & d'Allest, A. M. (2007), 'Normal eeg of premature infants born between 24 and 30 weeks gestational age: terminology, definitions and maturation aspects.', *Neurophysiol Clin* **37**(5), 311–323.

Vecchierini, M.-F., d'Allest, A.-M. & Verpillat, P. (2003), 'Eeg patterns in 10 extreme premature neonates with normal neurological outcome: qualitative and quantitative data.', *Brain Dev* **25**(5), 330–337.

Victor, S., Appleton, R. E., Beirne, M., Marson, A. G. & Weindling, A. M. (2005a), 'Spectral analysis of electroencephalography in premature newborn infants: normal ranges.', *Pediatr Res* **57**(3), 336–341.

Victor, S., Appleton, R. E., Beirne, M., Marson, A. G. & Weindling, A. M. (2005b), 'Effect of carbon dioxide on background cerebral electrical activity and fractional oxygen extraction in very low birth weight infants just after birth.', *Pediatr Res* **58**(3), 579–585.

Volpe, J. J. (1998), 'Neurologic outcome of prematurity.', *Arch Neurol* **55**(3), 297–300.

Wang, Y. & Agarwal, R. (2007), Automatic detection of burst suppression, *in* 'Engineering in Medicine and Biology Society, 2007. EMBS 2007. 29th Annual International Conference of the IEEE', pp. 553–556.

Weisman, O., Magori-Cohen, R., Louzoun, Y., Eidelman, A. I. & Feldman, R. (2011), 'Sleep-wake transitions in premature neonates predict early development.', *Pediatrics* **128**(4), 706–714.

Weiss, L. G., Oakland, T. & Aylward, G. P. (2010), *Bayley-III clinical use and interpretation*, Academic Press.

Welzing, L., Kribs, A., Eifinger, F., Huenseler, C., Oberthuer, A. & Roth, B. (2010), 'Propofol as an induction agent for endotracheal intubation can cause significant arterial hypotension in preterm neonates.', *Paediatr Anaesth* **20**(7), 605–611.

Wertheim, D. F., Murdoch Eaton, D. G., Oozeer, R. C., Connell, J. A., Dubowitz, L. M., Dubowitz, V., Willetts, R. & Wootton, R. (1991), 'A new system for cotside display and analysis of the preterm neonatal electroencephalogram.', *Dev Med Child Neurol* **33**(12), 1080–1086.

West, C. R., Harding, J. E., Williams, C. E., Gunning, M. I. & Battin, M. R. (2006), 'Quantitative electroencephalographic patterns in normal preterm infants over the first week after birth.', *Early Hum Dev* **82**(1), 43–51.

Wikström, S., Ley, D., Hansen-Pupp, I., Rosén, I. & Hellström-Westas, L. (2008), 'Early amplitude-integrated eeg correlates with cord tnf-alpha and brain injury in very preterm infants.', *Acta Paediatr* **97**(7), 915–919.

Wikström, S., Pupp, I. H., Rosén, I., Norman, E., Fellman, V., Ley, D. & Hellström-Westas, L. (2012), 'Early single-channel aeeg/eeg predicts outcome in very preterm infants.', *Acta Paediatr* **101**(7), 719–726.

Witte, H., Putsche, P., Eiselt, M., Schwab, K., Wacker, M. & Leistritz, L. (2011), 'Time-variant analysis of phase couplings and amplitude-frequency dependencies of and between frequency components of eeg burst patterns in full-term newborns.', *Clin Neurophysiol* **122**(2), 253–266.

Witte, H., Schack, B., Helbig, M., Putsche, P., Schelenz, C., Schmidt, K. & Specht, M. (2000), 'Quantification of transient quadratic phase couplings within eeg burst patterns in sedated patients during electroencephalic burst-suppression period.', *J Physiol Paris* **94**(5-6), 427–434.

Wong, L. & Abdulla, W. (2006), 'Time-frequency evaluation of segmentation methods for neonatal eeg signals.', *Conf Proc IEEE Eng Med Biol Soc* **1**, 1303–1306.

Wong, L. & Abdulla, W. (2008), Automatic detection of preterm neonatal EEG background states, *in* 'Acoustics, Speech and Signal Processing, 2008. ICASSP 2008. IEEE International Conference on', pp. 421–424.

Yan, M., Hou, Z. & Gao, Y. (2011), A bilateral brain symmetry index for analysis of EEG signal in stroke patients, *in* 'Biomedical Engineering and Informatics (BMEI), 2011 4th International Conference on', Vol. 1, pp. 8–11.

Yerushalmy-Feler, A., Marom, R., Peylan, T., Korn, A., Haham, A., Mandel, D., Yarkoni, I. & Bassan, H. (2014), 'Electroencephalographic characteristics in preterm infants born with intrauterine growth restriction.', *J Pediatr* **164**(4), 756–761.e1.

Zheng, Y., Wang, G., Li, K., Bao, G. & Wang, J. (2014), 'Epileptic seizure prediction using phase synchronization based on bivariate empirical mode decomposition.', *Clin Neurophysiol* **125**(6), 1104–1111.

Zwanenburg, A., Meijer, E., Jennekens, W., van Pul, C., Kramer, B. & Andriessen, P. (2012), 'Automatic detection of burst synchrony in preterm infants.', *Conf Proc IEEE Eng Med Biol Soc* **2012**, 4720–4723.

Curriculum

Ninah Koolen was born in The Hague, The Netherlands on December 18, 1988.

She received a M.Sc. degree with distinction in Biomedical Engineering (2011) from the KU Leuven, Belgium. During her studies she finished a two months' student summer project on the normal kinematics of the cervical spine at the Biomechanics section. She spent her next summer in Thailand, doing an internship at the Prince of Songkla University, Hat Yai and at the National Metal and Materials Technology Center, Bangkok. During her last year, she finished a master thesis under supervision of Prof. dr. ir. S. Van Huffel, entitled "Reliability of statistical features describing neural spike train in the presence of classification errors".

In October 2011 she joined STADIUS, Department of Electical Engineering (ESAT), KU Leuven as a PhD student under the supervision of Prof. dr. ir. Sabine Van Huffel, Prof. dr. Gunnar Naulaers, Prof. dr. ir. Maarten de Vos and Prof. dr. Sampsa Vanhatalo. She worked on neonatal signal processing in close collaboration with the Department of Development and Regeneration, Neonatology, University Hospital, Leuven and in collaboration with the NeoGuard project (https://neoguard.net). During these 4 years, she received an IWT PhD research grant on strategic basic research. She visited the BABA (BAby Brain Activity) lab in the Children's Hospital, Helsinki University Central Hospital, under supervision of prof. dr. S. Vanhatalo for a total of six months (short stay May 2014, Oct-Dec 2014 and April-June 2015). Thereto, she received two FWO travel grants for a long stay abroad. Her research focused on developing interpretable signal processing algorithms with application on brain maturation. The objective is to assist medical doctors at the Neonatal Intensive Care Units (NICUs), when assessing the brain development of the premature neonates.

Besides research, she has been engaged in science communication, contributing to several demonstrations and pre-university outreach workshops.

Publication list

Articles in internationally reviewed journals

1. Koolen, N., Jansen, K., Vervisch, J., Matic, V., De Vos, M., Naulaers, G., Van Huffel, S. (2014). Line length as a robust method to detect high-activity events: Automated burst detection in premature EEG recordings. Clinical Neurophysiology, 125 (10), 1985-1994.

2. Koolen, N. *, Dereymaeker, A. *, Räsänen, O., Jansen, K., Vervisch, J., Matic, V., De Vos, M., Van Huffel, S., Naulaers, G., Vanhatalo, S. (2014). Interhemispheric synchrony in the neonatal EEG revisited: activation synchrony index as a promising classifier. Frontiers in Human Neuroscience, 8, art.nr. 1030.
   * joint first author

3. Koolen, N., Dereymaeker, A., Räsänen, O., Jansen, K., Vervisch, J., Matic, V., De Vos, M., Van Huffel, S., Naulaers, G., Vanhatalo, S. (2015). Early development of synchrony in cortical activations in the human. Neuroscience, under review.

4. Dereymaeker, A. *, Koolen, N. *, Vervisch, J., Ortibus, E., Jansen, K., De Vos, M., Van Huffel, S., Naulaers, G.(2015). The suppression curve as a quantitative approach for measuring brain maturation in preterm infants. Clinical Neurophysiology, under review.
   * joint first author

5. Matic, V., Cherian, P., Koolen, N., Naulaers, G., Swarte, R., Govaert, P., Van Huffel, S., De Vos, M. (2014). Holistic approach for automated background EEG assessment in asphyxiated full-term infants. Journal of Neural Engineering, 11 (6), art.nr. 066007.

6. Matic, V., Cherian, P., Jansen, K., Koolen, N., Naulaers, G., Swarte, R., Govaert, P., Van Huffel, S., De Vos, M. (2015). Improving reliability

of monitoring background EEG dynamics in asphyxiated infants. IEEE Transactions on Biomedical Engineering, accepted for publication.

7. Matic, V., Cherian, P., Koolen, N., Ansari, A., Naulaers, G., Govaert, P., Van Huffel, S., De Vos, M., Vanhatalo, S. (2015). Objective differentiation of neonatal EEG background grades using detrended fluctuation analysis. Frontiers in Human Neuroscience, 9, art.nr. 189.

Papers in proceedings of international conferences

1. Koolen, N., Dereymaeker, A., Räsänen, O., Jansen, K., Vervisch, J., Matic, V., De Vos, M., Naulaers, G., Van Huffel, S., Vanhatalo, S. (2015). Data-driven metric representing the maturation of preterm EEG. Proc. of the 37th Annual International Conference of the IEEE Engineering in Medicine and Biology Society. EMBC 2015. Milan, Italy, Aug. 2015 (pp.1492-1495).

2. Koolen, N., Decroupet, O., Dereymaeker, A., Jansen, K., Vervisch, J., Matic, V., Vanrumste, B., Naulaers, G., Van Huffel, S., De Vos, M. (2015). Automated Respiration Detection from Neonatal Video Data. Proc. of the 4th International Conference on Pattern Recognition Applications and Methods. ICPRAM 2015. Lisbon, Portugal, Jan. 2015 (pp. 164-169).

3. Koolen, N., Dereymaeker, A., Jansen, K., Vervisch, J., Matic, V., De Vos, M., Naulaers, G., Van Huffel, S. (2014). Development of an interhemispheric symmetry measurement in the neonatal brain. Proc. of the International Conference on Pattern Recognition Applications and Methods. ICPRAM 2014. Angers, France, Mar. 2014 (pp. 765-770).

4. De Meester, J., Batselier, K., Koolen, N., Hunyadi, B., Decuyper, J., Vanden Bosch, E., Vandewalle, J., Dehaene, W. (2013). The mathematics in your ears. The role of math in integrated STEM via the modeling of hearing aids. Proc. of the 41th SEFI Conference. SEFI. Leuven, Belgium, Sep. 2013 (pp. 1-8).

5. Verveckken, J., Geth, F., Beerten, J., Hunyadi, B., Leemput, N., Van Roy, J., Tielens, P., De Smedt, V., Iacovella, S., Höschle, H., Koolen, N., De Clercq, H., Driesen, J., Gielen, G., Puers, B., Vandewalle, J., Van Huffel, S., Belmans, R., Deconinck, G., Dehaene, W. (2013). Development of open-source interactive smart energy house for K12 engineering eduction on residential energy efficiency. Proc. of the 41th SEFI Conference. SEFI. Leuven, Belgium, Sep. 2013 (pp. 1-12).

6. Geth, F., Verveckken, J., Leemput, N., Van Roy, J., Beerten, J., Tielens, P., De Smedt, V., Iacovella, S., Hunyadi, B., Koolen, N., De Clercq, H., Gielen, G., Puers, B., Van Huffel, S., Belmans, R., Deconinck, G., Dehaene, W., Driesen, J. (2013). Development of an Open-Source Smart Energy House for K-12 Education. Proc. IEEE Power and Energy Society Annual Meeting. IEEE PES General Meeting 2013. Vancouver, Canada, 21-25 July 2013 (pp. 1-5).

7. Verveckken, J., Geth, F., Hunyadi, B., Beerten, J., Leemput, N., Van Roy, J., Tielens, P., De Smedt, V., Iacovella, S., Koolen, N., De Clercq, H., Driesen, J., Gielen, G., Puers, B., Vandewalle, J., Van Huffel, S., Belmans, R., Deconinck, G., Dehaene, W. (2013). Developing Engineering-oriented Educational Workshops Within a Student Branch. Proc. IEEE EUROCON 2013. Zagreb, Croatia, 1-4 July 2013 (pp. 933-939).

8. Koolen, N., Jansen, K., Vervisch, J., Matic, V., De Vos, M., Naulaers, G., Van Huffel, S. (2013). Automatic burst detection based on line length in the premature EEG. Proceedings of the International Conference on Bio-inspired Systems and Signal Processing. BIOSIGNALS 2013. Barcelona, Spain, 11-14 Feb. 2013 (pp. 105-111).

9. Matic, V., Cherian, P., Jansen, K., Koolen, N., Naulaers, G., Swarte, R., Govaert, P., Visser, G., Van Huffel, S., De Vos, M. (2012). Automated EEG inter-burst interval detection in neonates with mild to moderate postasphyxial encephalopathy. Proc. of the 34th Annual International Conference of the IEEE Engineering in Medicine and Biology Society. EMBC 2012. San Diego, California, USA, Aug-Sep 2012 (pp. 17-20).

10. Koolen, N., Gligorijevic, I., Van Huffel, S. (2012). Reliability of statistical features describing neural spike trains in the presence of classification errors. Proc. of International Conference on Bio-inspired systems and Signal Processing. BIOSIGNALS 2012. Vilamoura, Portugal, Feb. 2012 (pp. 169-173).

Abstracts in proceedings of international conferences

1. Koolen, N., Dereymaeker, A., Räsänen, O., Stjerna, S., Jansen, K., Vervisch, J., Matic, V., De Vos, M., Naulaers, G., Van Huffel, S., Vanhatalo, S. Data-driven method for tracking early EEG maturation. Proc. of the 9th International Conference on Brain Monitoring and Neuroprotection in the Newborn. BMN 2015. Cork, Ireland, Oct. 2015.

2. Dereymaeker, A., Koolen, N., Jansen, K., Vervisch, J., De Vos, M., Van Huffel, S., Vanhatalo, S., Naulaers, G. Interhemispheric synchrony

reflecting the maturation of callosal and cortico-cortical connections in premature EEG. Proc. of the 9th International Conference on Brain Monitoring and Neuroprotection in the Newborn. BMN 2015. Cork, Ireland, Oct. 2015.

3. Thewissen, L., Smits, A., Caicedo, A., Koolen, N., Allegaert, K., Naulaers, G. Effect of propofol on cerebral hemodynamic parameters and amplitude-integrated EEG in newborns. Proc. of the 9th International Conference on Brain Monitoring and Neuroprotection in the Newborn. BMN 2015. Cork, Ireland, Oct. 2015.

4. Matic, V., Cherian, P.J., Ansari, A.H., Koolen, N., Govaert, P., Naulaers, G., Van Huffel, S., De Vos, M. Metrics for the Background EEG Assessment in Asphyxiated Infants. 37th Annual International Conference of the IEEE Engineering in Medicine and Biology Society (EMBC). Milan, Italy, Aug. 2015.

5. Koolen, N., Dereymaeker, A., Jansen, K., Vervisch, J., Matic, V., De Vos, M., Naulaers, G., Van Huffel, S. (2015). The suppression curve as a new respresentation of the premature EEG maturation. Proc. of the 24th Annual Computational Neuroscience Meeting. CNS 2015. Prague, Czech Republic, Jul. 2015.

6. Hunyadi, B., De Clercq, H., Koolen, N., Desmedt, V., Iacovella, S., Deconinck, G., Gielen, G., Puers, R., Van Huffel, S., Dehaene, W. A pre-university outreach activity on human-computer interfaces. Proc. of the Gender and STEM Conference. Berlin, Germany, July 2014.

7. Koolen, N., Jansen, K., Vervisch, J., Matic, V., De Vos, M., Naulaers, G., Van Huffel, S. (2012). Automated burst detection in the EEG of the preterm newborn. Proc. of the 7th International Conference on Brain Monitoring & Neuroprotection in the newborn. BMN 2012. Tampa, USA, Sep. 2012.

8. Koolen, N., Jansen, K., Vervisch, J., De Vos, M., Naulaers, G., Van Huffel, S. (2012). Background EEG analysis of the preterm newborn: automated burst detection. Proc. of the 40th annual meeting of the International Society of Oxygen Transport to Tissue. ISOTT 2012. Brugge, Belgium, Aug. 2012.



FACULTY OF ENGINEERING SCIENCE
DEPARTMENT OF ELECTRICAL ENGINEERING
STADIUS CENTER FOR DYNAMICAL SYSTEMS, SIGNAL PROCESSING AND DATA ANALYTICS
Kasteelpark Arenberg 10 box 2446
B-3001 Leuven
ninah.koolen@esat.kuleuven.be